237
3-7-79

PR. 2980

LBL-8883
UC-66
CONF-7810170 --

SECOND

INVITATIONAL WELL-TESTING SYMPOSIUM

PROCEEDINGS

October 25-27, 1978
Berkeley, California

MASTER

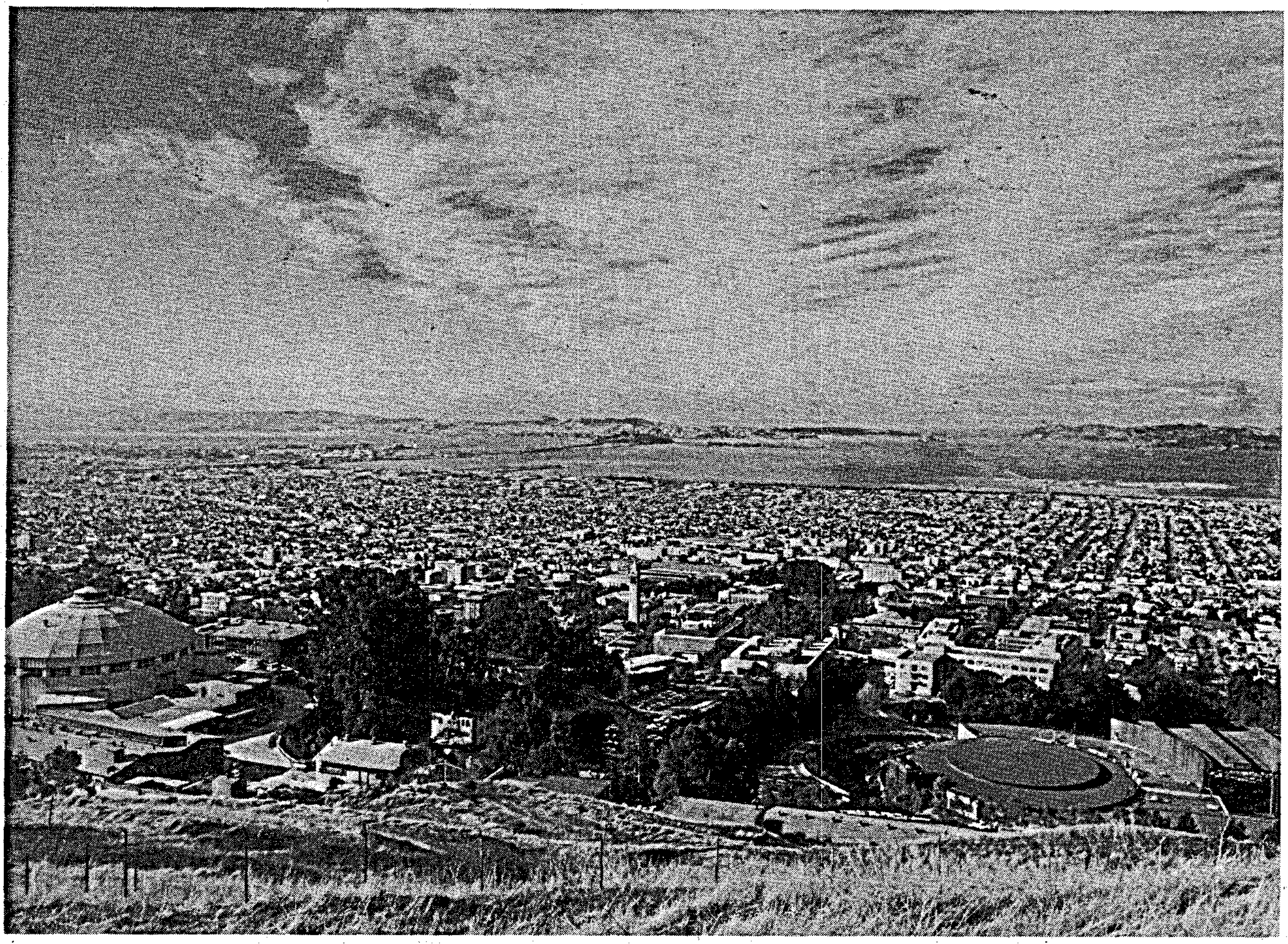

Sponsored by

U.S. Department of Energy
Division of Geothermal Energy

Through the

Earth Sciences Division
Lawrence Berkeley Laboratory
University of California

Prepared for the U.S. Department of Energy under Contract W-7405-ENG-48.

Printed in the United States of America
Available from
National Technical Information Service
U.S. Department of Commerce
5285 Port Royal Road
Springfield, VA 22161
Price Code: A07

LBL-8883
UC-66
CONF-7810170

SECOND INVITATIONAL WELL-TESTING SYMPOSIUM PROCEEDINGS

Lawrence Berkeley Laboratory
October 25-27, 1978

PREFACE

After the first Invitational Well Testing Symposium held at Berkeley, California, October 1977 (Ref. LBL-7027), many participants and the Well Testing Community as a whole expressed their interest in holding a second Symposium which would concentrate on a specific subject. It was decided to devote the second symposium to the important topic — injection of fluids underground — with the following sections to round out the meeting:

- Measurements and Case Histories
- Analysis and Interpretation
- Chemistry and Physics
- Special Problems

As in the past the goals of the symposium were for professionals in the fields of petroleum engineering, hydrology, and energy related earth sciences to meet and exchange information, ideas, and solutions to outstanding problems. The symposium was held to evaluate the state of the art of injection of fluid underground, and its application to geothermal systems in particular. The symposium was supported by the Geothermal Energy Division of the United States Department of Energy.

The Earth Sciences Division selected a second symposium organizing committee, under the chairmanship of Professor Paul A. Witherspoon. Members were Ron C. Schroeder and Werner J. Schwarz. The symposium and the proceedings were coordinated by Werner J. Schwarz.

The symposium provided the over 120 participants a forum in which to exchange ideas and present new information on fluid injection underground The emphasis was on reviewing existing capabilities, identifying current limitations, and generating new ideas for meeting the Department of Energy/Division of Geothermal Energy goals of power-on-line by 1980. The introduction was chaired by Ron C. Schroeder, and Professor Paul. A Witherspoon gave the keynote address.

The participants represented the major national laboratories Federal and State Government, Industry, Utilities, independent Consultants, 5 major Universities, France, El Salvador, Iceland, India, Italy and Mexico.

Abstracts and papers from non Lawrence Berkeley Laboratory authors and are being reproduced unchanged. Lawrence Berkeley Laboratory papers were reviewed by the Earth Sciences Division's Publications Committee and by the Technical Information Department.

CONTENTS

Chemistry and Physics
(Session Chairman: O. Weres)

Special Problems
(Session Chairman: J. P. Sauty)

INJECTION TESTING AT RRGI-4 RAFT RIVER, IDAHO IDAHO NATIONAL ENGINEERING LABORATORY

W. L. Niemi and L. B. Nelson
EG&G Idaho, Inc.
Idaho Falls, Idaho

INTRODUCTION

Injection testing of a 866 m (2840 ft) deep well, RRGI-4, within the Raft River KGRA began in March and concluded in June 1978. The purpose of the testing was to determine the hydrogeologic characteristics of an intermediate zone above and adjacent to the primary geothermal producing zone(s) and to ascertain the feasibility of injecting "cold," unaerated water into a zone hydraulically connected to the producing zone(s). This paper discusses the results and conclusions drawn from the longest duration test, conducted between May 30 and June 9, 1978, of the testing program. Reservoir Engineering hydrogeologists consider the data produced by this test to be the most representative of that portion of the Raft River KGRA penetrated by RRGI-4. The results of all testing, production, and injection conducted at RRGI-4 will be published at a later date by EG&G Idaho, Inc.

The Raft River facility is being developed to assist in the commercialization of moderate-temperature geothermal resources. The initial Raft River power system will attempt to generate five megawatts of electrical power from a 143 °C (290 °F) resource by using a binary organic cycle.[1]

Geologic Structure

Southern Idaho's Raft River valley (Figure 1) lies in a north-trending basin, warped and down-faulted in late Cenozoic time. The basin is filled to an inferred depth of 1800 to 2000 m (5900 to 6600 ft).[2] Faults located near the Raft River facility (Figure 2) include the Narrows Structure, thought to be a northeast-trending normal fault, dipping steeply toward the southeast, and the Bridge Fault, a north-trending fault, dipping steeply toward east.

RRGI-4 (Figure 3) located 475 m (1559 ft) south of RRGE-1 is 866 m (2840 ft) deep and is cased to a depth of 560 m (1840 ft). RRGI-4 penetrates alternating sand, gravel, silt, and tuff (Figure 2) of the Raft River and Salt Lake Formations. Geologic relationships (Figure 2) indicate that the Narrows Structure should have been penetrated by RRGI-4. No evidence of faulting was revealed from return drill cuttings to total depth and borehole geophysical logging to a depth of 554 m (1820 ft). Faulting is suggested by the anomalously high temperature of 120 °C (250 °F) at a depth of 560 m (1840 ft).

Well Construction

Table I lists construction characteristics of RRGI-4 and the observation wells used during the testing of RRGI-4. RRGE-1, RRGE-2, and RRGE-3 penetrate the geothermal resource. Monitor wells (MW) monitor pressure changes in aquifers, above the geothermal resource, which supply water for irrigation and domestic uses.

The variation in well depths and casing of observation wells and the complex and heterogeneous hydrogeologic system did not facilitate the interpretation of observation well data. The production, at various times, of RRGE-1, RRGE-2, and MW-2 and the drilling of RRGP-5 resulted in additional factors which had to be considered when interpreting the data. Observation well data were unsuitable to calculate or estimate the aquifer parameters: intrinsic transmissivity kh, transmissivity T, storativity ϕch, and/or storage coefficient S.

Hydrogeology

The spatial configuration of the fault zones, the Narrows Structure and the Bridge Fault, and the hydrogeologic characteristics of the fault zones and the surrounding rock are only generally understood with subsurface detail lacking.[2] RRGI-4 appears to be on the downthrown side of the Narrows Structure. Geothermal waters leaking from the fault zones migrate laterally toward the southeast as part of the valley flow system. Hot water can therefore be encountered in both the valley flow system, immediately down gradient of the fault zones, and in the fault zones.

Water chemistry data[3] indicate two sources for water in the geothermal resource. RRGE-1 and RRGE-2, which penetrate the Bridge Fault, represent one chemical type. RRGE-3, USGS-3, and RRGI-4, of the other chemical type, are thought to either penetrate the Narrows Structure or to be completed in a zone whose waters originate in the Narrows Structure.

If RRGI-4 penetrates the Narrows Structure, the injection of water into RRGI-4 can be expected to generate greater hydraulic responses in the upper portion of the fault zone than in unfractured rock. Observation well USGS-3 appears to be located in the upper portion of the fault zone. MW-1 apparently monitors the pressure in the unfractured rock adjacent to the Narrows Structure.

INJECTION TEST - MAY 30 TO JUNE 9, 1978

Method of Evaluation

The Jacob straight-line modification[4] of the Theis Nonequilibrium Equation was applied in analyzing pressure changes occurring within the Raft River KGRA during the RRGI-4 testing. The Jacob method utilizes a semilogarithmic graph of pressure buildup on the arithmetic scale versus the time since injection began on the logarithmic scale. The pressure drawdown or buildup data, plotted as a straight line when u, the Theis variable of integration, is less than or equal to 0.01. This condition occurred when the quantity of water being released from or taken into storage between the injection well and the point of observation was negligible compared to the changes in storage at a

TABLE I

Observation Wells Used During the Testing of RRGI-4

Well	Radius†	Depth	Casing‡
RRGE-1	1559 ft N 475 m	5000 ft 1524 m	3600 ft 1097 m
RRGE-2	5400 ft NNE 1650 m	6500 ft 1981 m	4200 ft 1280 m
RRGE-3	5300 ft SSE 1620 m (not monitored)	5400 ft 1645 m	4227 ft 1288 m
USGS-3	2300 ft W 700 m	1423 ft 434 m	900 ft 274 m
MW-1	700 ft SSE 210 m	1309 ft 399 m	1200 ft 366 m
MW-2	1850 ft SE 560 m	570 ft 170 m	540 ft 160 m
BLM	4000 ft NNW 1220 m	413 ft 126 m	--- ---
BLM Offset	4000 ft 1220 m	405 ft 123 m	65 ft 20 m
RRGI-4	--- ---	2840 ft 866 m	1820 ft 555 m

†Distance in feet (ft) and metres (m) and direction from RRGI-4 with N = North, NW = Northwest, NNE = North-Northeast, W = West, SSE = South-Southeast, and SE = Southeast

‡Cased depth

radius greater than that of the observation point. The u condition was satisfied in RRGI-4 after less than one-tenth of a minute of injection, when the effective radius of RRGI-4 was assumed to be one foot.

When using the Modified Nonequilibrium Equation, the change in pressure in pounds per square inch (psi) per logarithmic cycle (s_{10}) is used to calculate T (the product obtained by multiplying the aquifer thickness by its hydraulic conductivity, a measure of the ease with which water, under field conditions, can be transmitted through a porous material) and kh (the product of the intrinsic permeability, k, of the aquifer and its thickness, h). Due to the heterogeneous hydrologic character of the Raft River KGRA, no T or kh was calculated. An apparent T and an apparent kh was estimated to use as a basis for comparing tests. The apparent kh, expressed in millidarcy-feet (md-ft), was estimated through the formula

$$kh = \frac{5759\ Q\mu}{s_{10}}$$

where

Q = injection rate in gallons per minute (gpm)
μ = water viscosity in centipoises (cp) at 120 °C, and
s_{10} = the change in psi per log cycle.

The apparent T, expressed in gallons per day per foot of buildup (gpd/ft), was estimated through the formula

$$T = \frac{kh}{1000}\left(\frac{\gamma}{\mu}\right)(.3284147)$$

with

kh = the aquifer intrinsic transmissivity
γ = the water density at 250 °F in pounds per cubic foot (lg/ft), and
μ = the water viscosity at 120 °C in cp.

The apparent T and the apparent kh are not considered to be factual hydrogeologic entities.

Data Collection

Wellhead pressures were measured at RRGI-4 with a Heise pressure gauge and a Soltec strip chart recorder. Injection rates were quantified by passing the water through an orifice of known diameter and measuring the pressure differential across it. The temperature of the injection water and the injection rate were recorded on continuous recorders. Surface instrumentation was used to monitor wells RRGE-1, RRGE-2, USGS-3, MW-1, and MW-2. This instrumentation consisted of a digiquartz pressure transducer model 2200-A-002 interfaced to a Hewlett-Packard thermal printer model 5150 via a Parascientific digiquartz pressure computer model 600. A 60-degree, V-notch weir was used to monitor changes in artesian flow at the BLM well. A Stevens A35 water level recorder was used to measure the depth to water level in the BLM offset well.

Unsuccessful attempts were made to measure downhole pressure changes within RRGI-4 with a Hewlett-Packard temperature-pressure probe. The borehole geophysical logging cable failed due to electrical shorting within the cable, perhaps caused by the corrosive and electrically conductive action of geothermal water leaking through the cable's teflon insulation.[5]

Test Results

A 700 gpm (44 lps) injection test was initiated May 30 and terminated June 9, 1978. The test was conducted for 13,300 minutes and was terminated because the water levels in RRGE-2, which supplied water for injection, dropped to the level of the pump bowls. Initial wellhead pressure at RRGI-4 was 25 psig, suggesting that the wellbore was relatively cold. The shutin pressure following injection was 298 psig.

The deviation of points from a linear trend during the initial 25 minutes of injection were related to fluctuations in the injection rate. The injection rate varied as much as ±10 percent. The lowest acceptable variation in the injection rate during a test should be ±3 percent, but greater control of injection rates could not be attained with the procedures and equipment used.

The increase in pressure above the linear trend to the high point at 100 minutes is caused by the density effects of injecting increasingly hotter water of lower density. The decrease in pressure between 100 to 120 minutes is perhaps related to aquifer adjustments to the lower viscosity injection water, relative to formation water.

Ten pump outages occurred during the test. The effect of a pump outage on pressure buildup can be seen in Figure 4 after 120 minutes as data points which lie below the linear trend.

An apparent kh of 31,000 md-ft and an apparent T of 2600 gpd/ft were estimated from a Jacob graph of pressure buildup. The placement of the straight line after 120 minutes may be slightly in error due to pump outages. No analyzable pressure falloff data was obtained due to failure of recording instruments.

Increased wellhead pressure was observed at USGS-3 after 500 minutes (Figure 5). Pressure changes at MW-1 (Figure 6) were difficult to interpret due to water sampling of the well prior to RRGI-4 injection. The pressure increase at USGS-3 after 10,000 minutes was apparently 2.82 times greater than the increase at MW-1. This comparison assumed an initial pressure at MW-1 equal to an earlier injection test. The larger response in wellhead pressure farther from the injection well suggests a heterogeneous and/or anisotropic aquifer system.

Discussion of Results

The temperature of injection water rose from 66 °C (150 °F), the minimum temperature of injection and transfer piping preheating, to 134 °C (273 °F) during the test (Figure 4). The temperature of water being driven from the wellbore into the receiving zone(s) therefore depended on the time since injection commenced.

Examination of Figure 4 reveals an upward deviation in the data occurring between 25 and 120 minutes. The deviation is believed to be caused by temporally dependent densities and viscosities related to temperature variations between the injection water, the water in the wellbore, and the formation water. Small temperature changes of the water entering the receiving zone(s) can be expected for probably at least 10 minutes following the initiation of injection. Borehole fluid density changes can also be expected to be small during this period. Pressure buildup data collected at the wellhead during the initial 10 minutes of injection can be expected to have relatively small errors.

The linear segment in Figure 4 from 0.45 to 25 minutes implies that relatively small viscosity and density effects were occurring during this period, assuming no boundary effects. A large portion of the point scatter in the first 25 minutes is caused by variations in injection rate. Twenty minutes is the time required to inject approximately one borehole volume of water to a depth of 710 m (2340 ft). The increase in pressure, after 25 minutes, above the initial linear trend is presumed to be caused by the decreasing water density and viscosity of the hotter water as injection progresses with viscosity. The linear trend after 120 minutes has approximately the same slope as the initial linear trend. The authors believe that thermal quasi-equilibrium was established after 120 minutes. At that time the viscosity and density of the injection water was stabilized. The decline in wellhead pressure between 80 and 120 minutes is caused by the lower viscosity of the higher temperature injection water.

The maximum upward displacement of the pressure buildup above the initial linear trend appears to be related to the wellhead pressure immediately prior to injection. This wellhead pressure is strongly influenced by wellhead water temperature and the extent of preheating of the injection well. An injection test conducted on March 30, 1978 (Figure 7) did not show the upward displacement of pressure buildup as the well was thoroughly preheated before injection began, as shown by the initial wellhead pressure of 66 psig.

CONCLUSIONS

Conclusions derived from the May 30 to June 9, 1978 injection test at RRGI-4 include:

1. The response of the observation wells to injection into RRGI-4 confirmed the hydrogeologic conclusions indicated by geologic and geochemical relationships that RRGI-4 and USGS-3 penetrate the same fracture or fracture system, the Narrows Structure. The pressure responses in USGS-3, 700 m (2100 ft) to the west of RRGI-4, were greater than those in MW-1, 210 m (700 ft) to the south-southeast. It is concluded that MW-1 does not penetrate the fracture system but is in unfractured rock adjacent to and overlying the Narrows Structure. RRGI-4 and USGS-3 are on the downthrown side of the Narrows Structure with the structure being penetrated at shallower depths in USGS-3 than in RRGI-4.

2. No boundaries were detected during 222 hours of injection into RRGI-4. Although RRGI-4 penetrates a fault zone, it is believed that no boundaries were detected as pressure responses were integrated very rapidly within the fault zone and adjacent unfractured rock.

3. The temporally dependent borehole fluid temperature during injection is a significant factor which must be considered when analyzing the pressure buildup data. Downhole temperature-pressure probes must be used to determine aquifer responses during testing. The probe should be opposite the top of the uppermost highly transmissive zone and it should remain in the borehole until pressure changes occurring within the borehole correspond with those at the wellhead.

4. The aquifer parameters, intrinsic transmissivity kh, transmissivity T, storativity ϕch, and storage coefficient S, could not be determined quantitatively due to the heterogeneous and complex nature of the hydrogeology of the Raft River KGRA and the variation in well depths and casing of observation wells.

5. The wellhead and the injection water should approximate aquifer temperature before and during injection testing, to prevent pressure changes related to temporally dependent densities and viscosities.

References

1. "Regional Hydrothermal Commercialization Plan, Rocky Mountain Basin and Range Region," Dept. of Energy, 1978.

2. P. L. Williams, D. R. Mabey, A. A. Zohdy, H. Ackermann, D. B. Hoover, K. L. Pierce, and S. S. Oriel, "Geology and Geophysics of the Southern Raft River Valley Geothermal Area, Idaho, USA," Second U.N. Symposium on the Development and Use of Geothermal Resources, Proc., Vol. 2, 1976, p. 1273-1282.

3. H. L. Overton, "Hot Water Flow in Raft River Reservoir," in publication, 1978.

4. P. A. Domenico, Concepts and Models in Ground-Water Hydrology, McGraw-Hill, 1972, p. 405.

5. R. C. Stoker, personal communication, 1978.

This work was performed under the auspices of the U. S. Department of Energy, Division of Geothermal Energy.

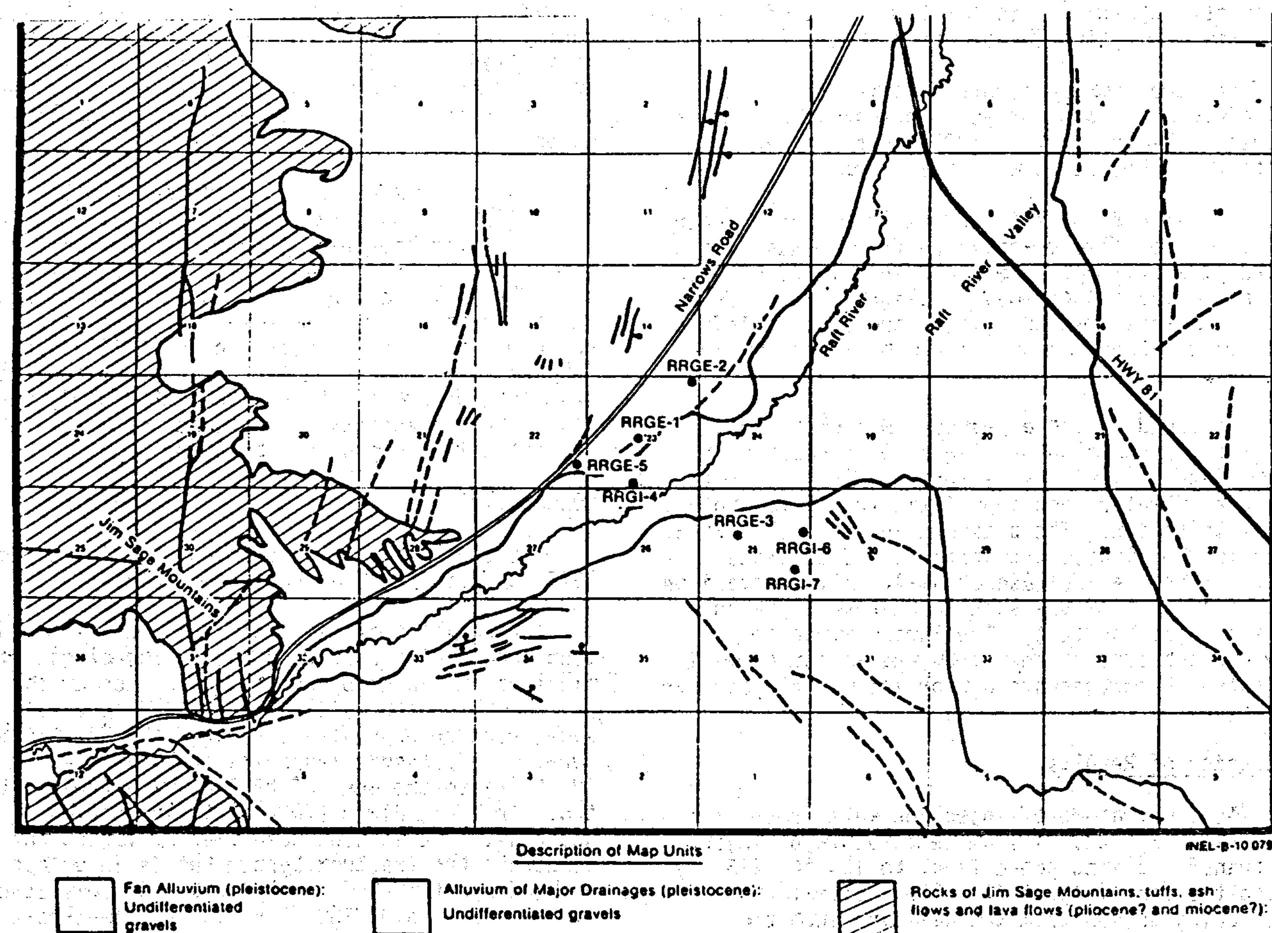

Fig. 1. Surfacial geology and faults of the Raft River Valley.

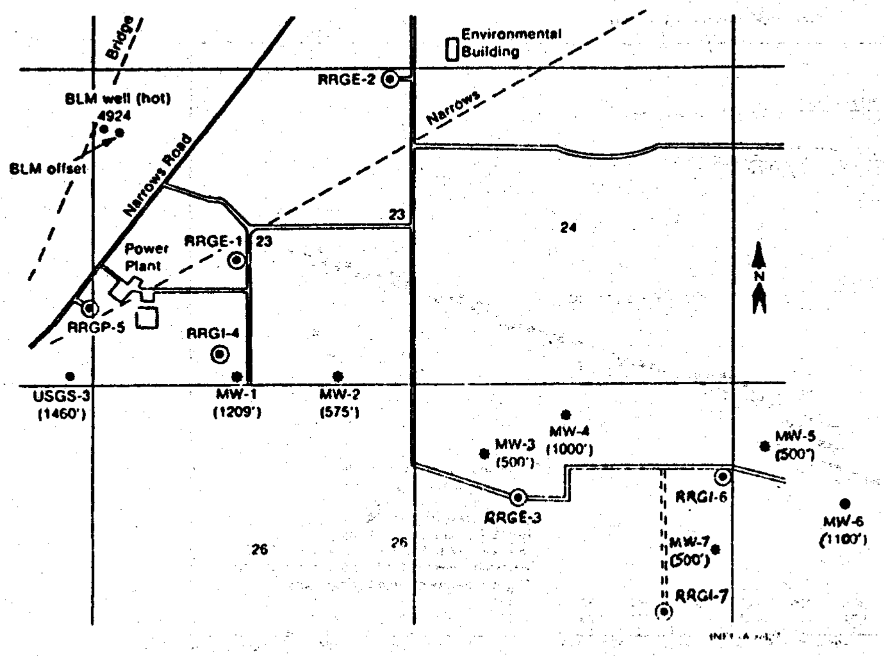

Fig. 2. Raft River Facility with geologic structure and well location.

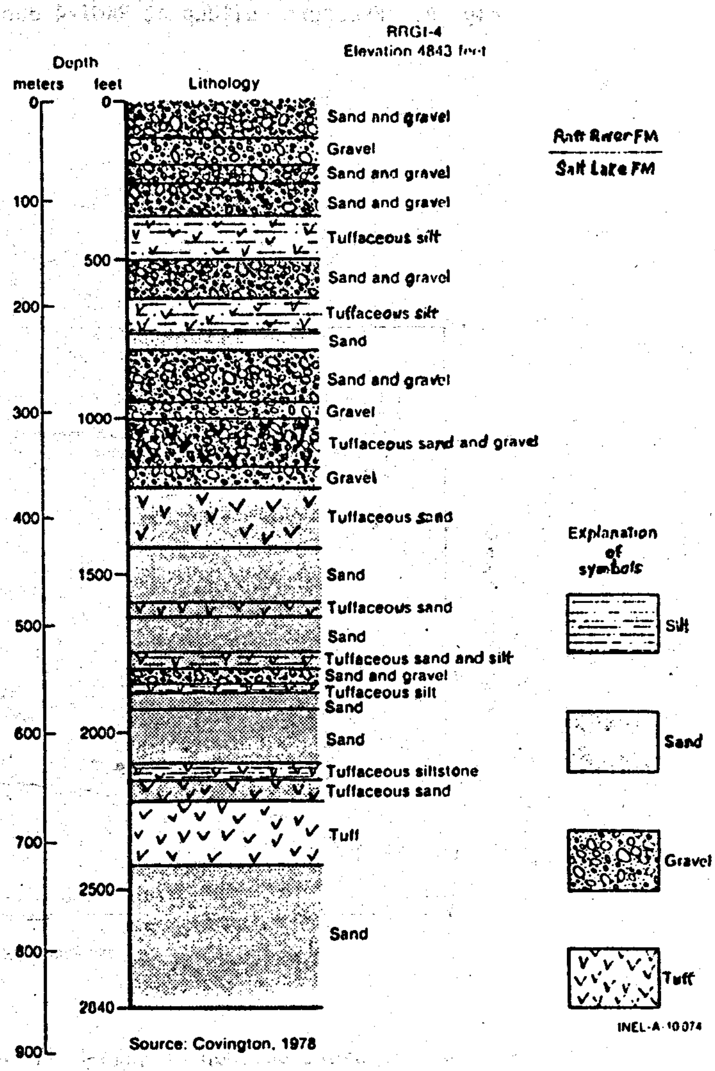

Fig. 3. Lithologic log RRGI-4.

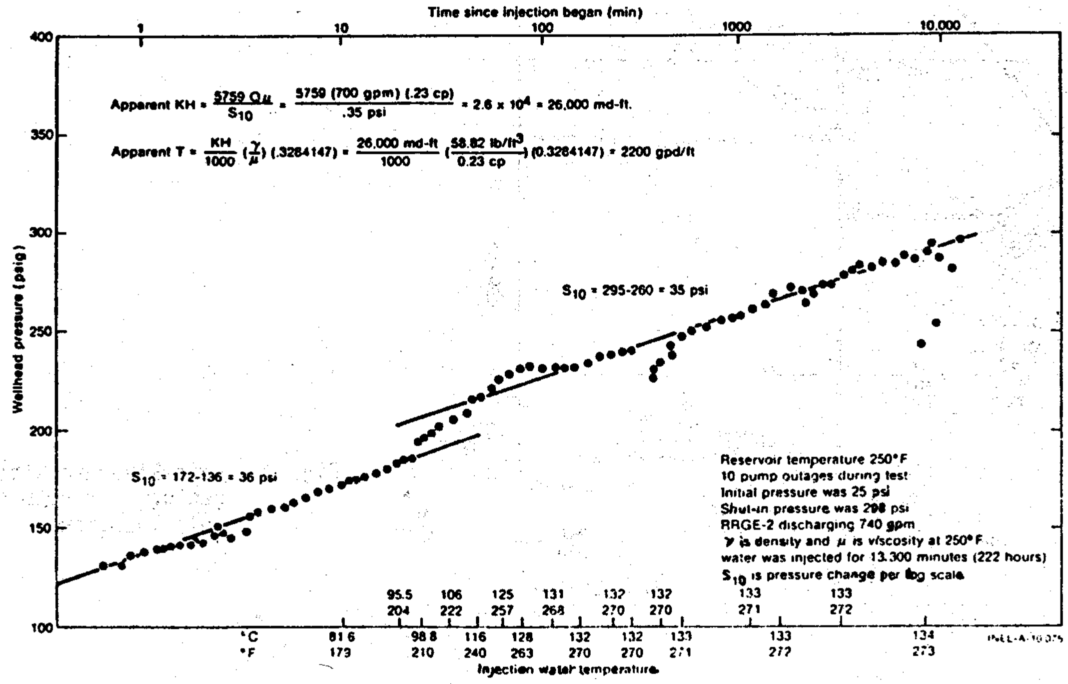

Fig. 4. Pressure buildup at RRGI-4 during May 30, 1978, 700 gpm injection test.

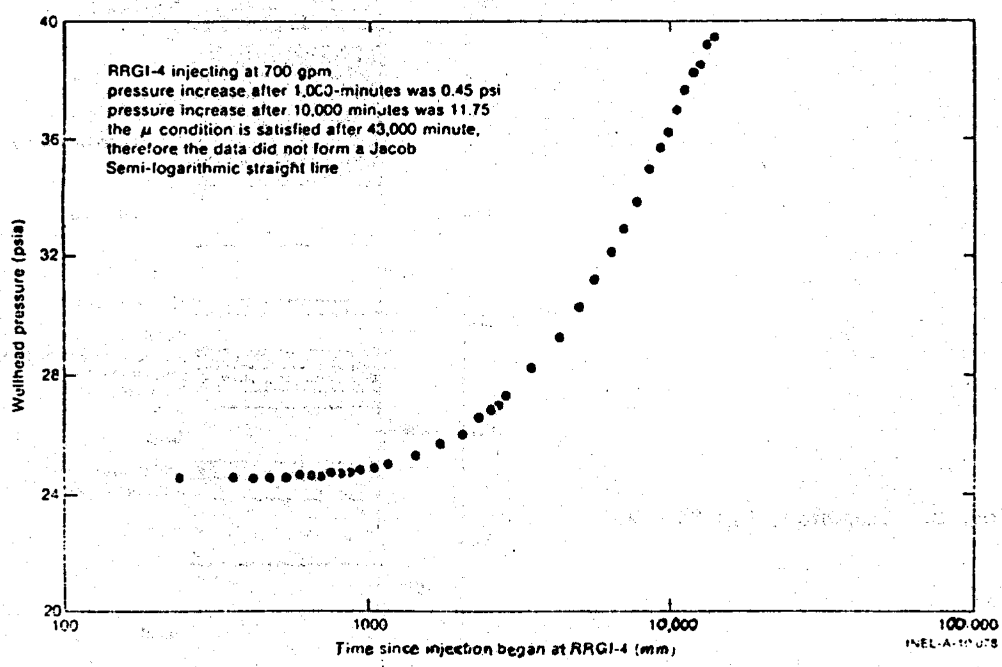

Fig. 5. Pressure buildup at USGS-3 during May 30, 1978, injection test at RRGI-4.

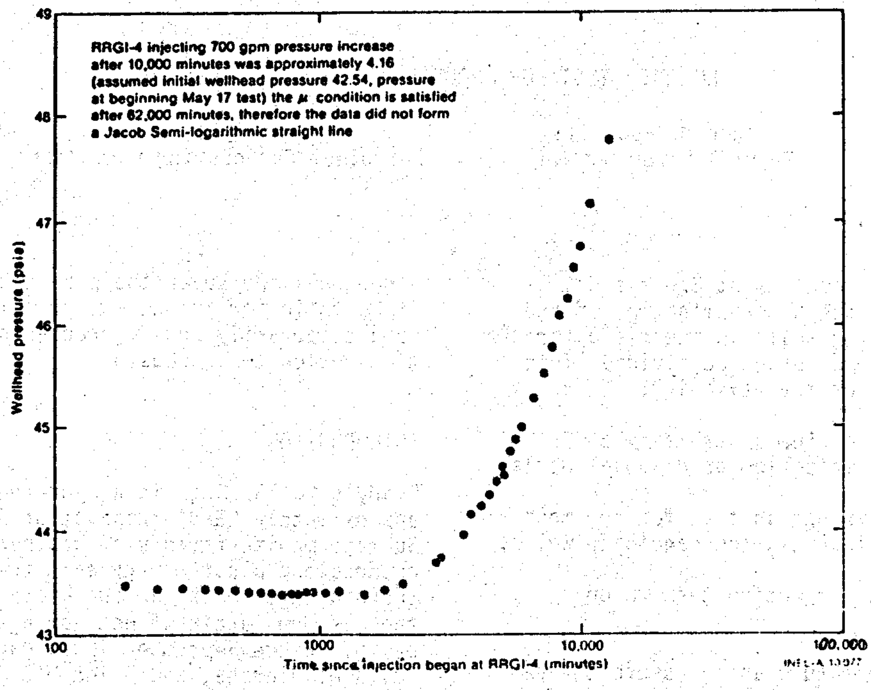

Fig. 6. Pressure buildup at MW-1 during May 30, 1978, injection test at RRGI-4.

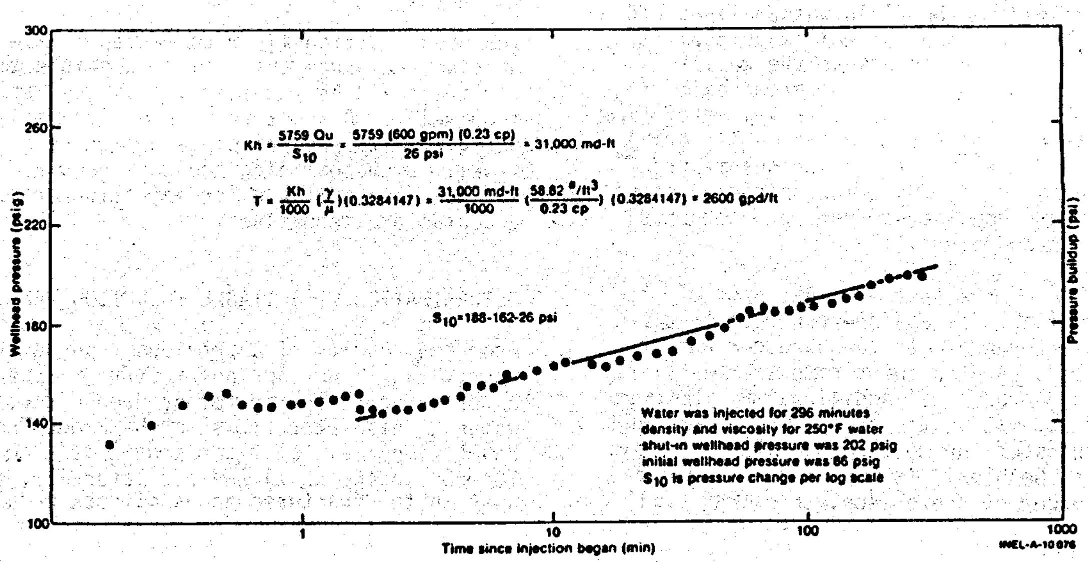

Fig. 7. Pressure buildup at RRGI-4 during March 30, 1978, 600 gpm injection test.

INJECTION TEST FOR BRADY'S HOT SPRINGS, NEVADA

Jacob M. Rudisill
Thermal Power Company

Herman Dykstra
Petroleum Engineering Consultant

ABSTRACT

An evaluation of the resource at Brady's Hot Springs, Nevada included a determination of the suitability of existing wells in the field for the disposal or injection of produced fluids. This evaluation consisted of the following:

1. The determination of the suitability of existing wells as injection or disposal wells.
2. The design of an injection test for the most promising of the investigated candidate wells.
3. Performance of the injection test which included:

   (a) pre-test temperature and pressure surveys.
   (b) selection and installation of a satisfactory wellhead.
   (c) pre-injection differential temperature and spinner surveys.
   (d) injectivity test of well, measuring wellhead pressure versus injected flow rate.
   (e) temperature, gamma and spinner surveys during constant, low flow rate injection.
   (f) spinner surveys at various flow rates and locations to determine the relative ability of particular zones of the well to accept water.
   (f) measurement of interference effects on neighboring wells.

The data obtained in the field was analyzed and interpreted to determine the well's suitability as an injector. Such factors as the well's present casing condition, the apparent exit regions of the water, the relative volume of flow leaving these exit points, and the well's drilling record impacted the analysis. Various means of correcting undesirable injection characteristics of the well were considered from both technical and economic standpoints.

The conclusion of the test was that none of the wells were suitable as an injector because of pressure interference with the producer and the subsequent concern of a short time thermal breakthrough to the producer. Additionally, the cost and risk of attempting to correct the cement and casing programs of the most perspective injector were found to be high. It was therefore recommended, in order of preference, to either drill a new well, workover the perspective well to make it suitable for injection, or utilize a disposal pond temporarily before proceeding with the injection option to be chosen.

INTRODUCTION

Brady's Hot Springs is a hydrothermal area located approximately 28KM northeast of Fernley, Nevada. Surface manifestations of geothermal activity occur along a north-northeast trending fault zone (herein referred to as the Brady Thermal Fault) at the eastern margin of Hot Springs Flat, a small basin. Since September 1959, Magma Power Company, its subsidiaries, and Union Oil Company (as Earth Energy Company) drilled 11 wells in the area. In 1977, Magma's 160-acre lease in the Section 12 was assigned to Geothermal Food Processors (GFP) for the purpose of providing heat from the wells on this acreage for the dehydration of food. GFP made an application to the Geothermal Loan Guarantee Program (GLGP) for assistance in financing the effort, and consequently the GLGP office turned to the U.S. Geological Survey (USGS) for a resource evaluation. The USGS in turn recommended that a pump flow test was necessary to truly determine the ability of the acreage's wells to provide the requisite water flow rate, temperature, and composition for the plant's operating life time of at least 15 years. Consequently, Thermal Power Company was contacted and procured to design, arrange, conduct and evaluate a pumped test program to satisfy these questions.

The USGS additionally recommended in their original resource evaluation that injection wells for the field be investigated as well as production wells. A short term injection test was thus designed with the principle objective of finding a well (or determining the work required to render such a well) suitable for injection or suggesting acceptable alternatives.

DETERMINATION OF SUITABLE INJECTION WELL

From the results of a previous reservoir assessment, Brady's Hot Springs reservoir appears to be a fractured reservoir fed by deep circulating water. This water flows up the Brady Thermal Fault (a normal fault striking N 19°E and dipping 70°-80° to the west) and out laterally, east and west in the fractured zones of rock paralleling the fault (see Figure 1). During the production test of Brady 8 (B-8), pressure interference was manifested and measured in the form of dropping water levels in the wells B-1, B-3 and B-4. The pressure response in B-1 and B-4 (B-3 was plugged with calcite and thus had delayed pressure response) was immediately reflective of changes in the production rate of B-8. When the production test was terminated, water levels rose in a logarithmic manner to their original levels. These results, coupled with the geological evidence, lead to the conclusion that Brady's highly fractured and highly connected reservoir would supply sufficiently hot water to the GFP plant for its expected 15-year life.

As shown in Figure 1 all of the wells in the field save B-8 and Earth Energy-1 (EE-1) are very shallow with correspondingly shallow casing points. EE-1 did not have a measurable pressure response, however, during the production tests and testing of B-8. Additionally, EE-1 is the deepest well available to GFP. The well's condition is presented schematically in Figure 2. EE-1 has proven production from slots at depth (4820 ft. - 5050 ft.) of 120 gpm and suspected production from perforations at 3600 ft. - 3700 ft. and 3200 ft. - 3300 ft. It has a casing program which, given a good primary cement job, might be satisfactory for use as an injector. Since production from B-8 was determined to be from a region around 700 - 800 ft., then injection in EE-1 at the +3200 ft. plus zones was thought to be sufficiently separated from production in B-8 to prevent temperature breakthrough. None of the other wells available to GFP possessed any of these characteristics; on the contrary, the other wells' shallow casing programs and direct communication with the producer rendered them unsuitable as injectors. Thus EE-1 was selected as the most suitable possible injector.

DESIGN OF INJECTION TEST

A short term injection test was designed to answer the following objectives in a time constrained and cost effective manner:

1. Determine the injectivity of EE-1.

2. Determine the zones in the well which accept water during injection.

3. Determine as quantitatively as possible the relative ability of each of these zones to accept water.

4. Use the data gained above to ascertain the suitability of EE-1 for GFP on a production basis.

To accomplish these objectives in a expeditious manner it was decided to store fresh water on site, inject water in the well at an intially varying rates, log the well while injecting at a constant rate, and then re-test the injection of injectivity of the well to determine whether any changes of the well's injectivity had occurred over time. Neighboring well's water levels were to be measured throughout the testing of EE-1.

PERFORMANCE OF THE INJECTION TEST

The performance of the injection test consisted of the following actions:

(a) Static temperature surveys.

Static temperature surveys were run with Kuster type wireline tools as well as single-conductor surface reading instruments. Three surveys were studied and are shown in Figure 3. The 3 surveys showed very large differences in nominal temperatures but displayed the same relative chagnes in temperature. The presence of the shallow acquifer at 700 ft. was clearly shown as well as a possible additional water source at 1900 ft. Interflow between the perforations at 1900 ft. and 3250 ft. was also clearly shown.

(b) Wellhead selection and installation.

Because of the field's sub-hydrostatic pressure, wells in the Bradys' Field did not have valve-operated wellheads. Due to safety considerations, a Series 309 9-5/8-in. by 8-in. casing head was selected for and welded onto EE-1. It was then felt that the wells were equipped to safely sustain any unforeseen pressure buildup during the injection test.

(c) Pre-injection surveys.

Differential temperature and spinner surveys were run in EE-1 previous to the injection of any water. The differential temperature portion of the log was not diagnostic. The spinner survey disclosed that a small amount of an interflow was occurring in EE-1 between the perforations of around 1900 ft. and those of around 3200 ft.

(d) Injectivity tests.

Water was next injected in EE-1 while pressure at the wellhead was measured. The results are plotted in Figure 4. The well accepted water on a vacuum up to 300 gpm, at which point pressure rose at a rate of 0.4 psi/gpm. Maximum wellhead pressure encountered was 160 psig at 700 gpm. Testing beyond this point did not occur because strong pressure response in B-8, the producer, was noted at 700 gpm.

(e) <u>Injection surveys</u>.

Spinner and gamma surveys were run in EE-1 during a constant injection rate of 150 gpm. After the response in B-8 had been noted, it was deemed very important to find out where the water was exiting EE-1. It was determined from temperature surveys that all injected water left the well through regions above 3290 ft. Through spinner and gamma surveys, it was determined that water was leaving at the lap of the 9-5/8-in. and 7-in. casings at 371 ft. - 493 ft. as well as at the perforations at 1920 ft.

(f) <u>Survey at varied flow rates</u>.

Spinner and gamma surveys were taken at various flow rates to determine what percentage of the flow was leaving at the 3 regions of interest. It was determined that the upper regions above 1940 ft. accepted proportionately more water as the flow rate increased. As shown in Figure 5, the percentage of flow existing above 1940 ft. was about 40% at 100 gpm and rose to almost 80% at 700 gpm. Of that proportions accepted about equal amounts at 150 gpm, but at higher rates the liner lap accepted proportionately more.

(g) <u>Interference effects</u>.

Water levels at wells B-1, B-3, B-4 and B-8 were taken during the injection test. B-3 and B-4 sustained no measurable interference affects. B-1 displayed a reaction to the start of injection but not to differences in flow rates over such a short period of time. B-8 showed tremendous response when flow rates approached 600 gpm. In fact, the well commenced to flow when injection rates in EE-1 rose above 600 gpm. Figures 6 and 7 displayed respectively the water levels of the 4 wells during the test and the water level of B-8 in relation to the injection rates.

EE-1'S SUITABILITY AS AN INJECTOR

From the field work, it was apparent that EE-1 in its present condition did not accept the design injection rate of 700 gpm without pressure interference at B-8, the producer. Water injected down EE-1 leaves the wellbore through 3 exit points:

1. the 9-5/8-in. - 7-in. lap at 371 ft.

2. the perforations at 1880 ft. - 1940 ft.

3. the perforations at 3200 ft. - 3300 ft.

It appears that the upper regions are causing the interference with B-8. Accordingly, the injecting of water in zones above 2000 ft. must be avoided if EE-1 is to be used as an injector. Referring to the schematic of EE-1 in Figure 2, this could be accomplished by running smaller pipe into the 4½-in. liner below 2000 ft. and cementing back to surface. The tremendous pumping penalty imposed prevents this course of action from being a viable option. Alternatively, one could consider pulling the 4½-in. liner, reaming out a larger hole below the 7-in., and running a somewhat larger casing through the 7-in. down to the preferred depth. This operation poses a high drilling risk as well as a rather severe pumping penalty, and was thus also deemed a less-than-preferable action.

Two other alternatives appeared available to GFP. A temporary surface disposal system could be cleared with the applicable Nevada State agencies. This system could be employed until GFP determined the ultimate course of action to take - whether to drill a new injection well, or attempt to rework EE-1 in the latter manner detailed above. It was recommended to GFP to pursue all alternatives with the ultimate objective of disposing the water underground.

FIGURE 1

A CARTOON DEPICTING
THE DYNAMICS OF THE
BRADY HOT SPRINGS RESERVOIR

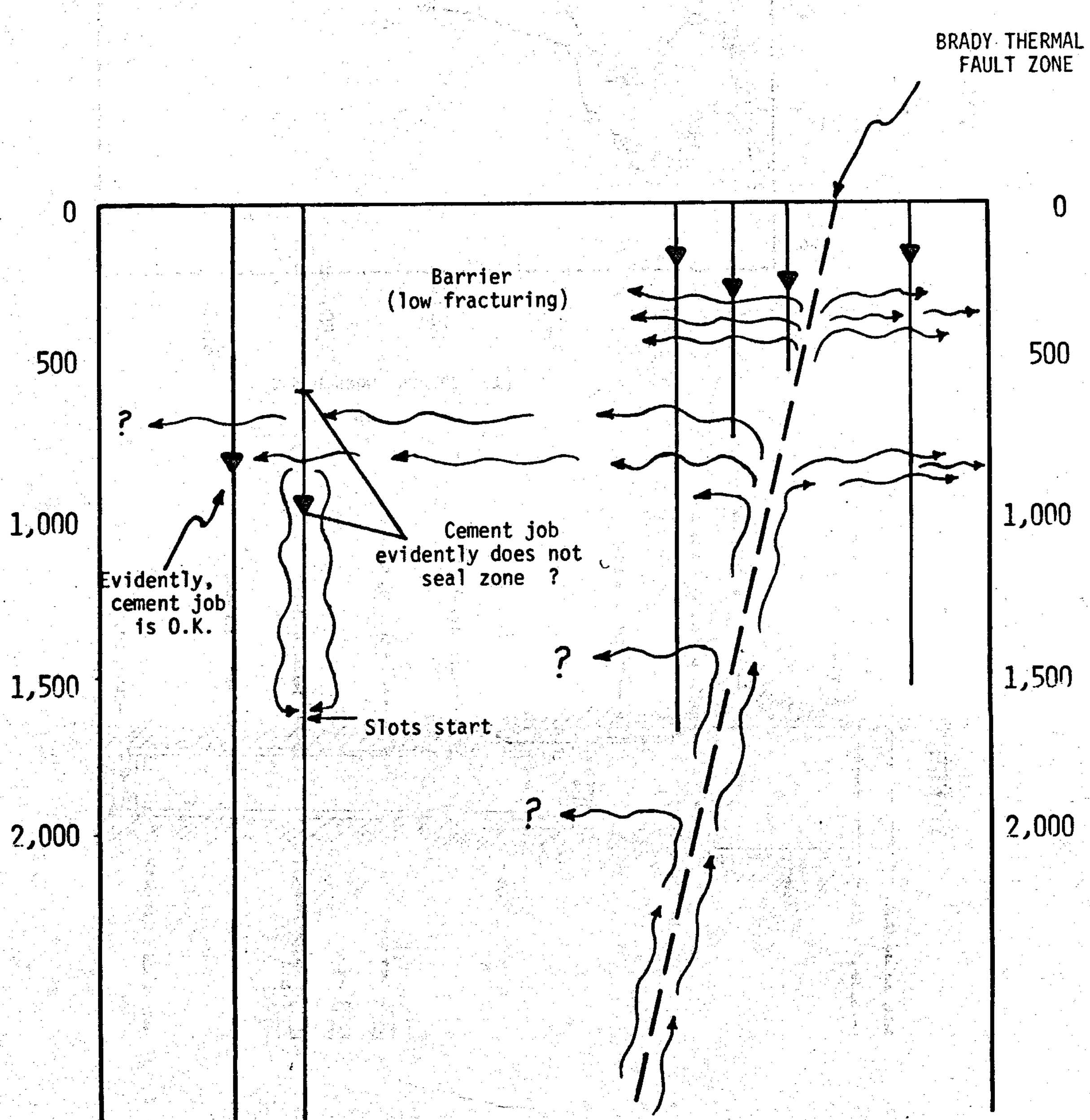

FIGURE 2

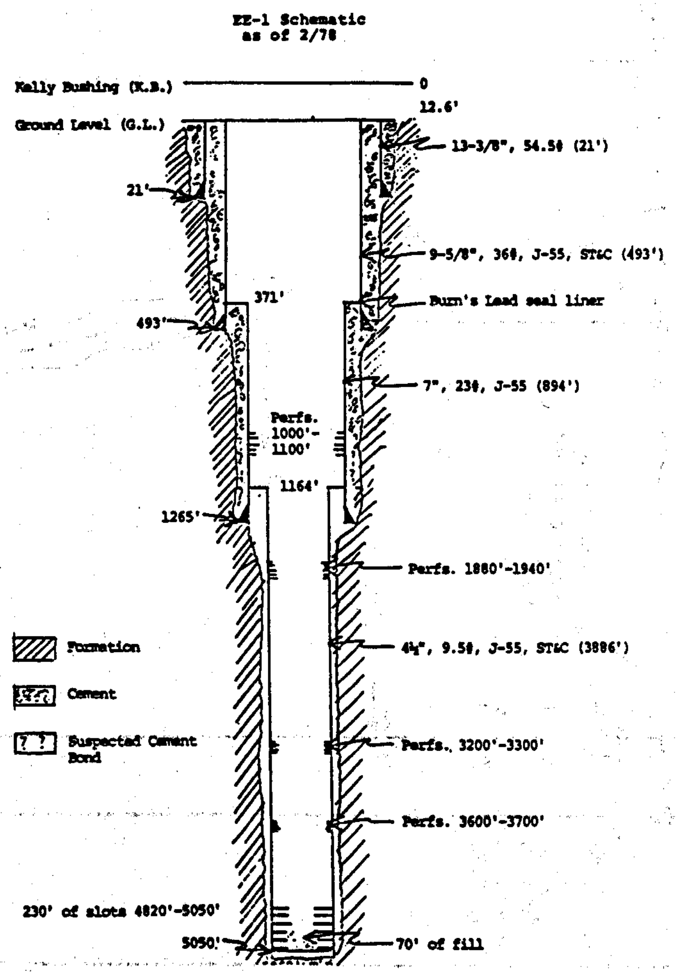

FIGURE 3

STATIC TEMPERATURE SURVEYS

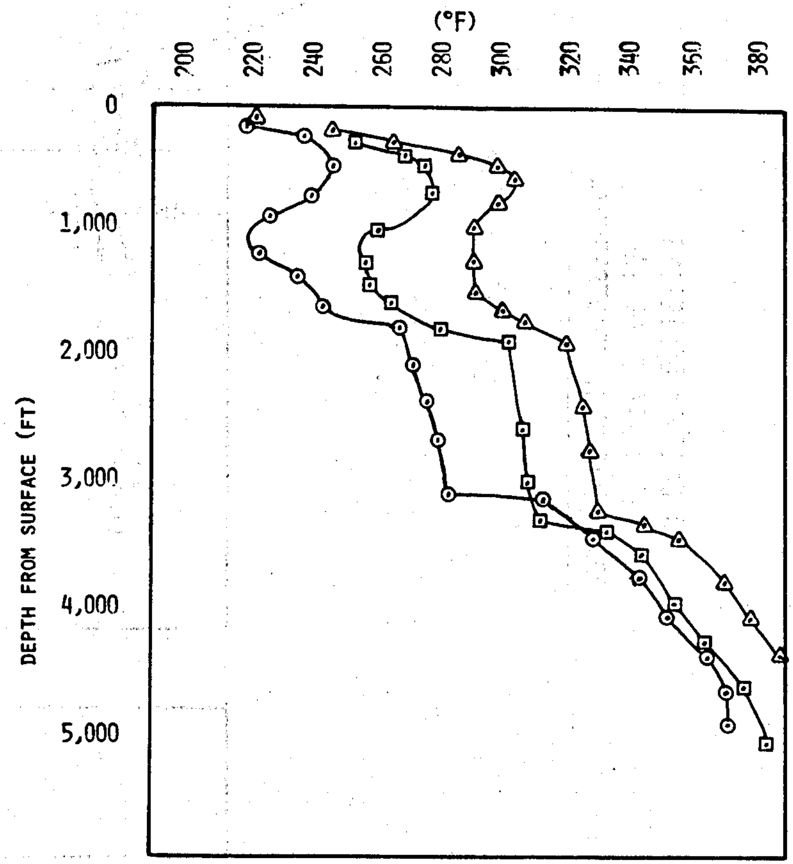

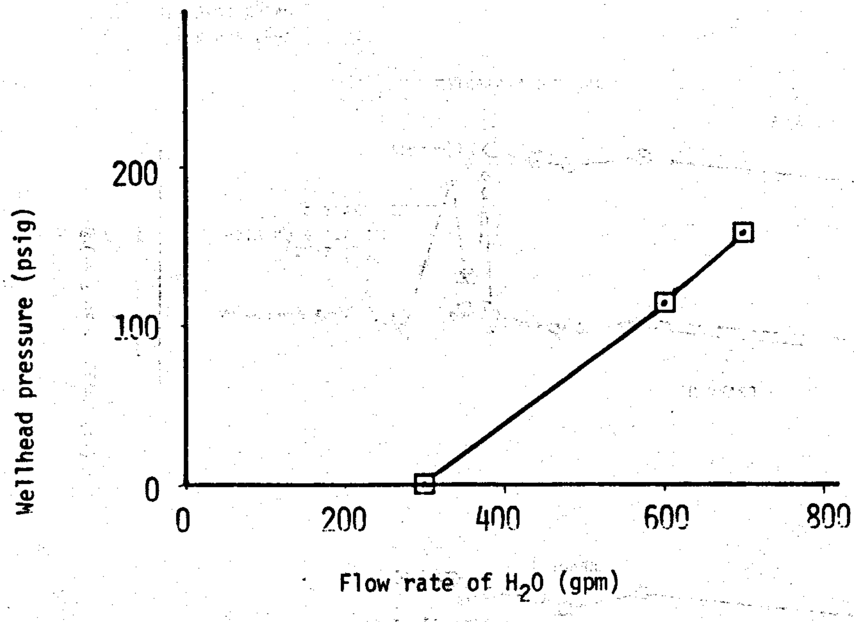

EE-1's injectivity curve--the graph of wellhead pressure (psig) versus flow rate (gpm)

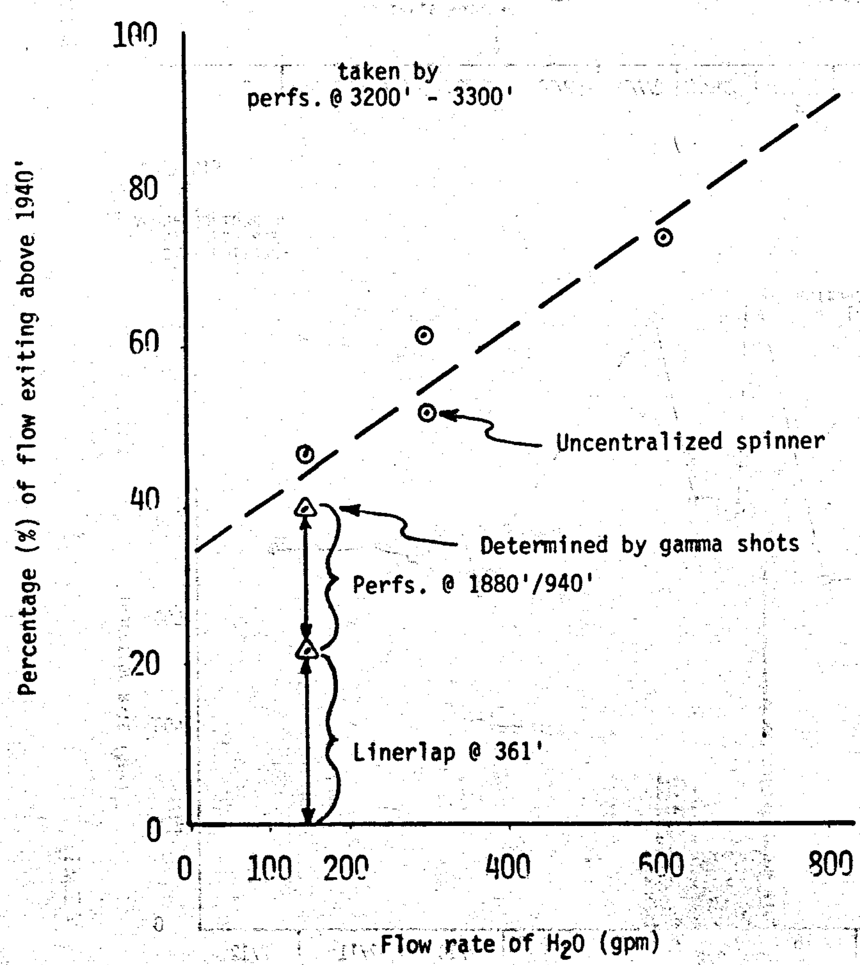

The graph of the % of flow rate exiting above 1940' in EE-1 versus flow rate (gpm)

FIGURE 6

WATER LEVEL IN B-3, B-8
B-4, AND B-1

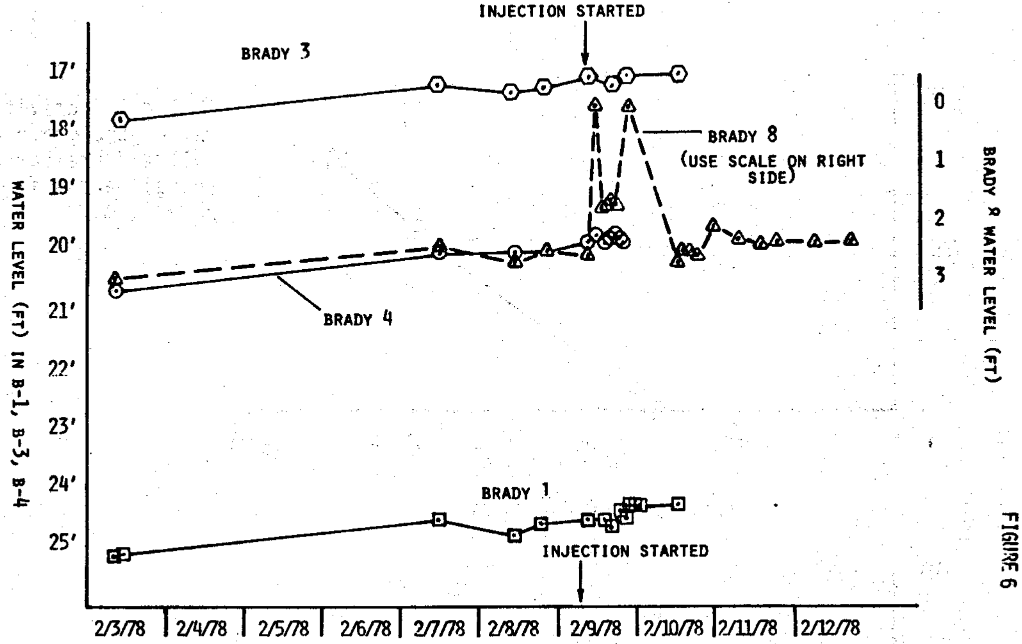

FIGURE 6

FIGURE 7

THE PLOT OF BRADY 8'S
WATER LEVEL AND
INJECTION RATE

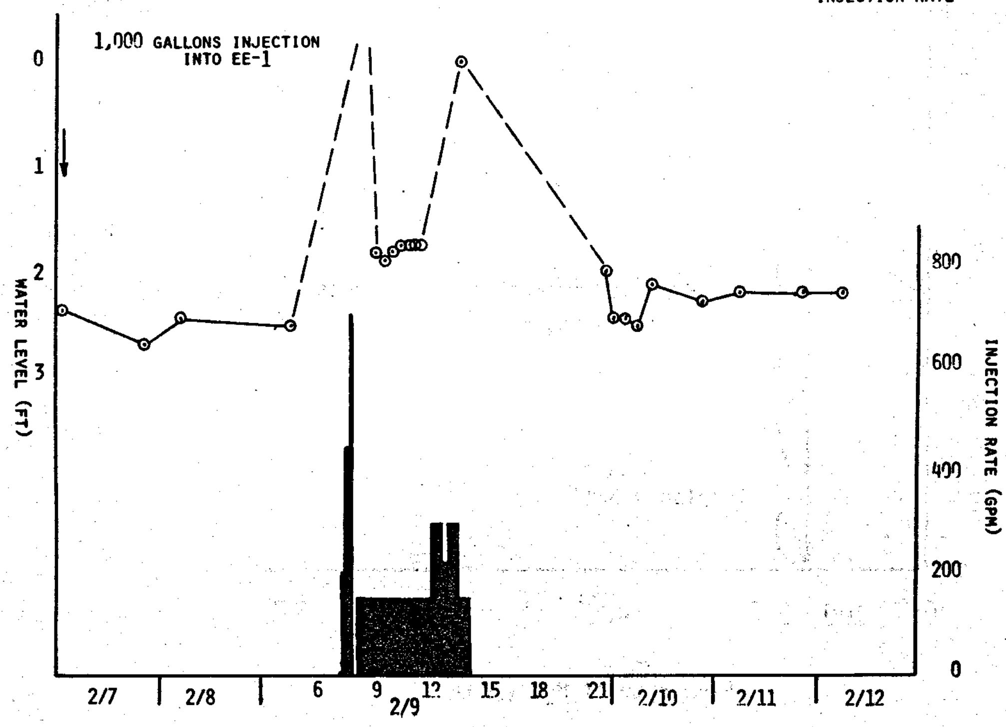

FIGURE 7

EXTRACTION-REINJECTION AT AHUACHAPAN GEOTHERMAL FIELD

Gustavo Cuellar, Mario Choussy and David Escobar
Comisión Ejecutiva Hidroeléctrica del Río Lempa
Superintendencia de Recursos Geotérmicos
San Salvador - El Salvador

ABSTRACT

A review of the geology and thermodynamics of the Ahuachapan Geothermal Field is given. The intensive mass extraction of the steam-water mixture started after the first unit began operating. The total mass extraction until August 1978 reached 50,478 kilotons. A continuous program of measurements was made in order to obtain a complete history of pressures, temperatures, and chemistry changes of the reservoir fluids as a result of the controlled extraction-reinjection system.

INTRODUCTION

In order to increase the production of electric energy in El Salvador, a program of geothermal studies was started in 1965. It allowed the development of the Ahuachapan Geothermal Field.

The first result of such investigations was the installation of two 30MW medium pressure units.

The first unit was commissioned in May 1975 and the second in June 1976. They provided during 1977 32.3% of the total electric energy generated in the country, proving their reliability, and increasing interest in the use of the underground steam as a source of energy production.

At the present time, the third unit, of 35MW capacity, is being installed and is expected to be in operation in January 1980.

New geothermal areas are presently under investigation where recent drillings have proved the existence of temperatures up to 300°C and extensive fractured zones.

In this paper is presented a series of data from the Ahuachapan Geothermal Field in production stage, which will give an opportunity for better understanding of the reservoir characteristics after a tracers study and the development of a mathematical model are implemented.

GEOLOGICAL SETTING

The general geological structure of El Salvador has been interpreted as a major structural trough which cuts approximately east-west across the southern part of the country. This trough has since been largely filled by Quaternary cones that compose the main volcanic chain of the country. Structurally the country can thus be divided into three units: a tilted block bordering the Pacific Ocean and dipping towards it, a median valley of variable width, and an uplifted northern zone composed of a number of complex fault blocks. The simple features assumed by Williams and Meyer Abich (1955), although probably true in general terms, are in fact more complex than is apparent from this model. In particular, the form of the median valley is not a simple parallel-sided rift. The uplifted southern and northern sides represent a series of blocks which have been faulted and tilted to give the present day structure.

The Ahuachapan Geothermal Field is associated with the southern flank of the central Salvadorean graben median trough, the northwestern sector of the Cerro Laguna Verde volcanic group. This group constitutes a complex extrusive structure developed during Quaternary times near the Pliocene tectonic block of Tacuba-Apaneca, the regional faults of which have controlled first the sinking of the graben and subsequently the emanation of volcanic products.

The field and its north and northwest extensions up to the Paz River, which appear to be a subelliptical basin filled by the most recent volcanic rocks, are lower to the north and northwest, reflecting the subsidence of the graben.

The geothermal field, partly defined so far by deep well drilling, is located in the southern part of the above mentioned basin.

Both the regional and the local structure are controlled by systems of faults and fractures oriented along three main directions: to an E-W system, which is approximately the trend of the main graben, belongs a series of steps faults which limit the field to the north. To the W, the field is bound by a second system of faults which strike NE. Finally, superficial hydrothermal activity is associated with the most recent system of faulting and fracturing which has a NNW trend. This youngest faulting probably has an important function in that it rendered permeable the reservoir formations of Ahuachapan Geothermal Field.

The stratigraphic sequence of the Ahuachapan area is described as follows: (see Fig. 1.)

- Laguna Verde volcanic complex: Andesitic lava flows and some pyroclastics (Holocenes). Thickness up to 200 m.

- Tuff and lava formation: Tuffs prevail in the upper part and lava intercalations in the lower part (Pleistocene). Thickness up to 500 m.

- Young agglomerate: Volcanic agglomerate with occasional lava intercalations (Pleistocene). Thickness up to 400 m. It is essentially impermeable and forms the caprock of the geothermal reservoir.

- Andesites of Ahuachapan: Lavas with pyroclastic intercalations (Plio-Pleistocene). Thickness up to 300 m. It is the reservoir producer formation: It has a typical secondary permeability caused in part by the columnar jointing related to cooling and in part by the contact surfaces of the different formations, but mainly derived from tectonic fracturing. In Fig. 2 can be seen the top of the Andesitic formation.

- Ancient Agglomerates: Agglomerates with breccia intercalations in the lower part. Thickness in excess of 400 m.

HYDROGEOLOGY

Shallow Aquifer. The shallow aquifer consists of tuffs and detritic-talus pumices covering the lavas of the Lagnua Verde complex. This is an unconfined aquifer recharged by rain water infiltration, feeding several springs on the slopes of the Laguna Verde and Laguna de Las Ninfas volcanoes, located at the contact with the underlying lavas which constitute the aquiclude of this system.

The variations in flow rate are controlled by precipitation, showing very fast response. The waters are generally of calcium carbonate type, locally sulfatic with residues below 0.5 gm/liter. This very shallow aquifer is of local interest only in the uphill area of the geothermal field.

Saturated Aquifer. The saturated aquifer consists of fractured lavas and pyroclastic deposits of the tuff and lava formation, while the young agglomerate, of low or no permeability, represents the impermeable basal stratum. Recharge takes place by direct infiltration which gives origin to a shallow free surface, tapped by several wells for domestic purposes and surfacing at several springs on the plain north of the geothermal area.

The piezometric surface in the area of the plain exhibits a concave shape which is open toward the north, having a gradient (and therefore a principal flow component) in a northern direction. The response of the piezometric level to the variations in rainfall is much slower than in the case of the shallow aquifer.

The water is of calcium-sodium carbonate type, with residues generally below 0.4 gm/liter. An exception to this rule is a group of springs, of which the most important one is the Salitre Spring, with a flow rate of 1000 liter/sec, and a temperature of 70°C. It differs in the chemistry of its water (sodium-chloride type) and its much higher residues (06-1.7 gm/liter). These differences relative to the general properties of the saturated aquifer are attributed to admixture with waters from the underlying saline aquifer which migrate along fractures.

The Saline Aquifer. The saline aquifer corresponds to the geothermal reservoir of the Ahuachapan Field and consists of a sequence of andesitic lavas (andesitic Ahuachapan formation) where the geothermal wells were drilled.

The permeability of the Ahuachapan andesites is predominantly secondary, due to fractures, which explains the circulation losses observed during drilling operations. The permeability of the aquifer is therefore extremely anisotropic and variable; however, it is logical to assume that the zones of highest transmissivity are oriented along the previously mentioned fault and fractured principal directions.

CHARACTERISTICS OF THE AHUACHAPAN WELLS

Up to this time, 29 wells have been drilled in the Ahuachapan Field with depths between 1524 m and 591 m. All the wells are located in an approximate area of 4 km^2, the zone of the production wells being only 2.0 km^2, with a minimum spacing of about 150 m. No significant interference among them has been detected.

The wells are distributed as follows: ten production wells provide steam for the first and second unit, three wells will provide steam for the third unit, two production wells are kept as stand by, four wells for reinjection purposes, and ten as exploratory wells.

A typical completion of production and reinjection wells is shown in Fig. 3 which, according to a good knowledge of the geological condition, has been standardized for the whole field.

The characteristics of the production wells are presented in Table 1, including depths and elevations of the top of Ahuachapan andesite formation. From the production characteristics it can be observed that there exists no relation between the well depth and mass discharge; however, they are associated with the elevation of the top of the formation, since the wells which go through the structural high show discharges with enthalpies corresponding very closely to the water adiabatic expansion at 230°C (initial temperature in the reservoir) and to the reservoir pressure.

It is worth pointing out that the wells with higher steam percentage, Ah-6 and Ah-26, correspond exactly to the structural high of the reservoir. Both of them show that 78% of the steam fraction is from the reservoir and 22% from the adiabatic expansion of the reservoir water. This does not apply to the well Ah-24, however, which is located in the same structural high (Fig. 2). This discrepancy is believed to be due to the sealing of only the more superficial fractures during the drilling process.

Table 1. Characteristics of the production wells.

Well	Separator pressure (kg/cm^2g)	Mass discharge rate (kg/sec)			Enthalpy (kcal/kg)	Steam rate/ total rate	Total depth (m)	Top of andesitic formation (meters above sea level)
		Total	Steam	Water				
Ah-1	5.4	85.08	12.50	72.58	235	0.15	1205	300
Ah-4	5.9	99.46	23.33	76.13	281	0.23	640	315
Ah-5	5.4	49.97	5.56	44.41	217	0.11	952	284
Ah-6	5.5	32.96	13.61	19.35	367	0.41	591	383
Ah-7	5.3	44.98	7.64	37.34	245	0.17	950	285
Ah-20	5.3	47.28	11.94	35.34	286	0.25	600	370
Ah-21	5.6	82.22	11.94	70.28	235	0.15	849	350
Ah-22	5.4	70.68	16.34	54.34	277	0.23	659.5	315
Ah-24	5.3	51.93	7.50	44.43	233	0.14	850	380
Ah-26	5.3	21.44	8.89	12.55	367	0.41	804	391
TOTAL:		586.00	119.25	466.75				

REINJECTION

1. Reinjection Program

The search for a better way to dispose of the hot saline water and to maintain the reservoir pressure at stable conditions, led to the starting of a reinjection program.

The reinjection program started in August 1975 when Ah-2 (a well for production purposes but with low permeability) was converted to reinjection by using residual water of well Ah-4 at atmospheric conditions. Under these conditions a flow of 126 ton/h had been injected into well Ah-2. In January 1976, injection tests under pressure were started between well Ah-7 as producer, and well Ah-8, being injected. Separating pressure was used as a driving force between the wells with water without any contact with the atmosphere, thus avoiding silica scaling, allowing the reinjection at higher temperatures (±160°C), and increasing the reinjection capacity. In April 1976, the system Ah-1, Ah-29 with A-29 as a reinjected well, was put in operation, and in October the system Ah-6, Ah-21 with A-17 as a reinjected well was put in operation. It is important to point out here that well Ah-17 received at the beginning waters from Ah-6 and, since it showed great absorption capacity, accepted water also from Ah-21.

2. Completion of the Reinjection Wells

The reinjection wells have, at the present time, two kinds of completion: i) the ones which were designed for production purposes and transformed lately to reinjection wells (Ah-2 and Ah-8). These wells still keep their completion, having the production casing cemented down to the top of the reservoir and the open hole to the bottom. ii) Wells with double-purpose (production-reinjection) which have the production casing cemented down to the top of the reservoir and, after, hanged casing down to the bottom of the andesitic formation.

Regarding their location with respect to the production wells, reinjection wells Ah-17 and Ah-29 (double purpose) are very close to the production wells and their lithological columns show a considerable reservoir thickness (400 m and 325 m, respectively). However, wells Ah-2 and Ah-8 are farther away from the production zone, showing a shorter reservoir thickness (105 m and 75 m, respectively).

3. Reinjection Well Capacity

The capacity of the reinjection wells is closely related to the formation's permeability and to the reinjection pressure. In Ahuachapan, three of the wells (Ah-29, Ah-17, and Ah-8) show absorption capacities greater than the actual

Table 2. Summary of the total reinjection program for Ahuachapan reinjection wells.

Well	As of (date)	Reinjection pressure (kg/cm^2g)	Mass capacity (ton/hour)	Total capacity (ton/hour)
Ah-2	Aug. 1976	atm.	130	130
Ah-8	Jan. 1976	4.9	200.4	330.4
Ah-2	Mar. 1976	6.0	114.9*	445.3
Ah-29	Apr. 1976	5.1	306.4	751.7
Ah-17	Oct. 1976	5.9	167.1	918.8
Ah-17	Dec. 1977	6.1	306.1*	1224.9

*Increment with respect to initial well reinjection capacity.

amount of reinjected fluid, whereas well Ah-2 started absorbing, at atmospheric pressure, only 126 ton/h and later, using the separation pressure of well Ah-4, increased to date to 245 ton/h. The quantities of reinjected fluids are illustrated in Table 2.

4. Reinjected and Extracted Mass

To more clearly understand reservoir behavior, we can divide the extraction in the Ahuachapan Field into two periods: the first period includes the development of the field, extending from August 1968 to July 1975; the second period includes the field production, from July 1975 up to now.

The total mass extracted and reinjected during the above periods is shown in Table 3.

As can be seen from Table 3, the reinjected mass has been, up to the present time, 29.5% of the total mass extracted and 39.9% within the production period.

5. Reinjection Control

Several questions arising from the reinjection program led to the elaboration of a program to study injection effects on the field condition. As a part of the program, measurements of temperature and pressure in the production and non-production wells were taken. Results are shown in Fig. 4, where an immediate pressure response to the variations in the reinjection-extraction can be found. However, the temperatures show slow variations and are probably masked by other kinds of changes. In order to detect small pressure changes, a continual recording pressure gauge has also been installed in well Ah-25. These data are still to be processed.

Study of the chemical monitoring in the well discharge has been very useful because the concentration in the injected water hints at its preference path. Change in permeability has been detected with Spinner equipment in the reinjection well to detect the absorption zones. As observed in Fig. 5, well Ah-2 has permeability in the zone between 200 and -250 masl and none in the bottom. Well Ah-7 absorbs all the injected water immediately after the bottom of the hanger liner. This can be interpreted as water circulation through the annulus ring going to the total lost circulation zone. In the open hole the formation has a low permeability. Well Ah-29 shows permeability through its whole free column, even though the water may flow to the annulus ring, but to a smaller extent than in well Ah-17.

6. Effects of the Reinjection-Extraction Rate

The different changes in the original conditions of the reservoir are due to the different reinjection-extraction rates operated on the field. The reservoir behavior during production has been, according to experience in other places, typical of a water-dominated field. However, the general trend depends on the reinjection rates.

In this paper, we are going to make some comments on the effects caused by the extraction-injection rate following changes of pressure, temperature, and chemistry of discharged fluids.

6-a. Pressures

Figure 6 illustrates the reservoir pressure changing as a function of the accumulative net mass extraction, showing the two periods mentioned above. At the beginning, the reservoir has a pressure (at 200 masl) close to 36 kg/cm^{2}g, which is greater than the saturation pressure at the measuring temperature (232°C); then, as a result of the extraction, the pressure reached new equilibrium values depending on the extraction rate, having a value of 35.6 kg/cm^{2}g in July 1975. During this period, strange values were detected in 1971, which are possibly due to the first injection tests. Pressure variation of only 0.4 kg/cm^{2}g in spite of the large amount of mass extraction suggests the presence of recharge.

During the production period, the pressure decreases rapidly, reaching values close to the saturation pressure; then follows a stabilization period controlled by the reinjection effects, and the developing of a steam zone in the reservoir.

Figure 4 presents in more detail the changes in pressure during the production period, showing also the different extraction-reinjection rates. The dependence of pressure on the reinjection and extraction rates and therefore on the net mass extraction can be clearly seen. With the starting of intensive production, pressure decreased but tended to stabilize once the new equilibrium state was reached as a consequence of reinjection and the development of a steam zone in the structural high of the reservoir. It seems difficult to determine which of the two effects is the dominant one.

Pressure distributions in the reservoir before and after the start of intensive extraction in

Table 3. Extracted and reinjected mass during development and production periods at Ahuachapan.

Mass	I. Development period (August 1968-July 1975)	II. Production period (July 1975-present)	Total (both periods)
Extracted (tons)	23,317,800	48,228,933	71,546,733
Reinjected (tons)	1,850,060	19,218,384	21,068,444
Net extracted (tons)	21,467,740	29,010,549	50,478,289

July 1975 are shown in Fig. 7. The pressure spreads southward where more permeability has been found. Toward the east and west, where lack of permeability limits the reservoir, the pressure response has been minimal.

6-b. Temperature

The maximum temperatures measured in the reservoir are shown in Fig. 8. Such distribution is somewhat influenced by well depth, by reinjection, and by the development of the steam zone in the structural high.

A low temperature zone is seen in the region of well Ah-6, corresponding to the structural high of the reservoir. The phenomenon has taken place in a remarkable way here, due to the pressure decrease, even though reinjection well Ah-17 is very close. It is believed that the predominant effect is due to boiling, since the temperature decreased in the zone before the operation of the reinjection well. The above distribution also shows that temperature increases (1) in the SW direction, which seems to be associated with the zone of greater recharge, and (2) in the SE direction, corresponding to a smaller permeability where the convective process of heat transfer plays a bigger role.

6-c. Chemical Indicators

1. Silica Temperature in the Reservoir

The silica temperature has been calculated from the silica concentration in the reservoir during the years 1975 and 1978.

Figure 9 shows that in 1975 the 230°C isothermal line included all the production wells, but in 1978 all of them were outside of the same isothermal line except wells Ah-7, Ah-21, and Ah-1.

Reinjection of waste water at 160°C with a high saline concentration has some chemical and thermodynamic effects. A slight water cooling in the reservoir is noticeable; on the other hand, because of the higher silica concentration of the injected water, the solubility equilibrium is established at the real reservoir temperature.

2. Chloride in the Reservoir

The isochloride lines in the reservoir are presented in Fig. 10, illustrating the preferential path taken by the injected water in wells Ah-17 and Ah-29.

The injected water in Ah-29 goes partly toward the central field, and partly eastward. If the observed cooling effect is produced by the injected water, then it can be concluded that the injection in Ah-17 affects the reservoir temperature the most, since the preferential path of the water coming from Ah-17 is toward the center of the field. In conclusion, as indicated by the increase in salinity of the discharge from the wells, the injected water in Ah-17 and Ah-29 goes partly to the center of the field.

CONCLUSIONS

The conclusions resulting from the intensive extraction can be summarized as follows:

1. The reservoir pressure decreased below the saturation pressure corresponding to the reservoir temperature. This causes the beginning of a boiling process in the formation, developing a steam zone in the structural high.
2. The temperature reaches equilibrium in response to the new pressure.
3. A decrease is observed in the total mass extraction as a consequence of the decreasing pressure; however, this does not indicate a remarkable decrease in the amount of available steam.
4. A tendency toward stabilization of pressure is observed as a result of both control of the reinjection rate and development of a steam zone.

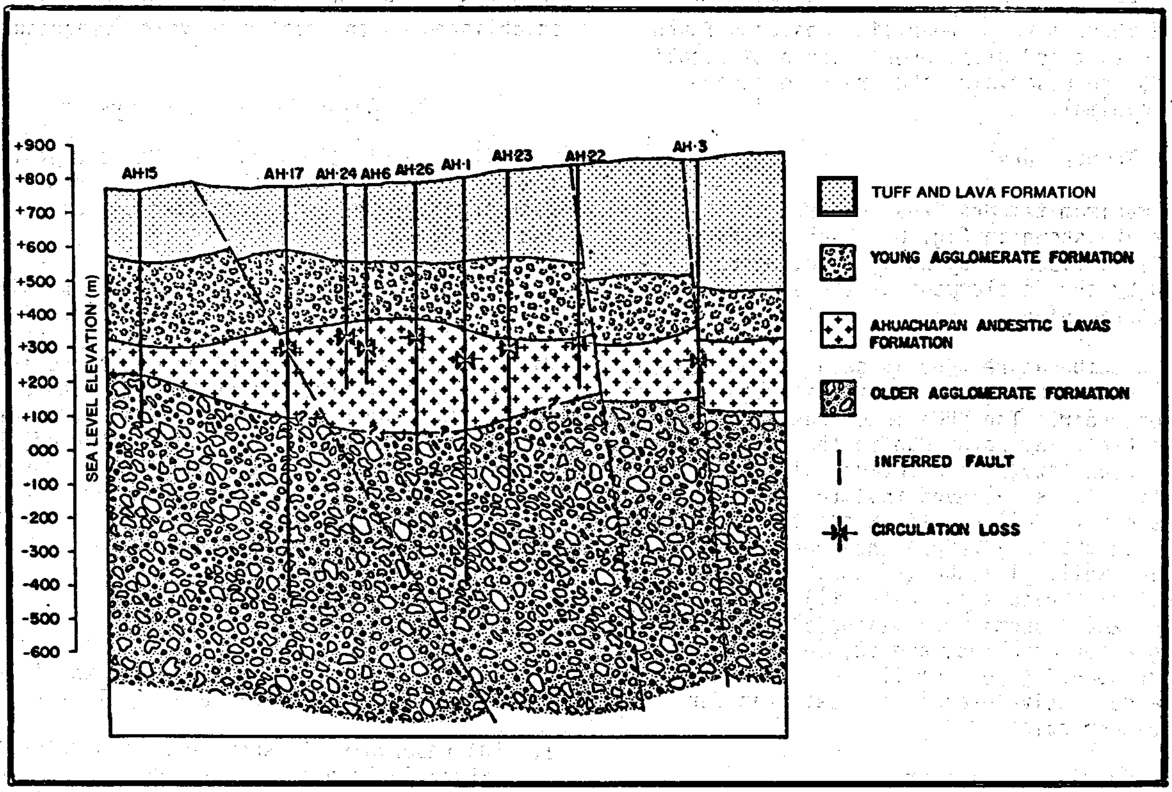

Fig. 1. Geological section of Ahuachapan geothermal field.

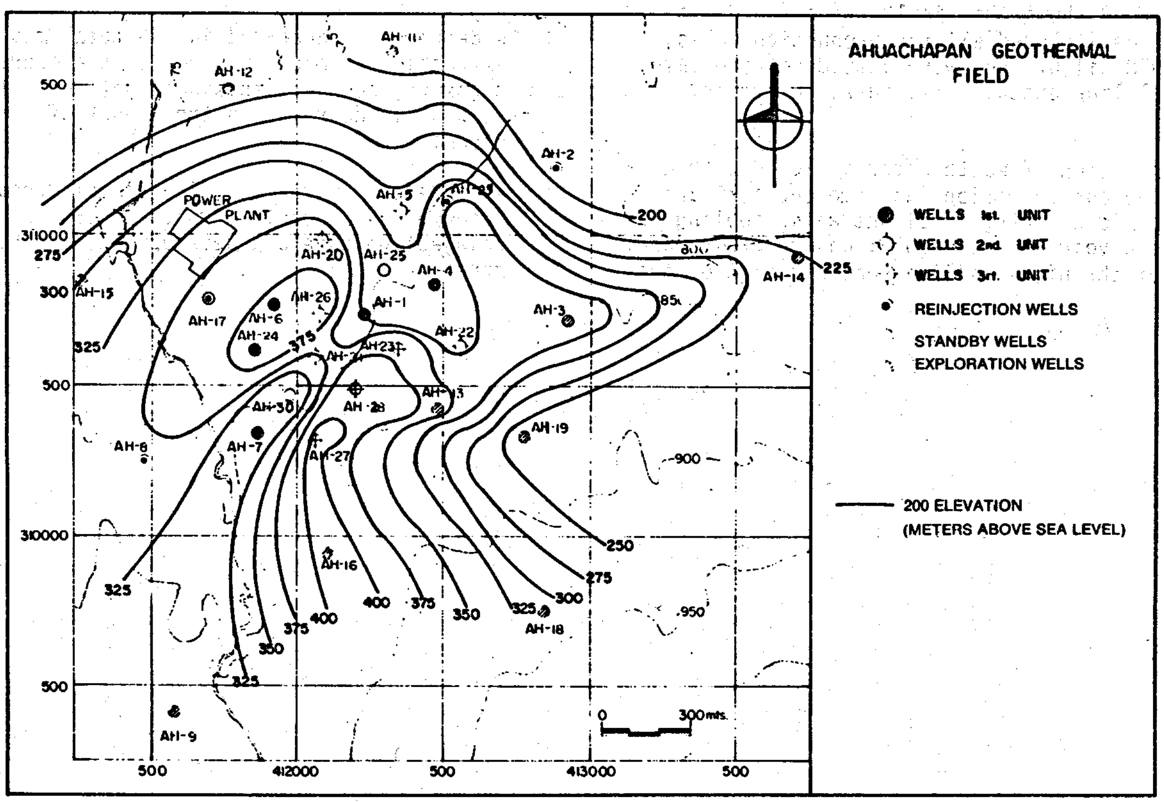

Fig. 2. Map of structure at top of Ahuachapan andesite formation.

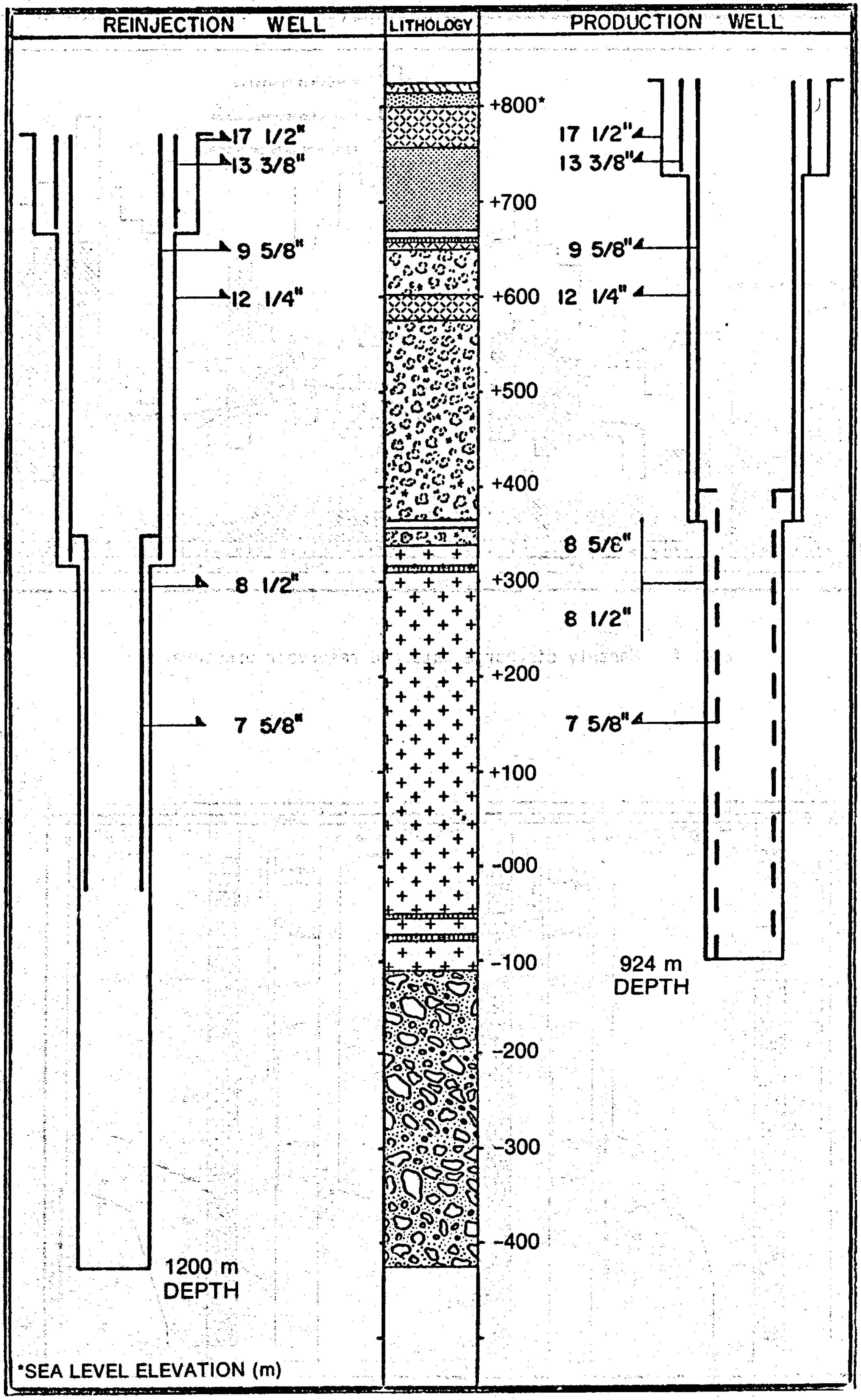

Fig. 3. Typical completion of the Ahuachapan wells.

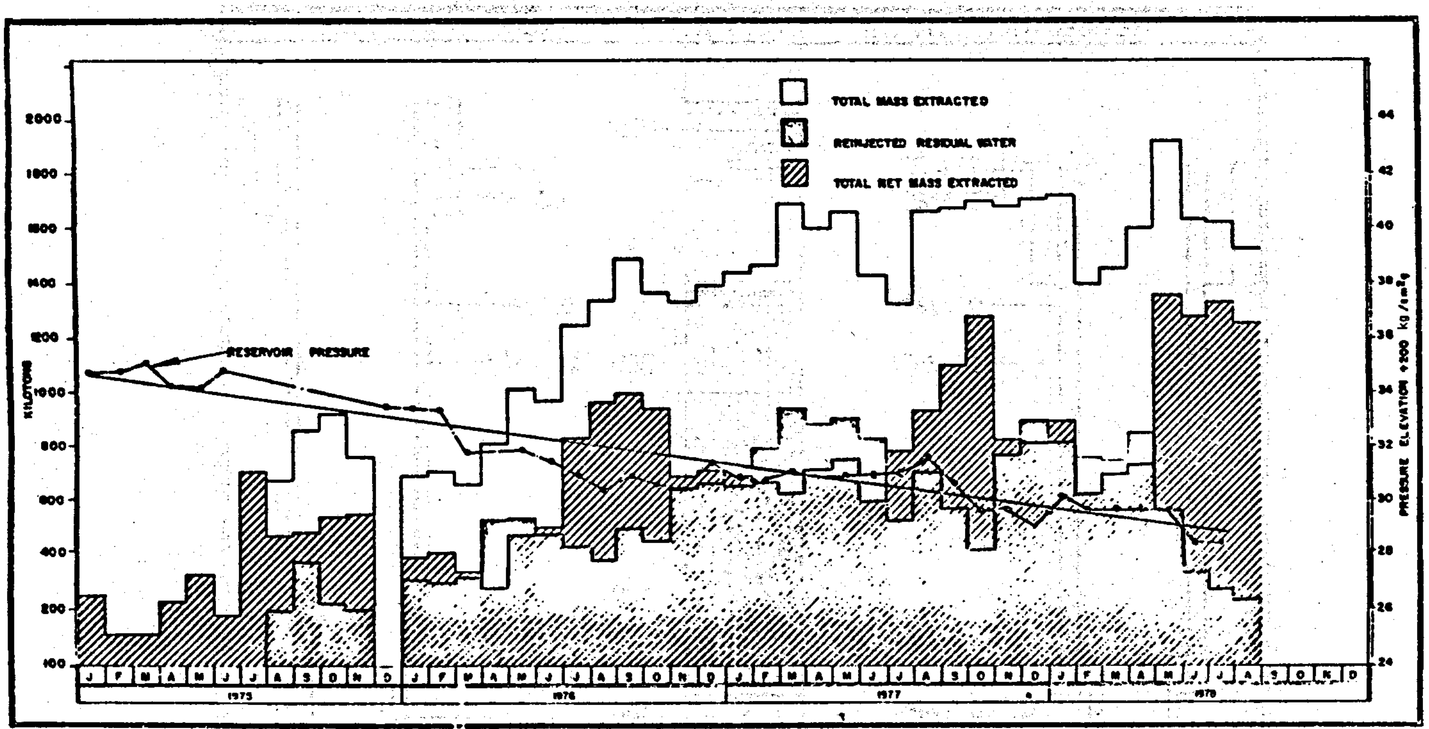

Fig. 4. Monthly discharge rate and reservoir pressure.

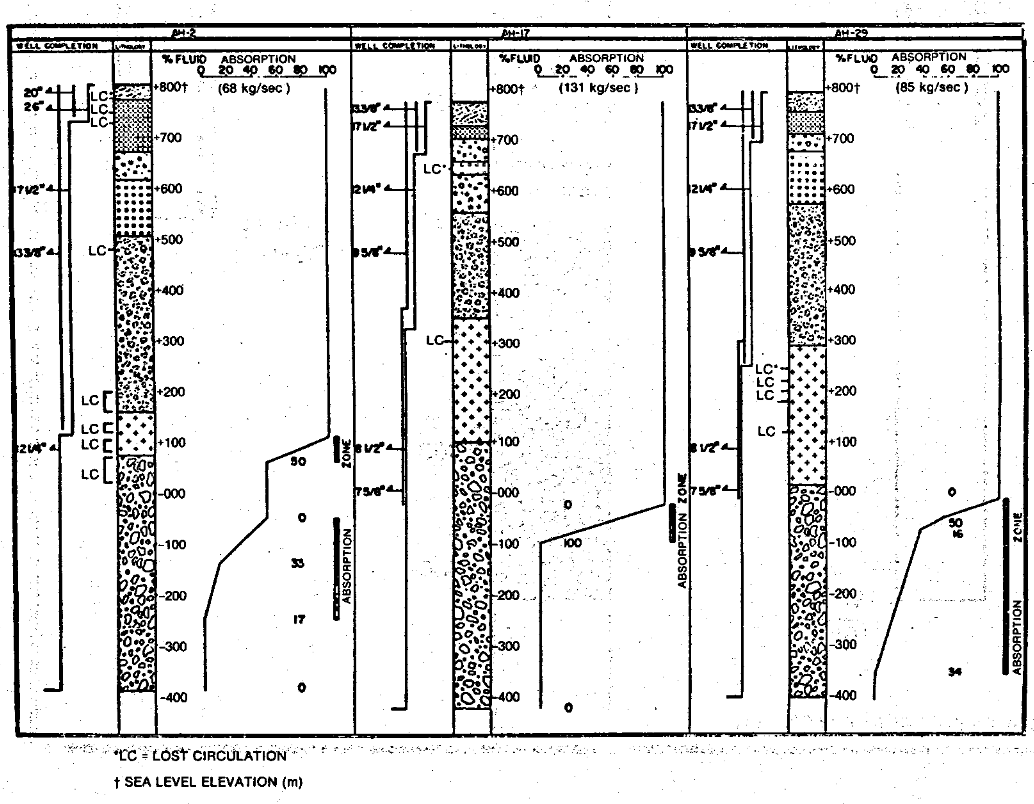

Fig. 5.

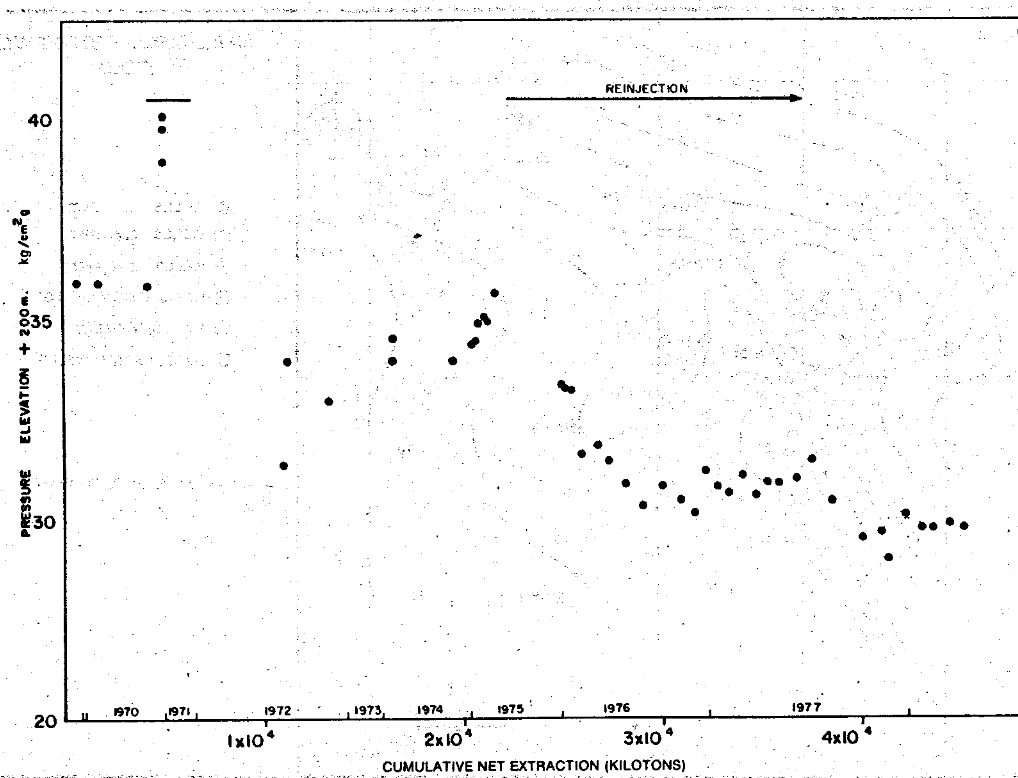

Fig. 6. Pressure trends with mass extraction.

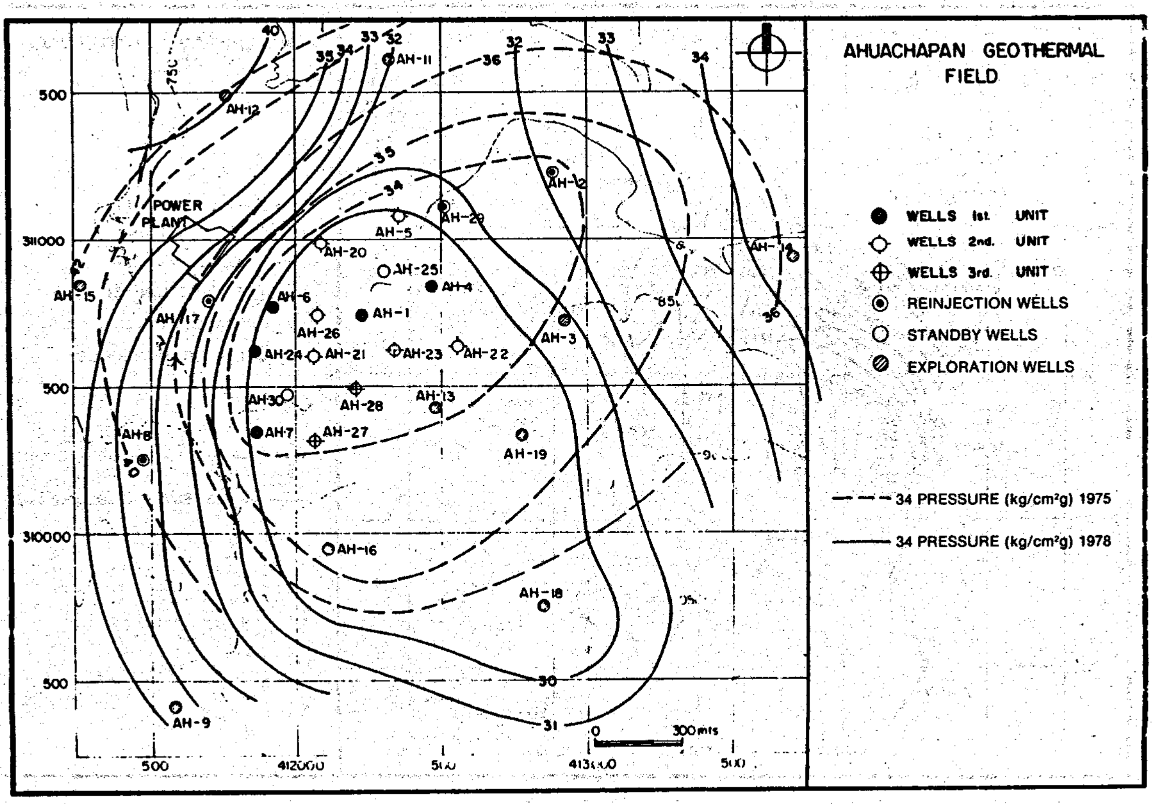

Fig. 7. Pressure distribution at 200 masl.

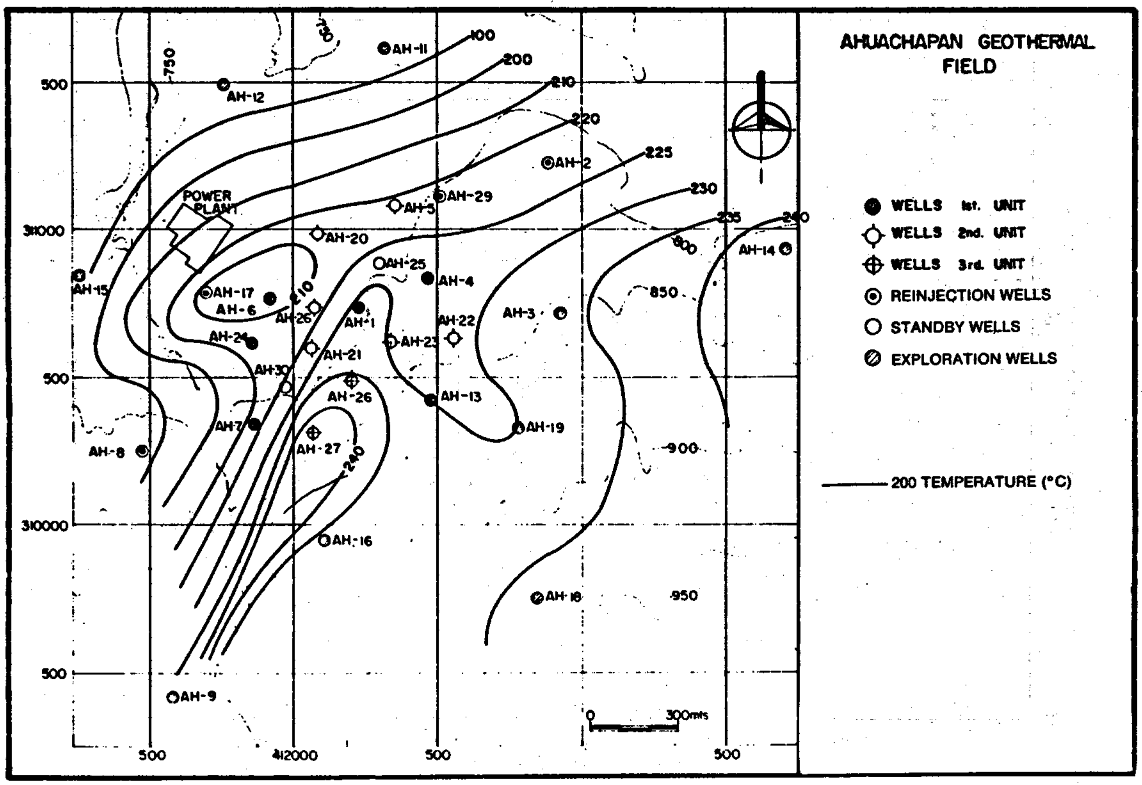

Fig. 8. Maximum temperature for geothermal wells.

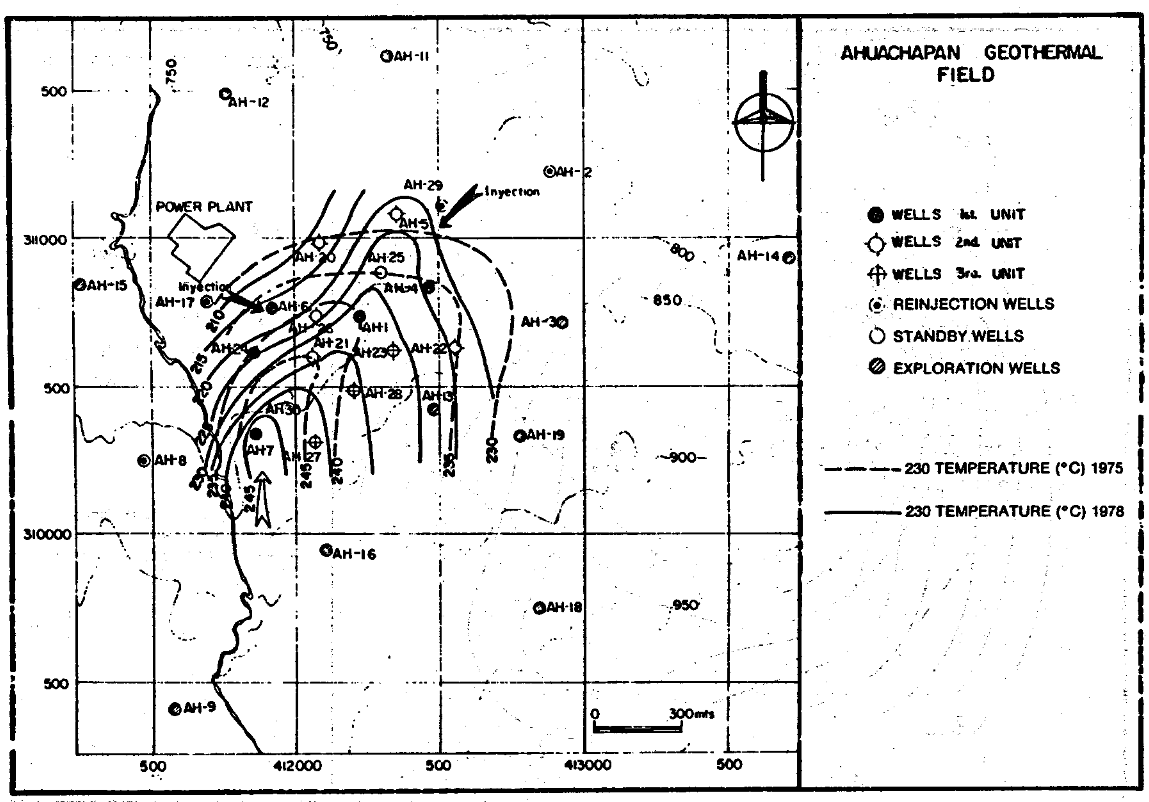

Fig. 9. Map of silica temperatures.

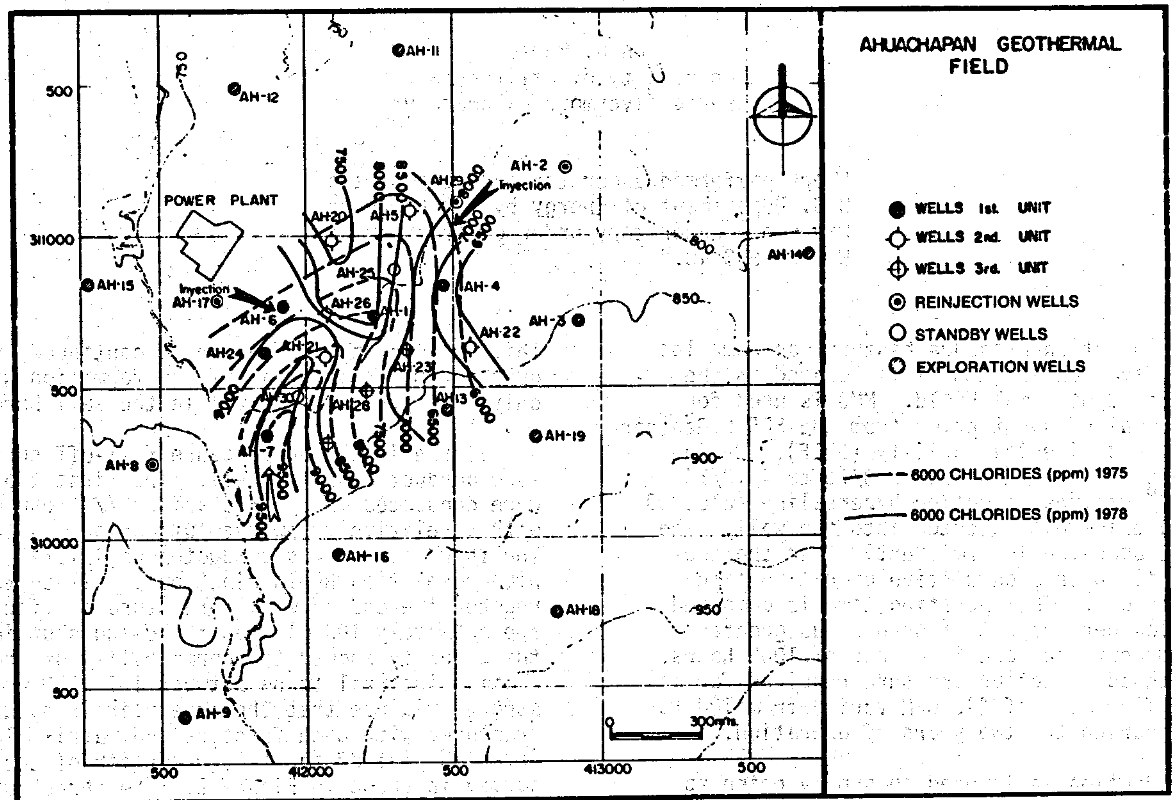

Fig. 10. Chlorides isoconcentrations.

A CASE STUDY OF A SALTON SEA GEOTHERMAL BRINE DISPOSAL WELL

By

John G. Morse
University of California
Lawrence Livermore Laboratory

"Work performed under the auspices of the U.S. Department of Energy by the Lawrence Livermore Laboratory under contract number W-7405-ENG-48."

An injection pressure history was compiled for the Magmamax #3 (MM3) well located in the Salton Sea Geothermal Field. MM3 is used for the disposal of spent brine from the SDG&E Geothermal Loop Experimental Facility (GLEF). During two years of operation from 5/3/76 to 4/13/78, 2.1 X 10^8 gallons of cooled hypersaline (210,000 ppm TDS) brine was injected into the well. The well was operated intermittently over the two-year period with a cumulative operating time of 7886 hours. The operating time is composed of 33 flow periods with four periods greater than 700 hours and one in excess of 1000 hours. The wellhead injection pressure required for an average flow rate of 443 GPM varied from 100 to 500 PSI during the two years of operation.

Production wells used to supply brine to the GLEF are Magmamax #1 (MM1) and Woolsey #1 (WW1). The Magmamax and Woolsey wells shown in Figure 1 were drilled in 1972. MM2 is a stand-by injection well and MM4 is an observation well. During the period from 5/3/76 to 4/13/78 MM1 was the primary production well contributing over 2/3 of the total brine production for the GLEF.

In 1973 and 1974 two short production tests were conducted using brine from MM1. 1.8 X 10^6 gallons and 1.6 X 10^6 gallons, respectively, were injected into MM3. During these tests, high scaling rates were observed in the surface equipment and a high suspended solids load observed in the brine. When initially operated, MM3 required no surface injection pressure for injection flows of 600 GPM. The weight of the cooled brine in the wellbore was sufficient to push the fluid into the formation.

In May of 1976, when the GLEF was put into operation, MM3 required a surface pressure of 100 PSI or greater to inject flows of 600 GPM. Brine injection during the 1973 and 1974 tests produced significant impairment of the MM3 well. The principal impairment mechanism being the plugging of the well bore injection interval by scaling and deposition of suspended solids.

MM3 is completed to a depth of 3065 ft. with a slotted liner from 2600 to 3065 ft. Temperature logs taken after shut-in show fluid to be entering the formation over a 200 ft. interval from 2600 to 2800 ft. Several spinner surveys run toward the end of the first year show fluid leaving the well bore over only a 4 ft. interval of the slotted liner indicating that most of the liner had been plugged. The injection interval had been underreamed prior to setting the slotted liner creating an annulus around the well casing. This annulus appears to permit continued injection over a 200 ft. interval of the formation with only a 4 ft. open interval in the well bore.

Three injection pressure fall-off surveys were conducted on the well. The first two surveys were conducted on 5/14/76 and 3/2/77 respectively, with a relatively low resolution logging tool. The third survey was conducted on 4/13/78 with a high resolution HP logging tool. All surveys reached the end of well bore storage effects at approximately 100 minutes following shut in. The third survey showed the permeability of the injection interval to be between 150-1000 md with strong evidence that the reservoir is naturally fractured with both fracture and matrix flow. A detailed plot of the latter portion of the third survey is shown in Figure 2. The three surveys show successively increasing well impairment or dimensionless "skin" factors of +110, +153, and +163 respectively.

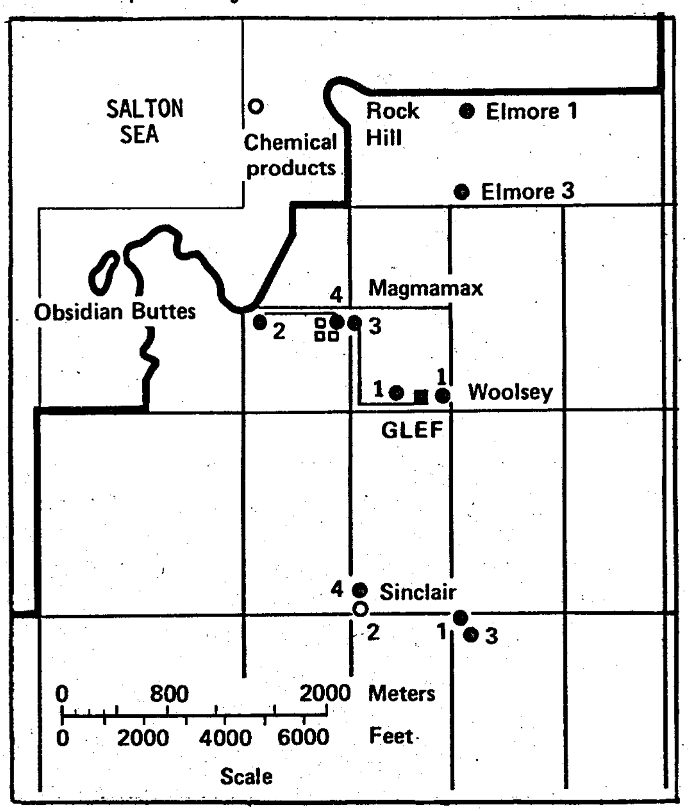

Figure 1: Geothermal Wells Used in Support of and in the Vicinity of the Magma-Narco Jointly Operated Geothermal Loop Experimental Facility (GLEF).

During the first year of operation, the spent brine was untreated prior to injection. During this period, the injection temperature was between 93-99°C and the well head injection pressure increased from 100 to 500 PSI. During the second year several workovers were conducted on the well and the brine was partially treated using settling tanks (2-3 hours residence time) prior to injection. During this period, the injection temperature was between 77-82°C with an injection pressure that ranged from 175 to 300 PSI. The net effect of the partial treatment and workovers was to reduce the rate of increase in injection pressure and to maintain the pressure within an acceptable operating range. The effect of these remedial measures is also seen in the smaller increase in measured skin damage between the second and third fall-off surveys described above.

The injection pressures shown in Figure 3 have a rather distinctive pattern during the second year of injection. When injection is first started 400 to 500 PSI is required to "breakover" the well. The injection pressure then drops to about 175-200 PSI for a 443 GPM flow rate. As injection continues the required pressure rises steeply. A detailed look at the last 1000 hour period of continuous injection shows the injection pressure to be increasing at a rate characteristic of a 10-50 md reservoir (see Figure 3). This "apparent" permeability is probably due to the severe nature of the wellbore damage and resulting reduction in effective "h" near the wellbore from 200 to 4 feet.

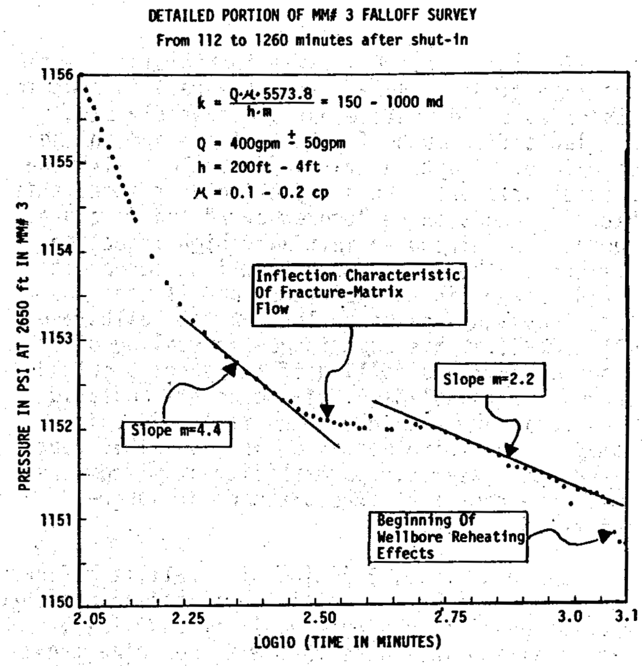

Figure 2: Details of Latter Portion of Pressure Drop-off Survey Conducted in Magmamax #3 on 4/13/78.

Figure 3: Plot of Magmamax #3 Injection Pressure from 5/3/76 to 4/13/78 for Flowrate of 443 GPM.

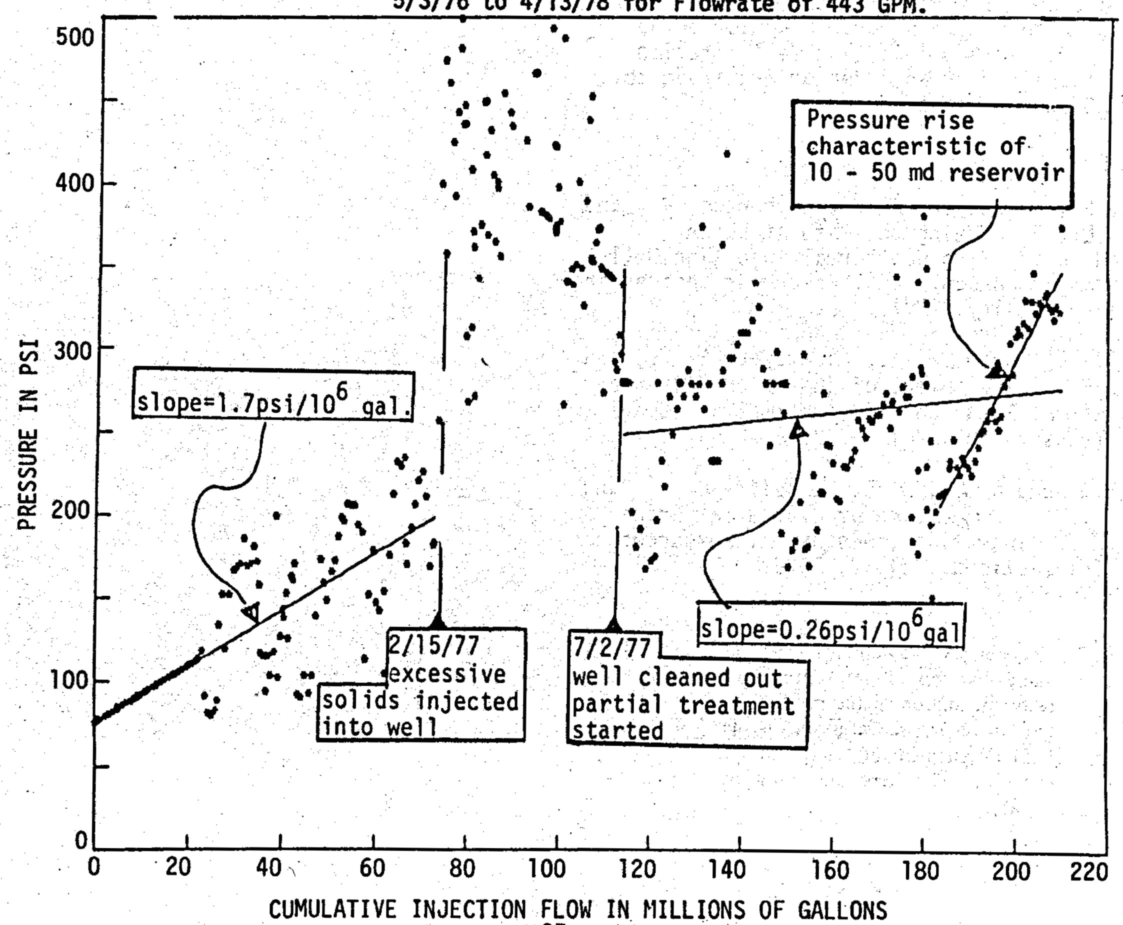

There are possibly three mechanisms affecting the injection pressure. When the well is shut-in, suspended solids settle out and possibly plug available flow paths in the wellbore and on the sand face. Fractures may tend to close with the reduced pressure. When injection is resumed this plugging needs to be "broken over" and fractures reopened requiring an initially high injection pressure. The second mechanism is a permanent "skin damage" in the well bore and at the sand face, causing a pressure loss at the wellbore of 175-200 PSI. This skin is due to scaling of the slotted liner and filling of the annulus outside the wall with solids. Well workovers and acid treatments are not able to correct this skin damage. The third mechanism is a possible zone of reduced reservoir permeability away from the well bore caused by precipitation of super-saturated silica.

In this study, lifetime of a well is defined as the operating time until the injection pressure exceeds on-site pumping capability (500 PSI). Data from MM3 indicates that with no brine treatment, well lifetime is about 150 days and with settling tanks about two years. This estimate is in close agreement with results of membrane filter tests conducted using Salton Sea brine (Owen, et al., 1977). Recently, Magma Power and Lawrence Livermore Laboratory have shown that a reaction clarifier used in conjunction with pressure filters can significantly improve injectability of Salton Sea brine (Quong, et al. and Tewhey, et al., 1978). Using this treatment process dissolved silica is reduced to below saturation and suspended solids are reduced to less than 5 ppm (1 μm in diameter) (Quong, et al., 1978). With this type of pre-injection brine processing Salton Sea injection well lifetime could be increased by an order of magnitude to between 20 and 30 years.

References

Owen, L. B., Kasameyer, P. W., Netherton, R., and Thorson, L.,"Predicting the Rate at Which Suspended Solids Plug Geothermal Injection Wells", Third Workshop on Geothermal Reservoir Engineering, Stanford University, 1977.

Tewhey, J. D., Chan, M. A., Kasameyer, P. W., and Owen, L. B., "Development of Injection Criteria for Geothermal Resources", Geothermal Resources Council Transactions, Vol. 2, 1978.

Quong, R., Schoepflin, N. D., Tardiff, G. E., and McLain, F. R., "Processing of Geothermal Brine Effluents for Injection", Geothermal Resources Council Transactions, Vol. 2, 1978.

A COST-EFFECTIVE TREATMENT SYSTEM FOR THE STABILIZATION OF SPENT GEOTHERMAL BRINES

Robert H. Van Note
Technical Consultant
Envirotech Corporation
San Mateo, California

John L. Featherstone
Manager, Technical Services
Imperial Magma Company
El Centro, California

Bernard S. Pawlowski
Sales Engineer
Envirotech Corporation
Garden Grove, California

ABSTRACT

In view of the rising costs for fossil fuel and the realization that such fuels are exhaustible, increasing attention has been focused on the earth's heat as a source of energy. It has been estimated that geothermal resources in the United States alone could produce 140,000 megawatts of power over a life expectancy of 30 years. This is the equivalent of 140 nuclear generating units. However, there are unsolved problems associated with utilizing geothermal brines to produce energy. Recent test work conducted at the Imperial Valley, California, provides a solution to one of these major problems.

A treatment system has been developed in which spent geothermal brines from a flash-tank heat-extraction plant are stabilized to permit reinjection of the treated brine while maintaining the integrity of the wells over an extended period. This treatment system is both cost-effective and environmentally sound. It incorporates the following unit process operations:

- Reconstituting the minerals which were dissolved from the geothermal strata formations in a Reactor-Clarifier by solids contact precipitation reactions.
- Polishing of the clarifier effluent in a gravity dual-media filter.
- Thickening and storage of sludge produced in the Reactor-Clarifier.
- Dewatering of the sludge to an optimum cake moisture suitable for handling and land disposal.

INTRODUCTION

A project was initiated in July 1975, at the Salton Sea Known Geothermal Resource Area in Imperial Valley, California, to demonstrate the viability of converting the underlying geothermal brines to energy. The project includes four wells drilled by Imperial Magma. Two of the wells, Magmamax #1 and Woolsey #1, are production wells; the other two, Magmamax #2 and Magmamax #3, are injection wells. Brine from Magmamax #1 now feeds a four-stage flash heat-extraction plant at the Geothermal Loop Experimental Facility, operated by the San Diego Gas & Electric Company and the Department of Energy. Spent brine from the flash system is transported by pipeline approximately 5,000 feet to Magmamax #3 well, and injected back into the formation.

The spent brine at the point of injection is supersaturated with respect to heavy metals and silica (Table 1), whose precipitation, along with plugging of the strata with discrete suspended solids in the brine, has adversely affected the integrity of the injection well. The viability of the complete project is in jeopardy unless cost-effective methods can be devised to stabilize the spent brine before injection.

Table 1. Chemical analysis of spent geothermal brine treated in pilot plant reactor-clarifier.

Constituent	Concentration - ppm
Sodium	53,276
Potassium	10,259
Calcium	22,414
Chloride	134,483
Iron	272
Manganese	685
Zinc	207
Lead	53
Copper	>1
Barium	129
Silicon as SiO_2	293
Magnesium	177
Total Dissolved Solids	228,448
pH	5.6
Temperature range	180°F-200°F 82°C- 93°C

In December 1977, personnel of Imperial Magma and Envirotech Corporation met to discuss methods of treating the spent brine to produce a non-scaling liquid suitable for well injection. At that time, it was conceived that auto-precipitation of minerals in the spent brine could be achieved in a solids contact clarifier, producing an effluent of stable saturated levels of silica and heavy metals.

Accordingly, a pilot plant Reactor-Clarifier, furnished by Envirotech Corporation to Imperial Magma, was installed adjacent to Magmamax #3 injection well and operated continuously 24 hours, per day, 7 days per week from February 28, 1978 to April 12, 1978, constituting the first phase of test work.

REACTOR-CLARIFIER

The fundamental component of the spent geothermal brine treatment system is the Envirotech Reactor-Clarifier, which is a tank of 8'0" diameter x 10'6" sidewater depth. All external surfaces are insulated to minimize heat loss of the spent brine. Area of the clarification zone is 37.7 square feet. The unit operates on the principle of solids-contact clarification. Large volumes of sludge (10 to 15 times the volume of feed) are recirculated internally through a draft tube/impeller arrangement to a reaction well. Previously precipitated sludge recirculated in this manner comes in intimate contact with the feedstream in the reaction well, providing seed nuclei on which dissolved solids in the feedstream precipitate under controlled conditions of temperature, reaction time, and solids concentration.

The resultant liquid/solid mixture flows from the reaction well into the clarification compartment, where liquid and solids are separated by gravity. Treated liquid overflows into collection launders at the upper surface of the unit. Rake arms move the settled sludge to a thickening cone at the bottom center of the tank, where the thickened sludge is discharged by gravity or pumps.

The results of this test work have led to a contract for a 55'0"-diameter Envirotech Reactor-Clarifier having 2,375 feet of total surface area, able to treat the total flow of spent brine from a 10-MW, two-stage, flash heat-extraction demonstration plant.

DESIGN EXPERIMENT

The first-stage test program was designed to develop a viable and cost-effective system for treating spent geothermal brine and for handling and disposing of sludges produced in the treatment.

The objectives of the design experiment were to:

- Test the original concept of auto-precipitation of minerals in the spent brine.
- Determine design criteria of the Reactor-Clarifier for sizing on a commercial scale, including:
  - Upflow rate
  - Reaction-well retention time
  - Solids concentration in reaction well.
- Measure the silica and turbidity concentrations of the effluent from various designs of Reactor-Clarifiers.
- Measure the quantities of solids precipitated in and discharged from the Reactor-Clarifier.
- Determine the thickening and dewatering characteristics of sludge produced, and the best dewatering equipment to use.
- Correlate all data collected to:
  - Determine design criteria for the Reactor-Clarifier that would most efficiently produce stable saturated levels of silica in the effluent.
  - Establish criteria for polishing the Reactor-Clarifier effluent.
  - Determine sludge handling and disposal requirements.
  - Estimate order of magnitude costs for spent-brine treatment and sludge handling and disposal for a 55 MW geothermal energy plant.

PILOT PLANT TEST RESULTS

Summary

Average test data from the pilot plant, presented in Fig. 1, are summarized for optimum design criteria as follows:

- No chemicals are required in the treatment of spent geothermal brines.
- Upflow Reactor-Clarifier Rate = 0.72 GPM/ft^2.
- Solids Concentration in Reaction Well = 2.5%.
- Reaction Time in Reaction Well = 17 minutes.
- Effluent Quality at Design Criteria
  - Silica - 172 ppm
  - Turbidity - 15 NTU (44 ppm s.s.)
- Sludge Produced:
  - 1.7 lb/day per GPM
- Sludge Characteristics:
  - From Reactor-Clarifiers : 4.5% solids
  - From Thickener : 10% solids
  - From Filter Press : 65% solids

Details of these summary results follow.

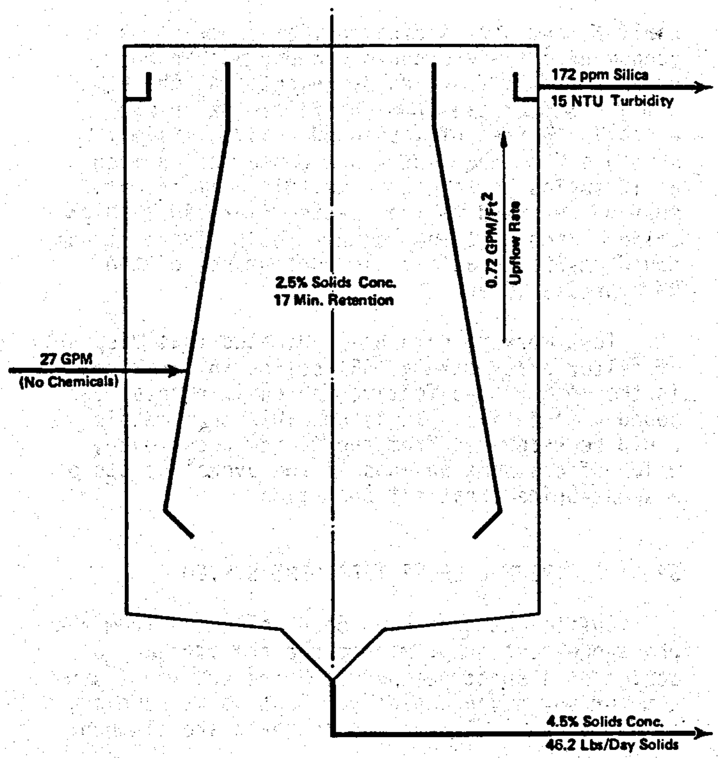

Fig. 1. Summary of pilot plant results.

Brine Treatment

Test results indicate that the quantity of silica remaining in solution in the Reactor-Clarifier effluent is a function of the insoluble solids concentration held in the reaction well. As shown in Fig. 2, a stable solubility level of 172 ppm SiO_2 is achieved when the solids concentration in the reaction well approaches 2.5% solids by weight. Further increases above the design concentration range do not markedly improve silica removal.

The capacity of a Reactor-Clarifier is dependent upon the settling rates of precipitated solids in the unit. It cannot be operated at an upflow rate greater than the settling rate of the precipitated solids; otherwise, clarification would not occur. In accordance with the Kynch theory, solids in hindered settling exhibit settling velocities inversely proportional to the solids concentration in the zone through which they settle. This is verified in Fig. 2. Upflow rates as high as 1.33 GPM/ft^2 can be maintained in the Reactor-Clarifier when relatively low solids concentrations in the reaction well are held at approximately 1.2% solids by weight. As these concentrations are increased, upflow rates must be reduced accordingly; down, for example, to a measured low of 0.62 GPM/ft^2 at a solids concentration of 2.63%.

In achieving a cost-effective process, there exists a compromise between the continuous production of stable saturated effluent from the Reactor-Clarifier and the maximum permissible upflow rate in the unit. Test data show that an optimum solids concentration of 2.5% by weight can be maintained in the reaction well while permitting a maximum design upflow rate of 0.72 GPM/ft^2 to produce the desired stable saturated effluent of 172 ppm SiO_2.

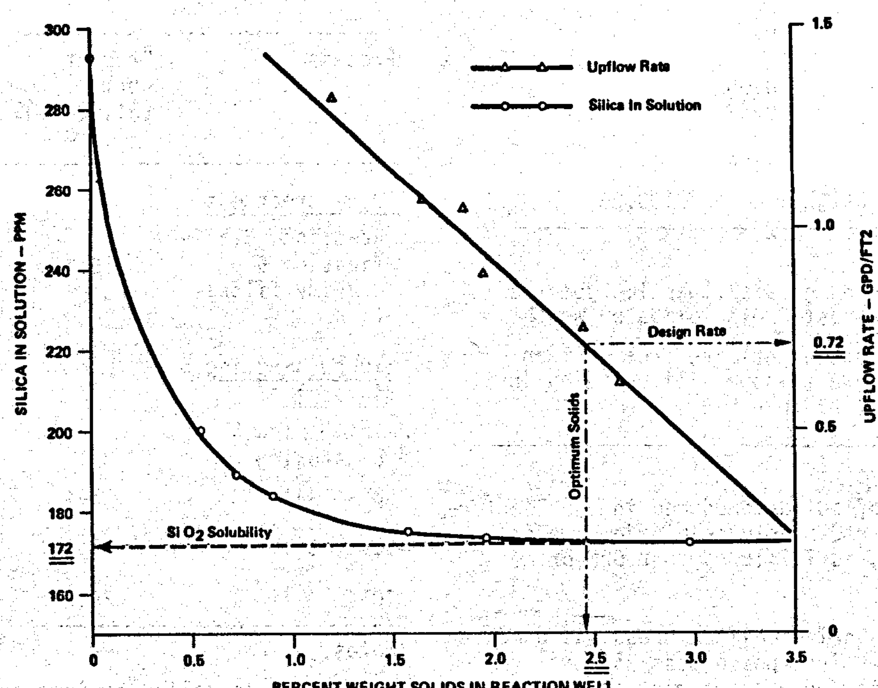

Fig. 2. Removal of silica by solids contact clarification processing.

Sludge Handling and Disposal

Insoluble solids produced in the Reactor-Clarifier by auto-precipitation (no addition of foreign chemicals or seed material) were collected from the Reactor-Clarifier sludge blowdown and analyzed. A proximate chemical analysis of these insoluble solids is presented in Table 2. Silicon is the major constituent of the total insoluble solids, representing approximately 90% by weight, as silica and possibly other complex silicate forms. Heavy metals including iron, strontium, manganese, lead, and copper appear to precipitate as sulfide and oxide minerals and, perhaps, as other complex forms.

Table 2. Proximate chemical analysis of insoluble solids in Reactor-Clarifier sludge.

Constituent	Weight-% solids	ppm
Silicon as Si	(42.82)	
as SiO_2	91.75	
Silver		97
Copper	0.13	
Nickel		23
Manganese	0.31	
Magnesium	0.08	
Lead	0.18	
Iron	0.85	
Cobalt		4
Chromium		18
Arsenic		85
Calcium	7.92	
Aluminum	0.02	
Barium		6
Boron	0.02	
Cadmium		2
Rubidium	0.01	
Selinium		73
Zinc	0.06	
Strontium	0.63	
Cesium		33
Sulfur	1.06	
Total constituents weight:	103.05%	

Notes:

1. All concentrations greater than 100 ppm are expressed to nearest 0.01% solids by weight.
2. Total constituent weights are greater than 100%, possibly due to some silicon being in complex forms other than SiO_2.

The quantity of solids produced in the Reactor-Clarifier, as measured by sludge blowdown under optimum conditions, is 1.7 lb/day per GPM brine fed to the unit.

An Envirotech-Shriver Filter Press was used near the end of the first-phase test work to determine the dewatering characteristics of the sludge on this device. These tests showed that the sludge could be dewatered easily, producing a filter press cake of 65% solids by weight. Earlier test work indicated that centrifuges and vacuum drum filters could produce a cake no greater than 50% solids by weight. At the same time, the filtrate from the filter press was essentially free of suspended solids, while the centrate from the centrifuge contained as much as 1% solids by weight. The filtrate/centrate must be returned to the Reactor-Clarifier. High solids concentrations in this recirculated stream could adversely affect the performance of the Reactor-Clarifier.

Test work to date has indicated that disposal of filter press cake at 65% solids in lined ponds is the most cost-effective and environmentally sound alternative. It is possible that metals could be recovered from the filter press cake, which offers some savings in the overall costs of a spent-brine treatment operation.

SPENT GEOTHERMAL BRINE TREATMENT SYSTEM

Sufficient data have been collected from the phase-one test program to prove the adequacy of design of a spent geothermal brine treatment system for any given capacity. Test work, however, is continuing. The following tests are planned:

- Phase 2 - Pilot plant operations including a Reactor-Clarifier, Gravity Sand/Anthracite Filter, Sludge Thickener, and Filter Press on the same pilot scale as reported above (to be started approximately July 15, 1978).

Table 3. Order of magnitude costs for spent brine treatment and sludge handling and disposal for a 55-MW geothermal generating station.

Process	Present worth ($1,000,000)	Unit Costs ¢/1,000 gallons	Unit Costs Mills/KWH
Brine treatment			
Reaction, Clarification & gravity filtration	15.2	11	0.9
Sludge handling & disposal			
Thickening & dewatering	8.4	6	0.5
Disposal	3.1	2	0.2
Sub Total	11.5	8	0.7
TOTAL	26.7	19	1.6

Notes:

Includes installed capital costs and O&M costs.
Life of plant = 30 years.
On-line plant factor = 90%.

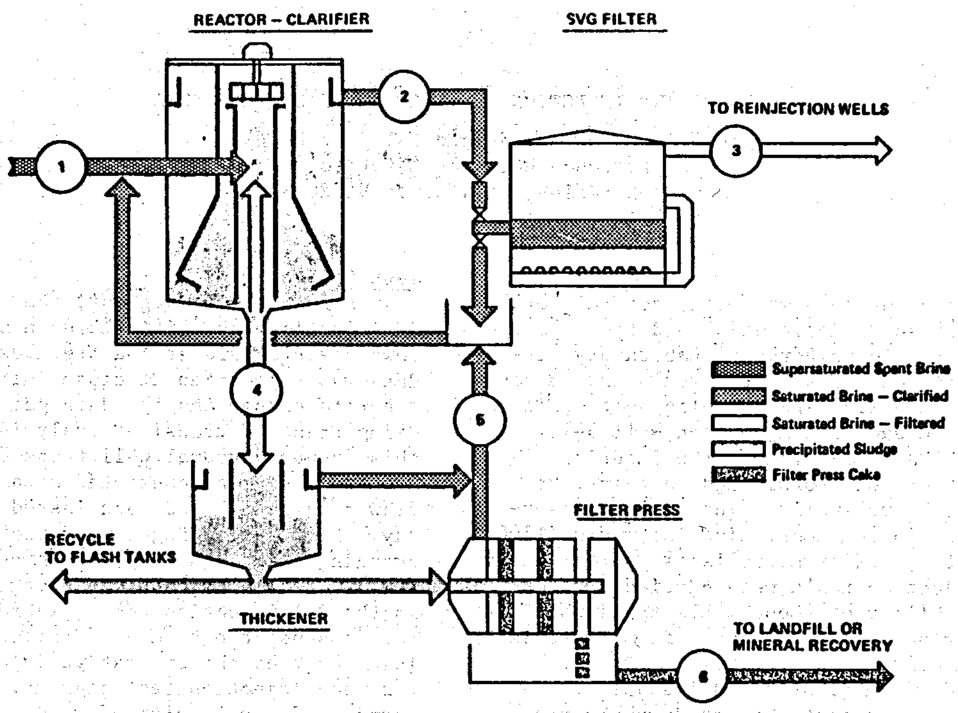

Fig. 3. Stabilization of spent geothermal brines.

- Phase 3 - Demonstration plant operation including a Reactor-Clarifier, Gravity Sand/Anthracite Filter, Sludge Thickener, and Filter Press to treat spent geothermal brine from a 10-MW heat-extraction plant facility. (To be started approximately February 15, 1979.)

The brine treatment systems used for both Phase 2 and Phase 3 test programs will be as shown in the simulated flowsheet in Fig. 3. Commercial operation of a spent geothermal brine treatment system is expected at this time to be the same as that shown on the flowsheet.

ORDER OF MAGNITUDE COSTS

Based upon test results presented above and upon cost information derived from projects of similar nature and size, order of magnitude costs for spent-brine treatment and sludge handling and disposal for a 55-MW geothermal generating station are presented in Table 3.

As shown, it is estimated that the unit cost on a present-worth basis for brine treatment is 11¢/1,000 gallon brine treated (0.9 mills/KWH). Estimate for sludge handling and disposal is 8¢/1,000 gallon brine treated (0.7 mills/KWH) for a total treatment cost of 19¢/1,000 gallon brine treated (1.6 mills/KWH). Chemical costs are not included in this analysis, in that it is felt that chemical addition in any form is not required to produce the required effluent qualities. If chemicals were to be used, 2¢ to 5¢/1,000 gallon brine treated should be added to these estimates.

RESULTS OF TWO INJECTION TESTS AT THE EAST MESA KGRA

Donald G. McEdwards and Sally M. Benson
Lawrence Berkeley Laboratory
Berkeley, California 94720

INTRODUCTION

In 1977, in accordance with contractural work for the U.S. Bureau of Reclamation and the Department of Energy, Lawrence Berkeley Laboratory performed two injection tests on two wells in the East Mesa KGRA. These wells were Republic Geothermal Well 18-28 and Bureau of Reclamation Well 5-1. The East Mesa KGRA is located in the Imperial Valley of Sourthern California and contains, at present, 15 geothermal wells. The average reservoir temperature in the completion intervals (1500-2700 meters) of the existing wells is approximately 180°C. The injection tests were carried out to determine the ability of these wells to dispose of the spent brine that is produced from the existing production wells.

Well 18-28 was monitored continuously for four months with a Hewlett-Packard downhole pressure and temperature gauge. Three separate injection episodes were monitored. The first two were each four-day tests with step changes in the injection rate. The third injection period lasted approximately 40 days and also included step rate changes.

Well 5-1 downhole pressure response during injection was monitored for five days using a silicon oil filled capillary tube connected to a paro-scientific pressure transducer. The injection rate schedule consisted of 6 step changes.

This paper will discuss the reservoir parameters (kh/μ, $\phi chre^2$) obtained from the analysis of transient pressure data and the skin values associated with the individual wells. The quality of the data obtained using a silicon oil-filled capillary tube in a cold injection well will also be discussed.

WELL 5-1 INJECTION TEST

Well Characteristics and Injection Scheme

Well 5-1 is completed with 7 4/8 inch casing to a total depth of 1828 meters. It is perforated or slotted from 1237 meters to 1828 meters. Fluid injected into Well 5-1 is geothermal brine produced from nearby BuRec Well 6-2. Fluid is stored in a six-acre holding pond where it is cooled to approximately 20°C. The pond fluid is then filtered, acidized and pumped into a holding tank at the 5-1 wellhead. Two positive-displacement injection pumps of 150 and 220 gpm capacity, respectively, may be used singly or in combination for fluid injection. Downhole pressures are monitored utilizing a 1280 meter, .054"I.D. stainless steel tubing filled with silicon oil. The downhole pressure response is transmitted through the oil in the tubing to the paro-scientific transducer (resolution .01 psi). Surface printout equipment can record the pressure data at one second or longer intervals depending on the rapidity of the pressure change.

Test Design

For each test segment, the step rate change in injection was initiated upon achieving a stable downhole pressure at the previous rate. Pressure data was then taken at close intervals following the rate change and the data gathered was analyzed using pressure transient analysis techniques. In this manner, several well tests could be conducted. Each test segment consisted of a relatively small flow rate change and each lasted approximately one day. Flow rate changes were accomplished by changing injection pumps or using them in combination. A total of six test segments were performed in the 5-1 injection test. Table I lists the flow rate change, the time of duration, the total fluid injected and the cumulative injection to that time for each injection test segment. Table II is a summary of the results of these six test segments. For each segment, the date, type of analysis used for the pressure data, the test results and comments regarding the tests are given. In addition, an injectivity index is listed that is derived from stabilized downhole pressures and current flow rates for each test segment.

Interpretation and Discussion of Transient Pressure Data

As Table II clearly shows, the values of transmissivity vary from 18,000 md-ft/cp to 100,000 md-ft/cp. The injectivity index, not surprisingly, also varies and tends to be larger at the higher levels of injection than at the lower levels of injection. The value of $\phi chre^2$, which is a measure of well damage, is quite small on the average, indicating a large positive skin for nominal values of the lumped parameter ϕch. This anamolous behavior among well test results may be explained by postulating the existance of a vertical fracture in the well. Two direct lines of evidence support this theory. Excerpts from the BuRec 5-1 injection log of January 27, 1976 shown in Figure 1, give a brief survey of events regarding Well 5-1. In summary, the wellhead pressure dropped from 1200 to 450 psi within 10 hours on that date. A wellhead pressure of 1200 psi, when added to the static head is sufficient at a depth of 5,000 ft (opposite the perforations) to fracture the reservoir rock. Emperical data support this conclusion. The other piece of evidence supporting the vertical fracture theory is the results of a spinner survey taken immediately after the 5-1 injection test was completed. The spinner survey comprised three injection rates; 150, 220 and 370 gallons per minute. For each survey going to 6,000 ft., it is clear that no flow was entering the perforations below 4400 feet. Only one stop of the spinner tool indicated flow, and that was at the very top of the perforations. Figure 2 shows the results of these 3 spinner surveys. At the present time, a dilation mechanism due to increased flow rate is being considered as a possible cause for the

TABLE I. SUMMARY OF WELL 5-1 INJECTION TEST

FLOW RATE (gpm)	ΔQ(gpm)	Total Hours (hours)	Fluid Injected	Cumulative Injection
150	150	16	144,000 gals	144,000 gals
220	70	22	290,400 gals	434,400 gals
0	-220	2	0	434,400 gals
370	370	24	532,800 gals	967,200 gals
220	-150	24	316,800 gals	1,284,000 gals
150	-70	7	63,000 gals	1,347,000 gals
0	-150	shut in	--	1,347,000 gals total injection

TABLE II. SUMMARY OF WELL 5-1 INJECTION TEST AND RESULTS

Date	Injection Rate	Test	ΔQ	Type of Analysis	kh/μ	$\phi c h r_e^2$	Comments	II ΔQ/DP
12/1/77 @1618	150	-	150	--	-	--	No analysis due to affect of cooling of the well or the pressure data.	--
12/2/77 @1003	220	1	70	MDH	18,000	.088		
				Two Rate (Mathews)	19,000	.1259		.886
12/3/77 @0932	0	2	-220	--	--	--	Well not shut in long enough to measure reservoir response.	.088
12/3/77 @1005	370	3	370	MDH Two Rate	42,000 25,000	$1.01x10^{-7}$ $3.37x10^{-5}$	Not shut in long enough before well was opened up.	.867
12/4/77 @1000	220	4	-150	MDH Two Rate	100,000 90,000	$5.3x10^{-7}$ $5.01x10^{-8}$		2.0
12/5/77 @940	150	5	-70	MDH	32,000	$5.61x10^{-5}$		.972
12/5/77 @1646	0	1	-150	MDH Two Rate	39,000 37,000	5.10^{-3} $5.8x10^{-12}$	Pressure data available only for 120 minutes after shut-in due to the heating of the oil in the tubing.	.508

wide range of values of transmissivity among the individual test segments. It should be remembered however, that little is known about the pressure-transient response of cold water injection into a fracture in a hot reservoir. Acknowledging all of the above difficulties in interpretation it does seem significantly clear, that in spite of the presence of the vertical fracture, the well has been damaged as indicated by the very small values of $\phi chre^2$. It is felt that the damage to the well and fracture is probably caused by chemical incompatibility of injected fluids and fluid present in the fracture, and/or particulate plugging

Also complicating this analysis is the response time of an oil filled capillary tube to large pressure changes in the well. This response time is roughly 20 minutes for oil at 70°F and 4200 feet of tubing (see paper by C. Miller and J. Haney this proceedings). The validity of this response time calculation is clearly seen in Figures 3, 4 and 5 which display pressure versus log time for test segments 3, 4 and 5. It will be seen on each figure that the semi-log straight-line portion begins approximately 20 to 30 minutes after the flow change initiation. The straight line is, however, convincing enough for analysis purposes.

WELL 18-28 INJECTION TEST

Well Characteristics and Injection Scheme

Well 18-28 is completed with a 7" casing to a total depth of 2440 meters. Roughly 75 meters of this length are jet perforated. A spinner survey indicates that fluid enters the reservoir only through this 75 meter interval. It is believed calcium carbonate scaling is responsible for the plugging of the remainder of the perforated section. The fluid injected into Well 18-28 is geothermal brine produced from Well 38-30 or Well 16-29. The fluid is pumped from the production well to the injection well by a positive displacement pump. Downhole pressure during injection was obtained with a Hewlett-Packard downhole pressure gauge located at 1520 meters. Pressure data was recorded by a thermal paper printer at intervals between 40 seconds to 10 minutes. The temperature of the injected fluid at the wellhead ranged from 65°C to 93°C. The Hewlett-Packard tool was also used to monitor downhole temperature. The injected fluid had increased in temperature approximately 14°C downhole. Figure 6 shows a plot of the flow rate from 38-30 and 16-29 that was injected into Well 18-28 as well as concurrent pressure readings.

Test Design and Interpretation

The 18-28 injection test was run concurrently with a series of production tests and interference tests on several Republic Geothermal wells. Thus, the tests were not designed specifically to obtain the type of data ammenable to transient pressure analysis. Flow rates were highly variable and downhole pressures were not stabilized prior to rate changes. Nevertheless, from two different methods of analysis consist t results were obtained. Pressure data were first analyzed using a least squares computer matching program. This analysis yielded a kh/μ of approximately 70,000 md-ft/cp with increased value of skin for successive segments of the test. The second type of analysis consisted of analyzing falloff data from three successive segments of the test (either Miller-Dyes-Hutcheson technique or the two-rate analysis technique). Figures 7, 8 and 9 show the results of these analyses. As seen from the figures, these analyses also yield values of approximately 77,000 md-ft/cp with increasing values of skin for successive segments of the test. This increase in the value of skin is consistent with evidence of increasing scaling in the well as seen by increasingly large injection pressures. These increasingly larger injection pressures, however, never approach values that would indicate fracturing of the formation at depth.

SUMMARY

BuRec Well 5-1 is fractured at the top of the perforations. The average transmissivity value for this well is approximately 43,000 md-ft/cp. The well appears to have been damaged even after fracture had occured. The mechanism for damage is most likely the same one responsible for the presence of the fracture in the first instance. This experience with Well 5-1 has shown that the fracturing of the well in a geothermal reservoir will not necessarily increase its injectivity. This is becuase the mechanism of plugging or scaling is not abated permanently when a well is fractured and the fracture becomes progressively damaged as did the well bore itself previously.

Well 18-28 is being progressively damaged under injection. This is seen in the increasing values of positive skin values. Its transmissivity value of 70,000 md-ft/cp has been obtained from several types of analysis. The well is not fractured from evidence on hand at present. The rapid increase in skin value between injection tests indicates something of a chemical nature is occuring in the well, again, probably similar to the 5-1 chemical incompatibility problem between the injected fluid and the geothermal brine at depth.

TIME	GPM	WELLHEAD PRESSURE	COMMENTS
1200	100	1200	At 1245 lowered gpm to 90, wellhead pressure 900 psi.
1400	90	1000	At 1410 increased gpm to 95.
1600	95	350	To raise level in tank put diesel on idle at 1730.
2200	100	450	Cannot bring pressure to 1000 psi due to injection tank pumping too much (2215). At 2330 injection tank almost empty. Shut down to allow it to fill up.

Drop in wellhead pressure from 1200 to 450 psi at same flowrate indicates fracturing.

Fig. 1. Excerpts from BuRec 5-1 injection log, 1/27/76.

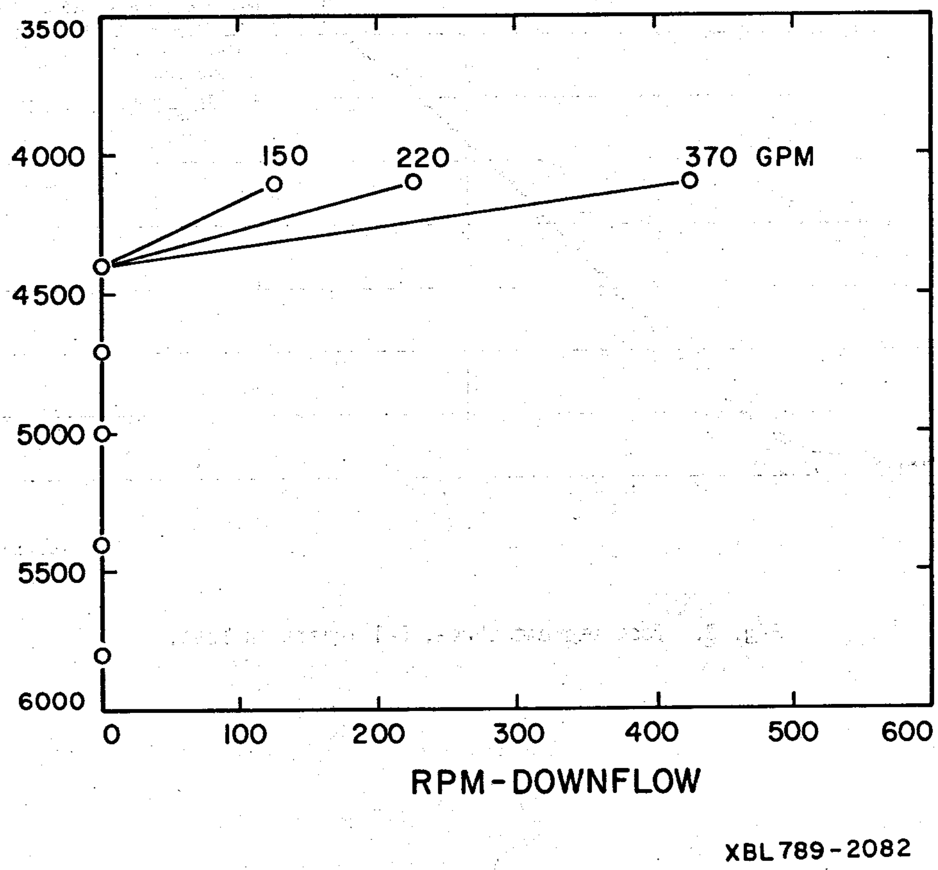

SURVEY DATA - well injecting

		RPM - low rate	medium rate	high rate
Stops	4100	125	225	425
	4400	0	0	0
	4700	0	0	0
	5000	0	0	0
	5400	0	0	0
	5800	0	0	0

Open intervals 4061' to 5276' perforations
5003' to 6003' slotted

Fig. 2. Spinner surveys taken in well 5-1.

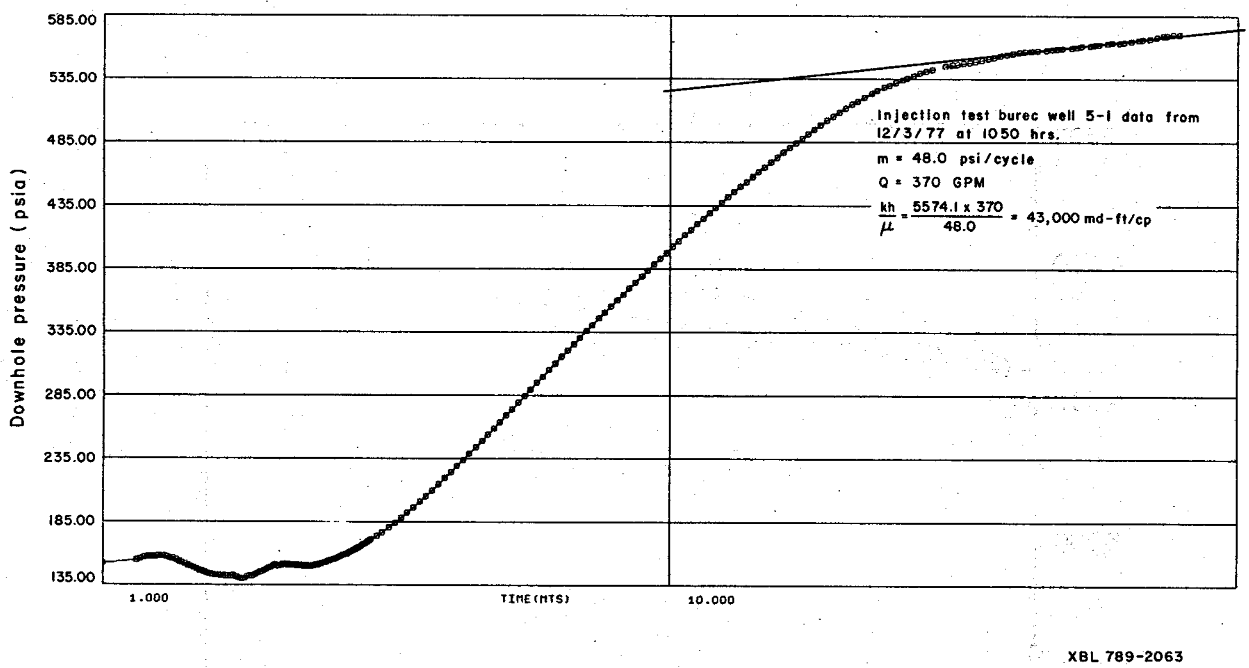

Fig. 3. Test segment three, 5-1 injection test.

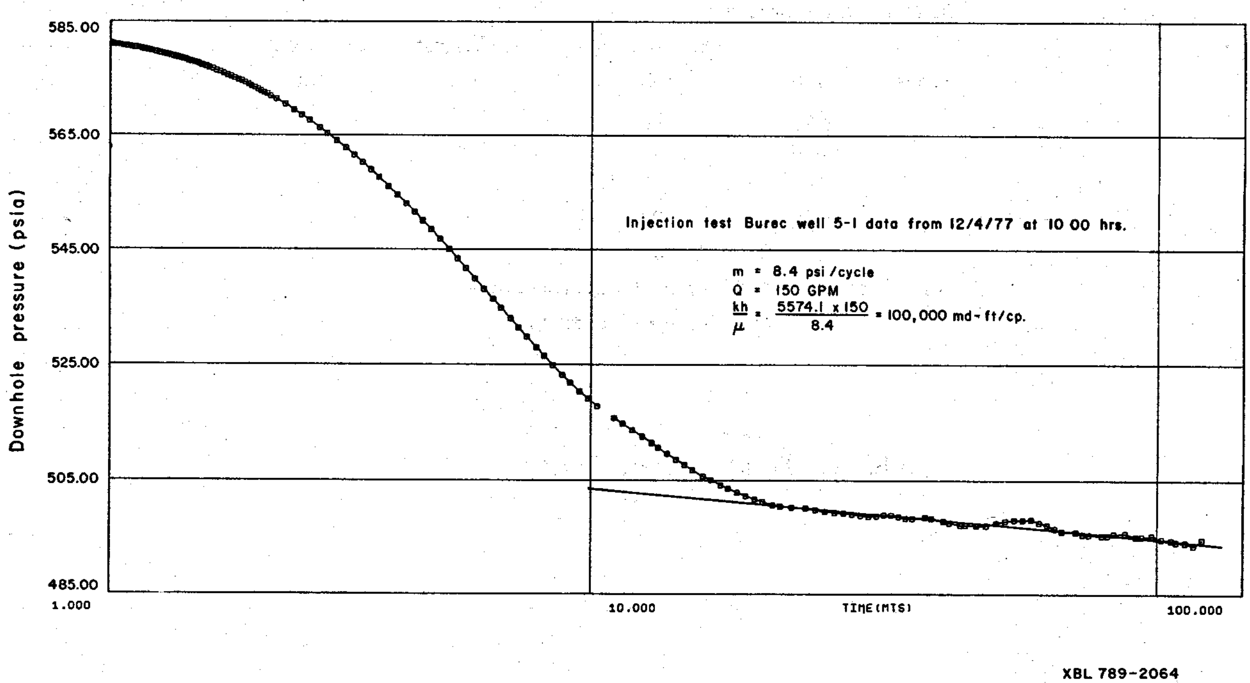

Fig. 4. Test segment four, 5-1 injection test.

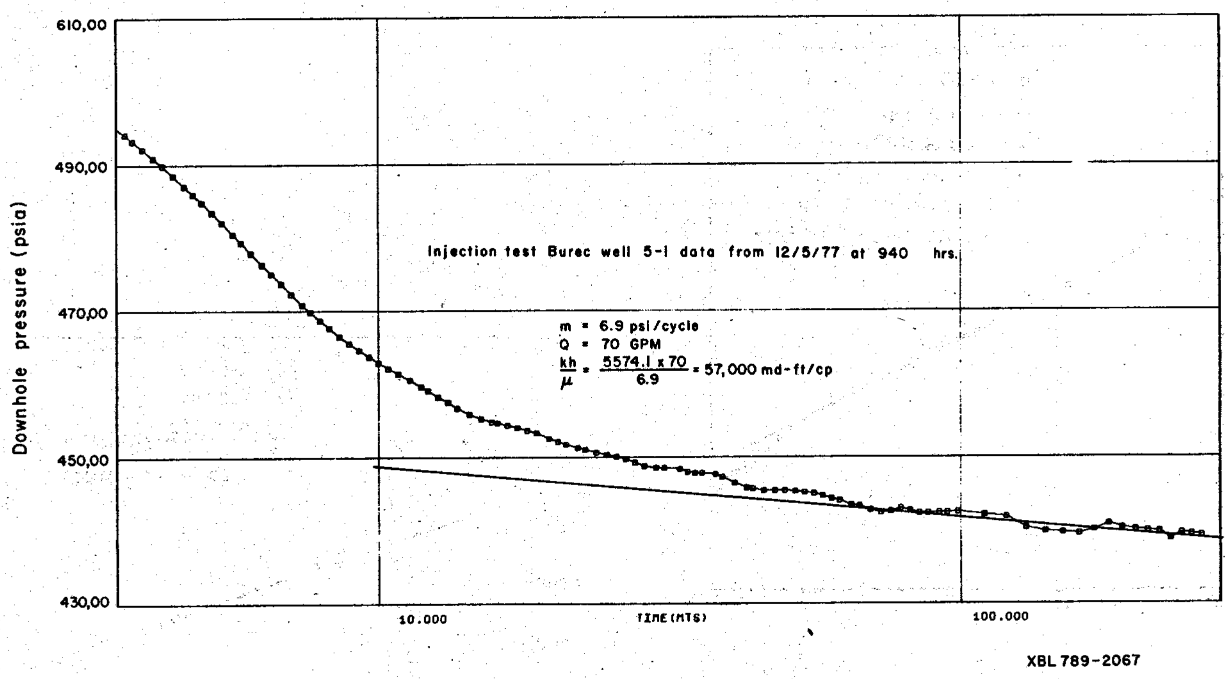

Fig. 5. Test segment five, 5-1 injection test.

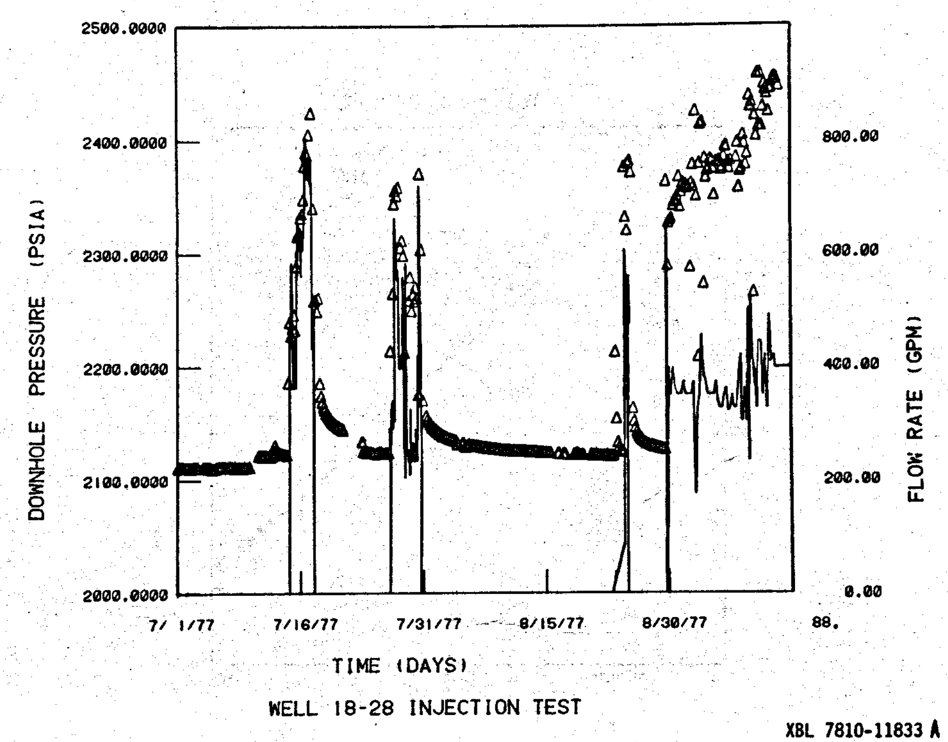

Fig. 6. Pressure and injection rate during 18-28 test.

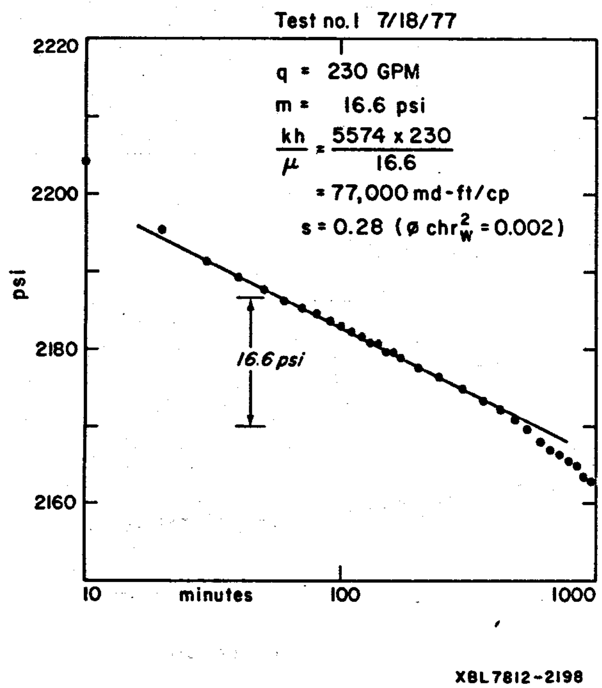

Fig. 7. Test segment no. 1, 18-28 production test.

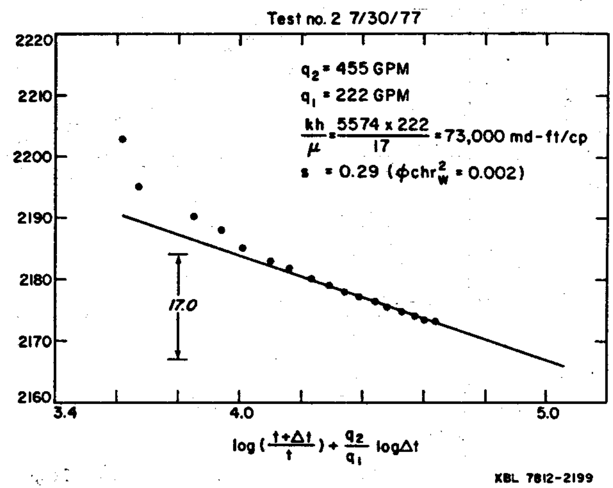

Fig. 8. Test segment no. 2, 18-28 production test.

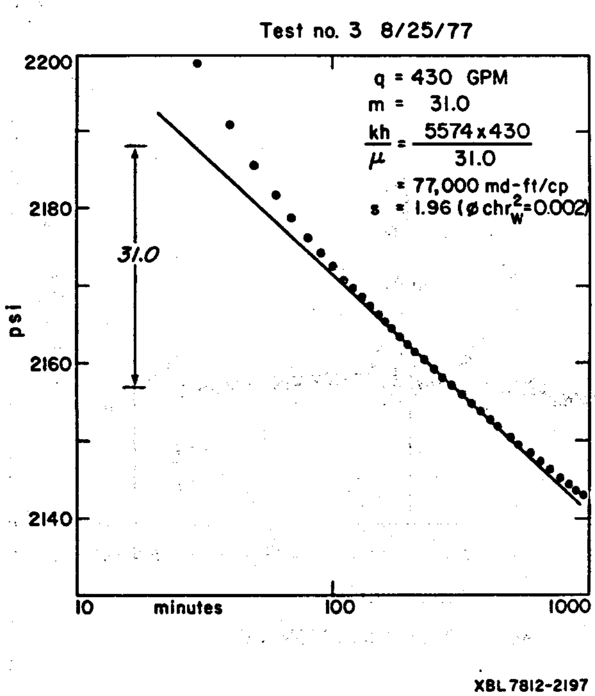

Fig. 9. Test segment no. 3, 18-28 production test.

DEVELOPMENT OF A HIGH RESOLUTION DOWNHOLE PRESSURE INSTRUMENT FOR HIGH TEMPERATURE APPLICATIONS

E. P. Eernisse
T. D. McConnell
A. F. Veneruso

Sandia Laboratories - Division 4736
Albuquerque, New Mexico 87115

ABSTRACT

As part of the Geothermal Logging Instrumentation Development Program being conducted by Sandia Laboratories for the Department of Energy's Division of Geothermal Energy, high resolution, quartz crystal based, downhole pressure instruments are being developed. Under a joint no-cost contract, Sandia and Paroscientific, Inc., of Redmond, Washington, are working to upgrade a Paroscientific transducer for operation at 275°C. In addition, Sandia Laboratories has been investigating various design configurations and fabrication techniques for high temperature quartz resonators and their associated electronic circuits.

The goal of these efforts is to achieve a resolution of 0.01 psi in a 0 to 7000 psi range and in temperatures up to 275°C. The progress and plans for this project will be reviewed and hardware samples will be displayed.

INTRODUCTION

The assessment of geothermal energy resources by means of well logging instruments is hampered because the downhole high temperatures, which are typically over 200°C, far exceed the operating regimes of ordinary electronics and transducers. A similar difficulty occurs in deeper oil and gas wells and steam injection wells for tertiary recovery. One of the most useful borehole measurements for well testing is a high resolution, pressure logging tool.[1,2] This instrument is essential in correlating well flows with pressure or fluid level changes and drawing inferences about the reservoir's production potential and its ability to transport and store fluids. Presently, the highest pressure resolution measurements are made with commercially available quartz resonator transducers.[3,4] However, the present technology of devices is limited to operation below 125°C; also the measurement's resolution is severely impaired by temperature gradients typically encountered by instruments moving downhole.

To correct these technical deficiencies, development activities are underway as part of the Geothermal Logging Instrumentation Development Program being conducted by Sandia Laboratories for the Department of Energy's Division of Geothermal Energy. Specific goals for the pressure transducer are 7000 psi full scale capability, 275°C upper temperature limit, and a resolution of 1 ppm, i.e., a minimum detectable fluctuation of about 0.01 psi on top of a full scale pressure background. Also, it is desirable to have measurement hysteresis in the measurements less than 1 ppm (i.e., the change in reading when approaching a given pressure from above and below).

One approach taken at Sandia is similar to the Hewlett-Packard design[3]; this is a thickness-shear mode plate resonator with a uniform force, proportional to pressure, acting around the perimeter of the resonator plate. As discussed in the following pages, numerous technological changes are necessary, however, to move the temperature range up to 275°C.

Another approach being investigated is that of the Paroscientific* flexure mode transducer[4]; this offers higher pressure sensitivity, but lower frequency stability than the resonator plate approach.

This article reviews the two concepts and then discusses the basic technology considerations of the Sandia design. Preliminary results of pressure measurements with the Sandia design at 275°C are presented to demonstrate viability of high temperature operation.

TRANSDUCER CONCEPTS

As described in Figures 1 and 2, the quartz resonator pressure transducer operates on the principle that mechanical resonance frequencies, which are linear elastic phenomena, are shifted by nonlinear effects. Thickness mode quartz resonators have extremely stable mechanical resonances (i.e., frequency variations less than 1×10^{-10} per month) due to the high purity of quartz, to cleanliness of

*Paroscientific, Inc., 4500 - 148th Ave., Redmond, Washington 98052

COMMERCIAL WELL LOGGING TOOLS

UTILIZING QUARTZ RESONATOR TRANSDUCERS

(Rough Comparable in Performance
.01 - .1 psi Resolution, 125°C
Maximum)

● **PAROSCIENTIFIC**

[FLEXURE MODE, HIGH PRESSURE SENSITIVITY
BUT LOW FREQUENCY STABILITY]

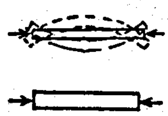

● **HEWLETT-PACKARD**

[THICKNESS SHEAR MODE, LOW PRESSURE SENSITIVITY
BUT HIGH FREQUENCY STABILITY]

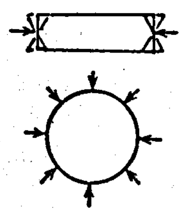

FIGURE 1

DIGITAL QUARTZ PRESSURE TRANSDUCERS
Paroscientific, Inc.

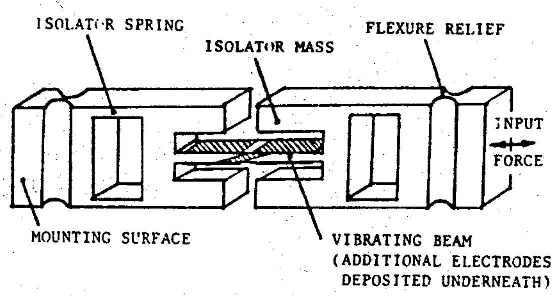

Quartz crystal resonator.

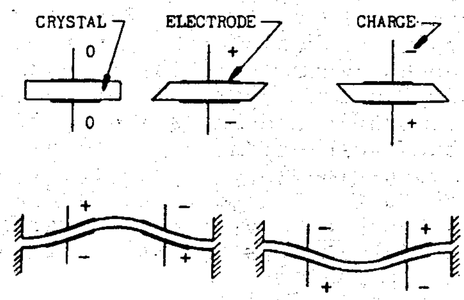

Piezoelectric excitation.

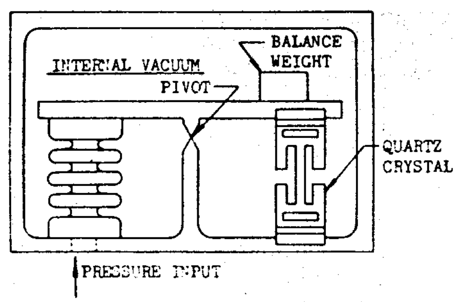

Absolute-pressure transducer.

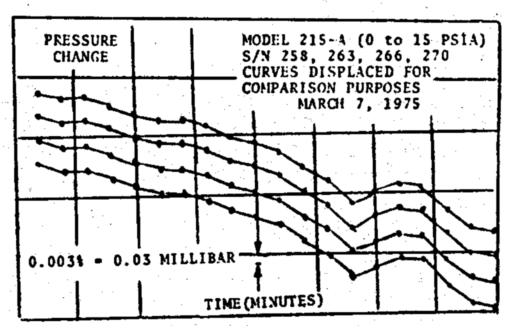

Barometric tracking.

FIGURE 2

fabrication and packaging, and to careful resonator design for obtaining well defined, high Q mechanical resonant modes. The flexure mode crystals are somewhat less stable because of lower mechanical Q. Frequency stabilities in environments where temperature is constant and there are no mechanical biases (initial stresses) acting on the resonator plate have been observed up to 2×10^{-12} over a 10 second period for the thickness mode designs and 1×10^{-9} for the flexure mode designs. Stabilities of 1×10^{-9} over time periods of hours are now routine for thickness modes and 1×10^{-7} for flexure modes. The high resolution of quartz resonator transducers comes from this inherent frequency stability and the fact that pressure induced stresses can reversibly shift the resonant frequencies as much as 1×10^{-3} for the thickness modes,[5,6] and 1×10^{-1} for the flexure modes.[4]

The proposed Sandia pressure transducer concept is shown in Figure 3. A

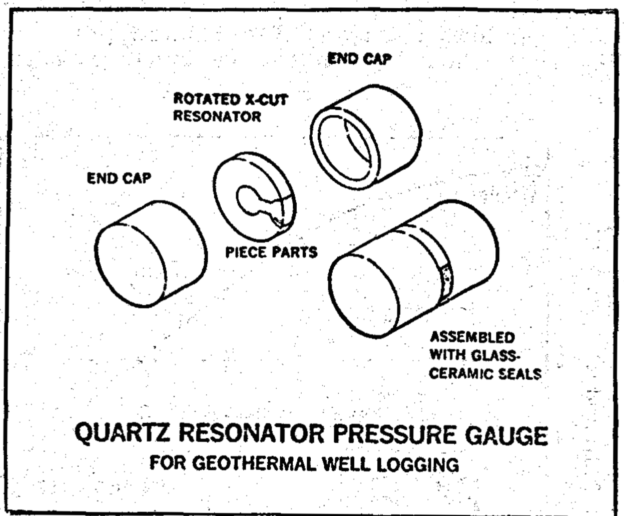

FIGURE 3

circular resonator plate is enclosed by two hollowed-out quartz end caps of the same crystallographic orientation as the resonator plate. The net force on the resonator due to the pressure is radially directed and uniformly distributed around the perimeter. This gauge concept is similar to that offered commercially for lower temperature applications.[3] These radial forces cause frequency shifts through nonlinear elastic behavior of the quartz crystal.

The Paroscientific transducer, shown in Figure 2, is another promising candidate for high temperature operation. Frequency shift for this approach arises from the influence of the axial force on the natural frequency of the vibrating beam (like the tuning of a guitar string). This flexure mode approach[4] has inherently higher sensitivity to pressure than the shear mode approach[3] used by Hewlett-Packard. Under a joint no-cost contract, Sandia and Paroscientific are working to upgrade a Paroscientific transducer for operation to 275°C. Key areas under development are fabrication and bonding techniques for high temperature operation.

TECHNOLOGY FOR SANDIA DESIGN

The Sandia Quartz resonator design, shown in Figure 3, was made to explore frequency variations due to initial stresses and temperature changes. This configuration was also used to investigate the suitability of different electrode materials, crystal bonding agents, and fabrication procedures. Each of these important topics are examined in detail below.

Frequency vs Temperature Effects

Unfortunately, small changes in temperature can shift the resonant frequencies by amounts comparable to the stress-related frequency changes, particularly for the thickness mode designs. It is therefore necessary to choose the resonator design (crystallographic orientation of the resonator structure) such that temperature effects are small compared to stress effects. This means operation, as shown in Figure 5, for a thickness mode design, at a turnover point in the frequency-temperature (f vs T) characteristic of the resonator so that the linear, or first-order, temperature effects are eliminated. The thickness shear vibrational modes of plate resonators are the most useful plate modes because they exhibit turnovers in their f vs T characteristics. All of the high frequency stability accomplishments in the past have come from plate resonators operating in the thickness-shear mode of vibration. The commercially available plate resonator transducer of interest here[3] utilizes the common BT-cut resonator with a parabolic f vs T. For high temperature operation at 275°C, the curvature of f vs T (second order effect) is large and equal to 0.19 ppm/°C^2. Thus a temperature change of 1°C causes a frequency shift $\Delta f/f$ of 1.9×10^{-7}. Since 0.01 psi causes a $\Delta f/f$ shift of 1×10^{-9} in most transducer designs, this high curvature places stringent requirements on the temperature environments.

One of the first steps taken in development of this high temperature technology was a search for crystallographic orientations where temperature effects of f were minimum around 300°C. The rotated X-cut was identified as the most useful orientation. The details of this orientation have been recently published[7]. It is identified as the $(xy\ell)\ \theta$ orientation in standard notation[8] (see Figure 4). A typical f vs T plot is shown in Figure 5. The f vs T characteristic of the common AT-cut is included in Figure 5 for comparison. As seen in Figure 5, the overall frequency shifts are

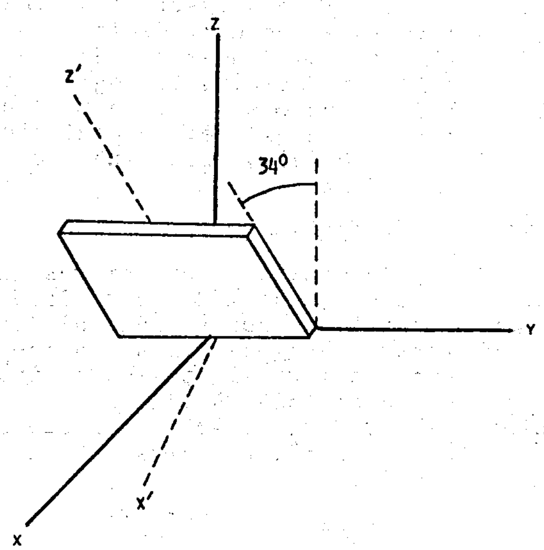

ROTATED X-CUT QUARTZ

(xyℓ) 34°
or (yxwℓ) 30°, 34°

FIGURE 4. Crystallographic orientation

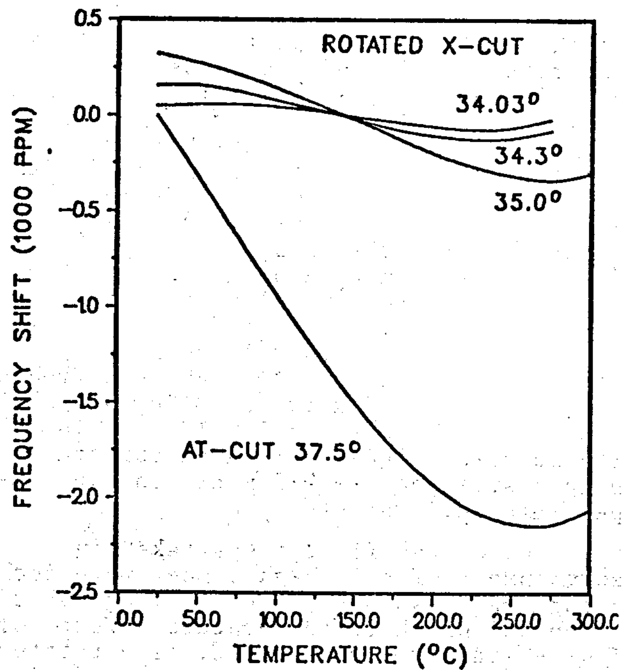

FIGURE 5

markedly less for the rotated X-cut and the curvature at the 275°C turnover point is less as compared to the AT-cut. The rotated X-cut has a curvature at 275°C of 0.04 ppm/°C^2 as compared to 0.12 for the AT-cut and 0.19 for the BT-cut. It is clear that the rotated X-cut has distinct advantages for oven-controlled applications where temperature cannot be controlled.

Response of Resonator Plate to Initial Stresses

The response of the thickness mode resonator plate to radially directed forces can be calculated at room temperature with the published values for the third-order elastic coefficients. This has been done for numerous crystallographic cuts including the rotated X-cut and published in the frequency control literature.[5] The shift is given by

$$\frac{\Delta f}{f} = KT$$

where T is the uniform initial stress caused by the symmetric force due to pressure and K is dependent on crystallographic orientation. Figure 6 shows K for the technologically im-

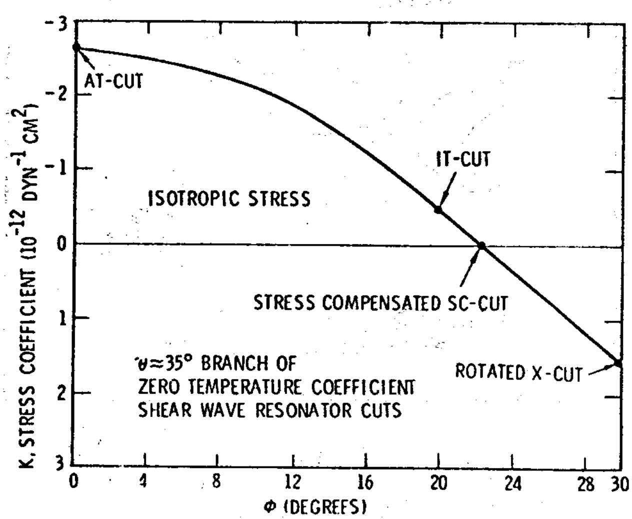

FIGURE 6. Stress coefficient for the important (yxwℓ)ϕ, 34° branch which contains the widely used TA-, IT-, SC-, and the Rotated X-cuts.

portant family[8] of thickness-shear mode cuts (yxwℓ)ϕ, θ which have a turnover point in their f vs T characteristics. The rotated X-cut is in this family and is given by (yxwℓ) 30°, θ. As seen in Figure 6, is has a K value of $+1.54 \times 10^{-12}$, which is magnitude-wise one of the largest to be obtained in quartz (compare this value to the others in Figure 6). The BT-cut, which is on the other technologically important branch of the (yxwℓ)ϕ, θ family with $\theta \approx -49°$, is the only other thickness shear mode cut of interest. It has a K value of 2.7×10^{-12}.

Electrode Considerations

Conventional electrode technology for quartz resonators used at low temperature involve Au electrodes on the acoustically active regions and Au electrodes with a Cr underlayer for the bonding areas. The hybrid circuit community has shown that Cr migrates at 300°C and loses adhesion. Unfortunately, separation of the Cr/Au electrode from substrates (usually Al_2O_3 ceramics) and wire bond failures are common. Considerable effort has therefore been spent on electrode technology; both Mo/Au and Nb/Au sputtered electrodes have been investigated.

Although the Nb/Au electrode system maintains adhesion after repeated cycling to 300°C in air, Rutherford backscattering studies show that O_2 migrates through the Au and reacts with the underlying Nb. If such electrodes are used on or near the acoustically active region, they will lower the resonant frequency and cause continuing downward drift in frequency of an order comparable to the frequency shifts due to pressure. The Nb/Au system was therefore abandoned in favor of Mo/Au.

The Mo/Au system has provided excellent adhesion to quartz in repeated temperature cycling and does not have the O_2 reaction problems of Nb/Au. Typical electrodes are keyhole patterns with 500 Å of Mo followed by 3000 Å of Au.

For the Sandia design, the Mo/Au electrodes are used for both the acoustically active region and the bonding areas.

Bonding Agent

The bonding agent chosen for assembly of the quartz pieces was Pyroceram 89 applied by silk screening or the equivalent VITA Tape applied as a tape on the mating surfaces. These are glass/ceramic materials with an organic binder. The binder is first burned out in a vacuum furnace. Temperature is then raised to just below the melting point of the glass bonding agent (400°C) and the system is repeatedly evacuated and backfilled with He or Ar. Then the temperature is raised to above the melting point of the glass to 455°C, the parts are mated, and the seal is made. The temperature is then held at 455°C for one hour to cause crystallization of the bonding agent. The resulting bond is a ceramic with a melting point far in excess of the sealing temperature and of any expected operating temperatures. The glass/ceramic was chosen because of this ability to make the initial seal as a glass and then convert to a mechanically stable ceramic form.

It has been found that the bonding agent dessolves the Mo/Au electrodes. The region where the electrode tab passes through the bond is therefore protected by 5000 Å of Cr deposited in a separate deposition. The Cr/bonding agent and Cr/Au interfaces have been found to hold up to temperature cycling, in contrast to the adherence failure of the Cr/quartz interface under temperature cycling. The results to date on this fabrication procedure have been satisfactory. Preliminary testing has not turned up any significant problems.

Experimental Pressure Measurements at 275°C

Measurements of pressure at 275°C have been accomplished. The rotated X-cut transducer was suspended from two electrical feedthroughs on the inside of a pressure bomb filled with silicone oil. This assembly was then heated in a furnace to 275°C. Wires from the feedthroughs were connected to an oscillator circuit outside the furnace. The oscillator's frequency was monitored as the bomb was pressurized with a hand pump. Independent pressure measurements were taken with a Paroscientific Model 600 Digiquartz Pressure Computer and Model 75K gauge located outside the furnace and connected into the pressure line with a "T" junction. The Paroscientific gauge has been checked in our standards lab with a dead weight tester to approximately 1 psi resolution (5000 psi full scale).

Results are shown in Figure 7 as

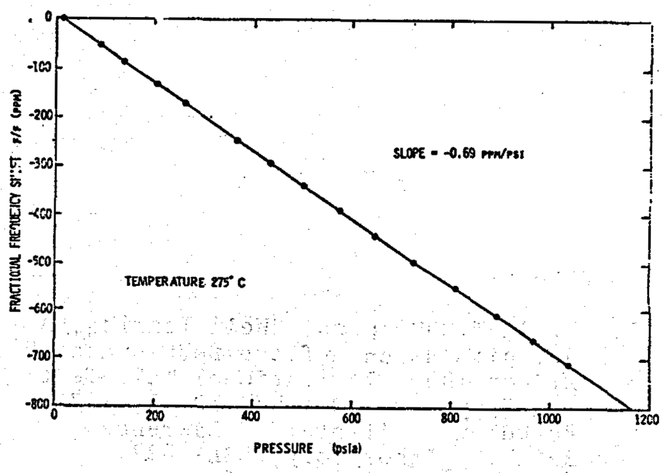

FIGURE 7

fractional frequency shift vs absolute pressure. Data repeatability and hysteresis effects were approximately 4 psi at 275°C and 2 psi at room temperature. These relatively high values seem to be related more to time-dependent flow of the viscous oil in the tubing of the experiment and temperature changes in the pressure bomb due to cold oil being pumped in during pressure increases than to effects in the quartz resonator itself. More careful design to limit the oil volume around the transducer and to preheat the oil during pressure-up will be necessary to demonstrate the full capability of the quartz resonator gauge.

CONCLUSIONS

This article is an interim report on the progress of technology developments for geothermal qualified quartz resonator pressure transducers. The feasibility of such devices is demonstrated in laboratory tests up to 275°C. Major areas under investigation are: crystal characterization at high temperature, design of pressure transducer configurations for geothermal use, and fabrication and bonding for high temperature operation of the crystal and other transducer components.

A vitally important aspect of this development work is the technology transfer to industry and the commercialization of geothermal qualified pressure transducers. For this, the ongoing developments have been closely linked with parallel activities in private industry, where similar transducers and complete tools are built and operated for petroleum logging.

REFERENCES

1. P. A. Witherspoon. "Well Testing, A Recapitulation of the Development," Proceedings, Invitational Well-Testing Symposium, October 19-21, 1977, Berkeley, California. Lawrence Berkeley Laboratory, LBL-7027, published March 1978.

2. H. J. Ramey, Jr., "Petroleum Engineering Well Test Analysis--State of the Art", Proc., Invitational Well-Testing Symposium, October 19-21, 1977. LBL-7027, March 1978.

3. H. E, Karrer and J. Leach, "A Quartz Resonator Pressure Transducer", IEEE Trans. Ind. Elec. and Control Instr. IECI-16, p. 44 (1969).

4. J. Paros, "Digital Pressure Transducers", Measurements and Data, Issue 56, Vol. 10, No. 2, March-April 1976.

5. E. P. EerNisse, "Quartz Resonator Frequency Shifts Arising from Electrode Stress", Proc. 29th Annual Frequency Control Symposium, p. 1 (1975).

6. A. Ballato, E. P. EerNisse, and T. Lukaszck, "The Force-Frequency Effect in Doubly Rotated Quartz Resonators", Proc. 31st Annual Symposium on Frequency Control, p. 8 (1977).

7. E. P. EerNisse, "Rotated X-Cut Quartz Resonators for High Temperature Applications", Proc. 32nd Annual Symposium on Frequency Control (1978).

8. "Standards on Piezoelectric Crystals", Proc. IRE 37, p. 1378 (1949).

NUMERICAL MODELING STUDIES IN WELL TEST ANALYSIS

Chin Fu Tsang, Michael Zerzan, Gudmundur Bodvarsson, Marcelo Lippmann, Donald Mangold, T.N. Narasimhan, Karsten Pruess and Ron Schroeder

Lawrence Berkeley Laboratory
University of California
Berkeley, California 94720

INTRODUCTION

Conventional well test analysis methods are commonly applied to well data from geothermal fields despite the isothermal assumptions of these techniques. At LBL we are involved in a series of studies in which we use numerical models to investigate the effects seen at a well producing from or injecting into a heterogeneous, non-isothermal system. This paper is a progress report on what we have learned. In the next section, the numerical models used for these studies will be briefly discussed. The following section is devoted to the description of and results from different cases studied using these models. Implications for the analysis of geothermal well data in light of these results will also be presented.

Numerical Models Used

In this work we use three reservoir simulators which were developed at LBL. These are a) Terzaghi, b) CCC and C) SHAFT78. They all use a numerical technique known as the Integrated Finite Difference method and are all designed to model complex three-dimensional systems. The first numerical model (Terzaghi) is an isothermal model, while the other two are non-isothermal, i.e. include both heat and fluid flow calculations. The model CCC specializes in liquid phase systems, while SHAFT78 is a two-phase code modeling steam-water flow. The capabilities of these three numerical models are summarized in Figures 1, 2 and 3. Both Terzaghi and CCC have been validated against many analytical solutions. SHAFT78 is a more recent model whose validation will be discussed at the Stanford Workshop (December 1978).

Cases Studied and The Results

A number of cases have been studied using the three numerical models described above. In this section we shall describe them and discuss the results.

Case 1: PUMPING TEST IN A TWO-LAYERED SYSTEM

In this case we studied the effect of a temperature gradient in a two-layered geothermal reservoir system on the pressure distribution. The initial temperature profile of the different layers and their properties are given in Figure 4 and Table 1. The upper and lower constant boundaries were assumed to be closed to fluid flow. A fully penetrating well was placed in the lower aquifer at the center of the system producing at a constant rate of a 100 tonnes per hour. The resulting pressure response was observed in the lower and upper aquifer at a distance of 12.76 meters from the axis. The results obtained from the numerical studies using CCC are given in Figure 5 and Tables 2 and 3.

In the lower pumped aquifer at a node located at a radial distance of 12.76 meters from the axis, the pressure changes in the isothermal and non-isothermal analyses are almost identical, especially at earlier times. The observed drawdowns compare reasonably well to values given by Hantush's[1] analytical solution (for $\beta \approx 5 \times 10^{-3}$), using the same reservoir parameters. Hantush's beta solution (which is valid for small values of time (in our case $t < 1115$ days)) assumes that the flow is horizontal in the lower aquifer and vertical in the shale break. In the upper unpumped aquifer there are some minor differences at early times between the pressure drawdown determined in the non-isothermal and isothermal cases. However, this differenc percentagewise diminishes with time (see Table 3). Reasonable agreement was obtained between the computed drawdowns in the upper aquifer and the corresponding analytical solution of Neuman and Witherspoon[2]. Generally the results indicate that isothermal data analyses of pumping tests performed in non-isothermal systems are warranted under the conditions:

1. The fluid properties used in the analysis should correspond to the averaged values of the producing aquifer.
2. The mass flow should be essentially horizontal in the pumped aquifer towards the producing well.

Case 2: NON-ISOTHERMAL RESERVOIR TEMPERATURE DISTRIBUTION

In this case we assume that areally the reservoir has a hot spot at a center represented by an area with radius 100 meters within which the temperature is 250°C. Outside of this radius the temperature goes down to a 100°C. The pumping test is carried out in a well at the center of the 250°C hot-spot. The pressure change versus the log (time) is plotted in the next figure (Figure 6). From this plot one may notice a normal Theis straight line at early times, then a change in slope is observed as the cold and hot water interface moves towards the wellbore. This break may be mistakenly interpreted as the presence of an imperfect barrier.

Case 3: COLD WATER REINJECTION PRESSURE

There is a practical need to know the reservoir pressure response due to the injection of cold water into a hot geothermal reservoir. In the present study we assume a uniform hot geothermal reservoir in which cold water is injected into a single well. The differences in viscosity and density between hot and cold water are quite significant and cannot be ignored. The results based on numerical model CCC are shown in Figure 7 where the pressure change is plotted against log (t/r^2) where t is the time and r is the radial distance from the well. We have assumed an injection temperature of 100°C and an initial aquifer temperature of 300°C. Thus at early times the pressure change follows the normal Theis solution corresponding to the original reservoir temperature. Then at a later time it begins to take off from the 300°C Theis straight line and follow a line which is parallel to the 100°C Theis line. This is reasonable because at the beginning the observation point in question is surrounded by the hot reservoir water and so the pressure response follows the 300°C reservoir hot water movement. Later on when the cold water front as arrived the fluid mobility has changed to the value corresponding to the lower temperature and consequently the 100°C Theis line will be followed. Hence, at very large times the expected pressure has a slope like the 100°C Theis line, but with a value substantially lower.

Case 4: PRODUCTION-INJECTION-PRODUCTION PROCEDURE

For this case we employed CCC to study the transient pressure response during a production-injection-production sequence. For this analysis a 100-m thick, 1,000-m radially symmetric reservoir is considered. The initial temperature and pressure as given by Figure 8 were used, with a flow rate of 2.5×10^6 kg/day.

The well is first pumped for five days (total time, t = 0-5 days): this is followed by five days of injection of 100°C water (t = 5-10 d); finally the well is pumped for another 15 days (t = 10-25 d). The pressure changes obtained at the center of the reservoir, 1.5 meters from the axis of the system is shown on Figure 9b. The pressure decreases normally during the first pumping period (t = 0-5 d); no temperature changes are observed. During injection the pressure increases as expected (t = 5-10 d); the temperature almost immediately drops as the cold water is injected.

During the final period of production (Figure 9b, t = 10-25 d) the pressure begins falling much faster than during the first period of pumping. Then it stabilizes to a more or less constant pressure value before continuing to decrease. The last part of the curve appears to be a continuation of the curve corresponding to the first pumping period. This response can be explained by studying the temperature and viscosity variation observed during this period (Figure 9a). During almost the first two days of the second pumping period the temperature remains low, then it slowly increases as the hotter water replaces the cold water being produced at the well. On the other hand, the viscosity of the liquid is high at the beginning and then rapidly decreases as the temperature rises.

For the same flow rate, the higher initial values of viscosity result in larger pressure decreases. As the temperature increases, and the viscosity decreases, the pressure stabilizes and then finally begins to drop again as a more or less constant temperature is attained. After about eight days the temperature in the reservoir is similar to that prevailing during the initial pumping period (t = 0-5 d). This explains why for later times the pressure curve for the second production period is almost a continuation of the dashed curve corresponding to the initial period of production (Figure 9b).

If we assume that the pressure during the initial pumping period (t = 0-5 d) are the observed pressures during a normal well test, we can perform a typical constant-temperature Theis well-test analysis. We find that we reproduce the reservoir parameters correctly so long as we use the density and viscosity constant corresponding to the average reservoir temperature. This justifies to a certain extent the application of usual pumping well-test methods to geothermal systems.

On the other hand, as discussed above, a very interesting pressure response curve is found when the well is pumped after a period of injection of colder water. This opens the possibility of using injection-production well tests to establish some of the thermal properties of the reservoir. We are in the process of making such a study.

Case 5: FRACTURED SYSTEMS

Many aquifers possess fractures. The numerical model, Terzaghi, which was developed at LBL, has the capability to model fluid flow through a fractured porous system. Thus the pressure response in a well intercepting fractures may be calculated numerically. To validate such a numerical model we have applied it to a simple case, where a well with a constant flowrate intercepts a vertical fracture. This problem has also been solved analytically by Raghavan[3]. The results are indicated in Figure 10 in a log-log plot. Three sets of calculations were made: the first with an infinite conductivity fracture; the second with finite conductivity fracture, and lastly the case of an infinite conductivity fracture with a 6" diameter well. Thus, the last set of calculations includes not only the effect of the fracture but also the effect of the wellbore storage. As can be seen from this graph the two sets of calculations compared very well with the Raghavan solution where it is applicable. This model will be used to examine more complicated situations where analytical solutions are not available. Examples include cases where the well intercepts more than one fracture and also cases where the fracture may be of varying aperture. Thus reservoir parameters may be estimated in these complicated cases where conventional well test analysis is not applicable.

Case 6: PRODUCTION FROM A TWO-PHASE GEOTHERMAL RESERVOIR

Geothermal systems are often two-phase either initially or after extensive production from an initially liquid system. In order to model the response of a two-phase reservoir, the code SHAFT-78 was developed at LBL. We ran the code on a set of problems simulating the response of a homogeneous reservoir to a constant mass withdrawal when the reservoir was initially uniformly two-phase (saturations of .1, .5, .9). Previous published results by Garg[4] indicate that under these assumptions the total kinematic mobility of the fluid near the wellbore*

$$\left(\left(\frac{K}{\nu}\right)_T \equiv K\left\{\frac{K_\ell}{\mu_\ell}\rho_\ell + \frac{K_v}{\mu_v}\rho_v\right\}\right)$$

can be inferred from a plot of P vs log t, and in fact, if m is the slope of the curve, then

$$\left(\frac{K}{\nu}\right)_T = \frac{2\pi m}{1.15q}$$

where

$$q = \frac{Kg}{m^3 s} \text{ (mass withdrawal rate)}$$

The SHAFT78 simulations were done with parameters tabulated in Table 4. Results are given in Table 5 and the accompanying figures (11, 12, 13). These results confirm the hypothesis. In addition, pressure was plotted as a function of log (t/r^2) and resulted in a straight line curve with slope close to that of the well pressure vs log (t) plot.

This indicates that observation well data could be used to infer $(K/\nu)_T$ in a two-phase system, hence agreement between $(K/\nu)_T$ at an observation well and at the producing well would be evidence that the field was two-phase rather than single phase with flashing near the production well bore.

In addition, saturation vs log (t/r^2) was plotted. As shown in Figure 15, no steep saturation gradients are produced as a result of production. Rather, a diffuse, broad front propagates out with a velocity proportional to $\sqrt{t}$. Changing the relative permeability curves (Figure 14) has a very slight effect on the saturation front, indicating that the result is not sensitive to the parameter governing liquid/steam transport in the simulation and that drawdown at a well in a two-phase system should be seen throughout the system.

The final figure (Figure 16) shows a plot of well head pressure vs log (time) in an initially liquid system. Once again, a straight line developes as exploitation progresses, resulting in a predicted $(K/\nu)_T$ value of .86E-8 (as compared to actual values which range from 1.4E-8 to 1.9E-8).

* Here K is permeability, μ is viscosity, and liquid and vapor phases are denoted by the subscripts ℓ and v respectively.

In addition, the flash front propagates at a velocity proportional to $\sqrt{t}$. However, plots of pressure vs log (t/r^2) result in a family of similar curves generated as each successive element flashes. Consequently qualitatively different pressure responses to the drawdown are found at observation wells located in the two-phase region and observation wells located in the liquid region. This supports the previously stated conclusion that observation well data can be used to distinguish between two-phase and flashing systems.

SUMMARY

In this work we have used numerical modeling to study a series of problems related to well test analysis. By looking at difference schematic cases we demonstrated:

(a) In certain cases effects (such as temperature boundaries) normally not included are important and thus care should be taken when analyzing geothermal well test data.

(b) By making use of numerical modeling more complicated procedures or situations may be analyzed, thus enriching the well test analysis method that can be used.

We are currently continuing with these studies with the hope of establishing new methods of reservoir evaluation.

REFERENCES

1. Hantush, M.S., 1960. "Modification of the Theory of Leaky Aquifers," J. Geophys. Res., v. 65, pp. 3713-3725.

2. Neuman, S.P., and P.A. Witherspoon, 1969. "Transient Flow of Groundwater to Wells in Multiple-Aquifer Systems," Berkeley, Department of Civil Engineering, Inst. Transp. Traffic Eng., University of California Publication 69-1, 182 p.

3. Raghavan, R., 1977. "Pressure Behavior of Wells Intercepting Fractures," Proceedings of First Invitational Well-Testing Symposium, October 19-21, 1977, Lawrence Berkeley Laboratory, LBL-7027, pp. 117-160.

4. Garg, S.K., 1978. "Pressure Transient Analysis for Two-Phase (Liquid Water/Steam) Geothermal Reservoirs," SSS-IR-3568 (R2).

Table 1

PUMPING TEST SIMULATION

Material Properties Used

	LOWER AQUIFER	SHALE BREAK	UPPER AQUIFER	CAPROCK
Intrinsic Permeability (md)	80	0.5	50	0.005
Porosity	.22	.40	.20	.40
Specific Storage (m-1)	10^{-4}	1.6×10^{-3}	10^{-4}	1.6×10^{-2}
Thermal Conductivity cal/sec m°C	10×10^{-3}	7.5×10^{-3}	10×10^{-3}	6.0×10^{-3}
Heat Capacity cal/g°C	0.250	0.230	0.250	0.230

Table 3

PUMPING TESTS SIMULATION - LARGER SYSTEM: PRESSURE DRAWDOWN (IN PASCALS) IN THE UPPER AQUIFER

TIME (days)	ISOTHERMAL (343.6°C)	NONISOTHERMAL
10	2.93×10^{1}	2.74×10^{1}
30	6.32×10^{2}	5.99×10^{2}
100	1.21×10^{4}	1.16×10^{4}
204	4.75×10^{4}	4.62×10^{4}
406	1.20×10^{5}	1.19×10^{5}

Table 2

PUMPING TEST SIMULATION - LARGER SYSTEM; PRESSURE DRAWDOWN IN THE LOWER AQUIFER

	ΔP (PASCALS)			DIMENSIONLESS			
				NUMERICAL		ANALYTICAL	
	NUMERICAL		ANALYTICAL	ISOTHERMAL (343.6°C)			
(days)	Isothermal (343.6°C)	Nonisothermal	Isothermal (343.6°C)	t_D	P_D	t_D	P_D
10	0.1418×10^{6}	0.1422×10^{6}	0.1380×10^{6}	352	3.26	352	3.17
30	0.1599×10^{6}	0.1604×10^{6}	0.1576×10^{6}	1055	3.67	1055	3.62
100	0.1750×10^{6}	0.1756×10^{6}	0.1749×10^{6}	3518	4.02	3518	4.02
406	0.1919×10^{6}	0.1927×10^{6}	0.1915×10^{6}	14270	4.41	14270	4.40

Table 4

RADIAL GRID DIMENSIONS
$\Delta r_1 = \Delta r_2 \;...\; \Delta r_{11} = 1m$
$\Delta r_{12} = 1.2\Delta r_{11} \;...\; \Delta r_{50} = 1.2\Delta r_{49}$
ROCK PROPERTIES
$\rho_{rock} = 2.65 \times 10^3$ kg/m^3
C_{rock} = 1000 J/Kg^{o}C
K_{rock} = 5.25 W/m^{o}C
Permeability = 10^{-13} m^2 (100 millidarcy)
Porosity = .2

Table 5

RESULTS FOR TOTAL KINEMATIC MOBILITIES $(k/\nu)_t$

INITIAL SATURATION (S_o) and PRESSURE (P_o)	$(k/\ )_T$ FROM P vs LOG (t) PLOT	$(k/\ )_T$ FROM P vs LOG (t/r^2) PLOT	TIME (SEC)	ACTUAL VALUE OF $(k/\ )_T$
P_o = 8.5 MPa S_o = .9	2.2146×10^{-7}	2.4265×10^{-7}	0. 1889. 7490. 10184.	2.3117×10^{-7} 2.2119×10^{-7} 2.2154×10^{-7} 2.2105×10^{-7}
P_o = 8.6 MPa S_o = .5	1.1610×10^{-7}	1.2266×10^{-7}	0. 3775. 7033. 19268. 45883.	1.2633×10^{-7} 1.1596×10^{-7} 1.1479×10^{-7} 1.1404×10^{-7} 1.1314×10^{-7}
P_o = 8.6 MPa S_o = .1	3.8239×10^{-7}	4.161×10^{-7}	0. 2336. 19327. 76549. 142060. 217406	5.5535×10^{-7} $4.-947 \times 10^{-7}$ 3.9253×10^{-7} 3.8568×10^{-7} 3.7956×10^{-7} 3.7866×10^{-7}

TERZAGHI

- THREE-DIMENSIONAL SIMULATION OF FLUID FLOW IN HETEROGENEOUS SYSTEM WITH COMPLEX GEOMETRY.
- USE INTEGRATED-FINITE-DIFFERENCE NUMERICAL TECHNIQUE.

CAN HANDLE:

POROUS-FRACTURE MEDIA

FRACTURE MEDIA

WELL BORE STORAGE

MATERIAL PROPERTIES DEPENDING ON STATE OF STRESS

Figure 1

SHAFT78

"SIMULTANEOUS HEAT AND FLUID TRANSPORT"

- THREE-DIMENSIONAL, STEAM-WATER, NON-ISOTHERMAL FLOW THROUGH POROUS MEDIA WITH COMPLEX GEOMETRY.
- EMPLOYS INTEGRATED-FINITE-DIFFERENCE METHOD.

CAN SIMULTANEOUSLY HANDLE:

1. CONDUCTION, TWO-PHASE FLOW IN AQUIFER SYSTEM.
2. TEMPERATURE DEPENDENCE OF ROCK AND FLUID PROPERTY PARAMETERS.
3. GRAVITATION EFFECTS.
4. SPATIAL VARIATION IN AQUIFER PROPERTIES.
5. INJECTION AND WITHDRAWAL.

Figure 3

CCC

CONDUCTION-CONVECTION-CONSOLIDATION

NUMERICAL MODEL (LAWRENCE BERKELEY LABORATORY)

MODELS 3-D WATER-SATURATED POROUS SYSTEMS

SOLVES FLUID AND HEAT EQUATIONS SIMULTANEOUSLY BY IFD (INTEGRATED FINITE DIFFERENCE METHOD)

CALCULATES CONSOLIDATION USING 1-D THEORY OF TERZAGHI

CAN HANDLE:

1. HEAT CONDUCTION AND CONVECTION BETWEEN RESERVOIR, CAPROCK AND BEDROCK.
2. FLOW OF WATERS OF DIFFERENT TEMPERATURES.
3. REGIONAL GROUND-WATER FLOW.
4. SPATIAL VARIATIONS OF AQUIFER PROPERTIES.
5. TEMPERATURE AND PRESSURE DEPENDENCE OF ROCK AND FLUID PROPERTIES.
6. VERTICAL CONSOLIDATION OF SATURATED FORMATIONS (DEFORMATION MAY BE NON-LINEAR AND NON-ELASTIC).
7. DIFFERENT BOUNDARY CONDITIONS.
8. GRAVITATION EFFECTS.

Figure 2

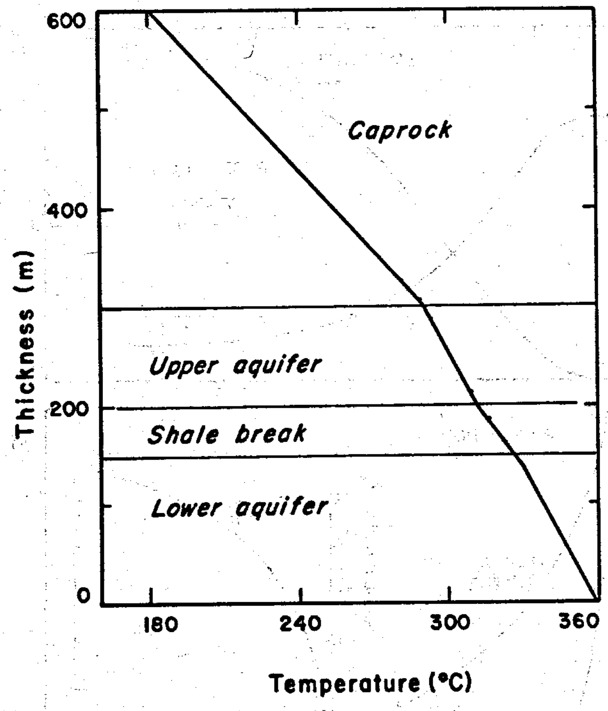

XBL 789-2079

Fig. 4. Two-layer system.

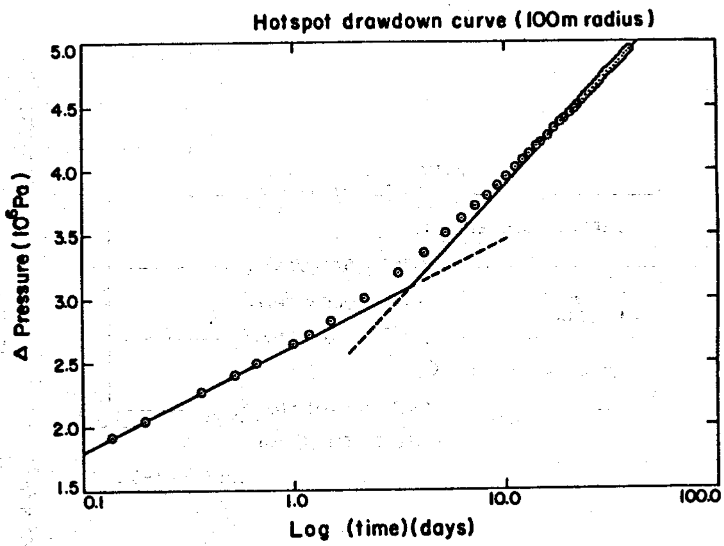

XBL 794-7398

Fig. 6. Hotspot drawdown curve (100 m radius).

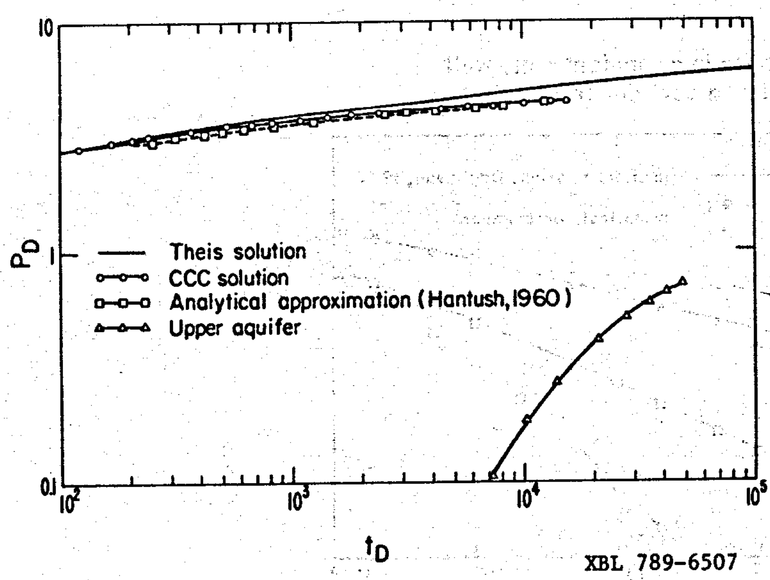

XBL 789-6507

Fig. 5. Two-layer system.

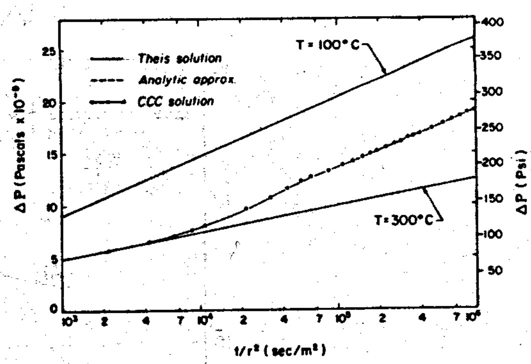

XBL 789 2077

Fig. 7. Pressure response for cold water injection.

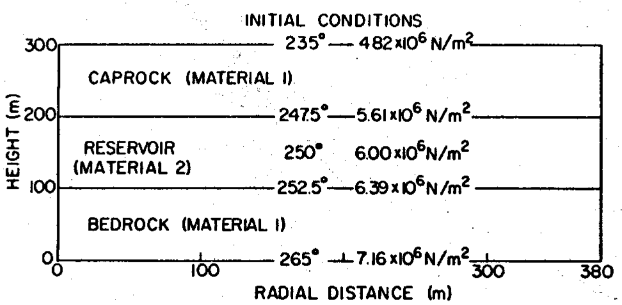

XBL 773-5213

Fig. 8. Production-injection-production.

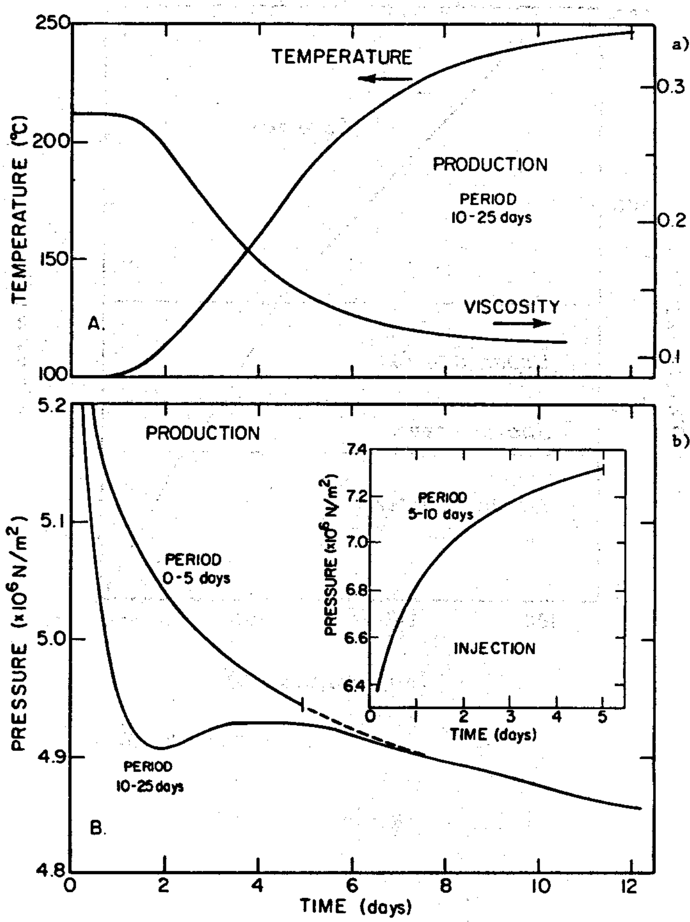

XBL 773-5217

Fig. 9. Production-injection-production simulation.

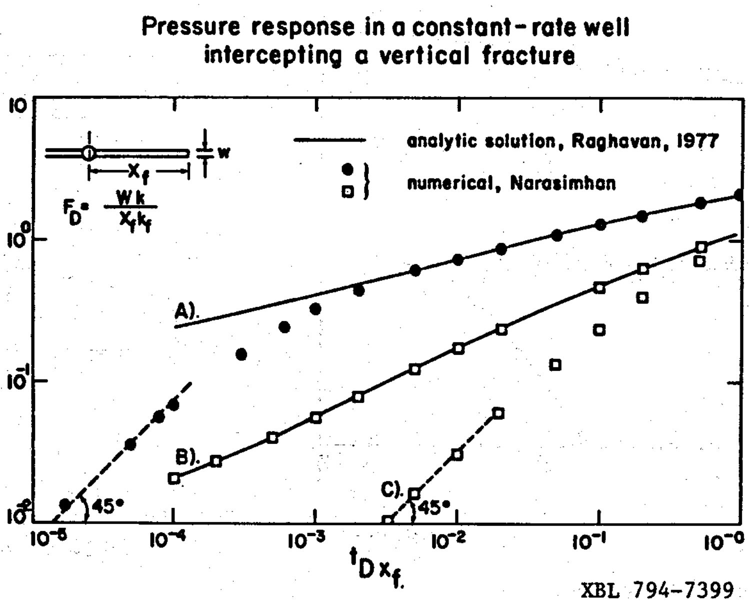

XBL 794-7399

Fig. 10A). Finite conductivity fracture; 10B) Infinite conductivity fracture; 10C) Infinite conductivity fracture with a 6" diameter well.

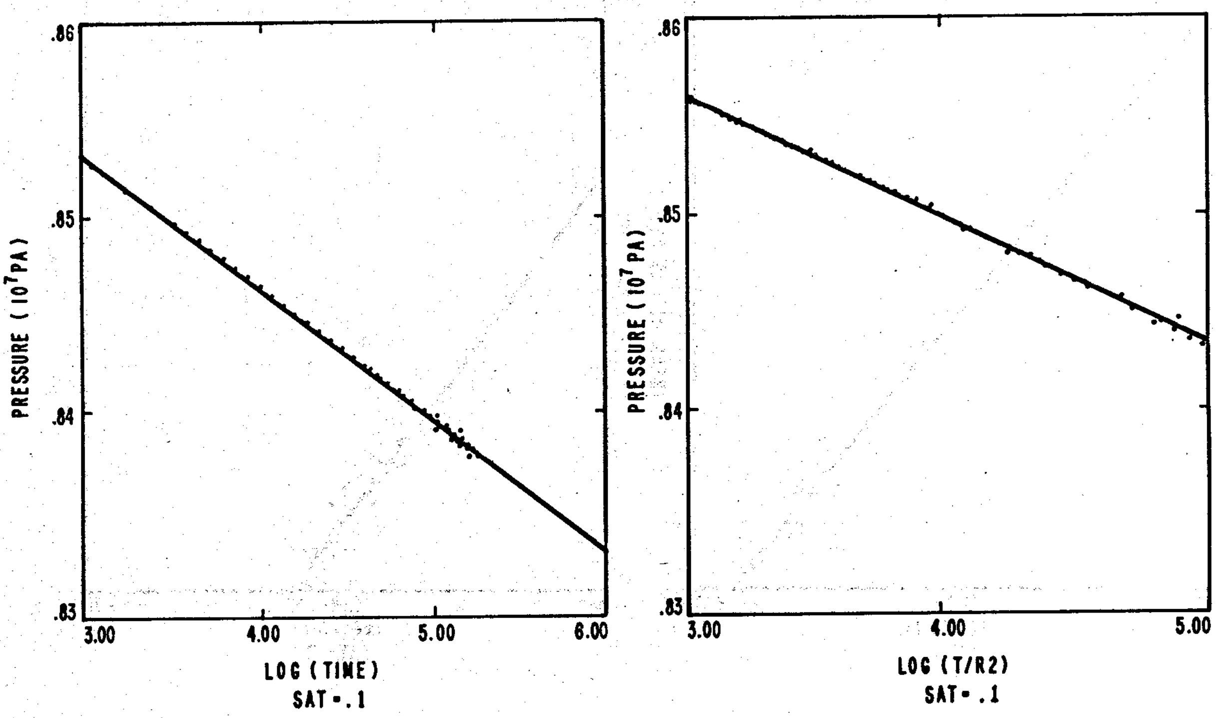

Fig. 11. Production drawdowns from a two-phase reservoir.

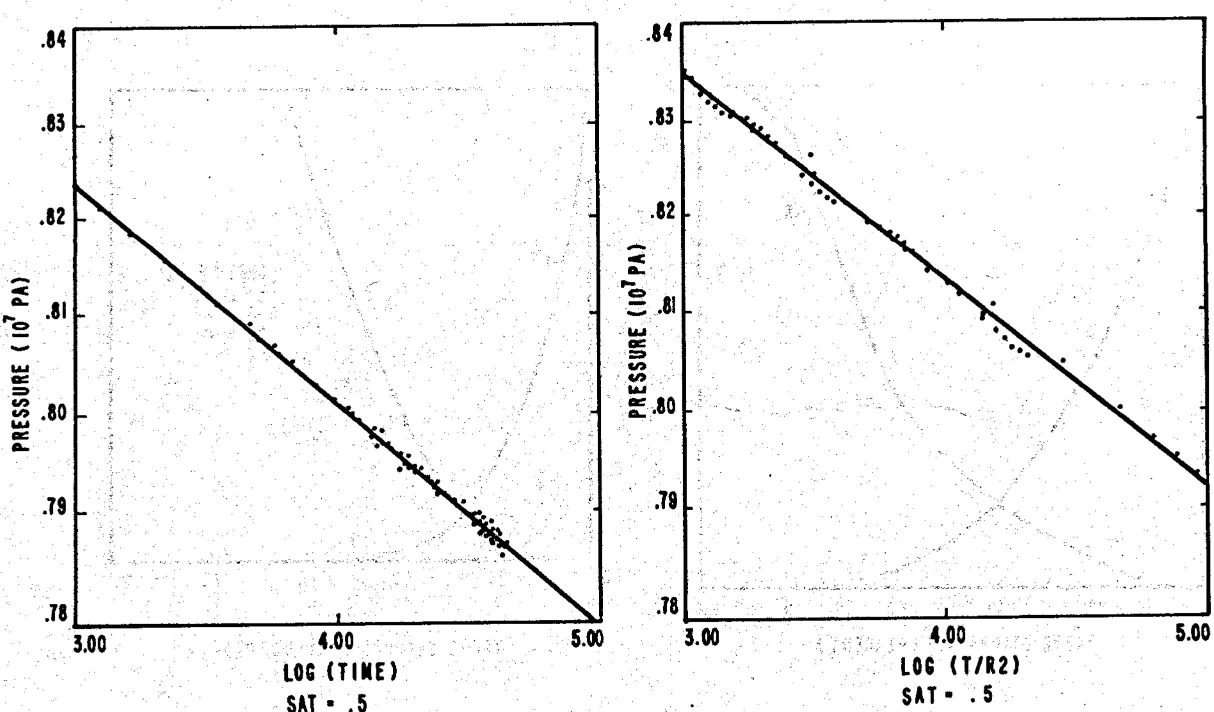

XBL 794-7396

Fig. 12. Production drawdowns from a two-phase reservoir.

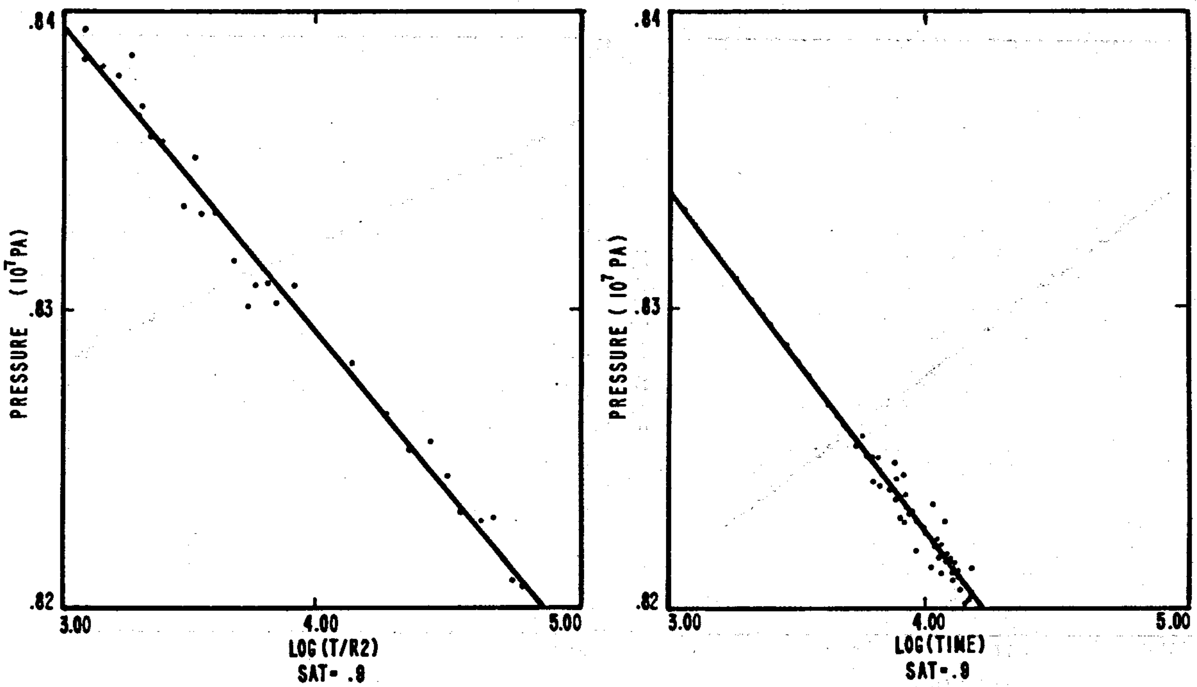

Fig. 13. Production drawdowns from a two-phase reservoir.

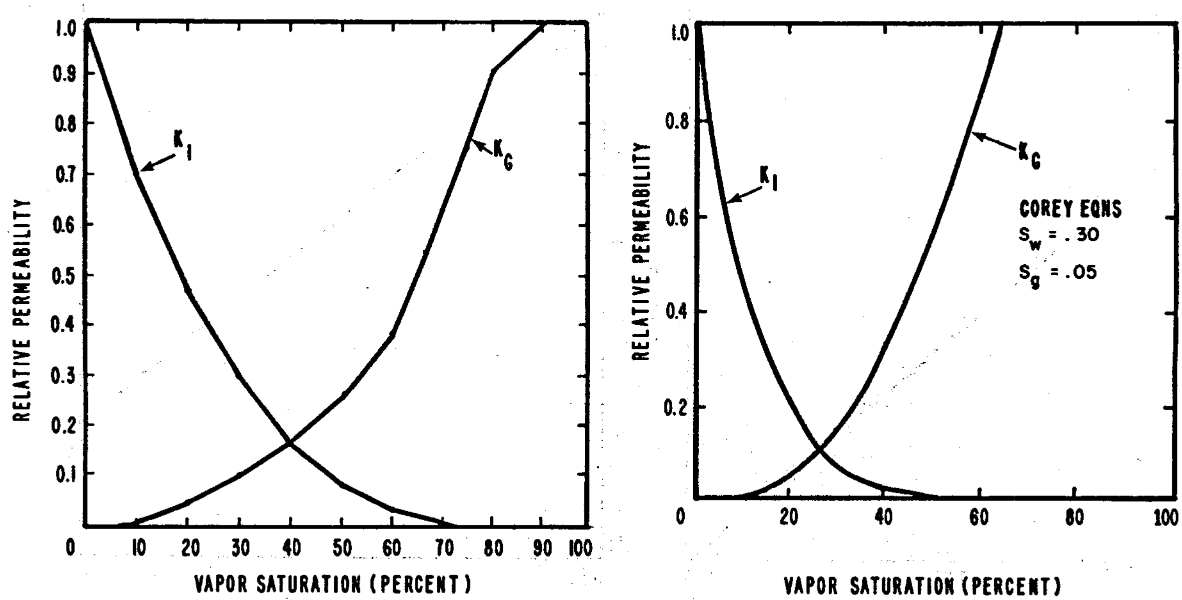

XBL 793-7395

Fig. 14. Relative permeability curves for water/steam.

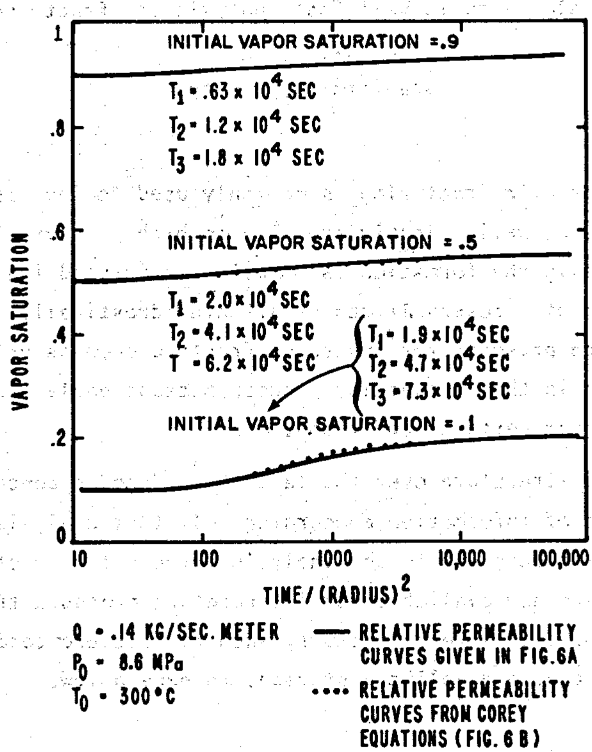

Fig. 15. Saturation profiles during production from a two-phase reservoir.

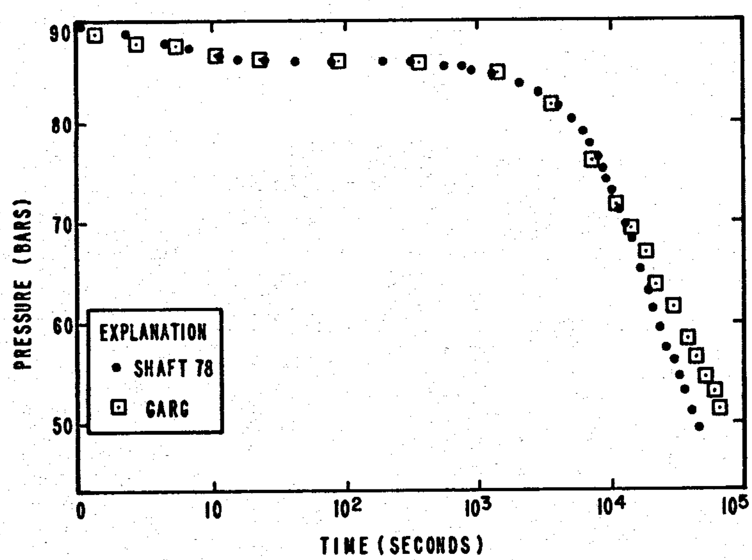

XBL 794-7397

Fig. 16. Production drawdown from a flashing reservoir.

Recent Developments in Well Test Analysis for Fractured Wells

H. Cinco-Ley
Stanford University

Hydraulic fracturing is commonly used to increase well productivity or well injectivity. Due to high pressure in injection wells the formation is sometimes fractured inadvertently. The behavior of a reservoir can be affected drastically if fractures are present; for instance, fracture compass orientation is a key factor in the reinjection process because early breakthrough may occur under certain conditions.

The literature over the last three decades contains a large amount of information concerning well test analysis, with special attention given to the analysis methods for fractured wells. Techniques are now available for interpreting pressure transient data influenced by several factors, such as fracture conductivity, fracture damage, and wellbore storage, to name a few.

PRESSURE FIELD PROPAGATION AND DENSITY CURRENTS

Gunnar Bodvarsson
School of Oceanography
Oregon State University

The injection of fluids into the subsurface results in pressure and flow transients which propagate through the formations. At moderate pressure amplitudes, the pressure field propagation in Darcy type porous media is governed by the well known simple diffusion equation with the diffusivity $a = b/\mu c$ where b is the permeability of the formation, μ the absolute viscosity of the fluid and c the total compressibility of the fluid saturated formation. The primary physical parameter involved in the diffusion of pressure fields of angular frequency ω in such media is the skin depth that is given by $d_s = (2b/\mu c\omega)^{\frac{1}{2}}$.[1]

The propagation of pressure fields with wave numbers k in a single fluid filled plane fracture of width h, where the inequality hk<<1 is satisfied, is governed by the equation

$$\rho(1 + \kappa hS)(\partial_{tt} + R\partial_t)p - hS\nabla_2^2 p = S(\partial_t + R)f \qquad (1)$$

where p is the fluid pressure in the fracture, ρ the density of the fluid, κ the compressibility of the fluid, R a resistance operator, S the stiffness operator for the half-space bounding the fracture, f is a source term and $-\nabla_2^2$ is the two-dimensional Laplacian. In the case of laminar flow regimes $R = 12\nu/h^2$, where ν is the kinematic viscosity of the fluid, and for Hookean half-spaces of infinite extent, the stiffness operator is defined by the somewhat unusual expression

$$S = (G/2(1-\sigma))(-\nabla_2^2)^{\frac{1}{2}} \qquad (2)$$

where G is the shear modulus, and σ the Poisson ratio of the material.

Considering the homogenous form of equation (1), pressure fields of wavelength L and assuming that

$$h \ll (1-\sigma)L/\pi\kappa G, \qquad (3)$$

such that the compressibility of the fluid can be neglected, we can distinguish between two different types of regimes of pressure propagation. In the case of oscillating fields with the angular frequency ω, the condition

$$\omega \ll 12\nu/h^2 \qquad (4)$$

implies a resistance dominated or diffusive field propagation with the skin depth

$$d = h[G/3\mu\omega(1-\sigma)]^{1/3} \qquad (5)$$

whereas, on the other hand, the condition

$$\omega \gg 12\nu/h^2 \qquad (6)$$

implies an inertia dominated wave propagation with the phase velocity

$$v = [hkG/2\rho(1-\sigma)]^{\frac{1}{2}}. \qquad (7)$$

Moreover, assuming that both (3) and (4) hold, equation (1) can be simplified to

$$\partial_t p - (h/\rho R)S\nabla_2^2 p = (1/\rho)Sf \qquad (8)$$

which is a diffusion type equation for the pressure field.

Density currents are of particular interest in Darcy type porous media. Consider the case of a fluid-saturated half-space at temperature T containing a spherical thermal anomaly at zero temperature. This situation can result from the injection of cold water into the half-space. Because of gravity, the spherical anomaly will sink with an initial velocity (SI-units) of

$$w = 2\alpha bgTC_f/C_r(\nu_i + \nu_e) \qquad (9)$$

where α is the thermal expansivity of the fluid, g the acceleration of gravity, C_f and C_r the volume heat capacities of the fluid and rock formations respectively, and ν_i and ν_e are the kimematic viscosities of the fluid inside respectively outside the thermal anomaly. The spherical anomaly will be deformed during descent.

Reference

[1]Bodvarsson, G., 1970. Confined fluids as strain meters. J. Geophys. Res. 75(14):2711-2718.

PRESSURE TRANSIENT ANALYSIS FOR GEOPRESSURED GEOTHERMAL WELLS

S. K. Garg, T. D. Riney and J. W. Pritchett
Systems, Science and Software
P. O. Box 1620
La Jolla, California 92038

ABSTRACT

Analytical solutions presently exist which form the basis for practical analysis of pressure transient data from isothermal single-phase (water, oil) and isothermal two-phase (oil with gas in solution, free gas) reservoir systems. A numerical model embodying the important mechanisms operating in geopressured geothermal reservoir systems has been applied in a series of parametric calculations simulating well drawdown/buildup to assess the applicability of the classical petroleum engineering/hydrology analysis procedures to geopressured systems. More specifically, the effects of irreversible formation compaction and methane saturation (and the associated changes in porosity, absolute permeability and/or total mobility) are studied. It is found that conventional well test analysis may be expected to yield reliable formation permeability (or mobility) data even when compaction occurs and methane evolves out of solution, but storativity estimates will be unreliable. Drawdown and buildup test data together can be used to diagnose irreversible compaction response of the formation.

INTRODUCTION

Geopressured strata underlie a band along the Gulf Coast of the United States about 750 miles long from the Rio Grande to the Mississippi estuaries which extends about 50-100 miles inland and a similar distance offshore (Fig. 1). The zone in which geopressures are most commonly found begins at a depth of about 10,000 feet and extends downward to about 50,000 feet. These strata contain undercompacted clays and sandstones, with interstitial fluids bearing the bulk of the total overburden pressure. The fluid pressure is generally well in excess of hydrostatic. Further, these waters are at elevated tempeatures and the high pressure, high temperature pore water is generally believed to be saturated with dissolved natural gas (principally methane).

The geopressured zones contain an enormous amount of energy in three forms:

1. Thermal energy in the fluid and sediments.
2. Mechanical energy in the geopressured fluid.
3. Chemical energy in the natural gas.

If only a small fraction of the total energy resource is economically recoverable, the geopressured zones would still represent a potentially enormous energy source.

The U. S. Department of Energy has undertaken an extensive deep drilling and well testing program to help evaluate the geopressured energy resource. Over 20 wells are planned for Texas and Louisiana sites during the next few years. The first of these, in Brazoria County, Texas, is currently being drilled and well test data should become available in early 1979.

In preparation for these data, Systems, Science and Software (S^3) has performed well test simulation studies to determine whether classical well test analysis techniques are likely to be applicable to geopressured reservoirs. This paper will present the results of these preliminary studies.

BACKGROUND

In petroleum engineering and groundwater hydrology, well tests are routinely conducted to diagnose the well's condition and to estimate formation properties. A major concern of well testing is the interpretation of pressure transient data. Practical procedures presently exist for analyzing pressure transient data from isothermal single-phase (water, oil) and isothermal two-phase (oil with gas in solution, free gas) systems.[2,3] The assumption of isothermal flow invoked in these analyses is justified for the testing of geopressured wells. However, a second major assumption invoked is that the formation compaction is small enough such that any associated changes in formation thickness and permeability may be neglected. This assumption is most likely inappropriate for geopressured systems. It is generally believed that geopressured reservoirs contain undercompacted sandstones/shales which will undergo substantial (and possibly irreversible) compaction upon fluid production; the formation compaction will be accompanied by significant changes in porosity and permeability. We will present a series of drawdown/buildup calculations designed to assess the applicability of classical petroleum engineering/hydrology procedures to geopressured systems; more specifically, we will examine the effects of irreversible formation compaction and changes in porosity and permeability. Before presenting the calculations, we will review the classical theory and its possible extension to geopressured formations.

CLASSICAL THEORY

We consider a fully penetrating well located in the center of an infinite reservoir of thickness h. We will neglect any variations in either formation or fluid properties in the vertical direction (this is a common assumption in pressure transient analysis). The geopressured reservoir may either be single-phase (liquid water with or without

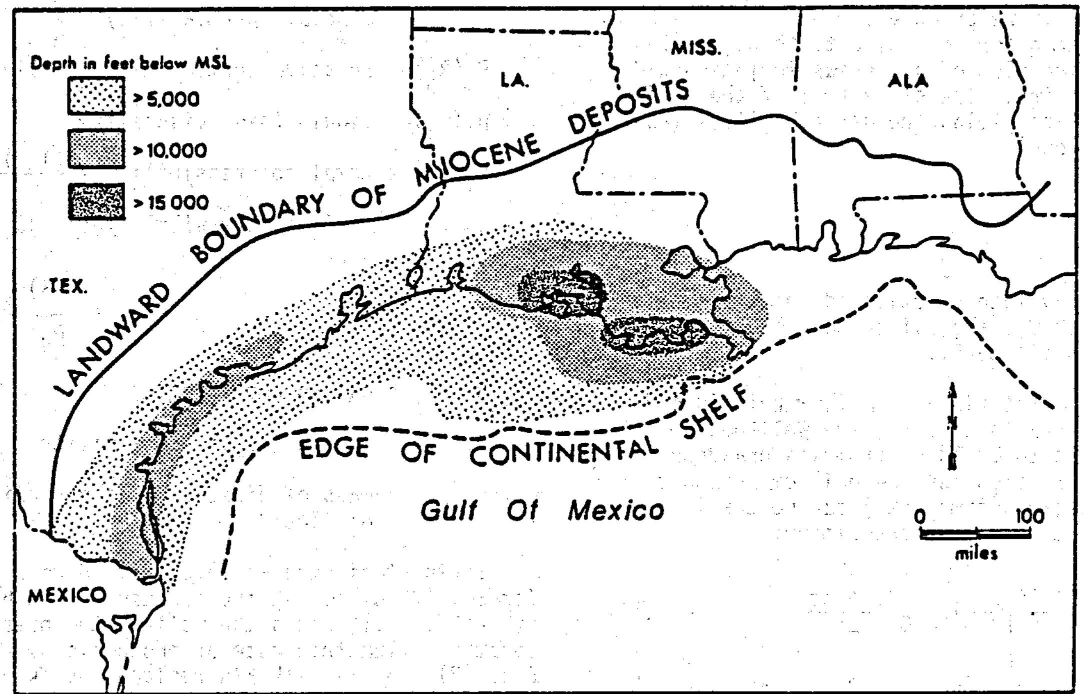

Figure 1. Geopressured zone in Miocene deposits, northern Gulf of Mexico basin [from Jones, 1975].[1]

dissolved gas), or two-phase (liquid water with dissolved gas, and free gas).

Single-Phase Flow

We shall consider the isothermal flow of a liquid of small compressibility. Assuming that (1) the pressure gradients are small, (2) the liquid has constant viscosity and (3) the formation has constant compressibility, and constant and horizontally isotropic permeability, the governing equation for radial Darcian flow can be written as follows:[2]

$$\frac{\partial^2 p}{\partial r^2} + \frac{1}{r}\frac{\partial p}{\partial r} = \frac{\phi\mu}{k} C_T \frac{\partial p}{\partial t} \qquad (1)$$

where

C_f = fluid compressibility

C_m = formation compressibility

C_T = total compressibility = $\frac{(1-\phi)}{\phi} C_m + C_f$

k = permeability

p = pressure

r = radius

t = time

ϕ = porosity

μ = fluid viscosity

We are interested in the solution of Eq. (1) for the case of flow into a fully penetrating well (located in an infinite reservoir of thickness h) at a constant volumetric rate of production (q). The basic solution for constant rate of production in conjunction with the principle of superposition, can be made to yield solutions for arbitrary rate histories. In this case, the solution for the well-bottom pressure (p_w) at an instant of time t after the start of the production at constant rate q can be expressed as:

$$p_w = p_i + \frac{q\mu}{4\pi\ kh}\left\{Ei\left(-\frac{\phi\mu C_T r_w^2}{4kt}\right)\right\} \qquad (2)$$

where

$$-Ei\,(-z) = \int_z^\infty \frac{e^u}{u}\,du.$$

For $\frac{4kt}{\phi\mu C_T r_w^2} > 100$, Eq. (2) is closely approximated by

$$p_w = p_i - \frac{1.15\ q\mu}{2\pi\ kh}\left[\log_{10}\frac{kt}{\phi\mu C_T r_w^2} + 0.351\right]. \qquad (3)$$

Equation (3) forms the basis of many well data interpretation techniques, e.g., pressure drawdown and buildup tests.

Drawdown. If we produce the well at constant volumetric rate q for some time t, then Eq. (3) implies that the plot of p_w versus $\log_{10}t$ should be a straight line. The slope (m_d) of the semi-log straight line yields the permeability k (assuming h is known):

$$k = \frac{1.15\ q\mu}{2\pi h\ m_d}\ . \tag{4}$$

Equation (3) may then be utilized to determine the storativity ($\phi h\ C_T$) and, if ϕ and h are known, total compressibility C_T.

Buildup. If at time t the flow rate is suddenly dropped from q to zero, the well-bottom pressure begins to build up from its drawdown value. An expression for the buildup pressure during this period (time > t) can be easily obtained from Eq. (3) by superposition:

$$p_w = p_i - \frac{1.15\ q\mu}{2\pi\ kh} \log_{10} \frac{t + \Delta t}{\Delta t} \tag{5}$$

where t denotes the buildup time. Equation (5) implies that a plot of p_w versus $\log_{10}[(t+\Delta t)/\Delta t]$ (usually called a Horner plot) should be a straight line. Let m_b be the slope of this straight line; then we have

$$k = \frac{1.15\ q\mu}{2\pi h\ m_b}\ . \tag{6}$$

In the limit $(t+\Delta t)/\Delta t \rightarrow 1$ (very large buildup times), Eq. (5) implies that $p_w \rightarrow p_i$ from below. For the sake of clarity, we shall denote this limit by p^*. Note that $p^* = p_i$ only for infinite reservoirs; for finite reservoirs p^* is in general different from p_i.

Two-Phase Flow

A theoretical framework for analyzing isothermal multiphase pressure tests in oil/gas reservoirs was developed by Martin.[4] Assuming that (1) the liquid and the (free) gas have constant but small compressibilities, (2) pressure and gas saturation gradilents are small, (3) the capillary pressure is negligible and relative permeabilities depend only upon the gas satuation, (4) the liquid and the gas have constant viscosities, and (5) the formation has constant compressibility, and constant horizontally isotropic permeability, the governing equation for radial Darcian flow can be written as:

$$\frac{\partial p}{\partial t} = \frac{(k/\mu)_T}{\phi\ C_T} \left[\frac{1}{r}\frac{\partial p}{\partial r} + \frac{\partial^2 p}{\partial r^2}\right] \tag{7}$$

where

$$(k/\mu)_T = k\left[\frac{R_\ell}{\mu_\ell} + \frac{R_g}{\mu_g}\right] = \text{total mobility.}$$

k = absolute permeability

$R_\ell(R_g)$ = relative permeability for liquid (gas)

$\mu_\ell(\mu_g)$ = liquid (gas) viscosity

C_T = total compressibility = $\frac{(1-\phi)}{\phi} C_m + C_f$

C_f = fluid compressibility $=(1-S)C_\ell+SC_g + \frac{(1-S)\rho_\ell}{\rho_g}\frac{\partial\alpha_\ell}{\partial p}$

S = gas volume fraction

$C_\ell(C_g)$ = liquid gas compressibility

α_ℓ = mass of dissolved gas per unit mass of liquid.

It is straightforward to write down solutions for Eq. (7) by noting the correspondence between it and Eq. (1). Thus the well-bottom pressure for constant volumetric rate of production is given by Eqs. (2) and (3) with k/μ replaced by $(k/\mu)_T$. The interpretation of pressure drawdown and buildup data for single-phase flow also carry over to the two-phase case with this substitution.

POSSIBLE EXTENSION OF THEORY

Application of the classical theory to wells drilled in geopressured strata requires special considerations of four characteristics of geopressured systems that may violate the assumptions on which the theory is based.

1. Formation compressibility (C_m) is very large.
2. Finite changes in porosity and, hence, permeability may be expected, i.e., $k = k(\phi)$ rather than a constant.
3. Formation compressibility may be different on loading ($\partial p/\partial t < 0$) and unloading ($\partial p/\partial t > 0$).
4. Two-phase flow effects are not well defined. The solubility of methane at the temperatures, pressures and salinities occurring in geopressured strata is uncertain and data governing the relative permeabilities of the gas and liquid components of the fluid are unavailable.

The objective of this study is to investigate the extent to which classical well test interpretation techniques may be applied to geopressured systems in spite of these special problems.

A possible extension of the classical theory may be readily obtained if we assume the irreversible compressibility of the formation is bilinear:

$$C_m = C_{mL} \text{ for } \partial p/\partial t < 0$$
$$= C_{mU} \text{ for } \partial p/\partial t > 0$$

and, for the time being, ignore the other three special characteristics of geopressured systems. Then the interpretation of pressure drawdown data is unchanged except C_m is replaced by C_{mL}. If we further assume that formation compressibility during buildup is given by C_{mU} throughout the reservoir (this is not strictly true as pore pressure may be declining in parts of the reservoir distant from the borehole), the bottom-hole pressure can be approximated by:

$$p_w = p_i + \frac{1.15\ q\mu}{2\pi\ kh} \log_{10} \frac{C_{TL}}{C_{TU}} - \frac{1.15\ q\mu}{2\pi\ kh} \log_{10} \frac{t+\Delta t}{\Delta} \quad (8)$$

where

$$C_{Tj} = \frac{1-\phi}{\phi} C_{mj} + C_f,\ j = L,U.$$

Equation (8), like Eq. (5), implies that the formation permeability k is given by Eq. (6). Given the initial pressure p_i, and the slope m_b, Eq. (8) may be solved to yield the ratio C_{TL}/C_{TU}. We shall show in the following that estimates for C_{TL}/C_{TU} obtained in this manner are only approximate due to the assumptions involved (i.e., use of C_{mU} to characterize formation compressibility during buildup, superposition in deriving Eq. (8) and ignoring the other special nonlinear effects in geopressured systems).

We note that as $(t + \Delta t)/\Delta t \to 1$ (very large buildup times), Eq. (8) implies that

$$p_w \to p^* = p_i + m_b \log_{10} \frac{C_{TL}}{C_{TU}} > p_i \quad (9)$$

rather than $p_w \to p^* = p_i$ from below as was the case for reversible compressibility. This will be shown to be a useful diagnostic for detecting irreversible formation compressibility from well test data.

In order to investigate the applicability of this extension of the theory to analyze pressure transient data in the presence of nonlinear formation behavior and two-phase flow effects characteristics of geopressured strata, the S^3 computer model MUSHRM was exercised in its one-dimensional radial mode for a series of calculations designed to simulate pressure drawdown and buildup tests. MUSHRM includes treatment of all of the important fluid/rock response mechanisms, and their interactions, that are believed to be operative in Gulf Coast geopressured reservoirs. A detailed presentation of the theoretical formulation upon which the geopressured reservoir version of MUSHRM is based and the numerical procedures it employs is provided elsewhere.[5] The pressure drawdown and buildup histories simulated with MUSHRM include treatment of all four of the characteristics of geopressured systems listed above. The calculated histories represent simulated experiments against which the applicability of the extended interpretation techniques will be investigated.

DESIGN OF SIMULATED WELL TESTS

In the MUSHRM calculations, large variations in formation compressibility are treated by using an incremental relationship to calculate changes in porosity with pore pressure. For the bilinear case,

$$\frac{\partial\phi}{\partial t} = (1-\phi_0)\ C_{mj} \frac{\partial p}{\partial t},\ j = L,\ U. \quad (10)$$

Finite changes of permeability with the large changes in porosity, $k = k(\phi)$, are represented by the Carman-Kozeny relation:

$$k = k_0 \left(\frac{\phi}{\phi_0}\right)^3 \left(\frac{1-\phi_0}{1-\phi}\right)^2 . \quad (11)$$

The finite difference method used in MUSHRM provides the required radial resolution of the pressure history thoughout the reservoir so that C_{mL} is used in regions undergoing loading ($\partial p/\partial t < 0$) and C_{mU} is used in regions undergoing unloading ($\partial p/\partial t > 0$).

The equation of state used for calculating the thermodynamic behavior of water-methane mixtures has been described elsewhere.[5] Because of the unavailability of relative permeability data for geopressured systems, two formulations were utilized in the calculations involving two-phase flow. One formulation, the Corey equations, assumes no gas flows until a critical saturation is exceeded,

$$R_\ell = (S_\ell^*)^4$$

$$R_g = (1 - S_\ell^*)^2\ (1 - S_\ell^{*2}) \quad (12)$$

where

$$S_\ell^* = (S_\ell - S_{\ell r})/(1 - S_{\ell r} - S_{gr})$$

$$S_\ell = 1 - S$$

$$S_{\ell r} = 0.3,\ S_{gr} = 0.05.$$

The second, a hybrid formulation, assumes free gas flow at any gas saturation (S > 0),

$$R_\ell = \left\{\frac{1 - S - S_{\ell r}}{1 - S_{\ell r}}\right\}^4 \text{ for } 1 - S > S_{\ell r}$$

$$= 0 \text{ otherwise} \quad (13)$$

$$R_g = S^2/(1 - S_{\ell r})^2 \text{ for } 1 - S > S_{\ell r}$$

$$= 1 \text{ otherwise.}$$

The reservoir rock is taken to be a sandstone with the following properties:

Rock grain density ρ_r = 2.65 gm/cm^3

Initial rock porosity = ϕ_0 = 0.2

Rock grain thermal conductivity κ_r = 5.25×10^5 ergs/sec-cm°C

Rock heat capacity c_r = 10^7 ergs/gm°C

Compressibility C_{mL} = 1.754 × 10^{-10} cm^2/dynes for $\frac{\partial p}{\partial t} < 0$

C_{mU} = variable (see Table 1) for $\frac{\partial p}{\partial t} \geq 0$

Absolute permeability k_0 (at $\phi = \phi_0$) = 0.2 × 10^{-9} cm^2 (∿ 20 md)

Formation thickness h = 5,000 cm.

The initial formation temperature is 150°C and the initial pore fluid pressure is 750 bars. Pressure drawdown and buildup histories were simulated forthe seven cases listed in Table 1. The pore fluid is assumed to be pure water for four cases (single phase flow); the other three cases treat pore fluids consisting of water/methane mixtures and involve two-phase flow (liquid water with dissolved methane, free methane gas). One calculation is designed to validate the classical interpretation methods against simulated well test data for characteristics typical of normally pressured formations (Case 1). Three simulations test the applicability of the extended theory for formations exhibiting irreversible formation compressibility (Case 2), porosity-dependent permeability (Case 3), and both variable compressibility and variable permeability (Case 4). Three simulations test the applicability of the extended theory when two-phase flow occurs under different assumptions for the gas mobility (Cases 5, 6 and 7).

SIMULATED WELL TEST ANALYSIS

The mass withdrawal rate in the simulated well tests is assumed to be 70 kg/sec (i.e., 14 gm/sec-cm over the formation thickness) for t < ∿ 1800 sec and 0 kg/sec for t > ∿ 1800 sec. The MUSHRM calculations used a radial grid with finer zoning near the wellbore (effective well radius of 13 cm). A detailed description of the zoning is presented elsewhere.[6]

In Case 1 (Base 1-Phase) the formation is assumed to exhibit identical compaction behavior during loading and unloading, and the permeability is taken to be independent of porosity; note that these are also the assumptions involved in deriving Eqs. (2), (3) and (5). The drawdown and buildup simulated histories for this case are shown in Figs. 2 and 3, respectively; the permeability values (18.9 × 10^{-11} cm^2 and 19.3 × 10^{-11} cm^2) inferred (assuming h = 5,000 cm; $\dot{M}$ = 70 kg/sec, ρ = 0.954 gm/cm^3, μ = 0.198×10^{-2} poise) are in reasonable agreement with the actual value of 20 × 10^{-11} cm^2. At least a part of the difference between the inferred and actual values is caused by changes in porosity (ϕ) and, hence, formation thickness h during the simulated drawdown/buildup. For example, during drawdown, porosity changes from 0.2 at t = 0 sec to 0.184 at t ∿ 1800 sec; this implies that h ($\Delta h/h = \Delta\phi/1-\phi$) decreases by approximately 2 percent. As remarked earlier, given k, Eq. (3) may be utilized to determine the total compressibility; the value of total compressibility obtained in this manner (∿ 7.95×10^{-10} cm^2/dynes) is also in satisfactory agreement with the actual value of 7.49×10^{-10} cm^2/dynes. Extrapolation of the straight line in Fig. 3 to $(t + \Delta t)/\Delta t = 1$ yields p* ∿ 748 bars; the slight difference between p* and p_i (= 750 bars) is due to the inapplicability of the semi-log approximation in the vicinity of $(t + \Delta t)/t = 1$. It is also worth noting here that the simulated buildup data lie above the straight line as $(t + \Delta t)/\Delta t \to 1$.

The next simulation, Case 2 (C-variable), treats a formation that exhibits irreversible compaction. In this case, the formation compressibility during loading (C_{mL}) and all other physical

Table 1. Parametric well test simulations (p_i = 750 bars, T_i = 150°C, C_{mL} = 1.754 × 10^{-10} cm^2/dynes).

Simulation	C_{mL}/C_{mU}	k	% CH_4	$S_{g,i}$	R_ℓ, R_g
#1 Base 1-Phase	1	k_0	0	---	---
#2 C-Variable	2	k_0	0	---	---
#3 k-Variable	1	$k(\phi)$	0	---	---
#4 C,k-Variable	2	$k(\phi)$	0	---	---
#5 Base 2-Phase	1	k_0	0.75	0.0058	Corey (S_{gr} = 0.05)
#6 High $S_{g,i}$	1	k_0	0.90	0.049	Corey (S_{gr} = 0.05)
#7 High R_g	1	k_0	0.61	0.0001	Hybrid (S_{gr} = 0)

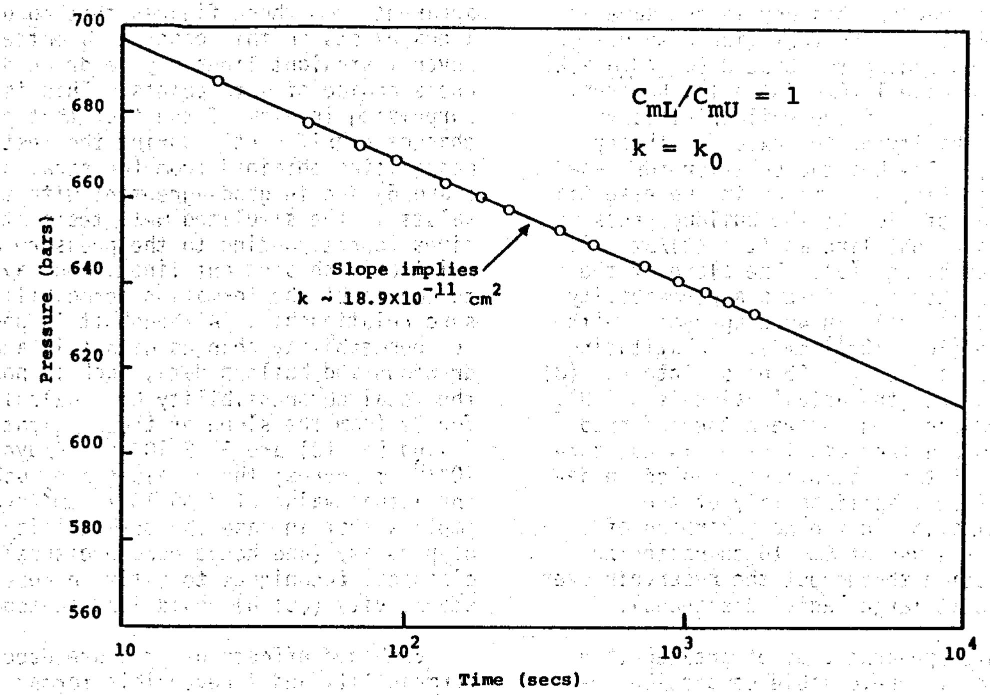

Figure 2. Drawdown history for Case 1 (Base 1-phase).

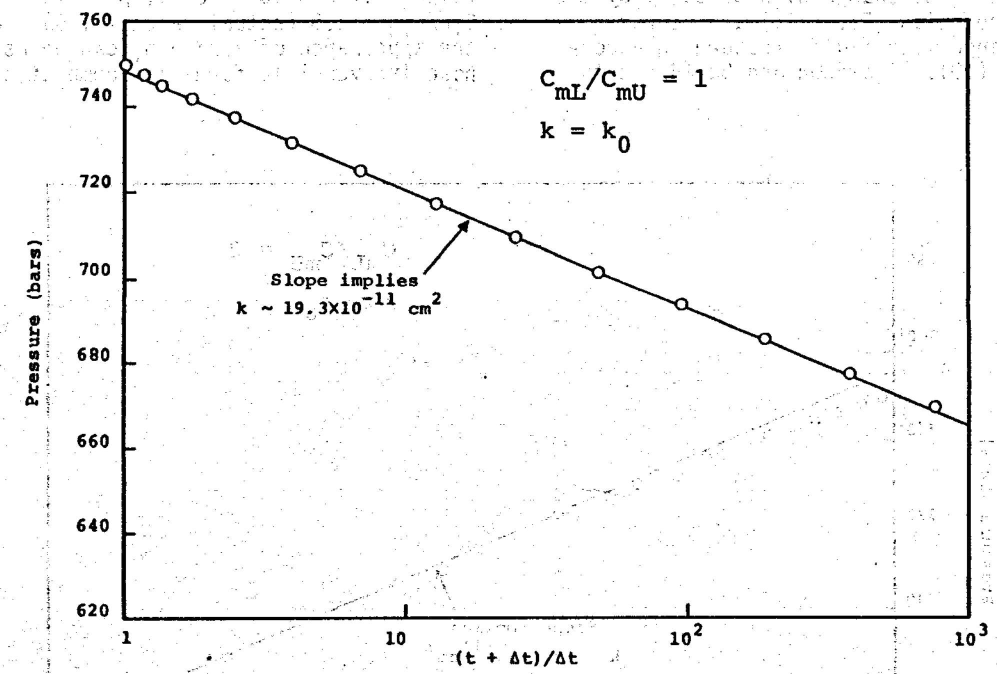

Figure 3. Buildup history for Case 1 (Base 1-phase).

parameters are the same as for Case 1; the interpretation of the drawdown history is the same as illustrated in Fig. 2. The formation compressibility during unloading for Case 2 (C_{mL}/C_{mU} = 2) is different from Case 1 (C_{mL}/C_{mU} = 1), however, and the interpretation of the buildup history tests the applicability of the extended theory, Eqs. (8) and (9). The buildup behavior for Case 2, illustrated in Fig. 4, differs in one essential respect from that of Fig. 3; the buildup pressure lies below the straight line as $(t + \Delta t)/\Delta t \to 1$. This is predicted by Eq. (9). The slope of the straight line in this case infers a permeability value (19.1×10^{-11} cm^2), in good agreement with the actual value (20×10^{-11} cm^2). Substituting the values for p_i and p^* ($\sim$ 755 bars) into Eq. (8) yields $C_{TL}/C_{TU} \sim 1.6$ (the actual value is ~ 1.9). The lack of good agreement between the inferred value of C_{TL}/C_{TU} and the actual value is not surprising in view of the assumptions invoked in deriving Eq. (8) (e.g., applicability of the semi-log approximation in the neighborhood of $(t + \Delta t)/\Delta t = 1$ and use of C_{mU} to characterize formation compaction throughout the reservoir even though $\partial p/\partial t < 0$ at large radial distances).

In any event, appearance of p^* greater than p_i is indicative of irreversible compaction behavior. Furthermore, the difference between p^* and p_i increases with the degree of irreversibility (see Garg, et al.[6] for further discussion of this question).

In Case 3 (k-variable), the formation permeability is assumed to change with porosity by the Carman-Kozeny relation (Eq. (11)) and, consequently, to change with fluid pressure in accordance with Eq. (10). Drawdown and buildup data are plotted in Figs. 5 and 6, respectively. It is apparent from these figures that no unique straight lines exists in this case; as a matter of fact, several straight lines may be drawn depending upon one's choice of data points. This is really not surprising in view of the fact that permeability changes significantly during the test. The permeabilities obtained from the straight lines (Figs. 5 and 6) are in good agreement with the actual values in the simulated well tests at appropriate times (corresponding to the pressure at the midpoint of each straight line), and may be utilized to construct the formation permeability-pore pressure relationship. Although it is possible to infer permeability changes with fair accuracy from drawdown and buildup data, such is not the case for the total compressibility C_T. Calculated values for C_T from the slope of the straight lines (Fig. 5) and Eq. (3) are 11.8 10^{-10} cm^2/dynes and 25.4 10^{-10} cm^2/dynes; these values are much larger than the actual value of 7.49 10^{-10} cm^2/dynes. This implies that in case the permeability is a function of porosity (and hence pore pressure), the use of classical techniques to estimate reservoir storativity ($\phi C_T h$) would lead to too high values.

Combined effects of pressure dependence of permeability and irreversible formation compaction are investigated in Case 4 (C,k-variable). As might be expected, the drawdown behavior is similar to that of Case 3. The buildup behavior for this case is shown in Fig. 7. The straight line drawn through points corresponding to large values of $(t + \Delta t)/\Delta t$ yields $k \sim 15.4 \times 10^{-11}$ cm^2 (actual value $\sim 17.3 \times 10^{-11}$ cm^2), p^* = 764 bars, and $C_{TL}/C_{TU} \sim 2.5$ (actual value ~ 1.9). Once again, the appearance of a $p^* > p_i$ can be used to diagnose irreversible formation compaction. The

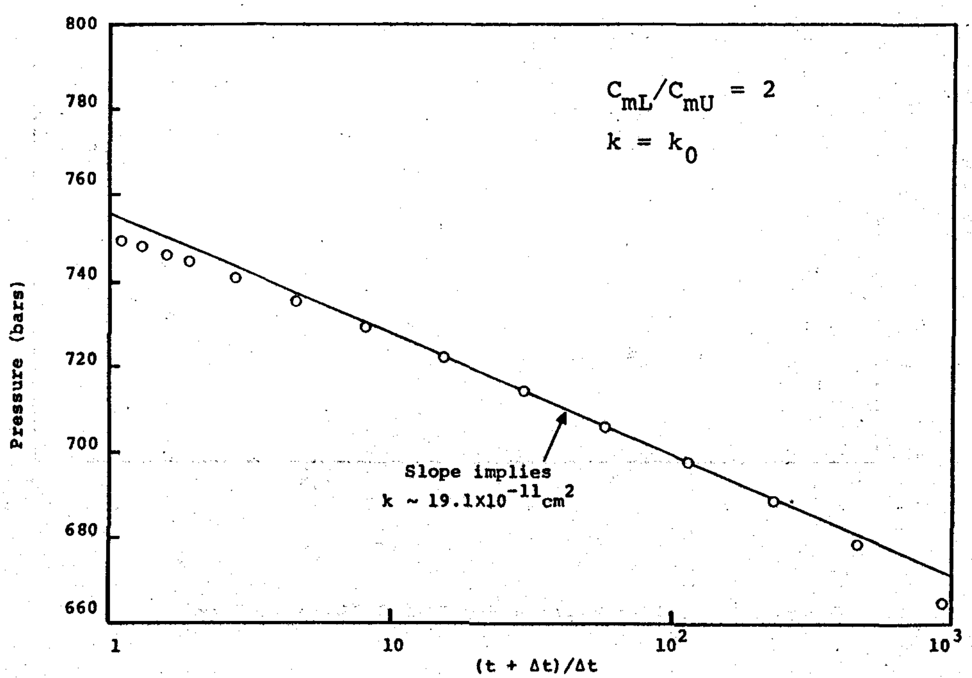

Figure 4. Buildup history for Case 2 (C-variable).

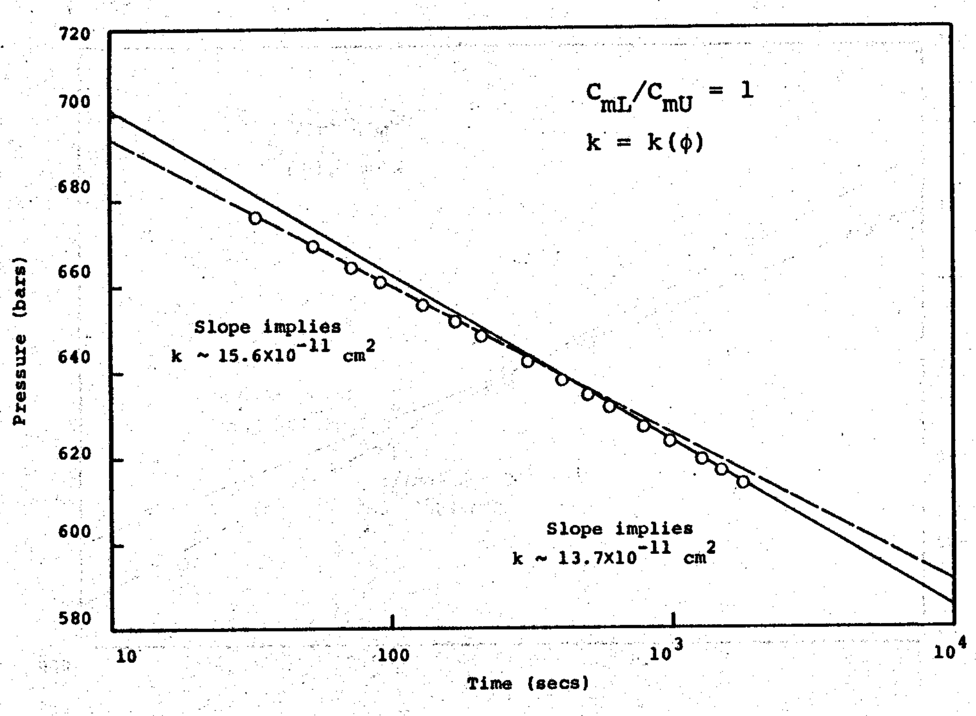

Figure 5. Drawdown history for Case 3 (k-variable).

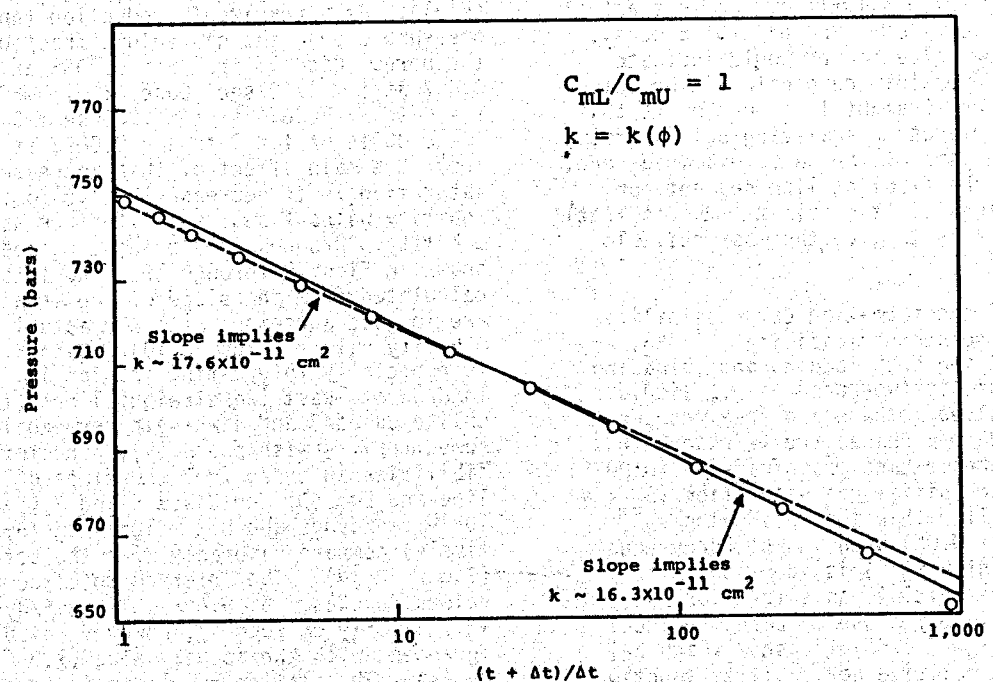

Figure 6. Buildup history for Case 3 (k-variable).

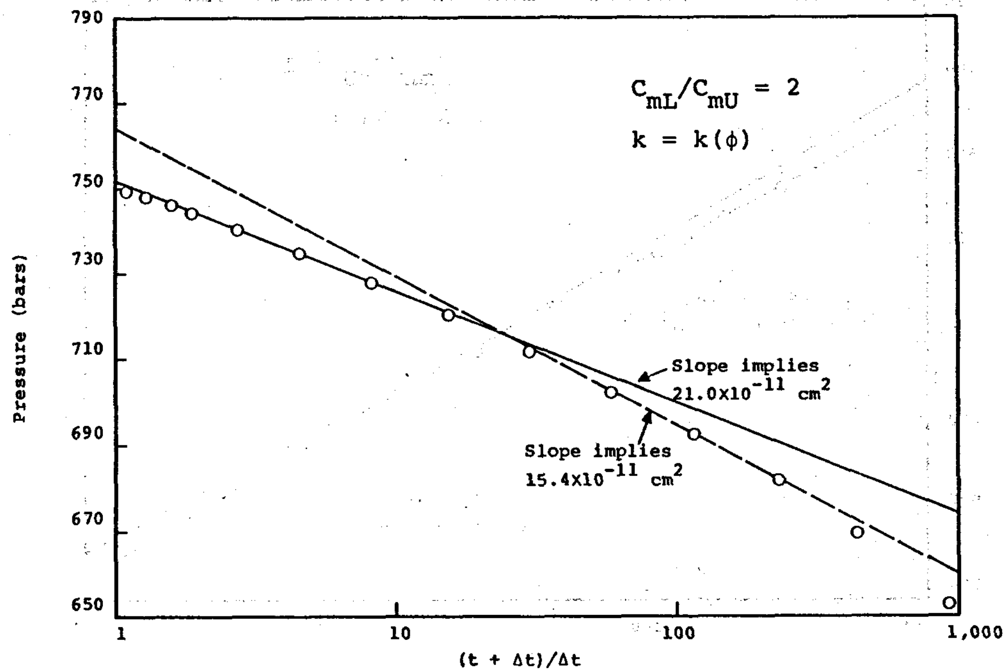

Figure 7. Buildup history for Case 4 (C,k-variable).

straight line passing through points for large buildup times, however, gives anomalous values for permeability (21.0×10^{-11} cm^2 against actual value of 18.3×10^{-11} cm^2) and p* (751.6 bars). Use of the latter value for p* would indicate little or no irreversible compaction. The selection of the proper straight line portion is thus of critical importance in analyzing buildup data. Based on the analysis of the cases examined here, it appears that the straight line segment for intermediate values of $(t + \Delta t)/\Delta t$ ($\sim 5 < (t + \Delta t)/\Delta t < \sim 200$ is likely to give the most reliable information.

In Cases 5-7 the formation compressibility (C_{mL}/C_{mU}) and absolute permeability ($k = k_0$) are held constant dûring both loading and unloading but the pore fluid is two-phase (i.e., liquid water with dissolved methane and free methane gas). Case 5 (Base 2-Phase) treats reservoir fluid in which the methane mass fraction (0.0075) corresponds to an initial gas saturation ($S_{g,i}$ = 0.0058) much smaller than the residual gas saturation (S_{gr} = 0.05) used in the Corey equations. Case 6 (high $S_{g,i}$) is identical with Case 5 except the initial gas saturation is ($S_{g,i}$ = 0.049) is very close to Corey residual gas saturation (S_{gr} = 0.05). Case 7 (high R_g) employs a hybrid relative permeability function, Eq. (13), with zero residual gas saturation and assumes a pore fluid with methane mass fraction selected to approximate 100 percent saturation without any free gas (actually $S_{g,i}$ = 0.0001). These three pressure drawdown/buildup simulations were chosen to investigate the effects of the presence of free methane in the pores and the use of different relative permeability functions.

In all three cases, the free gas, initially immobile, becomes mobile during the simulated well tests; however, most of the production comes from the liquid phase such that $q_T \sim q_\ell$ and $(k/\mu)_T \sim (k/\mu)_\ell$. As a result of production (and consequent pressure drop), the gas volume fraction goes up in the pores (Case 5; from S = 0.0058 at t = 0 to S = 0.067 at t $\sim$ 1760 sec; Case 6: from S = 0.049 at t = 0 to S = 0.074 at t $\sim$ 1800 sec; Case 7: from S = 0.00014 at t = 0 to S = 0.0093 at t $\sim$ 1730 sec); the main effect of this increase in gas saturation is to decrease the liquid (and total) mobility without substantially increasing the gas mobility. Drawdown histories for these cases are shown in Figs. 8 through 10. The total mobilities calculated from the slope of the straight lines are in good agreement with the actual range of mobility values (Figs. 8-10). Case 6 (high $S_{g,i}$) is especially interesting insofar as it is possible to draw at least two straight lines (this is not unlike Cases 3 and 4 wherein permeability was assumed to vary with porosity). The total compressibilities inferred from the slope of the straight line and Eq. (3) for Cases 5 and 7 ($C_T \sim 7.6 \times 10^{-10}$ cm^2/dynes and 8.2×10^{-10} cm^2/dynes respectively) compare favorably with the actual value (7.6×10^{-10}). The inferred total compressibility values for Case 6 (9.6×10^{-10} cm^2/dynes and 12.7×10^{-10} cm^2/dynes), however, display poor agreement with the actual value (7.9×10^{-10} cm^2/dynes). This latter result is in agreement with out earlier remark (c.f., discussion of Cases 3 and 4) that whenever permeability changes substantially during the test, the calculated compressibility (and hence storativity values) will be in error).

CONCLUDING REMARKS

From the results presented here, it is possible to draw three tentative conclusions regarding the applicability of the extended classical well test

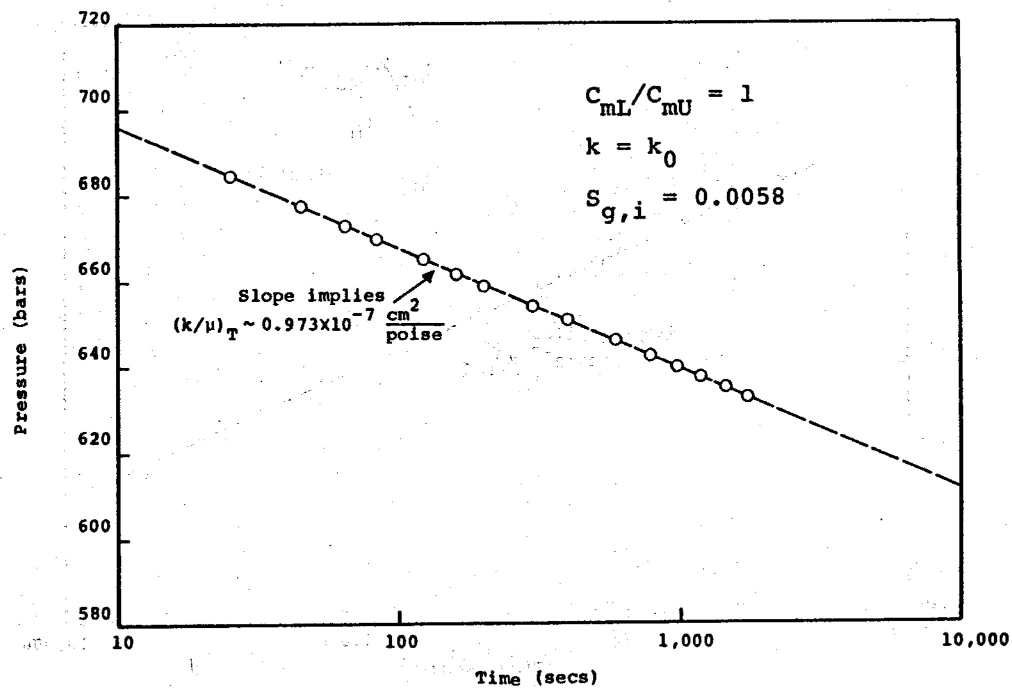

Figure 8. Drawdown history for Case 5 (Base 2-phase).

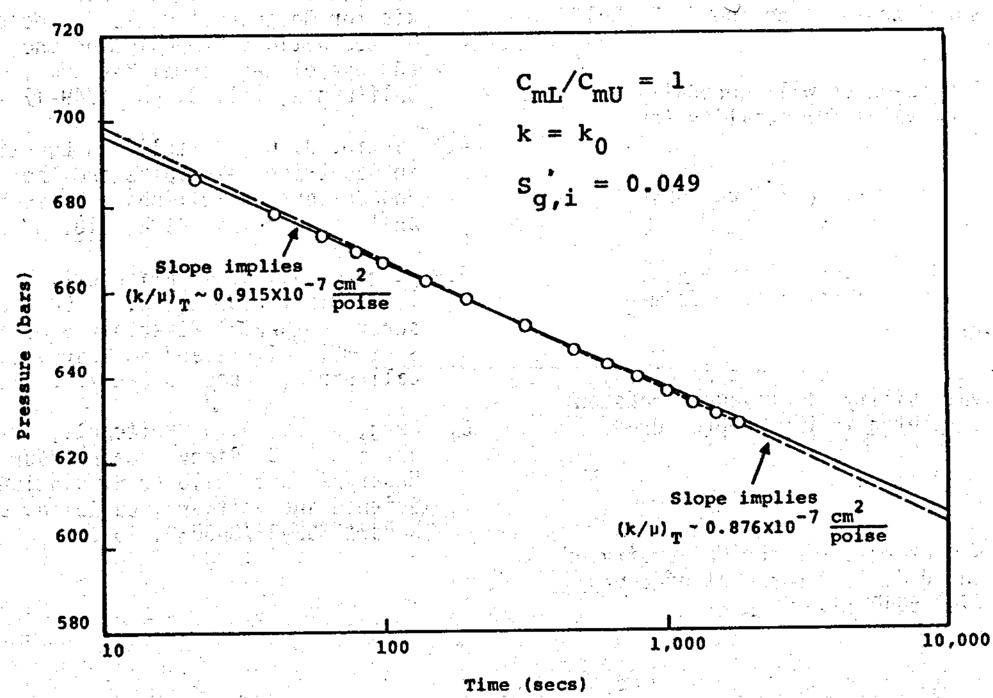

Figure 9. Drawdown history for Case 6 (high $S_{g,i}$).

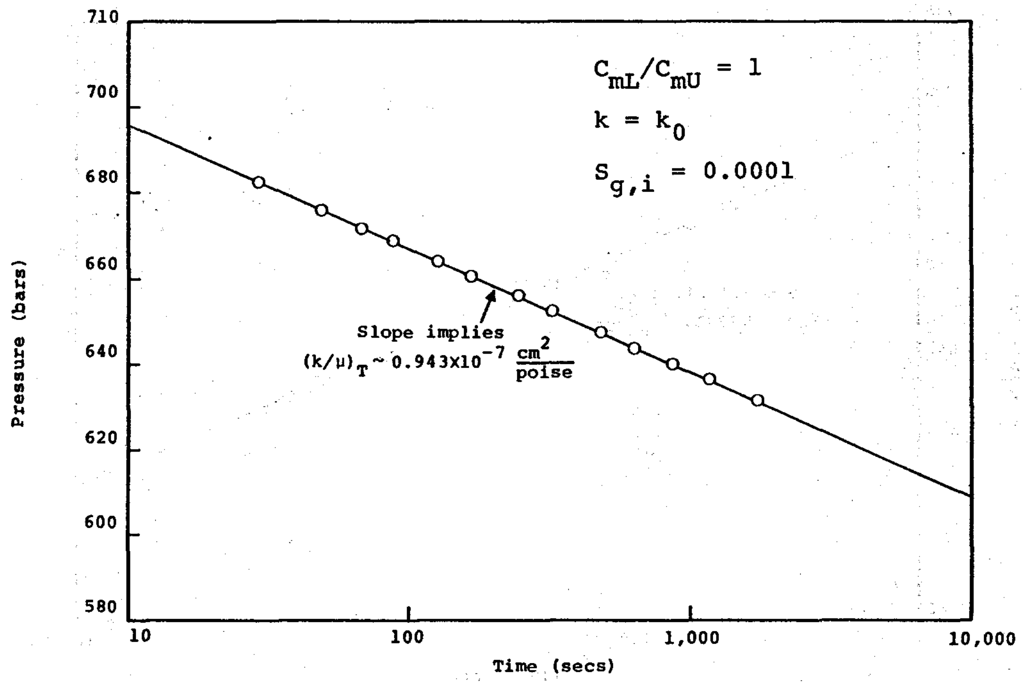

Figure 10. Drawdown history for Case 7 (high R_g).

theory to undercompacted sandstone/shale sequence found in geopressured zones along the U. S. Gulf Coast:

1. Classical procedures will generally yield a good value for mobility (or permeability.

2. Storativity estimates will be subject to large uncertainties.

3. Buildup (and drawdown) tests may be used to diagnose irreversible formation compaction.

Whether the procedures in fact prove practical must await the availability of pressure transient data from wells completed in the geopressured zone.

ACKNOWLEDGEMENTS

This work was performed for the University of Texas at Austin under U. S. Department of Energy Contract No. EY-76-C-5040-1S.

REFERENCES

1. Jones, P. H., "Geothermal and Hydrocarbon Regimes, Northern Gulf of Mexico Basin," Proceedings of First Geothermal Energy Conference, The University of Texas at Austin, pp. 15-89, June 2-4, 1975.

2. Matthews, C. S. and D. G. Russell, Pressure Buildup and Flow Tests in Wells, Society of Petroleum Engineers Monograph Volume I, Dallas, Texas, 1967.

3. Ramey, H. J., Jr., "Pressure Transient Analysis for Geothermal Wells," Proceedings Second United Nations Symposium on the Development and Use of Geothermal Resources, San Francisco, California, Vol. 3, pp. 1749-1757, 1975.

4. Martin, J. C., "Simplified Equations of Flow in Gas Drive Reservoirs and the Theoretical Foundations of Multiphase Pressure Buildup Analyses," Trans. AIME, 216, p. 309, 1959.

5. Garg, S. K., J. W. Pritchett, M. H. Rice and T. D. Riney [1977], "U. S. Gulf Coast Geopressured Geothermal Reservoir Simulation," Systems, Science and Software, La Jolla, California, Report SSS-R-77-3147, 1977.

6. Garg, S. K., J. W. Pritchett, D. H. Brownell, Jr. and T. D. Riney, "Geopressured Geothermal Reservoir and Wellbore Simulation," Systems, Science and Software, La Jolla, California, Report SSS-R-78-3639, 1978.

FLUID FLOW IN NATURALLY FRACTURED RESERVOIRS

T. D. Streltsova-Adams*
Rice University, Geology Department
Houston, Texas

SUMMARY

Analysis of fluid flow in naturally fractured reservoirs is discussed. Field records of pressure behavior in fracture formations reveal a variety of reservoir responses. These include the "bending of the pressure curve" type, the "specified initial slope" type, the "homogeneous reservoir" type, the "two-asymptotic lines" types, the "reverse distance-drawdown" type, etc. The characteristic behavior of fractured formations is not readily recognized and the divergence in interpreting the fracture flow behavior is well known. An apparent diversity of the fractured reservoir performance is discussed here by analyzing the characteristic pressure response of a double porosity model. A general approach for developing a fluid flow model is considered first. The pressure drawdown is presented then for two constituents of a double porosity media--fractures and matrix. The solution for the fracture flow is an alternative to that given by Warren and Root (1963). A conclusion is reached that a unique interpretation of the diversive response of a naturally fractured reservoir requires independent information that adequately specifies the reservoir properties.

INTRODUCTION

Analyses of known naturally fractured reservoir rocks show that fractures, having much greater conductivity to fluids than the intact rock, increase the overall permeability of the fractured rock mass. Enhanced fluid recovery, rapid pressure interference with distant wells, erratic productivity and diversity of the well pressure response are basic qualitative characteristics of the naturally fractured reservoirs. Quantitative analysis, which is provided by well testing, results in the effective, or thickness-weighted, reservoir permeability which depends on permeability of both the fractures and the porous blocks (matrix). If the permeability of an individual fracture considered as a linear channel is proportional to the fracture width, δ_{cm}, such that $\bar{k}_f = \delta^2 \times 10^8/12$ darcys (Muskat, 1946, Eq. 2, p. 425), the fracture permeability of a reservoir is determined as

$$k_f = (\delta/s)\bar{k}_f = \phi_f\bar{k}_f \qquad (1)$$

where s is the fracture spacing and ϕ_f is the fracture porosity defined as $\phi_f = (h/s)\,\delta/h = \delta/s$, h being the thickness of the reservoir and $(h/s)\delta$ - the total thickness of all the fractures in the reservoir. Effective permeability is thus influenced by the fracture pattern as well--its density, continuity, size, and orientation.

The diversity in the fracture pattern and the fracture-matrix properties is manifest in the reservoir performance which displays a variety of responses to an induced pressure change. It includes the characteristic s-shaped transient pressure response with two asymptotic parallel straight lines in a conventional semilogarithmic plot (Pollard, 1959; Warren and Root, 1963, 1965; Borevsky et al., 1973; Strobel et al., 1976; Crawford et al., 1976). Responses also include the pressure pattern similar to that of a homogeneous formation (Odeh, 1965), or the pressure behavior consisting of two distinct segments of different slope (Adams et al., 1968; Eagon and Johe, 1972), or the erratic pressure behavior with the drawdowns greater in more remote wells than in the nearer ones (Vecchioli, 1965; Barevsky et al., 1973; Streltsova, 1976). Peculiarities and nonconformity of the fractured reservoir performance have given rise to a divergence of views on the fractured reservoir behavior and the arguments on the flow interpretation are well known.

Two constituents of a fractured formation, matrix and fractures, each having its distinct porosity and permeability, have been recognized in developing the fractured reservoir flow models. The basic assumption in viewing the fractured medium is usually that the permeability of a fractured reservoir is due largely to the fracture permeability, while the fluids are contained primarily in the intergranular porous material, the matrix. Such is one of the assumptions put in the so-called double porosity model (Warren and Root, 1963), used in representing a fractured reservoir. In some cases, however, the matrix permeability can be quite comparable, if not greater than the fracture permeability. In some other cases, the fracture porosity, which usually is very low, may also be comparable to the matrix porosity. There are in fact unlimited variations in the fracture and matrix properties, the whole range of which is not accounted for by the double porosity model.

Fluid flow in a double porosity model is detailed below. The medium is assumed to consist of randomly distributed fractures breaking up the matrix into porous blocks of irregular size and shape. A general approach in developing a flow model is discussed first. The pressure drawdown distribution is then presented for two constituents of the media--the fracture and the porous block. The solution for the fracture flow is an alternative to that given by Warren and Root (1963). An apparent diversity in the performance of a naturally fractured reservoir is then discussed

*Present address: Reservoir Division, Exxon Production Research Co., P. O. Box 2189, Houston, Texas.

on the basis of analysis of the characteristic pressure response of a double porosity media.

Symbols used are specified where they first appear. A system of units commonly referred to as Darcy units is adopted here. To apply the results to oil field units the quantities $q/4\pi T_f$ and $T_f/\phi_f c_f h$ in Darcy units are to be replaced by the quantities 70.6 q/T_f and 0.00633 $T_f/\phi_f c_f h$ in practical oil field units, respectively.

A GENERAL APPROACH FOR DEVELOPING FLOW MODELS IN A NATURALLY FRACTURED FORMATION

Two different theoretical approaches are used in the study of fractured fluid-saturated rocks. One is concerned with individual fracture behavior, fracture criteria, and parameters of fracturing by laboratory measurements, core analysis, electric logs, use of tracers, etc. The second is concerned with the overall behavior of the fractured rock treating it as a continuum. The concept of a continuum as applied to the liquid flow in a porous media considers the macroscopic or averaged quantities of an arbitrarily located, but representative, elemental volume in the flow domain. Characteristics of the interconnected pores are assumed to be independent of the point of consideration, and the pore-fluid pressure is a continuous function of position. Fractures, as planes of mechanical discontinuity in a rock, strongly influence its hydromechanical properties. The response of fluids in fractures to pressure changes is almost instantaneous, whereas that in porous material is much slower. Therefore, there are two different pressure distributions, one in the fracture system, another in the matrix. During drawdown, the differential pressure response results in a flow from the matrix to the fractures. This matrix-to-fracture flow is time-dependent and produces a new equilibrium between the matrix and fracture pressures. Thus, two porosities with two different permeabilities could explain the features of flow in a fractured formation as the result of the reequalization of this pressure differential. Pollard (1959, p.42) has assumed the rate of flow "from the fine voids into the coarse fissures" to be proportional to the pressure difference in pores and fractures. The hydrodynamic aspects of flow in naturally fractured reservoir rock were first considered by Barenblatt and Zheltov (1960) and Barenblatt et al. (1960). Two overlapping continuum media, porous and fissured, each filling the entire flow domain, were assumed to represent a fractured formation. "Unlike the classical seepage theory, for each point of space, not one liquid pressure but two, p_1 and p_2, are introduced. The pressure p_1 represents the average pressure of the liquid in the fissures in the neighborhood of the given point, while the pressure p_2 is the average pressure of the liquids in the pores in the neighborhood of the given point" (Barenblatt et al., 1960, p. 1288). To obtain the representative average pressure values, an elemental volume characterizing the medium's properties was assumed to be of the size of a sufficiently large number of porous blocks traversed by an extensive network of fractures. The volume of the liquid v which flows from the porous blocks into the fissures per unit volume of rock was assumed on the basis of analysis of dimensions (Barenblatt et al., 1960, Eq. 1.2, p. 1289) to be

$$v = (\alpha/\mu(p_2 - p_1) \qquad (2)$$

where α was termed a new dimensionless characteristic of the fissured rock, μ being the liquid's viscosity.

The Barenblatt et al. (1960) theoretical approach was analogous to that developed earlier by Rubinstein (1948) in considering the temperature distribution in a heterogeneous material composed of two or more substances, such as a uniform mixture of a gas and a solid. In the latter study the flux of heat within each phase was assumed to obey Fourier's law. However, the flux of heat between the phases was assumed to obey Henry's law. The approach applied by Barenblatt and Rubinstein in analyzing a heterogeneous medium is an application of a general theory called the theory of interacting media or the theory of mixtures. Application of this theory has also been made in chemistry, specifically in studies of the diffusion of chemical species and mixtures; in soil mechanics, specifically in developing a theory of effective stress; in thermodynamics in studying multiphase media. A general mathematical development on interacting media, including thermodynamics and mechanical effects was developed by Truesdell in the late 1950s. However, it seems that the Truesdell statement concerning his priority ("...So far as I can learn, in my note of 1957 and in an unpublished report by H. Grad written about the same time are the first suggestions that the constituents of a flowing mixture of continua need not have a common temperature," Truesdell, 1969, p. 88) is not correct. Petroleum engineers had certainly developed these ideas some time before. The roots of this approach to analyzing heterogeneous systems go back even further. Perhaps the first work on the theoretical aspects of interacting media was that of Anzelius (1926) who considered the heat exchange between a fluid and solid constituents randomly distributed in the fluid. Each point of the space was represented by two temperatures: one for the solid constituent, another for the surrounding moving fluid. In 1938 Tichonov et al. (1946) independently arrived at the system of equations analogous to that of Anzelius (1926) in describing the dynamics of the gas adsorption on a porous adsorbent.

Models developed by Warren and Root (1963), Odeh (1965), Kazemi (1969), Wilson and Witherspoon (1970, 1974) have basically followed the same approach in considering a fractured formation as two coexisting systems of porous blocks and fractures. Warren and Root (1963) and Kazemi (1969) assumed a regular pattern of fractures breaking a rock mass into a systematic array of identical rectangular parallelepipeds. Odeh (1965) assumed a "homogeneously" fractured reservoir, with fractures arbitrarily distributed in a rock mass having porous blocks of various size and orientation. The fractured medium was assumed to have fracture permeability many times of the matrix permeability, while matrix porosity to be much greater than that of the fracture. Fluid flow was assumed to take place only through the system of fractures. Matrix, as a uniformly distributed fluid source, was assumed to release fluids to fractures, not contributing immediately to the wellbore. Eq. (2) was adopted to describe the interaction between the matrix and fractures as the matrix to fracture flow. In the Warren and Root (1963) notations this equation was written as (Warren and Root, 1963, Eq. 9, p.248):

$$\phi_1 c_1 \frac{\partial p_1}{\partial t} = \frac{\alpha k_1}{\mu}(p_2 - p_1) \qquad (3)$$

where subscripts 1 and 2 refer to the matrix and the fracture, respectively, and the parameter α has the dimensions of reciprocal area.

A model based on the assumptions specified above will be referred to in the following as the double porosity model. Subscripts "f" and "m" will be referred to as "fracture" and "matrix", respectively.

FLUID FLOW IN A DOUBLE POROSITY MEDIUM

An alternative solution to that of Warren and Root (1963) is described below. The subscripts denoting fracture parameters and matrix (porous block) parameters are correct here, but reversed in the original paper (Streltsova, 1976).

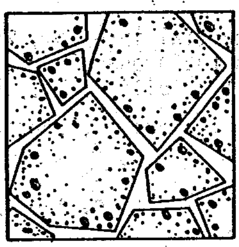

Fig. 1. Rock mass broken up into blocks of irregular size by fractures.

A naturally fractured formation (Fig. 1) is assumed to consist of a large number of randomly distributed, sized and oriented fractures breaking up the reservoir rock into porous blocks of irregular size and shape conventionally termed matrix. Flow to the wellbore in such formation, bounded from above and below by impermeable boundaries, is assumed to take place only through the system of fractures. The matrix is assumed to release fluids to the fractures. The differential equation for the fracture flow to the well is in this case

$$\frac{k_f}{\mu}\left(\frac{\partial^2 p_f}{\partial r^2} + \frac{1}{r}\frac{\partial p_f}{\partial r}\right) = \phi_f c_f \frac{\partial p_f}{\partial t} + v \qquad (4)$$

where v is the flow rate, i.e. volume of fluid released by the matrix per unit reservoir volume per unit time, into the fracture flow, and c_f is the fracture total compressibility.

This volume of fluid, v, which results from the matrix elastic response to the pressure difference between the points within and outside the porous blocks, is assumed to be proportional to the pressure gradient across the block and to the porous block conductivity:

$$v = \phi_m c_m \frac{\partial p_m}{\partial t} = \frac{k_m}{\mu h}\frac{p_f - p_m}{\ell}, \qquad (5)$$

or

$$\frac{\partial p_m}{\partial t} = \frac{k_m}{\mu \phi_m c_m h \ell}(p_f - p_m) = \alpha_1 (p_f - p_m) \qquad (6)$$

where ℓ is a linear parameter and $\alpha_1 = k_m/\mu\phi_m c_m h\ell$.

Eq. (6) is a first order linear equation, provided that α_1 is a constant, the solution of which is

$$p_f - p_m = \int_0^t \frac{\partial p_f}{\partial t} e^{-\alpha_1(t-\tau)} d\tau \qquad (7)$$

Multiplying the above by $\alpha_1\phi_m c_m$ to determine v from Eqs. (5)-(7) and substituting it into Eq. (4), the general differential equation for the fracture flow becomes:

$$\frac{k_f}{\mu}\left(\frac{\partial^2 p_f}{\partial r^2} + \frac{1}{r}\frac{\partial p_f}{\partial r}\right) =$$

$$= \phi_f c_f \frac{\partial p_f}{\partial t} + \alpha_1 \phi_m c_m \int_0^t \frac{\partial p_f}{\partial t} e^{-\alpha_1(t-\tau)} d\tau, \qquad (8)$$

where the right-hand side integral term represents the time-dependent matrix-to-fracture flow contribution.

This equation is analogous (except for notation) in the form to that obtained by Boulton (1963, p. 471) for the flow to a well discharging at a constant rate, q = const, from an unconfined aquifer, the solution for which has been found. Adopting this solution (Boulton, 1963, Eq. 14, p. 479), the fracture pressure drawdown may be written as

$$\Delta p_f = \frac{q}{4\pi T_f} W_f\,(r/B,\ \theta,\ \eta) \qquad (9)$$

$$W_f = \int_0^\infty 2J_0\left(\frac{rx}{B\nu}\right)\left\{1 - e^{-\frac{\alpha_1 t\eta}{2}(1+x^2)} \cdot \left[\cosh\left(\frac{\alpha_1 tc}{2}\right) + \frac{\eta(1-x^2)}{c}\sinh\left(\frac{\alpha_1 tc}{2}\right)\right]\right\}\frac{dx}{x},$$

where $B = (k_f/\alpha_1\phi_m c_m)^{\frac{1}{2}} = (k_f h\ell/k_m)^{\frac{1}{2}} = (T_f/T_m)^{\frac{1}{2}}$ (10)

$$c = [\eta^2(1+x^2)^2 - 4\eta x^2]^{\frac{1}{2}} \qquad (11)$$

$$\nu^2 = (\eta - 1)/\eta \qquad (12)$$

$$\eta = 1 + \phi_m c_m/\phi_f c_f \qquad (13)$$

$$\theta = 4\, T_f t/\phi_f c_f h r^2 \qquad (14)$$

$$T_f = k_f h/\mu \qquad (15)$$

and J_0 is the Bessel function of the first kind of zero order.

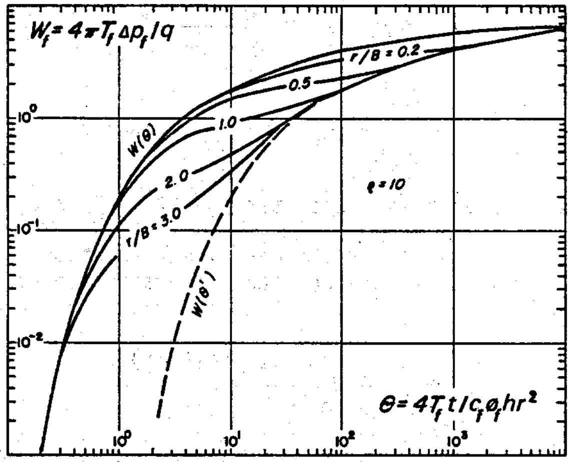

Fig. 2. Pressure drawdown function $W_f = 4\pi T_f \Delta p_f/q$, (Eq. 9), $\eta = 10$, plotted in logarithmic coordinates.

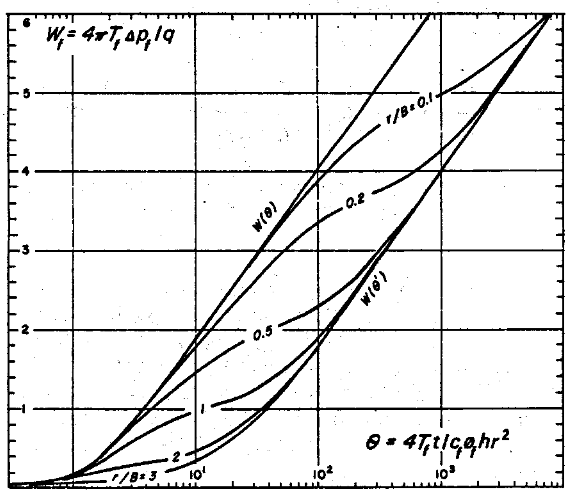

Fig. 3. Pressure drawdown function $W_f = 4\pi T_f \Delta p_f/q$, (Eq. 9), $\eta = 10$, plotted in semilogarithmic coordinates.

Values of the pressure drawdown function, $W_f = 4\pi T_f \, \Delta p_f/q$, computed from Eq. (9) for $\eta = 10$ and assumed values of parameters r/B and $\theta = 4t_D = 4T_f t/\phi_f c_f hr^2$ are shown plotted in the logarithmic and semilogarithmic coordinates in Fig. 2 and Fig. 3, respectively. For sufficiently small values of time, t, when t tends to zero, Eq. (9) gives

$$W_f(r/B, \theta) = \int_0^{\infty} 2J_0\left(\frac{r}{B}\, x\right) \frac{x^2}{x^2+1} \left\{1 - \exp\left[-\alpha_1 \eta t (x^2+1)\right]\right\} \frac{dx}{x} =$$

$$= \int_{1/\theta}^{\infty} \exp\left[-\, x - \left(\frac{r}{B}\right)^2 \frac{1}{4x}\right] \frac{dx}{x} \qquad (16)$$

If there were no matrix, $B \to \infty$, the pressure drawdown function, Eq. (16), will be further reduced to

$$W_f(\theta) = \int_{1/\theta}^{\infty} \exp\,(-x)\, \frac{dx}{x} \qquad (17)$$

which is the exponential integral, $W_f(\theta) = -\,Ei(-1/\theta)$, with the argument, θ, based on the fracture parameters. This curve is the left-hand side limiting curve on the Fig. 2, or the left straight-line segment in Fig. 3.

For large time, for the case when η tends to infinity, Eq. (9) gives

$$W(r/B, \theta') = \int_0^{\infty} 2J_0\left(\frac{r}{B}x\right) \left\{1 - \frac{1}{x^2+1} \exp \left[-\, \frac{\theta'(r/B)^2 x^2}{4(x^2+1)}\right]\right\} \qquad (18)$$

which when t tends to infinity further reduces to

$$W(\theta') = \int_{1/\theta'}^{\infty} \exp\,(-x)\, \frac{dx}{x} \qquad (19)$$

which is the exponential integral, $W(\theta') = -\,Ei(-1/\theta')$, with the argument, θ', based on the fracture transmissibility, T_f, and the combined, fracture and matrix, storage capacity:

$$\theta' = \theta/\eta = 4T_f t/(\phi_f c_f + \phi_m c_m)hr^2 \qquad (20)$$

The exponential integral curve (19) is the right-hand side limiting curve on the Fig. 2, or the right straight-line segment in Fig. 3. It is displaced from the left-hand side curve (17) horizontally by the amount η. The two asymptotic curves, the initial one (17) and the final one (19) are connected by the intermediate s-shaped (r/B) curves, the horizontal asymptotes of which are given by

$$W_f(r/B) = \Delta p_f/(q/4\pi T_f) = 2K_0(r/B), \qquad (21)$$

where K_0 is the modified Bessel function of zero order.

The fracture drawdown behavior described is analogous to that obtained by Warren and Root (1963), except the solution described is given for the whole range of the time variable, from zero to infinity, while the Warren and Root (1963) solution is approximated for $\tau > 100$. Parameters of the Warren and Root (1963) solution are related to those considered here as follows:

$$1/\omega = 1 + \phi_m c_m/\phi_f c_f = \eta \qquad (22)$$

$$\lambda = \alpha k_m r^2/k_f = r^2 k_m/k_f h\ell = (r/B)^2 \qquad (23)$$

$$\alpha = \alpha_1/(k_m/\mu\phi_m c_m) = 1/h\ell \qquad (24)$$

$$\tau = t_D = 0.25\,\theta \qquad (25)$$

where η, B and θ are defined by Eqs. (13), (10) and (14), respectively.

The pressure drawdown distribution in the matrix, the second component of the fractured medium, has been obtained by Streltsova (1976) in the form

$$\Delta p_m = \frac{q}{4\pi T_f} W_m(r/B, \theta, \eta) \tag{26}$$

$$W_m = \int_0^\infty J_0\left(\frac{r}{B}\frac{x}{\vartheta}\right)\left[2 - \frac{e^{a_1\alpha_1 t} + a_1 e^{-\alpha_1 t}}{1+a_1} - \frac{e^{a_2\alpha_1 t} + a_2 e^{-\alpha_1 t}}{1+a_2} - \frac{\eta(1-x^2)}{c} \cdot \left(\frac{e^{a_1\alpha_1 t} + a_1 e^{-\alpha_1 t}}{1+a_1} - \frac{e^{a_2\alpha_1 t} + a_2 e^{-\alpha_1 t}}{1+a_2}\right)\right]\frac{dx}{x}$$

where $a_1 = 0.5[c-\eta(1+x^2)]$, $a_2 = -0.5[c+\eta(1+x^2)]$ and c, ϑ and η are defined by Eqs. (11), (12) and (13), respectively.

An alternative and equivalent form of Eq. (26), obtained by application of the Laplace transform to Eqs. (4)-(7) has been obtained in the form (Vandenberg,[1] A., and Hardy,[2] J., private communication, 1977):

$$\Delta p_m = \frac{q}{4\pi T_f} W_m(r/B, \theta, \eta) \tag{27}$$

$$W_m = \int_0^\infty 2J_0\left(\frac{r}{B}\frac{x}{\vartheta}\right)\left\{1 - e^{-\frac{\alpha_1 t\eta}{2}(1+x^2)} \cdot \left[\cosh\left(\frac{\alpha_1 tc}{2}\right) + \frac{\eta(1+x^2)}{c}\sinh\left(\frac{\alpha_1 tc}{2}\right)\right]\right\}\frac{dx}{x},$$

i.e. the fracture and matrix pressure drawdowns (Eqs. 9 and 27) differ only in the sign of x^2 in the coefficient of sinh $(0.5\ \alpha_1 tc)$.

Values of the pressure drawdown function, $W_m = 4\pi T_f \Delta p_m/q$, computed from Eq. (26) (or Eq. 27) for $\eta = 10$ and assumed values of parameters r/B and θ are shown plotted in Fig. 4. To show the trend of the function behavior with the increase of η, the dashed lines depict the two limiting curves, r/B = 3.0 and r/B = 0.05, for $\eta = \infty$. The solution for $\eta = \infty$ has been given by Barenblatt et al. (1960, Eq. 5.21, p.1301) under the assumption of the negligible fissure compressibility, $c_f = 0$.

[1]Hydrology Research Division, Water Resources Branch, Dept. of the Environment, Ottawa, Ontario, Canada.
[2]Physics Dept., Carleton University, Ottawa, Ontario, Canada.

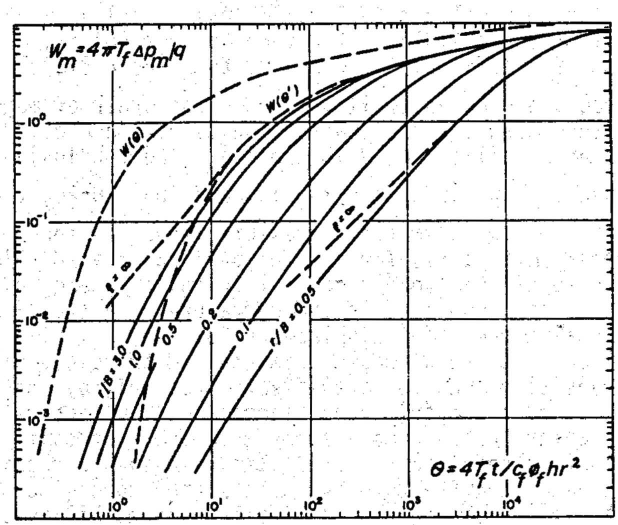

Fig. 4. Pressure drawdown function $W_m = 4\pi T_f \Delta p_m/q$, (Eq. 26 or 27), plotted in logarithmic coordinates.

ANALYSIS OF FRACTURE FLOW DRAWDOWN BEHAVIOR IN A DOUBLE POROSITY MEDIUM

Fracture pressure drawdown in a double porosity medium has a distinct behavior: the initial and late time pressure segments (Eqs. 17 and 19), parallel and displaced by an amount η(Eq. 13), are connected by a transitional curve which at early time deviates from the initial segment approaching a horizontal (defined by Eq. 21), then inflects from it merging at a later time with the final segment of the pressure curve. The pressure curve to the left and below the inflection point is described by Eq. (16), the pressure curve to the right and above the inflection point is described by Eq. (18). Zero slope of the transitional curve, with the inflection point at a horizontal, is pronounced when η has a large finite value (strictly it is for η tending to infinity).

Table 1. Calculation of the η parameter for assumed values of ϕ_m/ϕ_f

ϕ_m/ϕ_f	$(c_m+c_o)/(c_f+c_o)$	η
200.	40.	41.
150.	30.	31.
100.	20.	21.
50.	10.	11.
20.	4.	5.
10.	2.	3.
1.	0.2	1.2

Assuming some average values for compressibility of a fractured reservoir, the η values may be assessed as ranging from about 50 to a little over 1. Table 1 shows the calculated η values for a given ratio of fracture and matrix porosities and assumed reservoir matrix pore volume compressibility, $c_m = 10^{-5}$ psi^{-1}

(ranging usually from 2 x 10^{-6} psi^{-1} to 15 x 10^{-6} psi^{-1}, Jones (1975)), fracture compressibility, c_f = 9 x 10^{-5} psi^{-1} (according to Jones (1975), fracture compressibility is about an order of magnitude greater than that of the matrix) and oil compressibility, c_o = 10^{-5} psi^{-1}. The conclusion then follows that if ϕ_m/ϕ_f is less than 50-20, the limiting two asymptotic pressure lines are too close (η is 11-5) for a transional curve to develop a recognizable zero slope. The smaller the η value, the less pronounced is the curvature of a transitional curve. The displacement of the initial and final pressure drawdown segments and the slope of transitional curves are affected not only by the fracture and matrix capacitances, but by factors which are not encompassed by the double porosity model. These factors are: the relative permeabilities of the fracture and matrix (the double porosity medium considers only fracture permeability), the contribution of the matrix flow to the wellbore and the non-steady state matrix-to-fracture flow. Some discussion on the effect of these assumptions may be found in Boulton and Streltsova (1977 a,b; 1978) and Streltsova-Adams (1978).

Response of a fractured formation, which has limitless combinations of the matrix and fracture properties, may thus range from a pressure curve with zero intermediate slope to an almost uninflected curve with the slope determined by the closely spaced initial and final pressure segments. Therefore, the characteristic behavior of a fractured formation may not readily be recognized. It is not easy to relate the pressure data of an individual test to a conceptually known reservoir performance, which displays a wide variety of curve shapes. The problem of determining the fractured reservoir parameters is not unique. The reservoir behavior, dependent on variations in the fracture and matrix properties which are limitless, may be uniquely interpreted only if these properties are known independently. The study of rock properties changes during the production is of particular importance in analyzing the fractured reservoir performance. Pressure and temperature changes immediately affect the fracture permeability. Inelastic deformation of fractures may lead to the fracture closure with the result that fractures become ineffective for fluid flow. A combined drawdown and buildup test may give an insight into the compaction response of a formation. The use of multi-well pressure interference tests in combination with single well drawdown-buildup tests and core data information may eliminate step by step the uncertainties in interpreting the diversive behavior of a fractured formation.

REFERENCES CITED

Adams, A. R., Ramey, H. J. Jr., and Burgess, R. J., 1968, Gas well testing in a fractured carbonate reservoir, J. Pet. Technol., 20, 1187-1194.

Anzelius, A. R., 1926, Uber Erwärmung durchströmender medien, ZAMM, August.

Barenblatt, G. I., and Zheltov, Yu. P., 1960, Fundamental equations of filtration of homogeneous liquids in fissured rocks, Dokl. Akad. Nauk USSR, Mech., 132(3), 522-525.

Barenblatt, G. I., Zheltov, Yu. P., and Kochina, I. N., 1960, Basic concepts in the theory of seepage of homogeneous liquids in fissured rocks, J. Appl. Math. Mech. (USSR) 24(5), 1286-1303.

Barevsky, B. V., Samsonov, B. G. and Jazvin, L. S., 1973, "Metodika Opredelenia Parametrov Vodonosnich Gorizontov po Dannim Otkachek" (Aquifer Parameter Determination from Pumping Test Analysis), Nedra, Moscow (in Russian).

Boulton, N. S., 1963, Analysis of data from non-equilibrium pumping tests allowing for delayed yield from storage, Proc. Inst. Civ. Eng., 26, 469-482.

Boulton, N. S., and Streltsova, T. D., 1977a, Unsteady flow to a pumped well in a two-layered water-bearing formation, J. Hydrol., 35, 245-256.

Boulton, N. S., and Streltsova, T. D., 1977b, Unsteady flow to a pumped well in a fissured water-bearing formation, J. Hydrol., 35, 257-269.

Boulton, N. S., and Streltsova-Adams, T. D., 1978, Unsteady flow to a pumped well in an unconfined fissured aquifer, J. Hydrol., 37, 349-363.

Crawford, G. E., Hagedorn, A. R., and Pierce, A. E. 1965, Analysis of pressure buildup tests in a naturally fractured reservoir, J. Pet. Technol., 11, 1295-1300.

Eagon, H. B., and Johe, D. E., 1972, Practical solutions for pumping tests in carbonate-rock aquifers, Ground Water, 10(4), 6-13.

Jones, F. O., Jr., 1975, A laboratory study of the effects of confining pressure on fracture flow and storage capacity in carbonate rock, J. Pet. Technol., 1, 21-27.

Kazemi, H., 1969, Pressure transient analysis of naturally fractured reservoirs with uniform fracture distribution, Soc. Pet. Eng. J., 12, 451-462.

Muskat, M., 1937, "The Flow of Homogeneous Fluids through Porous Media," McGraw-Hill, New York.

Odeh, A. S., 1965, Unsteady-state behavior of naturally fractured reservoir, Soc. Pet. Eng. J., 3, 60-64.

Pollard, P., 1959, Evaluation of acid treatments from pressure build-up analysis, Trans. AIME, 216, 38-43.

Rubinstein, L. N., 1948, K voprosy o protsesse raspredelenia teplà v geterogennich sredach (Process of conduction of heat in heterogeneous media), Izv. Akad. Nauk SSSR, Ser. Geogr. Geofiz., 12(1), 27-45(in Russian).

Streltsova, T. D., 1976, Hydrodynamics of groundwater flow in a fractured formation, Water Resour. Res., 12(3), 405-414.

Streltsova-Adams, T. D., 1978, Well hydraulics in heterogeneous aquifer formations, Adv. Hydrosci., 11, 357-423.

Strobel, C. J., Gulati, M. S., and Ramey, H. J., Jr., 1976, Reservoir limit tests in naturally fractured reservoir - a field case study using type curves, J. Pet. Technol., 9, 1097-1106.

Tichonov, A. N., 1946, O stanovlenii electricheskogo toka v odnorodnom provodiaschem poluprostranstve (Electrical current in a uniform semispace), Izv. Akad. Nauk SSSR, Ser. Geozr. Geofiz., 10(3) (in Russian).

Truesdell, C., 1969, "Rational Thermodynamics," McGraw-Hill Book Company.

Vecchioli, J., 1965, Directional hydraulic behavior of fractured-shale aquifer in New Jersey, Symp. Dubrovnik, Int. Assoc. Sci. Hydrol., 318-326.

Warren, J. E., and Root, P. J., 1963, The behavior of naturally fractured reservoirs, Soc. Pet. Eng. J., 9, 245-255.

Warren, J. E., and Root, P. J., 1965, Discussion on "Unsteady-state behavior of naturally fractured reservoir" by A. S. Odeh, Soc. Pet. Eng. J., 3, 64-65.

Wilson, C. R., and Witherspoon, P. A., 1970, An Investigation of Laminar Flow in Fractured Porous Rock," Publ. No. 70-6, Dept. Civ. Eng., Univ. of California, Berkeley.

Wilson, C. R., and Witherspoon, P. A., 1974, Steady state flow in rigid networks of fractures, Water Resour. Res., 10(2), 328-335.

GEOTHERMAL BRINE INJECTION EVALUATION METHODOLOGY

R. QUONG, L. B. OWEN AND G. E. TARDIFF
UNIVERSITY OF CALIFORNIA, LAWRENCE LIVERMORE LABORATORY
LIVERMORE, CALIFORNIA

Introduction

Utilization of liquid-dominated geothermal resources in the U.S. will require subsurface injection of spent effluents as the most environmentally acceptable means of disposal. In many instances, the energy conversion cycle will cause processed geothermal fluids to become supersaturated in various chemical species which can subsequently precipitate. Direct injection of raw effluents, therefore, may, over the long term, be unacceptable because of wellbore and reservoir plugging resulting from deposition and continuing precipitation of solids. Injection evaluations have to define the requirements for both reservoir parameters and effluent quality before the potential for long term injectivity can be established. This paper describes standard oil field methodology we have adapted to establish brine quality and pre-injection processing requirements to insure long-term injectivity of Salton Sea Geothermal Field (SSGF) effluents. The brine processing work was completed in conjunction with a joint Magma-LLL reservoir evaluation program[1-3].

Standard oil field methodology consists of preliminary coreflooding, filtration and chemical stability tests to establish the potential for reservoir impairment[4-12]. Identification of impairment mechanisms leads to subsequent development of processing systems which consist typically of deaeration and treatment with inhibitors to control casing corrosion, addition of inhibitors to control biological and inorganic scales, and removal of particulates. Pilot facilities are installed and injectivity of the process fluid is evaluated again by combinations of core, membrane filter and chemical stability tests. These procedures minimize damage to injection wells during initial field development and permit estimates to be made of the expected operating lifetime of disposal wells.

The injection evaluation methodology is summarized in Figure 1. Injectability of fluids is established in the field on the basis of core and membrane filtration tests. The long-term post filtration chemical stability of effluents is established by incubation tests at injection temperature. Compatability of effluents with injection formation waters can be established by jar and incubation tests if connate waters are available. In the same fashion, adverse reactions between injected effluents and formation matrix materials can also be resolved if representative core materials are available for testing.

If the feasibility of direct injection of raw effluent is indicated by the initial field evaluation, a full-scale injection test can be carried out. If, however, effluents must be conditioned prior to injection, additional work is required to define and implement a pretreatment processing system. Following development of the pilot pre-injection processing system, injectivity tests are repeated to establish the cost benefit to be realized from installation and operation of the full-scale process.

Injectivity Tests

Work at the SSGF has led to the development of apparatus and procedures for rapid assessment of effluent injectivity[13,14]. Typical experiments have been performed at nominal injection temperatures of 90°C. Membrane filtration data, which can subsequently be used to estimate long-term injection well performance, are especially easy to acquire. We have successfully employed analytic models developed by Barkman and Davidson[10] to evaluate injection well performance based on membrane filtration data[15]. Core tests are also extremely useful, especially in the evaluation of potential reservoir impairment stemming from reactions between processed effluents and the reservoir matrix material.

Long-term incubation tests (2 to 30 days) were a key element in injectivity evaluations at the SSGF. The incubation tests were carried out at injection temperature (90°C) to establish the potential for precipitation of silica and other phases. These tests were also used to establish the stability of processed effluents. The primary advantages of incubation tests are: a) identifies potential for precipitation; b) leads to estimate of mass of precipitate formed and rate of formation; c) precipitating phases are identified; d) no need to rely on calculational techniques for estimating precipitation-potential. At present there are no proven techniques for establishing the precipitation rate of amorphous iron-silicates from SSGF-type brine because of the lack of data on temperature-dependent solubilities and kinetics.

Pre-Injection Process Development

An essential part of preinjection processing is the proper conditioning of the fluid and solids in preparation for clarification and/or filtration[16]. Conditioners include inorganic coagulants such as $Fe_2(SO_4)_3$, $Al_2(SO_4)_3$ and $FeCl_3$ and polyelectrolytes. Polyelectrolytes are water soluble polymers that ionize to form multiple positively or negatively charged active sites. The primary function of coagulants is to neutralize the charge on the surface of particles. Once the particles are destabilized, then aggregation and growth can occur, as well as adsorption onto filter media. Further agglomeration and enhancement of settling properties can be realized through use of inorganic or organic flocculants. The organic compounds are long chained, high molecular weight polymers with active sites for adsorbing and attaching onto the particles. This bridging action is an important factor in enhancing sedimentation.

Processing needs are initially investigated on a bench scale by conventional jar testing and analyses of critical species in incubated samples. Appropriate chemical treatment is first established by jar testing, followed by pilot scale testing.

Fluids which are supersaturated will require sufficient holding time to allow the precipitation process to proceed in appropriate solids handling equipment. Solids contact clarifiers accelerate the precipitation process by surface activation in addition to separating the bulk of the precipitated solids. Overflow from the clarifier can be polished to below 1 ppm suspended solids levels by methods such as multi-media granular or precoat pressure filtration. Chemical treatment is usually necessary, although some fluids may be adequately filtered without use of chemicals. Fluids which are undersaturated and contain low levels of suspended solids can be directly filtered, again with or without chemicals depending on the characteristics of the fluid and solids.

SSGF Results

The methodology discussed has been applied to Salton Sea Geothermal Brine effluents. Scaling caused by loss of silica from supersaturated SSGF brine effluents and plugging by deposition of silica particulates were identified as the causes of (SSGF) reservoir impairment. Conventional effluent treatment processes were investigated to lower silica to saturation rapidly by sludge contact, followed by coagulant aided clarification and final polishing by filtration. Particulate concentrations in the processed effluents were reduced to 1-2 ppm and brine injectivity confirmed by core and membrane filter methods. The cost of brine processing was estimated to be 20¢/1000 gallons based on a 50 MW plant producing 10 Mgd effluent. The methodology used to evaluate injection of SSGF brine is applicable to any geothermal resource.

References

1. Schroeder, R. C., 1976, Reservoir Engineering Report for the Magma-SDG&E Geothermal Experimental Site near the Salton Sea, California. Univ. Calif. Lawrence Livermore Laboratory, Rpt. UCRL-52094, 62 pgs.

2. Morse, J. G., 1979, Well Test and Evaluation of Reservoir Parameters in a Portion of the SSGF. Univ. Calif. Lawrence Livermore Laboratory, Rpt. UCRL-in press.

3. Thorsen, L. D., 1979, A Fast Analytic Simulator for Evaluation of Well Arrays. Univ. Calif. Lawrence Livermore Laboratory, Rpt. UCRL-in press.

4. Doscher, T. M. And Weber, L., 1957, The Use of the Membrane Filter in Determining Quality of Water for Subsurface Injection: Drilling and Production Practice, pgs. 169-179.

5. Hewitt, C. H., 1963, Analytical Techniques for Recognizing Water Sensitive Reservoir Rocks: Jour. Petroleum Technilogy, pgs. 813-818.

6. Johnston, K. H. and Castagno, J. L., 1964, Evaluation by Filter Methods of the Quality of Waters Injected in Waterfloods: U. S. BUreau of Mines, RI 6426, 14 pgs.

7. Mungan, N., 1965, Permeability Reduction Through Changes in pH and Salinity: Jour. Petroleum Technology, pgs. 1449-1453.

8. Farley, J. T. and Redline, D. G., 1968, Evaluation of Flood Water Quality in the West Montalvo Field: Jour. Petroelum Technology, pgs. 683-687.

9. Jordan, C. A., Edmondson, T. A. and Jeffries-Harris, M. J., The Bay Marchand Pressure Maintenance Project-Unique Challenges of an Offshore Sea-Water Injection System: Jour. Petroleum Technology, pgs. 389-396.

10. Barkman, J. H. and Davidson, D. H., 1972, Measuring Water Quality and Predicting Well Impairment. Jour. Petroleum Technology, pgs. 865-872.

11. McCune, C. C. 1977, On-site Testing to Define Injecction-Water Quality Requirements: Jour. Petroleum Technology, pgs. 17-24.

12. Keelan, D. K. and Koepf, E. H., 1977, The role of Cores and Core Analysis in Evaluation of Formation Damage: Jour. Petroleum Technolgoy, pgs. 482-490.

13. Netheron, R., and Owen, L. B., 1978, Apparatus for the Field Evaluation of Geothermal Effluent Injection: Geothermal Resources Council, Trans., Vol.2, pgs. 487-490.

14. Tewhey, J. D., Chan, M. A., Kasameyer, P. W. and Owen, L. B., 1978, Development of Injection Criteria for Geothermal Resources: Geothermal Resources Council, Trans., Vol. 2, pgs. 649-652.

15. Owen, L. B., Kasameyer, P. W., Netherton, R., and Thorson, L., 1977, Predicting the Rate by Which Suspended Solids Plug Geothermal Injection Wells: Proc. 3rd Workshop, Geothermal Reservoir Engineering, Stanford Geothermal Program, Kruger and Ramey, Ed., pgs. 163-171.

16. Quong, R., F. Schoepflin, N. D. Stout, G. E. Tardiff, and F. R. McLain, "Processing of Geothermal Brine Effluents for Injection", 1978, Trans. of the Geothermal Resource Council, Vol. 2, pp. 551-554.

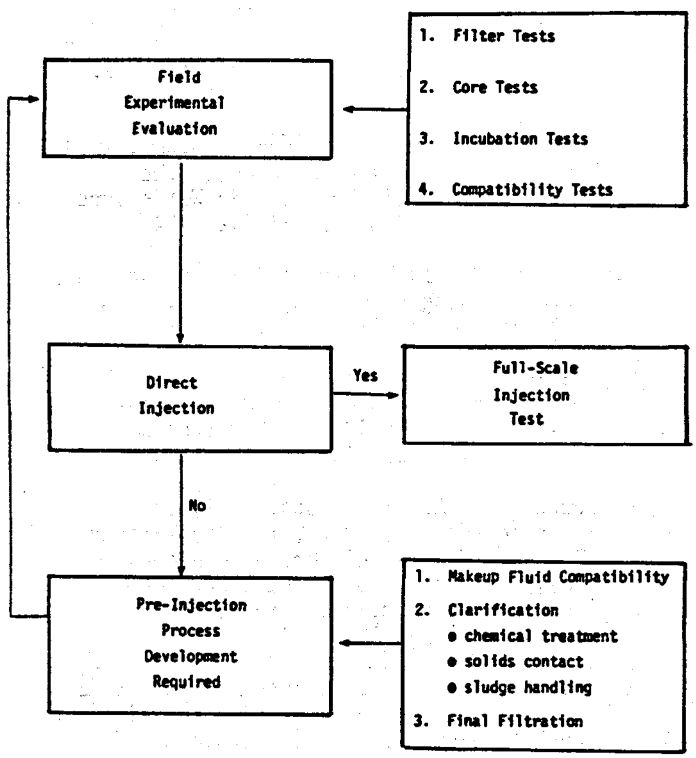

INJECTION EVALUATION METHODOLOGY

Figure 1

"Work performed under the auspices of the U.S. Department of Energy by the Lawrence Livermore Laboratory under contract number W-7405-ENG-48."

USE OF TRACERS IN GEOTHERMAL INJECTION SYSTEMS

by O. J. Vetter
Vetter Research
Costa Mesa, California

SUMMARY

The use of tracers is critical in geothermal injection systems. The hydrodynamic break-through of reinjected brine can be monitored in a very precise way using tracers. No other method is known which allows produced brine monitoring with the same precision. Thus, precalculated and monitored break-through profiles can be compared and the expected temperature front can be estimated in a very precise way. This use of tracers can be considered a "pre-warning" system.

The choice of tracers for geothermal reservoirs is rather limited. Tritiated water, introduced into the reservoir in a controlled manner, is the best choice. However, this monitoring technique eliminates the use of naturally occurring tracers for reservoir studies. The pros and cons for the use of naturally occurring tritium and other tracers are described.

Man-made tracers, particularly tritiated water, can be utilized to obtain quantitative data on reservoir parameters not available by other means. Pressure transient testing and tracer injection are complementary methods from which one can obtain the maximum information about critical reservoir parameters.

Present tracer techniques are hampered by a lack of information on the dispersion coefficient of the tracer in the flowing brine and the precise adsorption characteristics of the tracer on the rock material. Better quantitive evaluations of various reservoir characteristics will be possible if further research is conducted on the most critical adsorption properties under reservoir conditions.

INTRODUCTION

The new school of thought favors reinjection of heat-depleted brine into geothermal reservoirs. Proper reinjection of brine into geothermal reservoir can significantly extend the life of the reservoir and thereby increase the amount of recoverable energy compared to a simple production of the reservoir without reinjection of the heat-depleted brine. The present trend is towards reinjection and away from the disposal of the brine into a reservoir different from the producing zone.

The advantages of proper reinjection have already been indicated[1,2,3,7,8] and are, therefore, omitted from this presentation. However, in reinjection there are some real dangers: faulty reinjection can ruin a reservoir and its operation within a very short time. Unexpectedly high permeability flow channels caused by the generally unknown rock heterogenieties of a producing reservoir can lead to these problems. For example, if a premature break-through (hydraulic front) occurs within ten years instead of the calculated twenty years, the critical temperature front may arrive at the producing wells within fifteen years after start of reinjection instead of the calculated thirty years. The detrimental effects are obvious. Assuming the reservoir contains a recoverable energy of $\$10^{10}$ (approximately 1000 MW and 30 years life), the financial loss would then be on the order of $\$5 \times 10^{9}$.

The financial loss can still be enormous even if the reinjection problems are not as serious as those mentioned above. For example, if the decrease of the recoverable energy due to "faulty" reinjection is only 1%, the financial loss can still be significant. Assuming the conditions of the previous example ($\$10^{10}$ total recoverable energy; 1000 MW; 30 years life) the loss due to the 1% decrease is still $100 Million.

The industry is thus faced with a dilemma: reinjection problems ruin a reservoir within a very short time and no reinjection at all will result in a drastic decrease of the recoverable energy. The financial losses can be substantial in both cases. The only economically feasible solution to the problem would be the correct or optimized (i.e., non-faulty) reinjection of the heat-depleted brine. Unfortunately, the present uncertainties in determining the precise reservoir parameters which can lead to a "faulty" injection system, e.g., reservoir heterogenities such as fractures, high permeability streaks, faults, etc., make it impossible to design the absolute optimal reinjection system. Injection well spacing, location and completion are vital design features. In many instances these are still left to rough estimates because of the problems encountered in determining the precise location of the above-mentioned reservoir heterogeneities. Various types of pressure test methods (e.g., pressure pulse and interference testing) do not normally yield information exact enough to overcome these problems. For example, extremely high permeability channels in an otherwise "perfect" reservoir may be indicated by conventional pressure test work. However, only very rough estimates can be made regarding the precise locations, geometry and conductivity of these channels. If the reservoir consists of a highly fractured rock formation such as the hard rock in the Geysers (California), the Bacca field (New Mexico) or the Cesano field (Italy), the evaluation of the pressure tests data may become too coarse and may become technically of little value.

It is the opinion of the author that a workable approach to solving the problems can be made with well designed tracer tests. These can provide the most viable means of avoiding the possibility of major disasters in any reinjection system[9]. Monitoring of the tracers' concentrations in the produced brine will allow the operator to stop any "faulty" reinjection operation immediately upon arrival of the tracers in the producing wells. This early warning system will allow an opportunity to re-design or modify the entire injection system before a major financial disaster occurs. In addition, more sophisticated tracer tests can give a host of information about critical reservoir parameters which cannot be measured by any other available method. These sophisticated tracer tests consist of more than "just sticking any tracer" into the injected brine and looking for the first appearance of the tracer in the produced brine. This common "break-through determination" may still be adequate in some situations. However, additional and more useful reservoir data can be obtained with the same level of effort using more sophisticated tracer techniques. These techniques are not suggested as alternatives to the conventional transient analysis.

It is not suggested that reservoir tracer tests - no matter how sophisticated - should replace the more conventional pressure test work; on the contrary, tracer and pressure test work should supplement each other in the field. Pressure tests can provide specific information on the near wellbore region and average reservoir data on the far wellbore region. The tracer tests can allow us to analyze and interpret reservoirs at locations very remote from the wellbore.

BASIC CONCEPTS OF WELL TO WELL TRACER TEST WORK

The literature contains a large number of publications dealing with various types of tracers and tracer techniques in subterranean reservoirs. Most of these referenced publications deal with only one objective for well to well reservoir tracing[12-14]. The majority of the publications are concerned only with:

1) The recharge of the reservoir through the injected brine and/or through any other water source (nearby aquifer and surface water).

2) Injection brine break-through determinations.

The break-through determinations are by far the most frequent subject of the referenced publications. This concept is very simple: a tracer is added to the brine (or naturally occurring tracers in the brine are used for this purpose) to determine the time required for the tracer to occur in one or more producing wells. Only very few publications are concerned with quantitative evaluations of the tracer break-through data.

Properly designed tracer tests can yield much more data than that of simple "break-through" determinations. It can be shown that some of the vital reservoir heterogeneities (such as dimensions, conductivities, directions and locations of fractures and/or high permeability streaks) can be determined in a rather quantitative manner through tracer tests. In addition, sweep efficiencies, drainage radii and a number of other reservoir parameters can also be analyzed through more sophisticated tracer tests.

Basically, one can categorize reservoir tracer tests (well to well) into two major groups:

1) General tracer tests for reservoir monitoring or verifications.

2) Diagnostic tracer tests to evaluate specific reservoir problems or to obtain very specific information on certain reservoir parameters.

Different concepts may have to be used depending upon the various field conditions and the goals to be achieved through the tracer test work. In addition, tracer tests can also be operationally divided into two different basic categories:

1) Pulse (slug) injection of tracers.

2) Continuous tracer injection.

Here again, different objectives can be achieved depending upon the type of tracer injection.

Tracer Tests for General Reservoir Monitoring

Normally, very little information on some critical reservoir parameters is available when a new reinjection system is started. The same lack of concrete information is evident for a sometimes prolonged time period after the start-up of a new reinjection system. Adding a tracer, e.g., tritiated water, to the first water injected into the reservoir will load the reservoir with tracer. The subsequent constant monitoring of the produced water for this tracer would automatically allow a very convenient and economical reservoir verification method. In other words, this general tracer test at or soon after the start of a reinjection system can be considered a prewarning system: any hydraulic advance of the injected water faster than that expected or calculated would allow the necessary changes of the entire injection system before a temperature front is experienced in the producing wells. This would prevent major temperature damage to a reservoir due to missing the accelerated advance of the hydraulic front.

A plot of the tracer concentration in the produced brine vs. time will indicate many reservoir problems. Actually, time is a convenient but "incorrect" unit. The cummulative production instead of time should be used. However, if the brine injection and production rates in the field are kept constant after the tracer injection, the time unit becomes a "correct" unit. Two "typical" tracer elution profiles are indicated in Figure I.

The interpretation of these elution profiles is hampered by a number of problems:

1) The most obvious question is: what injection well contributes how much tracer to the total tracer concentration in the brine of any given production well?

2) The quantitative interpretation of the tracer elution profile, even if it would stem from only one injection well offers great difficulties.

The data obtained through this general tracer technique will not permit the precise determination of many critical reservoir parameters. It will, however, allow some estimates as to (a) which general areas of the field are particularly endangered and (b) the type of problems to be expected in the prolonged reinjection within these endangered reservoir areas. The main advantages of this method are:

1) It provides an early warning system if any severe sweep problems exist in the reservoir. Major damage due to premature break-through can be prevented at the earliest time.

2) This test is very economical and requires funds negligible compared to the value of the information.

3) The information from this general tracer test is of vital importance for designing the required subsequent reservoir tracer test work.

As the main conclusion, the author believes that this general tracer technique should be an integral and routine feature of any newly started reinjection system.

Specialized Tracer Tests

A new situation exists if a given reservoir area shows definite sweep efficiency problems. These problems can be indicated by:

1) A general tracer test.

2) Any type of pressure test work.

3) Production monitoring (brine composition and temperature).

The operator must now determine the extent of the problems, i.e., the location, direction, conductivity and geometry of the high permeability streaks leading to the undesired decrease in sweep efficiency. This is a very difficult task. As mentioned before, pressure test work is not suited to complete this task with the required precision, i.e., a different technique must be used to obtain these data.

A tracer test of a different nature can be utilized to gather the needed information. For example, a different tracer can be injected into each injection well within the suspected problem areas. Monitoring of the various tracers in the brines produced from various production wells will now allow the determination of flow patterns and flow barriers (e.g., faults) within the troubled reservoir area. However, the quantitative interpretation of these single tracer elution profiles is still rather difficult if not impossible as outlined in the following paragraphs.

Qualitative Tracer Tests. Tracer techniques are most commonly applied to the "determination" of an injection brine break-through. A tracer is added to the injected brine and the produced brine is monitored for the occurence of this tracer. A number of simplifications is commonly applied in this technique:

1) No adsorption of the tracer is assumed, even though by nature, every chemical used as a tracer must exhibit adsorption properties in any reservoir.

2) The accuracy and precision of the analytical determination of the tracer concentration in the produced brine is commonly ignored or grossly overestimated. This ignorance or overestimation may give misleading "results".

3) Stability of tracer.

Both assumptions or simplifications (adsorption, analytical and stability problems) will be discussed in more detail below and in later reports and publications[10,11]. Presently, we will assume that each tracer exhibits different adsorption properties and that most conventional tracers (e.g., nitrate, aldehydes, thiocyanate) cannot be determined with the required accuracy. Therefore, most of the conventional tracer studies give only a "yes or no" type answer, i.e., tracer is or is not detected in the produced brine.

An apparent "break-through" could be meaningless as the following example shows. If 100,000 m^3/day of the brine is reinjected and one (1) m^3/day channels to the producing wells within three months, a break-through determination would indicate a severe problem. In reality, no alarming situation exists because the other 99,999 m^3/day of injection brine may show a perfect sweep pattern in the reservoir. On the other hand, if none of these 100,000 m^3/day will channel to the producing wells within a year, no break-through would be indicated - but the entire hydraulic front could arrive in the producer within three years vs. the calculated twenty years. Even though no break-through was indicated in the latter example, a major problem exists in the reservoir.

Quantitative Tracer Tests. The quantitative evaluation of tracer elution profiles as shown in Figure 1 are rather difficult. The various peaks in these curves indicate various flow channels within the reservoir. High permeability streaks must exist in the reservoir if the predicted elution profile (based on uniform reservoir permeability) does not match the measured tracer elution profile. These high permeability streaks can be divided into two basically different categories:

1) Horizontally oriented streaks.

2) Vertically oriented streaks.

Figures 2 and 3 illustrate the basic differences between the two types of high permeability streaks.

In order to differentiate between the two types of streaks (horizontal and vertical), the tracer appearence must be analyzed in the production wellbore fluids as a function of depth. Even if this feature is added to a tracer test, it will not indicate the difference between the two types of high permeability streak orientation in reservoir locations further away from the bore of the production well because of mixing.

Another problem experienced in a quantitative evaluation of tracer elution profiles is the difficulty in determining the dispersion of the tracer in the reservoir fluid as the tracer front advances toward the production well. Many factors will affect this dispersion or mixing of advancing tracer with reservoir fluid. Diffusion, tortuosity of the porous medium and mixing due to the microscopic flow velocity profiles of the mobile fluid phase along the immobile (stagnant) connate water layers are only a few factors effecting the dispersion coefficient.

The different arrival times of the various injected fluids in the producing wellbore will cause various degrees of mixing (see Figure 4). This mixing through different arrival times will add to the degree of dispersion.

Sorption effects of the tracer introduce still another problem in quantitatively evaluating tracer tests. The various sorption characteristics of the tracer on the solid phase (rock material) will make it difficult to perform a quantitative interpretation of the tracer elution profile. One must be aware of the fact that there exists no nonadsorbing tracer. Even tritium, one of the tracers causing the least adsorption problems, will adsorb on the rock to an appreciable degree.

The chemical analyses of the produced fluids for their content of tracer is also an important consideration. The tracer must be detectable in concentrations under less than 1 mg/l or hugh masses of tracer will be required for an actual field tracer study. Figure 5 shows the implications of this requirement. The sensitivity and accuracy of many analytical methods commonly used for tracer test work are not sufficient to satisfy the needs of a quantitative field tracer study.

Finally, the chemical stability of many tracers in the hot geothermal reservoir may pose serious problems. Many tracers used for the much cooler oil reservoirs are not stable enough at the high temperatures of a geothermal reservoir. Thus, the choice of useful tracers becomes rather limited.

Summarizing, one can state that the present tracer technology (well to well tracing) provides semiquantitative data at best.

Suggested Improvements of Present Tracer Techniques

Multiple tracer injection could solve some of the problems outlined so far. "Multiple" can refer to different tracers being injected into different wells of the same field or different tracers injected into the same well. Figure 6 shows that ten tracers are sufficient for a field with a geometric location of wells to achieve both objectives:

1) Two different tracers injected into each injection well and

2) A different tracer combination for different wells.

If the ten tracers have different adsorption properties and if these adsorption properties are known, the principles of conventional liquid or gas chromotography could be applied to obtain quantitive results on various reservoir parameters through such a sophisticated tracer study. The principles of this new tracer technology will be outlined in a future paper[11].

CHOICE OF TRACER AND TRACING TECHNIQUES

The choice of a tracer for any tracing job mainly depends upon the tracing technique, which in turn depends upon the objective of the tracer study. In many instances, there are more than one objective for a tracer study, thus creating a number of problems for choosing the proper tracers and tracing technique. For example, a chosen tracer technique for a given objective may require the use of man-made tritiated water as a tracer, whereas other tracer objectives in the same reservoir may require the utilization of naturally occurring tritium. Naturally, the utilization of man-made tritium as a tracer will "contaminate" the reservoir, thus preventing any future use of naturally occurring tritium as a tracer in this reservoir. In these and similar cases, a decision must be made as to which one of the tracers is most desirable to fulfill the various objectives of tracer studies and reservoir management.

Man-Made Vs. Naturally Occurring Tracers

Naturally occurring tracers can be used at least theoretically to determine a number of important reservoir parameters:

1) Age determination of the reservoir water through tritium determinations if the intruding water consists of "recent" surface water.

2) Natural recharge of the reservoir with water from another aquifer or with surface water.

3) Flow patterns within a reservoir if the various waters in the reservoir have distinctively different compositions.

4) Break-through of reinjected water into the producing wells.

The first parameter (age determination of the reservoir water) requires that the naturally occurring tracer is tritium, whereas, any other tracer or tracer combination can serve for determining the other three parameters.

In most attempts using naturally occurring tracers for reservoir studies, an obvious problem exists: if the operator wants to conduct a tracer study involving man-made tracers, the man-made and naturally occurring tracers cannot be the same. As soon as the man-made tracer is introduced into the reservoir, it will be very difficult or impossible to distinguish between the man-made and naturally occurring tracer if the two tracers are the same. This means, the operator has to make a decision as to his preference: he must either use a man-made tracer different from the naturally occurring tracer or, if for any reason both tracers must be the same, he must then decide which type of tracer test is more important for his operation. The latter decision must be made more often than commonly expected. This decision can be very difficult because of the many pros and cons for the "*contamination*" of a producing reservoir with man-made tracers. In addition, this "contamination" can be irreversible, particularly if the most important tracer for geothermal injection systems, namely tritium, is used as a man-made tracer.

The decision as to what tracer and what type of tracer test to apply requires a thorough evaluation of advantages and disadvantages involved. In most cases, a compromise has to be made. To help the operator in making this decision, a critical evaluation of the various naturally occurring tracers and tracer tests involving these tracers is given in the following paragraphs.

<u>Age Determinations Through Tritium Measurements</u>. Age determinations through measurements of the concentration of naturally occurring tritium in reservoir brines are frequently suggested. Even though theoretically possible, the authors do not believe in the validity and technical usefulness of this method and the accumulated data. The reasons for this statement are manifold:

1) If tritium has recently entered the reservoir in the form of surface water, any age determination is limited to approximately fifty years (see Figure 8). This limitation is not given by a lack of accuracy of the tritium determination of the enriched samples (by conventional standards), but the rapid decay of the tritium (half-life time 12.35 years). After approximately four life cycles, the tritium concentration becomes so low that even excellent counting procedures (±1%) do not provide a measuring accuracy required for precise age determination (see Figure 2), i.e., only instrument background but not tritium will be measured.

2) If mixing between "recent" and old water occurred in the reservoir, the age determination becomes meaningless. Any recent recharge of the reservoir with surface water will cause mixing of old and recent water in the reservoir.

3) The tritium content of the water originally penetrating into the reservoir must be known for any age determination. This tritium concentration will depend upon the time of entering the reservoir. Any water entering the reservoir before 1945 (start of atomic bomb testing) will have a much lower tritium content than water entering the reservoir during the height of the atomic bomb testing. "Prebomb" and "Afterbomb" surface waters have again totally different tritium concentrations.

4) It must be assumed that the tritium in the surface water, penetrating through the soil and porous overburden layers, remains constant and does not become adsorbed on the porous medium on its way into the reservoir. This assumption is wrong since the upper 20-30 cm of soil already act as a "sink" for atmospheric tritium.

5) No pick-up of tritium in the reinjected water is allowed if age determinations are planned. For example, atmospheric air is blown through the cooling towers in the Geyser field. Any pick-up will greatly disturb later conclusions about the age of the reservoir water.

The author believes that using naturally occurring tritium for age determinations cannot be justified considering the above assumptions. Preventing the injection of man-made tritium into the reservoir to "save" it for age determinations using natural tritium is a very shortsighted measure.

<u>Utilization of Naturally Occurring Tracers</u>. Naturally occurring tracers besides tritium can be extremely useful in a few isolated cases. For example, Mercado[17] reports a case where potassium/sodium ratios of the produced brine from different producing wells was used to detect thief zones in the reservoir (see Figure 7). Other reported cases are the detection of casing leaks in producing wells by analyzing the injected, produced and native reservoir fluids.

Another argument often used in favor of using naturally occurring tracers is the analyses of produced and injected fluids and subsequent comparison of the two compositions. The intention is to determine the arrival of the hydraulic front through this comparison. This idea has a major shortcoming: if the injected fluid has the same composition as the produced fluid or if only slight compositional differences between the two fluids exist, the indicative changes in the produced fluid will be either non-existent or too small to be detected.

Radioactive Vs. Chemical Tracers

The author prefers radioactive over chemical tracers. This preference is dictated by a number of reasons:

1) Less tracer has to be injected because of the much higher sensitivity and accuracy of the radioactive tracer in the required analyses of the produced fluids (see Figure 5).

2) The price for the radioactive tracers is much lower than that for an equivalent amount of chemical tracer (see Figure 5).

3) Handling and other logistics are much easier in the case of radioactive tracers due to the comparitively small amounts of tracer required.

The disadvantages of using radioactive tracers are:

1) A special license is required.

2) Only highly-trained personnel are allowed to handle the tracer.

3) No accident is allowed.

CONCLUSIONS

1) General monitoring of geothermal reservoirs can be accomplished through the use of tracers. The tracer should be injected immediately after starting the reinjection.

2) Tritiated water is the most suitable tracer to accomplish this general reservoir monitoring and verification.

3) The conventional tracer technique of well to well tracing needs considerable improvement to allow a quantitative interpretation of the tracer elution profiles.

4) Measuring of the precise adsorption/desorption characteristics of the applied tracers must be known.

5) Tracer chromatography is a new technique which will allow a better interpretation of tracer elution profiles.

6) This chromatography technique must be proven in the laboratory and in the field.

7) Man-made tracers are better suited for reservoir tracing than naturally occurring tracers.

8) Age determinations through measurements of naturally occurring tritium are ambiguous at best.

9) Radioactive tracers are superior to chemical tracers.

LITERATURE REFERENCES

1) Tsang, C. F., Bodvarson, G., Lippman, M. J. and Rodriguez, J. R., "A Study of Alternative Reinjection Schemes for the Cerro Prieto Geothermal Field, Baja California, Mexico", Geothermal Resources Council, Transactions, Volume 2, pp. 659-662, July 1978.

2) Tansev, E. O. and Wasserman, M. L., "Modeling the Heber Geothermal Reservoir", Geothermal Resources Council, Transactions, Volume 2, pp. 645-647, July 1978.

3) Hanson, J. M. and Kasameyer, P. W. "Predicting Production Temperature Using Tracer Methods", Geothermal Resources Council, Transactions, Volume 2, pp. 257-258, July 1978.

4) Miller. R. J., "Enhanced Recovery Reservoir Engineering Aspects of Geothermal Development", Geothermal Resources Council, Transactions, Volume 2, pp. 457-459, July 1978.

5) Whiting, R. L. and Ramey, H. J., "Application of Material and Energy Balances to Geothermal Steam Production", Journal of Petroleum Technology, July 1969.

6) Garg, S. K., Pritchett, J. W. and Brownell, D. H., "Transport of Mass and Energy in Porous Media", Proceedings, Second United Nations Symposium on the Development and Use of Geothermal Resources, Volume 3, pp. 1651-1656, San Francisco, 1975.

7) Einarsson, S. S., Vides, A. R. and Cuellar, G., "Disposal of Geothermal Waste Water by Reinjection", Proceedings, Second United Nations Symposium on the Development and Use of Geothermal Resources, Volume 2, pp. 1349-1363, San Francisco, 1975.

8) Kubota, K. and Aosaki, K., "Reinjection of Geothermal Hot Water at the Otake Geothermal Field", Proceedings, Second United Nations Symposium on the Development and Use of Geothermal Resources, Volume 2, pp. 1379-1383, San Francisco, 1975.

9) Vetter, O. J., "Tritium Tracer as a Means for Reservoir Verification in Geothermal Reservoirs", Proceedings, EPRI Annual Geothermal Project Review and Workshop, pp. 1714-1723, Kah-Nee-Ta, Oregon, July 1977.

10) Vetter, O. J. and Crichlow, H. B., "Injection, Injectivity and Injectibility in Geothermal Operations: Problems and Possible Solutions", Phase I (Definition Study).

DOE/DGE Contract No. ET-78-C-03-2044.

11) Vetter, O. J. and Crichlow, H. B., "Reservoir Tracer Adsorption Chromatography", awaiting publication.

12) Brigham, W. E. and Smith, D. H., "Prediction of Tracer Behavior in Five-Spot Flow", SPE preprint 1130.

13) Reiss, J., Dyan, J. and Rappaport, D., "Methods for Calculating Tracer Distribution in Multiphase Plug Flow Systems", International Journal of Multiphase Flow, Vol. 2, No. 1, June 10, 1975.

14) Brigham, W. E., Reed, P. W. and Dew, J. N., "Experiments on Mixing During Miscible Displacement in Porous Media", Society of Petroleum Engineers Journal, VI, No. 1, March 1961.

15) Wagner, O. R., Baker, L. E. and Scott, E. R., "The Design and Implementation of Multiple Tracer Programs for Multifluid, Multiwell Injection Projects, SPE preprint 5125.

16) Wagner, O. R., "The Use of Tracers in Diagnosing Interwell Reservoir Projects", SPE preprint 5125.

17) Mercado, S. and Samaniego, F., "An Example of Fluid Migration Between Layers of the Cerro Prieto Geothermal Field", Second Invitational Well Test Symposium, University of Berkeley, Berkeley, October 25-27, 1978.

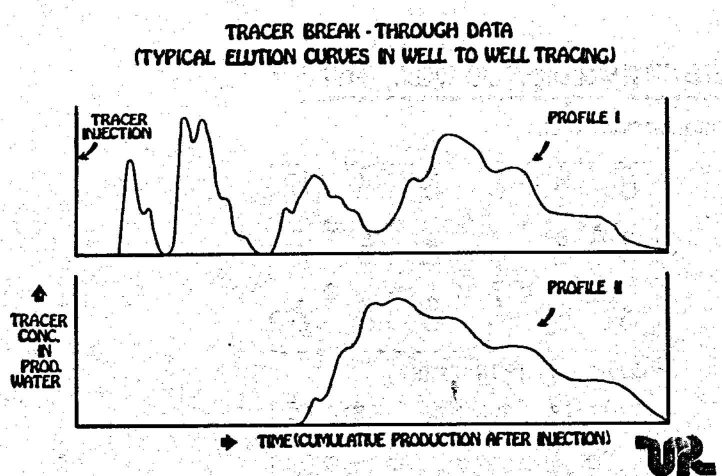

Figure 1

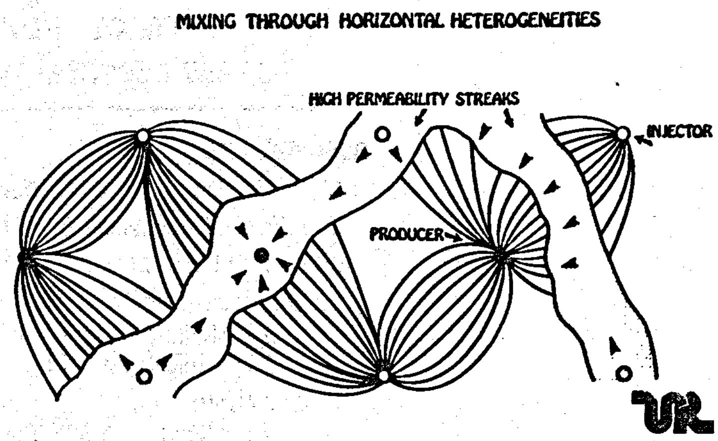

Figure 2

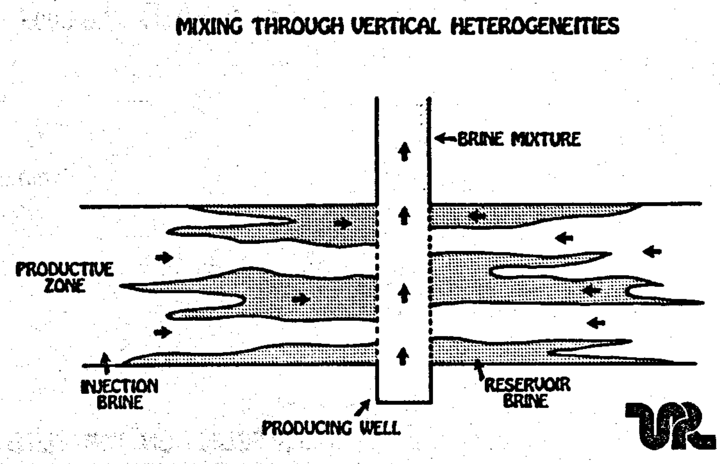

Figure 3

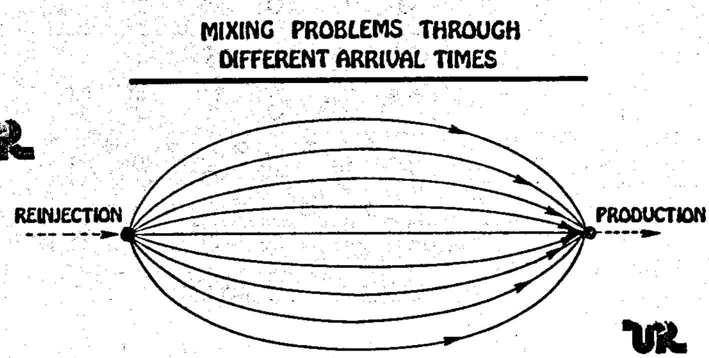

Figure 4

TRACER REQUIREMENT
(150 MW GEOTHERMAL POWER PLANT)

ASSUMPTIONS:

1.) Reinjection: 1.31×10^8 Lt/Day
2.) 10^{-2} % Of Reinjected Brine Must Be Found In Produced Brine
3.) Tracer Slug: 24 Hours
4.) Analytical Sensitivity:
    A.) Tritium: 2 DPM/ml
    B.) Chemical: 1 mg/Lt
5.) Cost/Unit:
    A.) Tritium: \$ 50.-/Curie
    B.) Chemical: \$ 0.30/Kg

TRACER JOB:

1.) Required Amount Of Tracer:
    A.) Tritium: 2.62×10^{15} DPM = 1178 Curies
    B.) Chemical: 1.31×10^6 Kg
2.) Total Cost Of Tracer:
    A.) Tritium: \$ 58.900.-
    B.) Chemical: \$393.000.-

Figure 5

TRACER SELECTION FOR FIELD WITH GEOMETRIC WELL PATTERN

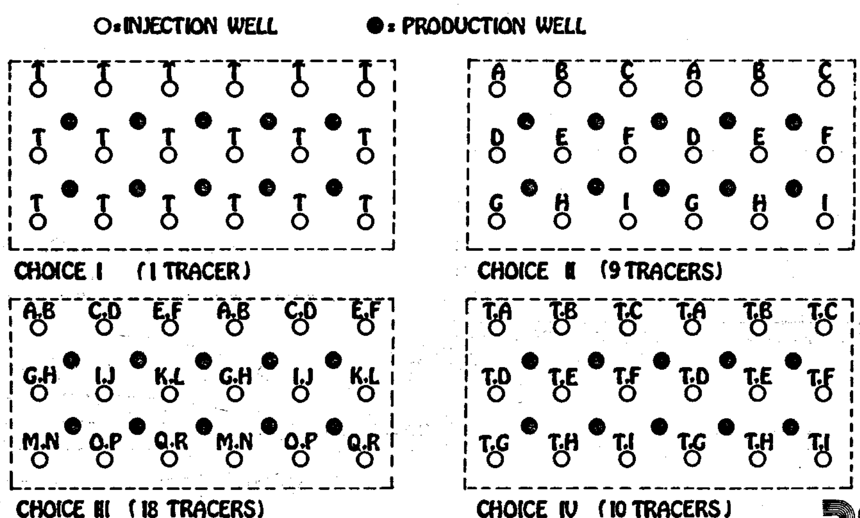

Figure 6

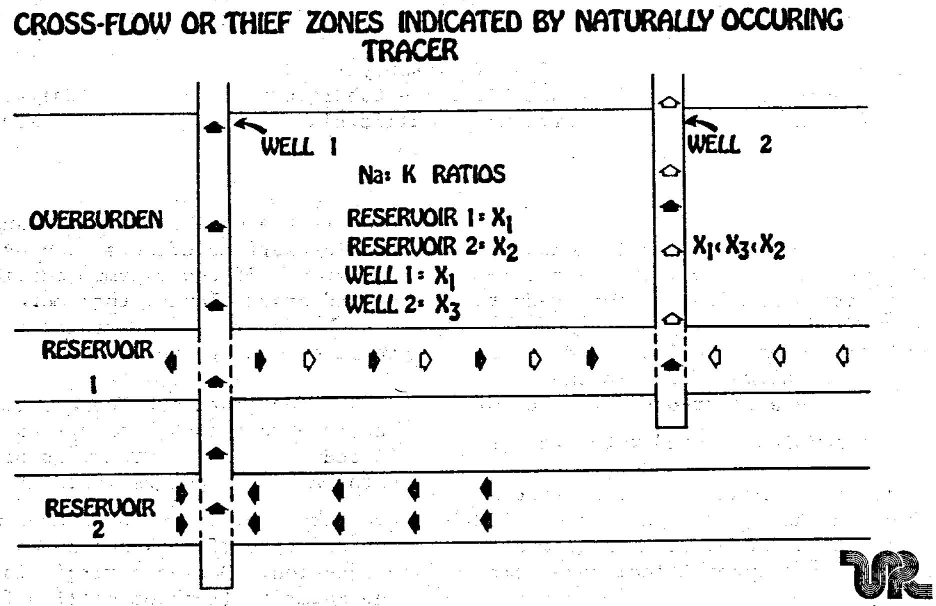

Figure 7

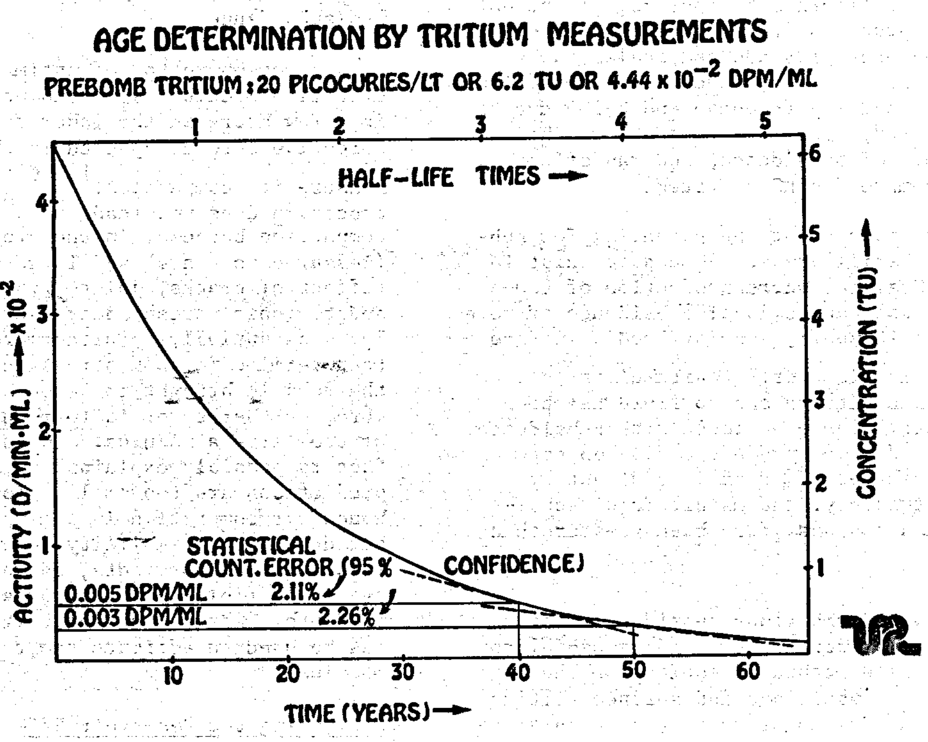

Figure 8

A METHOD OF USING *IN SITU* POROSITY MEASUREMENTS TO PLACE AN UPPER BOUND ON GEOTHERMAL RESERVOIR COMPACTION

John F. Schatz
Lawrence Livermore Laboratory
Livermore, California

Paul W. Kasameyer
Lawrence Livermore Laboratory
Livermore, California

James A. Cheney
University of California
Davis, California

ABSTRACT

Placing an upper bound on reservoir compaction requires placing a lower bound on the reservoir effective compaction modulus. Porosity-depth data can be used to find that lower-bound modulus in a young sedimentary basin. Well-log and sample porosity data from a geothermal field in the Imperial Valley, CA, give a lower-bound modulus of 7.7×10^3 psi. This modulus is used with pressure drops calculated for a reservoir to determine an upper bound on reservoir compaction. The effects of partial reinjection and aquifer leakage on upper-bound subsidence estimated from the compaction are illustrated for a hypothetical reservoir and well array.

INTRODUCTION

Systematic and large-scale withdrawal of fluids from subsurface reservoirs carries with it the potential for reservoir compaction and surface subsidence. It is desirable to have a method of estimating subsidence magnitude. Subsidence effects have been observed in association with oil and water withdrawal, and furthermore, have been identified as possible consequences of hydrothermal fluid production from geothermal reservoirs.[1-3] For example, in California's Imperial Valley, hot brines will be produced from a geologically young sedimentary sequence of sands and shales and cooler fluids will be reinjected. The compaction of this aquifer and layers above and below due to fluid pressure reduction may propagate to the surface in the form of subsidence, and may affect natural or man-made drainage systems.

Little is known about the potential for subsidence in geothermal areas. Some data exist for Wairakei, New Zealand, where production of geothermal fluids has caused local subsidence of more than 15 feet in 10 years, and involved a surface area 3000 feet in diameter.[3] Wairakei is in a volcanic geologic setting and no fluid has been reinjected there. The experience with subsidence caused by oil and water production may be more applicable to geothermal areas in sedimentary basins. Unfortunately, the magnitude of subsidence in these areas has often been greater than predicted.[4]

Before new and ambitious subsidence model development is considered, it would be useful to have an approximate method of estimating the greatest possible subsidence and surface tilting which could occur due to production at a particular field. If these maximum possible surface effects are acceptable, then the subsidence modeling effort could be terminated at an early and inexpensive stage. For example, that would be the case if the maximum possible subsidence caused smaller surface effects than natural tectonic activity. If the maximum possible surface effects are adversely large, then more accurate models must be developed to predict the <u>actual</u> subsidence to be caused by production.

To estimate subsidence, we must determine how the reservoir rock compacts as its pore pressure is reduced. The systematics of the mechanical deformation of porous sedimentary rock and soil are very similar.[5] Therefore, we adopt some of the concepts of soil mechanics for the following discussion. During a virgin loading increment, the material (rock or soil) deforms inelastically in response to a static load, and has a small modulus which we call its normal consolidation modulus. Recovery during an unloading increment, and recompaction during successive cycling up to the preconsolidation load is primarily elastic, and the material is much stiffer, deforming with its recovery modulus. To estimate reservoir compaction, we must find the reservoir effective modulus defined as the ratio of the production-caused pore pressure drop to compaction. For our purposes, we wish to place a lower bound on the reservoir effective modulus, because that is the one consistent with an upper bound for compaction and subsidence.

A common method of estimating the reservoir effective modulus is to subject a sample of rock in a few hours in the laboratory to the change in effective stress expected in the reservoir, and to measure its compaction.[1,3,6] Unfortunately, this procedure does not lead to an upper bound for compaction because, in the field, long-term (measured in years) and large-scale mechanisms (effect of cracks, joints, faults, fluid flow, and tectonic stress) decrease the effective modulus substantially. Furthermore, it is difficult to determine *in situ* stress accurately, and if the rock is brought to less than its *in situ* pressure, further error is introduced in the direction of too large a modulus. The neglect of these factors possibly explains why many subsidence predictions are too small. To estimate an upper bound for compaction in a manner consistent with our desire for simplicity we choose, instead of laboratory measurements, an interpretation of available field data for porosity as a function of depth. The compaction curve thus established can be used to estimate the reservoir effective modulus.

<u>Estimating the Reservoir Effective Modulus</u>

Consider the case of a geologically young sedimentary environment as discussed above. After sediment is deposited on the surface, its porosity decreases with depth as it is buried by new sediments above. The decrease in porosity results from mechanical consolidation caused by the increased effective stress plus additional porosity loss due to other mechanisms such as chemical deposition. If we could observe the porosity of a particular packet of sediment through time as its depth of burial increased, we could put a lower bound on the effective modulus of that material. Assuming that, on the average, the sediment type varies little with time, and that the material deposited in pores is either negligible or increases monotonically with depth, we can find that lower bound on the effective modulus for the entire reservoir from the present porosity vs depth curve. This procedure for finding a lower-bound reservoir effective modulus is correct even if the reservoir is preconsolidated or cemented.

The assumptions required by the above procedure for a lower bound on modulus are: (1) approximately constant material type and (2) increasing deposition with depth. With a longer list of assumptions: (1) constant material type, (2) no deposition, (3) no cementation, (4) no preconsolidation, and (5) no tectonically-caused porosity changes, our bound is the actual reservoir effective modulus.

Extensive porosity vs depth data are often not available as direct measurements. To illustrate our method, we use resistivity vs depth as interpreted from electric logs from a geothermal field. Then by using Archie's law for the case of highly saline water combined with salinity vs depth measurements, a porosity vs depth relationship may be determined. Results are shown in Figure 1, along with porosity determined by other methods for comparison.

At any depth in Figure 1, the porosity has considerable scatter in value. This is perhaps due to differences in initial porosity upon deposition and uncertainty in porosity estimates. However, despite this scatter, a definite trend is observed over an interval of several thousand feet. We choose to fit this trend with a logarithmic porosity law such that the reservoir effective modulus is given by

$$b = \frac{\gamma(1-\phi)}{\phi(\delta\, \ell n\, \phi/\delta z)} \qquad (1)$$

where

ϕ = porosity,
γ = average bouyant density of overburden, and
z = depth from surface.

This type of functional form has received considerable prior use and justification in the development of models of porous rock compaction.[5] The value of $\delta\, \ell n\, \phi/\delta z$ can be determined directly from a z vs $\ell n\, \phi$ plot as shown in Figure 1. For example, for a depth of 3000 feet and an average overburden bouyant density of 75 pounds/cubic foot

$$b = 7.7 \times 10^3 \text{ psi} \qquad (2)$$

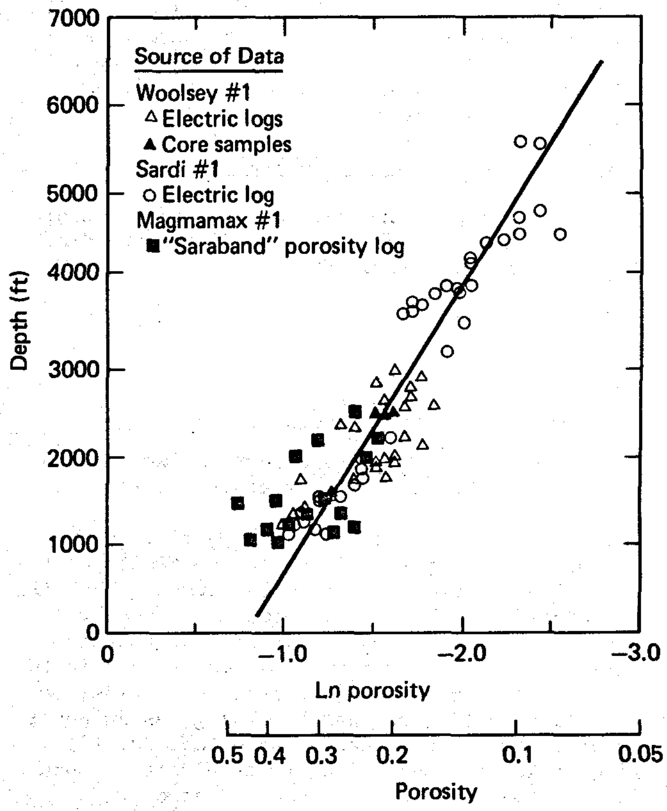

Figure 1. Porosity vs depth for selected wells near the Salton Sea Geothermal Field.

There are reasons why the seemingly small (as compared to hard rock) value of b given by Eq. (2) is a reasonable value for predicting an upper bound on reservoir compaction. For example, the value in Eq. (2) is within a factor of two of the moduli of sandy soils as measured in the laboratory at an applied pressure of 1500 psi.[7] Also, similar values were used with some success to match subsidence at the Wilmington Oil Field, Long Beach, CA, from pressure reduction data.[8]

Laboratory measurements on outcrop rock that is considered to be similar to reservoir rock give

$$b = 3.3 \times 10^6 \text{ psi} \qquad (3)$$

a value more than two orders of magnitude greater than Eq. (2). The test was a one-dimensional compression test at 3000 psi confining stress. Clearly, preconsolidation or cementation has given the outcrop rock a large modulus. This laboratory test demonstrates an extreme case of the need to be wary of determining reservoir effective modulus from laboratory tests. As a less extreme but more useful case, it would be desirable to do a laboratory compaction test on true reservoir rock, and to maintain pressure for several weeks or more (our test had a duration of several hours). Then, the magnitude of time-dependent effects could be observed. Furthermore, if reservoir compaction data becomes available, laboratory-to-field size effects might be investigated.

Example of Estimation of Subsidence

The estimated upper bound of surface subsidence resulting from a calculated pressure drop distribution is obtained by

$$\delta = \frac{h \, \Delta P}{3b} \qquad (4)$$

where

h = thickness of aquifer, and

ΔP = pressure drop due to flow (assumed to equal change in effective stress).

The factor of three reduction appearing in the denominator of Eq. (4) is a crude estimate of the reduction of surface subsidence caused by bulking and arching in the layers between the reservoir and the surface. Because of uncertainties in this factor, and our simple method of calculating subsidence from reservoir effective modulus, we have less confidence that Eq. (4) gives an upper bound to subsidence than we have that Eq. (1) gives a lower bound to reservoir effective modulus. Also, no attempt is made to account for thermal contraction due to the cooling of a geothermal reservoir. For these reasons, the results of this section should be viewed as an example of the application of our method of placing a lower bound on the reservoir effective modulus for compaction, rather than a precise calculation of an upper bound on subsidence.

The upper-bound subsidence estimates shown in Figure 2 a-d, have been calculated for a hypothetical aquifer and well array.[9] We choose to illustrate the possible effects of reinjection percentage and aquifer confinement on subsidence. Thirty years of production is assumed. Nine wells penetrate fully into an aquifer which is 200 m thick with a permeability of 200 mD and a fluid viscosity of 0.6 cp. The aquifer is assumed to be totally confined in Figures 2a and 2b and confined by a "leaky" 200 m thick, 5 mD aquitard in Figures 2c and 2d. The six production wells, located at the outside of the array, each have a liquid production rate of 0.04 m^3/s. Upper bound reservoir compaction is calculated using the modulus of Eq. (2) for calculated pressure drops. A recovery modulus 20 times larger is used for the region of pressure increase near the injection wells. Subsidence is calculated using Eq. (4).

Several observations can be made for this example. For a fully confined aquifer, injection significantly reduces the area and depth of the upper bound expected subsidence bowl. If the aquifer is leaky, then the area and subsidence due to aquifer compaction are not so strongly affected by injection rate. Of course, in this case, compaction within the aquitard should also be evaluated, and we have not done so.

In the results shown in Figure 2, the maximum land tilt is about 70 cm/km (after 30 years). This can be compared to observed natural tilting rates of about 0.8 cm/km/year in the vicinity of the Salton Sea.[10] If these natural rates are extrapolated to thirty years, they would result in a tilt of 20-30 cm/km. Thus, natural tilts (due presumably to tectonic activity) and our estimate of an upper bound on production-caused tilts for the hypothetical aquifer and array are comparable. We would say, that for this situation, geothermally-caused subsidence could not produce any adverse effects that could be distinguished from presently occurring natural processes. However, we could no longer say this for very different reservoir, array, or production conditions, such as a significantly higher production rate.

Comparison to Measured Subsidence at Wairakei

The production history at Wairakei has been previously modeled in two dimensions based on a reservoir cross section with considerable geologic input.[3] The calculated pressure drop in the area of maximum subsidence is compared to subsidence in Figure 3. Although our assumption of a young sedimentary basin does not apply to the volcanic setting of the Wairakei field, it is interesting to consider the Wairakei experience with respect to the difficulty in obtaining the appropriate reservoir compaction properties for long-term subsidence predictions.

The Wairakei work indicates:

- The ratio between pressure drop and surface subsidence changes with time, suggesting that the deformation of the reservoir and overlying rocks involves time delay and inelastic behavior.

- A modulus for the reservoir based on the average subsidence over twenty years corresponds to a rock modulus ten times larger than measured in the laboratory.

- If the factor of three in Eq. (4) is assumed to apply, and it is noted that the rate of subsidence has not slowed, even though the rate of pressure drop has decreased, then the difference between field results and laboratory tests are greater than a factor of thirty, and this factor will increase as subsidence continues.

- The ratio of pressure drop to the upper bound for subsidence (= 3b/h from Eq. (4)) based on the Imperial Valley data of Figure 1 is 2.2 bars/m. At Wairakei, the ratio established during twenty years of production is 12 bars/m; subsidence is continuing, and the ratio will probably decrease with time. These values are surprisingly similar,

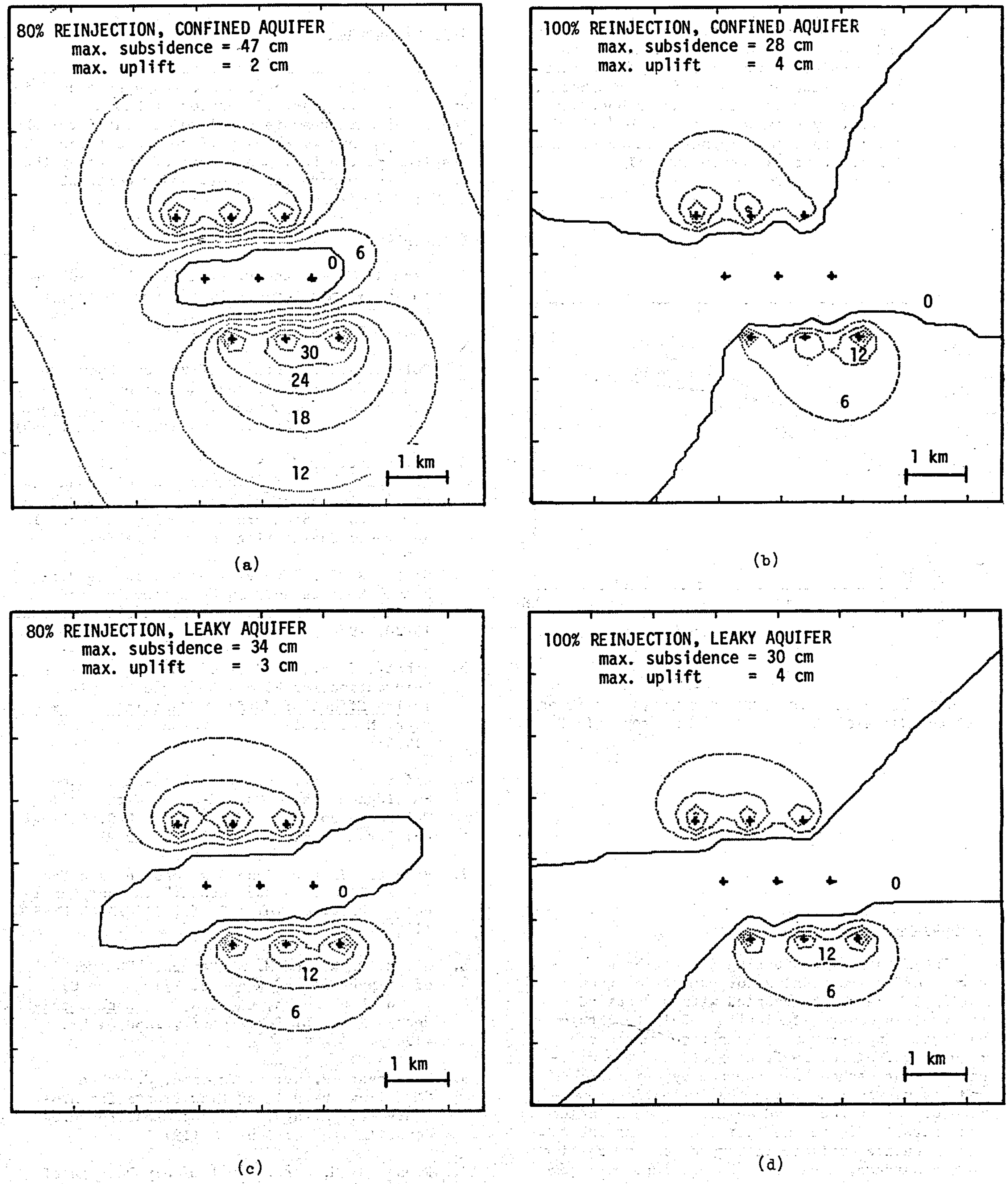

Figure 2. Examples of estimation of upper bound on subsidence using our method of finding a lower bound for the reservoir effective modulus. The hypothetical well array and aquifer are described in the text. Contour interval is 6 cm.

considering the differences in rock type and geologic history in the two areas. The modulus derived from *in situ* measurements at the wrong location works better in this case than the modulus based on laboratory measurements on the "right" rocks. This coindicence illustrates how difficult it can be to determine the appropriate reservoir modulus.

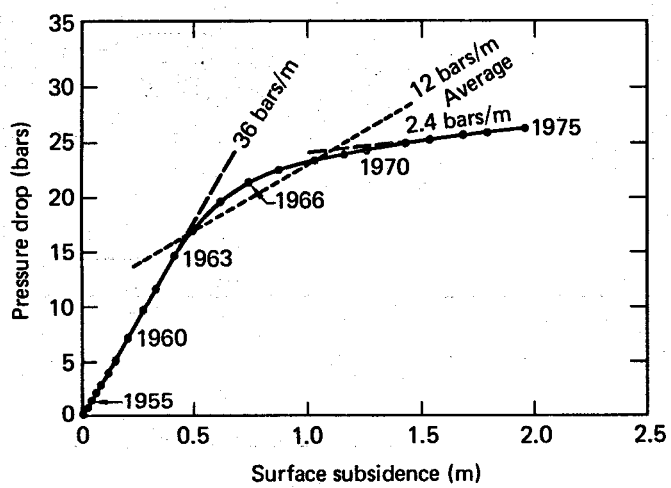

Figure 3. Reservoir pressure drop vs subsidence at the Wairakei Geothermal Field (from Ref. 3).

CONCLUSIONS

The method of evaluating a lower-bound reservoir effective modulus for compaction that is outlined here can be coupled with a detailed reservoir pressure simulation model to obtain an estimated upper-bound to long-term subsidence resulting from reservoir compaction. The validity of our method is supported by observations and discussion concerning the inelastic properties of porous rocks and soils. A model including thermal effects and aquitard compaction, a more accurate estimate of compaction propagation to the surface, more data on long-term rock compaction, and input from monitoring surface elevation during production could improve the estimate.

Acknowledgments

J. Tewhey and M. Chan of LLL provided core porosity estimates and the outcrop sample used in our laboratory test. J. Hanson of LLL modified the reservoir pressure model to account for leaky aquifers. This work was performed under the auspices of the U.S. Department of Energy by the Lawrence Livermore Laboratory under contract number W-7405-ENG-48.

References

1. Mayuga, M. N., and D. R. Allen, "Subsidence in the Wilmington Oil Field, Long Beach, CA, U.S.A." in Land Subsidence, Proc. of Tokyo Conf., IASH/AIHS-UNESCO (1969).

2. Poland, J. F., "Status of Present Knowledge and Needs for Additional Research on Compaction of Aquifer Systems," in Land Subsidence, Proc. of Tokyo Conf., IASH/AIHS-UNESCO (1969).

3. Pritchett, J. W., S. K. Garg, and D. H. Brownell, "Numerical Simulation of Production and Subsidence at Wairakei, New Zealand," in Summaries of Stanford University Geothermal Reservoir Engineering Workshop (1976).

4. Scott, R. F., "Overview of Subsidence Problem," Keynote Address on Evaluation and Prediction of Subsidence, Pensacola, FL, Jan. 15-20, 1978.

5. Schatz, J. F., "Models of Inelastic Volume Deformation for Porous Geologic Materials," in The Effect of Voids on Material Deformation, M. Carroll and S. Cowin, ed., ASME (1976).

6. Lofgren, B. E., and R. L. Klausing, "Land Subsidence due to Ground-Water Withdrawal Tulare-Wasco Area, California," U.S. Geological Survey Prof. Paper. 437-B (1969).

7. Roberts, J. E., "Sand Compression as a Factor in Oil Field Subsidence," in Land Subsidence, Proc. of Tokyo Conf., IASH/AIHS-UNESCO (1969).

8. Allen, D. R. and M. N. Mayuga, "The Mechanics of Compaction and Rebound, Wilmington Oil Field, Long Beach, CA, USA," in Land Subsidence, Proc. of Tokyo Conf., IASH/AIHS-UNESCO (1969).

9. Kasameyer, P. W., L. Thorson, C. McKee, "Modeling Thermal and Flow Fronts for Arbitrary Well Arrays," in Geothermal Resources Council, Transactions, 1 (1977).

10. Reese, S. M., Jr., "Preliminary Results of the 1976-1977 Imperial Valley Leveling Surveys," National Geodetic Survey (1977). See also N. B. Crow and P. W. Kasameyer, "Monitoring Natural Subsidence and Seismicity in the Imperial Valley as a Basis for Evaluating Potential Impact of Geothermal Production," in Geothermal Resources Council, Transactions 2 (1978).

AN EXAMPLE OF FLUID MIGRATION BETWEEN THE LAYERS ON THE CERRO PRIETO GEOTHERMAL FIELD

Sergio Mercado and Fernando Samaniego
Instituto de Investigaciones Eléctricas
Cuernavaca, México

ABSTRACT

This paper shows a field example of fluid migration between the layers of the Cerro Prieto Geothermal Field. The first part present results for well M-15. Measurements of the Na/K index are used to demonstrate the mixing of relatively warm water of the upper layer with the hotter water of the lower layer. The second part shows results for well M-21 and its replacement M-21A, completed at the upper layer.

INTRODUCTION

The Cerro Prieto Geothermal Field is located about 30 kms south of Mexicali, Baja California, México. In this field CFE has drilled a total of 55 wells, eighteen of which are now being used for eletricity generation at the first 75MW geothermoelectric plant that has been continuosly operated since 1973. Some of these eighteen wells were drilled more than ten years ago, and have shown collapse and related problems, causing the need for repair jobs. Several of these jobs have not been successful and the wells were plugged. Due to the fact that is was desired to use the same surface facilities of the plugged wells, replacement wells were drilled close to the original wells.

The average spacing of the first production wells is 200 m, and field measurements have shown interference between the wells. Recently drilled wells to be used for the second 75MW plant to start operation in 1979, have a spacing of 400 m; it is expected that this will decrease interference effects.

Since Cerro Prieto reservoir is of liquid dominated type, a great hot water volume with high salt content is wasted. Reinjection is being considered as an alternative for the disposal of the brine. Several authors have shown that the reservoir is a two layers system.[1,2,3,4]. This has to be considered in any modeling and field testing of reinjection. This paper shows a field example of fluid migration between the layers of the reservoir. Results were obtained from measurements at wells M-15, M-21 and their replacement wells, and also well M-39.

GENERAL BACKGROUND

Reservoir engineering studies commonly assume that the reservoir consists of a single layer, and has constant rock and fluid properties throughout. The actual occurrence of such reservoir is almost imposible. The environment in which sediments are deposited is very complex, and there are many possible chemical and physical changes that can occur, causing heterogeneities, some of them not necessarily obvious in the reservoir behavior. Perhaps the most common type of heterogeneity that we come across with is that which results from various cycles of sedimentation-a set of heterogeneous layers. There are two possible situations for these layers which have been thoroughly discussed in the pressure transient analysis literature:[5,6,7,8,9].
a) cross flow exist between the layers, and b) no-cross flow exists between the layers due to impermeable lamination. For the case of the layer system with no-cross flow, the only communication is by means of the common wellbore. It is well established that the behavior of the two cases is quite different.

The Cerro Prieto Geothermal Field is a heterogeneous system, composed of at least two main layers.[1,2,3,4]. Fig. 1 presents an areal view of the field. Shown in this figure are wells M-15 and M-21, which are the subject matter of this study. It is intented to show how chemical and physical measurements can be used to interpret the fluid mixing of the different layers ocurring in the reservoir. This field seems to fall on category b) of heterogeneous layer systems previously discussed. As will be shown later in this paper, completion and mechanical problems in the production pipes cause that fluid migrates from one layer to another, this being in some cases a severe problem, like the scaling caused by the mixing of hot and relatively warm water of the two main layers.

DISCUSSION

This section presents results for well M-15 and M-21. First results are discussed for well M-15. This well was drilled to a depth of 1286 m, developing problems during completion, like casing collapse. Repair jobs were carried out in 1970 and in 1973, when a 5" casing was cemented to a depth of 775 m. Due to the previously mentioned problems, the job was not successfull and the well was abandoned, filling it with mud to a depth of 809 m where the well was blocked up.[4,10].

After the lost of well M-15, it was decided to drill a replacement well, M-15A. This is located about 27 m from the original M-15 well, and its depth is 1264 m. Due to the closeness of the two wells, to the actual abandonment situation at M-15, and to the layer characteristics of Cerro Prieto, it is expected that some sore of interference and communication between the wells M-15 and M-15A would occur. Fig. 2 shows data of M-15A of the variation versus time of: a) temperature of fluid produced, b) Na/K index, and c) flashed steam production. The temperature of the fluid produced (Fig. 2.a) decreased sharply at the beginning and then took a more gradual descense, until reaching an almost constant temperature flow in 1976. It is important to notice in this figure the difference between the measured bottom-hole temperature before the start of production (point (1), 308 °C) and the temperature after two years (point (2), 258°C). The sharp reduction on temperature is reflected in a sudden rise of the Na/K index (Fig. 2.b) in the third quarter of 1974 and after a peak in mind 1975, it decreases slowly. With regard to steam production, the well produced 92 ton/hr in August, 1974, and went down to 60 ton/hr in three months (Fig. 2.c), finally stabilized flow was reached after two and a half years of production, and is about 44 percent of the initial steam flow of the well.

Table 1 shows data of the variation of the Na/K index and wellhead flowing pressure versus time for well M-15A. Also shown is data of the orifice used for the well. It can be observed that at beginning the Na/K index had a value of 7 units, in accordance with temperature data measured before the start of production for the deepest layer. After 20 days of production the index is 9.4 units. This is explained as been caused by migration of relatively warm water of average temperature of 214 °C coming from the upper layer of well M-15.

Fig. 3 presents a visualization of the situation at well M-15 and M-15A. Since the blocking of well M-15 was not caused intentionally, it is possible that some fluid move away from the upper relatively warm layer to the hot deeper layer at well M-15. Furthermore, this fluid of average temperature of 214 °C could flow through the deeper layer toward well M-15A just 27 m apart, and affect the temperature of the fluids produced.

Fig. 4 presents a more detailed visualization of the situation between these wells. The Na/K index for the temperature of 277 °C at well M-15A is of 7 units, and combined with the Na/K index of 12u for the relatively warm fluids coming from M-15, gives an average Na/K index for the fluid produced of 9.5 units. This is an arithmetic average of the indices of the two fluids. The downward flow in well M-15 can be caused among other things by difference in pressure between the layers or the higher density of the relatively warm fluids of the upper layer with respect to the lower density of the hot fluid of the deeper layer.

Table 2 shows the variation of the steam rate and the water-steam ratio versus time. It is observed that at the beginning (Fig. 2.c) the high steam rate had a water ratio of 2.7, but it increased, with some oscillations, with time. This situation has been already discussed to be a possible consequence of the mixing of relatively warm water with hot water. Another explanation for the decrease in the steam rate could be the presence of scaling detected at well M-15A by mechanical measurements. Fig. 5 illustrates the completion details at well M-15A. Casings of 11.3/4" and 7.5/8" have been cemented. This last casing has a slotted portion at the bottom, and besides the scale problem there seems to be others, like sand sloughing or casing collapse shown in this figure. The scale deposition may be explained by the mixing of different composition warm water with hot water. This scale appears to be even covering part of the bottom of the open casing.

Field data that support the existence of fluid migration between the layers is obtained from well M-39 (Fig. 1) located about 200 m from well M-15A. Fig. 6 shows a visualization of the interaction between these wells. In Fig. 6.a well M-39 is shut-in and M-15A is flowing with a steam rate of 40 ton/hr. In April 1976 (Fig.6. b) well M-39 starts production, while M-15 is producing 41 ton/hr. This causes that not all of the low enthalpy fluid go to well M-15. This is shown in Fig. 6.c, where steam production at M-15A has increased up to 51 ton/hr. In Fig. 6.d production at well M-39 has decreased, causing that more low enthalpy fluid flow toward well M-15A, decreasing the steam production to its previous level of 41 ton/hr.

With regard to well M-21, it was drilled to a depth of 1505 m, cementing casing up to a depth of 1080 m. As previously discussed for well M-15, well M-21 also developed problems during drilling and completion, like sand sloughing and tubing collapse.[4,10]. After unsuccessfull repair jobs, the well was plugged up to about 1000 m, remaining open in the lower part comunicating with the liner. After the lost of well M-21, its was decided to drill replacement well M-21A, located at only 21 m apart. This well was drilled to a depth of 1300 m, and has been a good producing well. Again, due to the closeness of the two wells, to the actual abandonment situation, and to the layer characteristics of Cerro Prieto, it is expected that some interference and communication would occur between the wells M-21, and M-21A.

Fig. 7 shows data for well M-21A of the variation versus time of: a)water-steam ration, b) steam production, and c)Na/K index. The water-steam ratio (Fig. 7.a) increased with time. At short times, it has a value less than one, an uncommon value for a Cerro Prieto well. A plausible explanation is that steam from the deeper layer (Fig. 8) migrates through well M-21 which is not completely blocked up, and then through the upper layer toward well M-21A. Fig. 7.b shows the flashed steam production versus time; as seen, it decrease with time, reaching approximately stabilized conditions at the end of 1976. Fig. 7.c shows the variation of the Na/K index, which ranges from 6 to 7 units.

Fig. 8 showing a detailed visualization of the situation at well M-21, can be used to explain the value of the index for the fluid produced. The fluid of the deeper layer at well M-21 have a Na/K index of 5 units, while the fluid at M-21A had originally a Na/K index of 7 units, which approximately averaged gives an index of 6.5 units, which is the index of the produced fluids. Thus, fluid migration between the layers could again explain the Na/K index behavior. Also the early high rate of high enthalpy steam can be explained by the migration of steam coming from the the deeper layer through the liner of M-21. For later times, the decrease in the steam rate and the increased in the water-steam ratio can possibly be explained by scale deposition in the reservoir caused by flashing.

CONCLUSIONS

The main purpose of this study has been to show a field example of the fluid migration between, the layers of Cerro Prieto Geothermal Field. From the results of this work the following conclusions have been drawn:

1. Fluid migration exists between the layers of the reservoir. For well M-15, this is indicated by measurements of the Na/K index, enthalpy and flow rate, which change due to migration from the upper warm water layer to the lower hot water layer.
2. The Na/K index can be used to analyze the structural properties of the reser-

voir and fluid migration characteristics. This information can be useful for reinjection purposes.

3. Field measurements indicate that the replacement wells are affected by the original wells due to fluid migration.

4. Well spacing of 200 m show interference effects.

5. For well M-21, fluid migration is from the hot lower layer to the warm upper layer. This flow consists mainly of steam.

6. There are at least two producing layers with different physical and chemical characteristics.

REFERENCES

1. Puente, J.: "Geology of the Cerro Prieto Geothermal Field", presented at First Symposium on the Cerro Prieto Geothermal Field, San Diego, Ca., Sept. 20-22, 1978.

2. Abril, A. and Noble, J.E.: "Geophysical Well Log Correlation Along Various Cross Sections of the Cerro Prieto Geothermal Field", presented at First Symposium on the Cerro Prieto Geothermal Field, San Diego, Ca., Sept. 20-22, 1978.

3. Mercado, S.: "Chemical Changes in Geothermal Well M-20, Cerro Prieto, México", Geological Soc. of America Bull., V. 20 (Dec., 1969) p. 2623-2630.

4. Mercado, S.: "Mecanismo de Producción de Pozos del Campo Cerro Prieto y su Relación con el Indice Na/k", presentéd at "Primera Reunión de Intercambio Técnico sobre Geotermia" organized by "CFE-Coordinadora Cerro Prieto", San Felipe, B.C.N., November 28-30, 1977.

5. Tarik, S. M., and Ramey, H.J., Jr.: "Drawdown Behavior of a Well with Storage and Skin Effect Communicating with Layers of Different Radii and Other Characteristics", paper SPE 7453, presented at the 53rd Annual Fall Technical Conference of SPE of AIME, Houston, Tex., Oct. 1-3, 1978.

6. Matthews, C. S., and Russell, D. G.: "Pressure Builup and Flow Tests in Wells", Monograph Series, Society of Petroleum Engineers of AIME, Dallas (1967) 1

7. Earlougher, R. C., Jr.: "Advances in Well Test Analysis",Monograph Series, Society of Petroleum Engineers of AIME, Dallas (1977)5.

8. Lefkovitz, H. C., Hazebroeck, P., Allen E. E., and Matthews, C. S.: "A Study of the Behavior of Bounded Reservoirs composed of Stratified Layers", Trans. AIME (1961), 222,43.

9. Cobb, W. M., Ramey, H. J., Jr., and Miller, F. G.: "Well Test Analysis for Wells Producing from two Commingled Zones of Unequal Thickness", Trans., AIME (1974), 257, 1035-1043.

10. Dominguez, A. B., and Vital B. F.: "Reparación y Control de Pozos Geotérmicos en Cerro Prieto, Baja California, México", Proc. Second U.N. Symposium on the Use and Development of Geothermal Energy, San Francisco, May 20-29, 1975, p. 1483-1495.

TABLE 1. Na/K Index for the Produced Fluids at Well M-15A

Date	Na/K	Diameter	Pressure psi
July 10,74	7.2	1/2"	686
July 15,74	7.0	3 "	563
July 15,74	7.6	3 "	526
July 16,74	7.5	4 1/2"	395
July 16,74	7.8		398
July 17,74	7.9	5 1/2"	300
July 17,74	7.7	6 "	293
July 19,74	8.6	6 "	300
July 22,74	8.7	6 "	298
July 29,74	9.4	6 "	321
Aug.,15,74			
Aug.,30,74	9.4	5 1/4"	280
Jan.,15,75	9.1	5 1/4"	212
Mar.,11,75	9.1	5 1/4"	200
Sept.,9,75			
Sept.11,75	10.7	8 "	158
Nov.,10,75	9.9	8 "	100
Mar., 8,76	9.6	8 "	97
May 24,76	9.4	8 "	102

TABLE 2. Variation as Time of Steam Rate and Water-Steam Ratio

Date		Flashed Steam Rate, ton/hr	Water-Steam Ratio
August	1974	92	-
Sept.		78	2.7
Oct.		73	3.0
Nov.		60	-
Jan.	1975	60	3.1
May		52	3.4
July		44	3.7
Oct.		47	4.5
Nov.		44	3.8
Jan.	1976	40	4.1
April		41	4.1
Aug.		53	3.2
Oct.		41	4

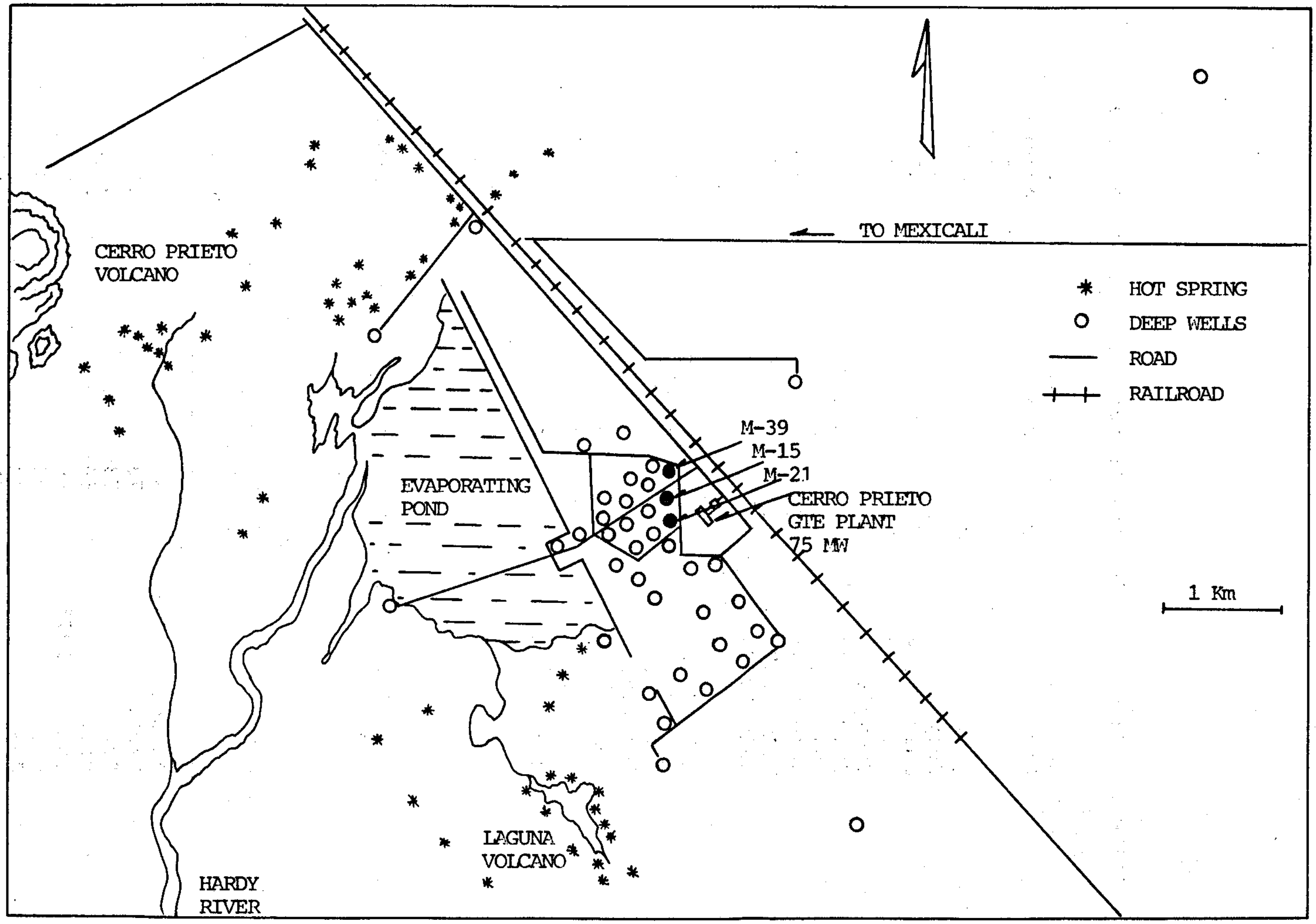

FIGURE 1. CERRO PRIETO GEOTHERMAL FIELD. LOCATION OF WELLS M-15, M-21 and M-39

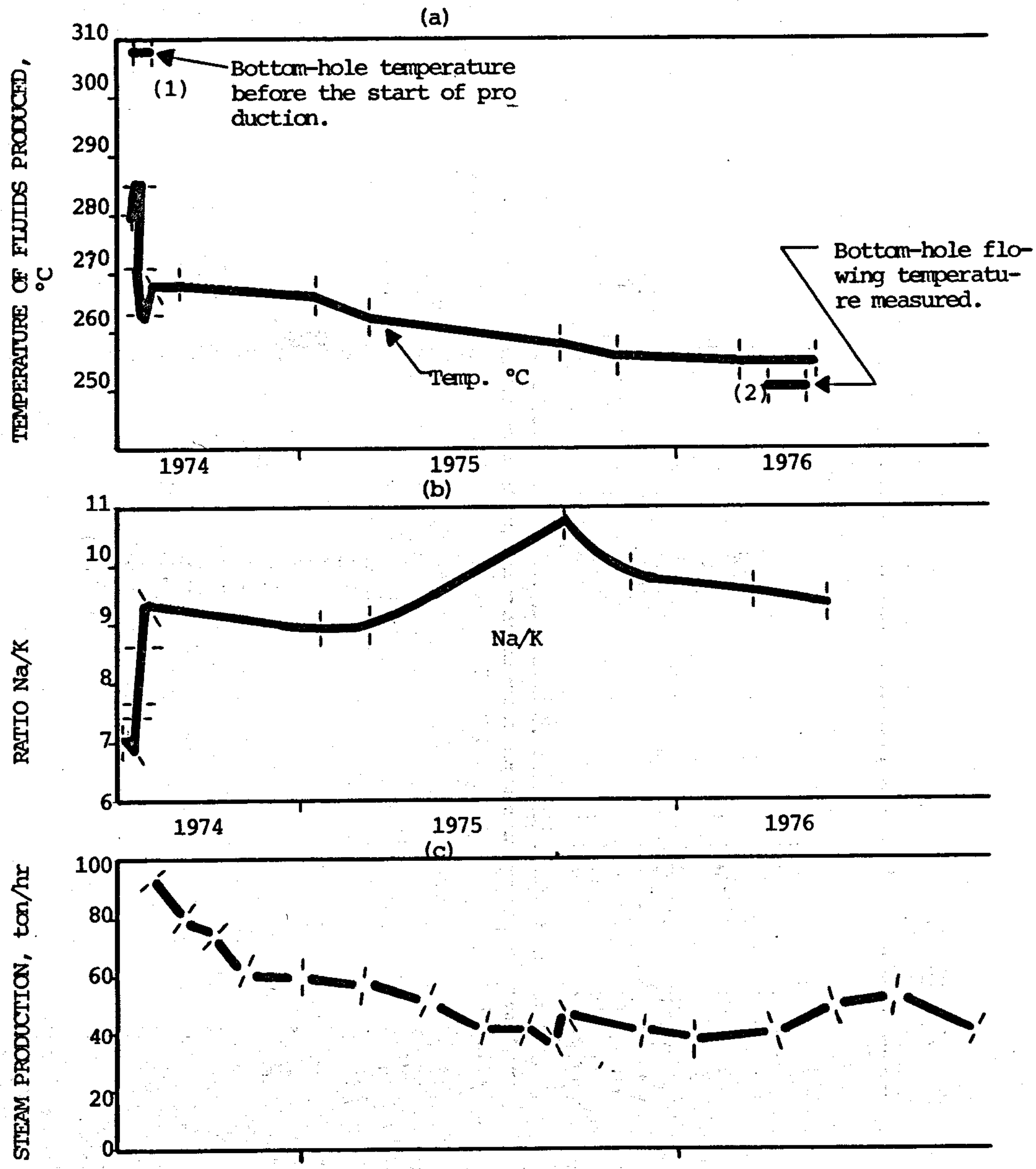

FIGURE 2. Well M-15A Variation vs. Time of:

(a) Temperature (calculated from Na/K ratios),
(b) Na/K Ratio, and
(c) Steam Production.

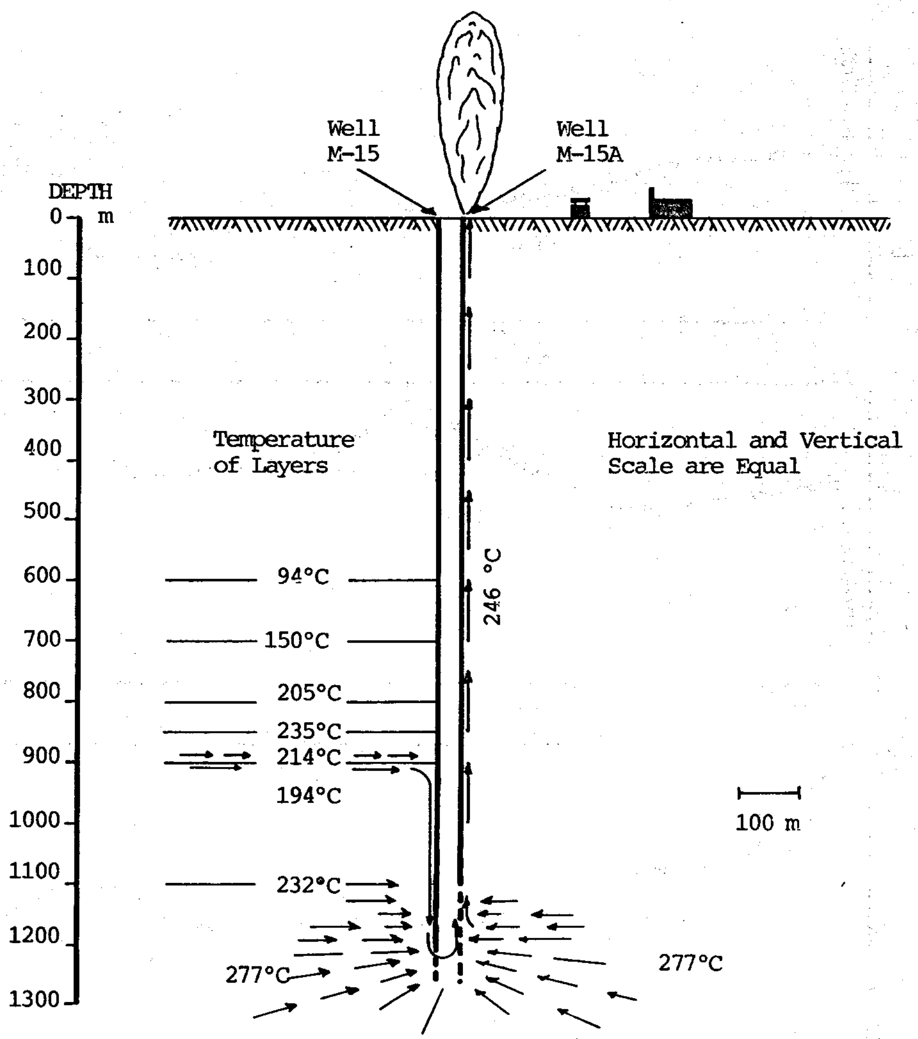

FIGURE 3. Visualization of Production Mechanism of Well M-15A

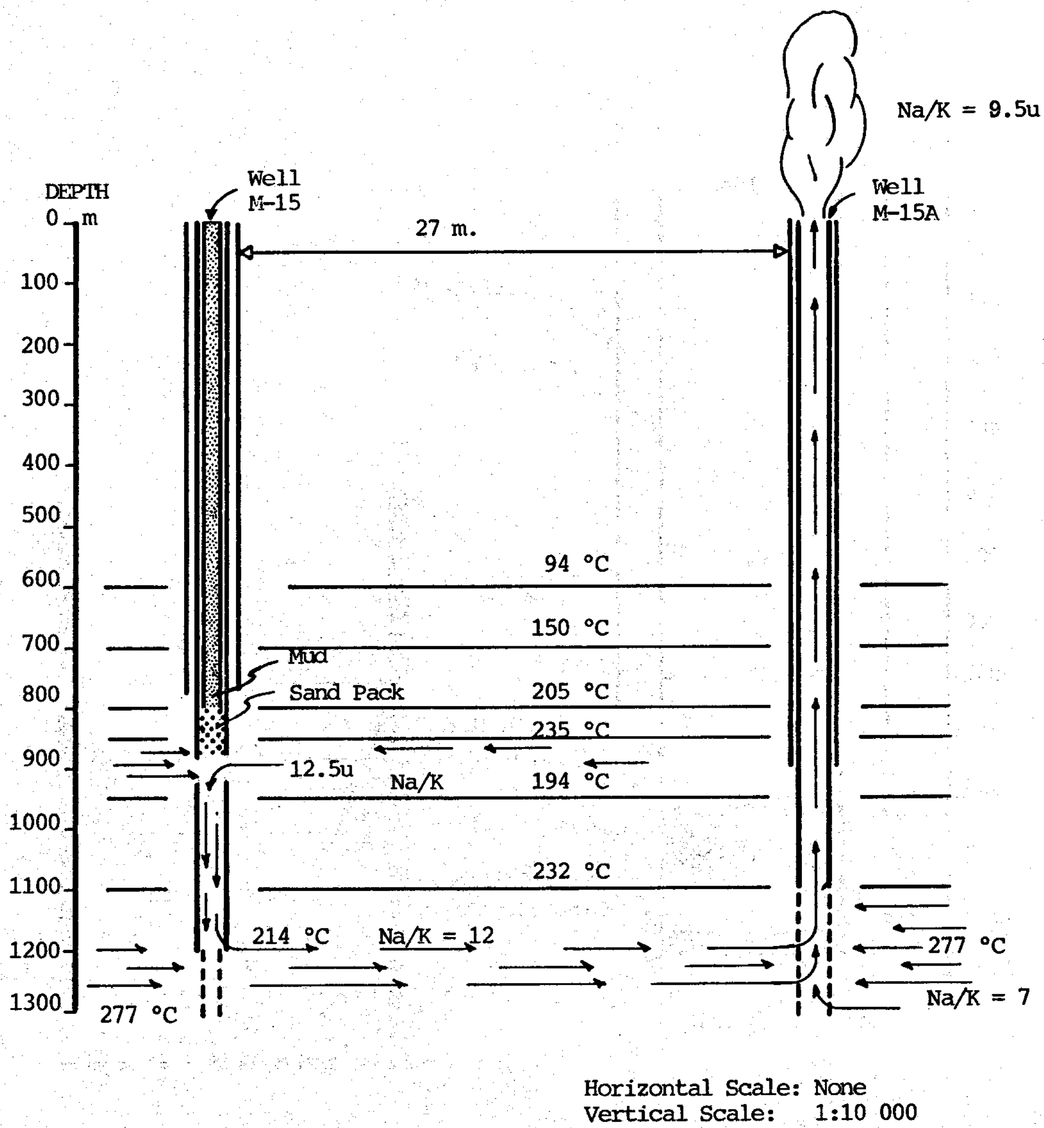

FIGURE 4. Detailed Visualization of the Production Mechanism of Well M-15A.

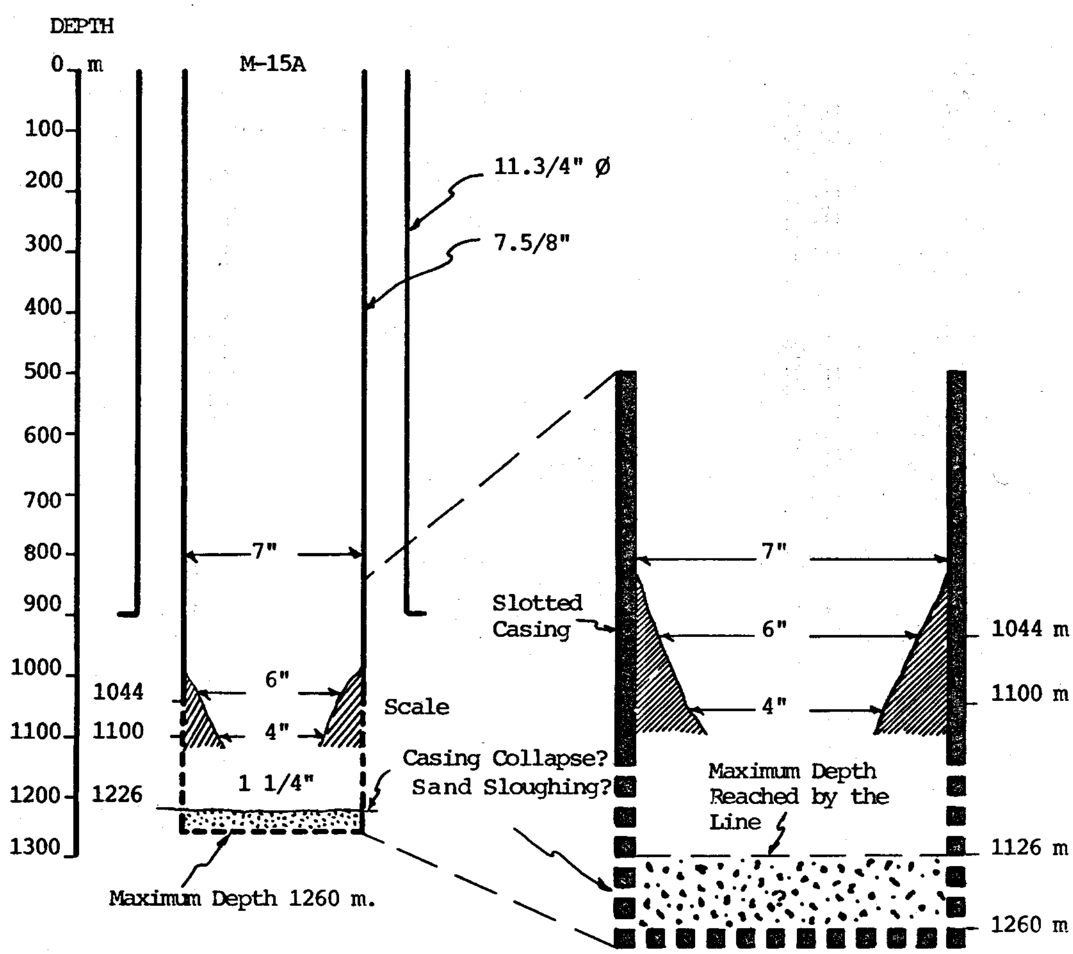

FIGURE 5. Squematic of Well M-15A Completion and Scale Deposition.

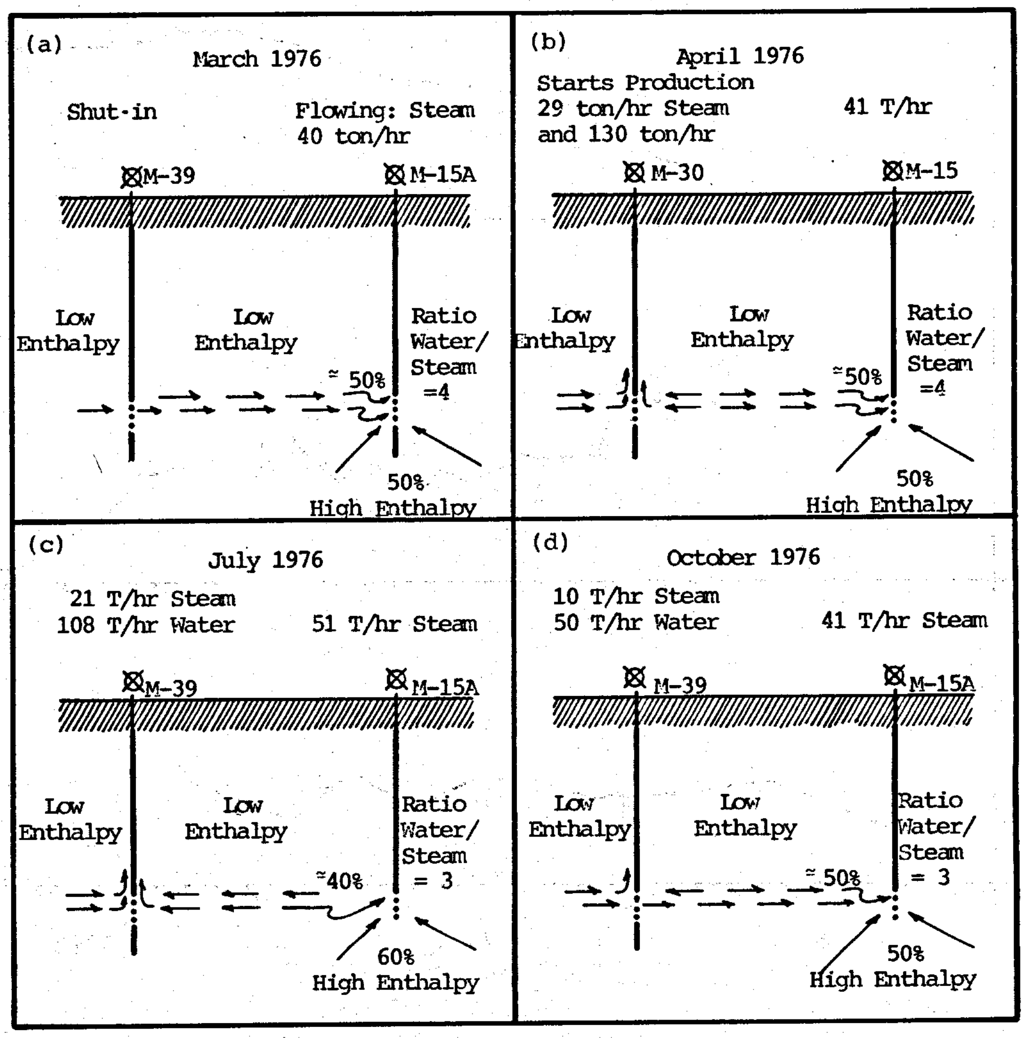

FIGURE 6. Fluid Migration Between Wells M-39 and M-15A

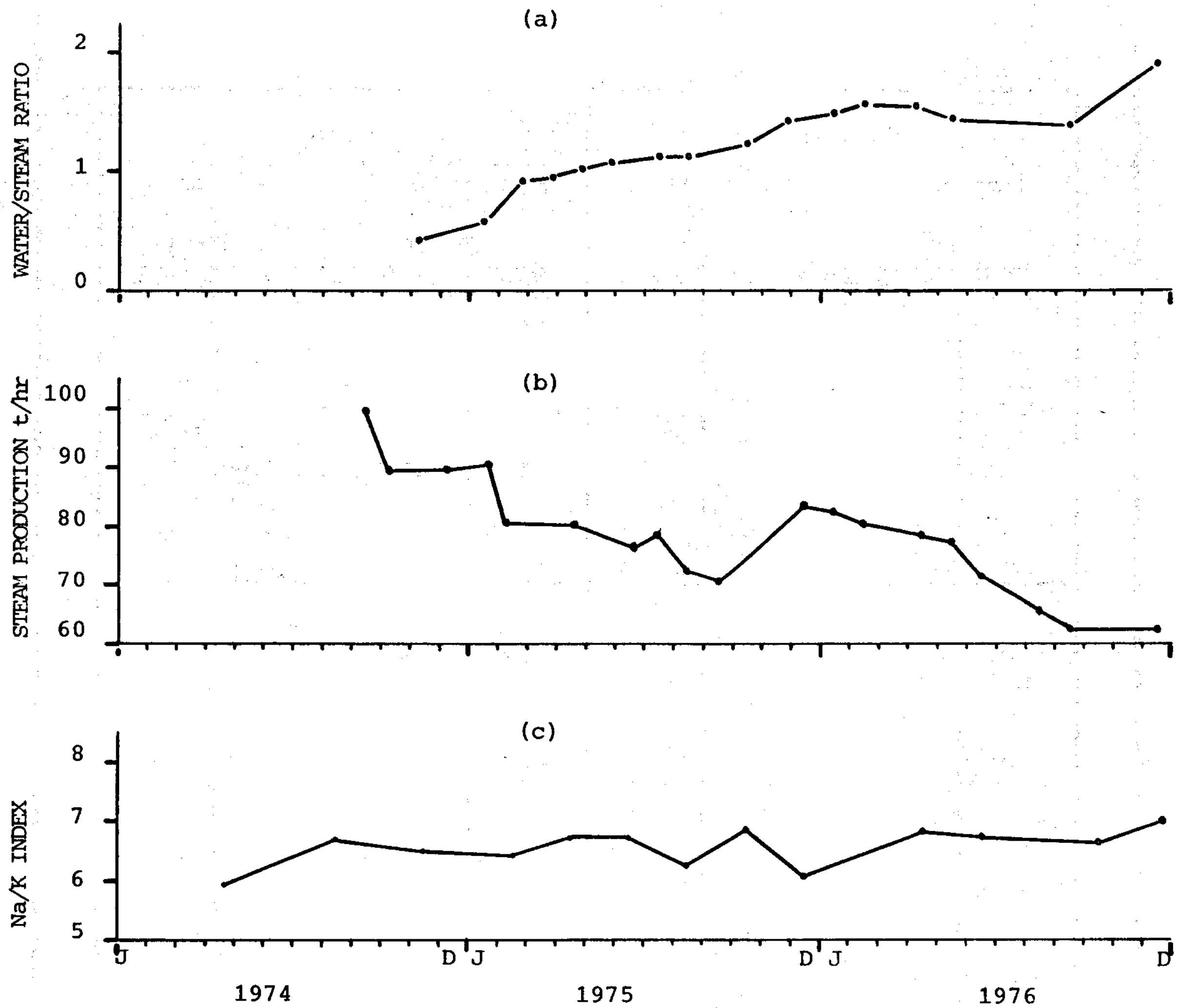

FIGURE 7. WELL M-21A, VARIATION VS. TIME OF:

(a) WATER TO STEAM RATIO,
(b) STEAM PRODUCTION, AND
(c) Na/K RATIO

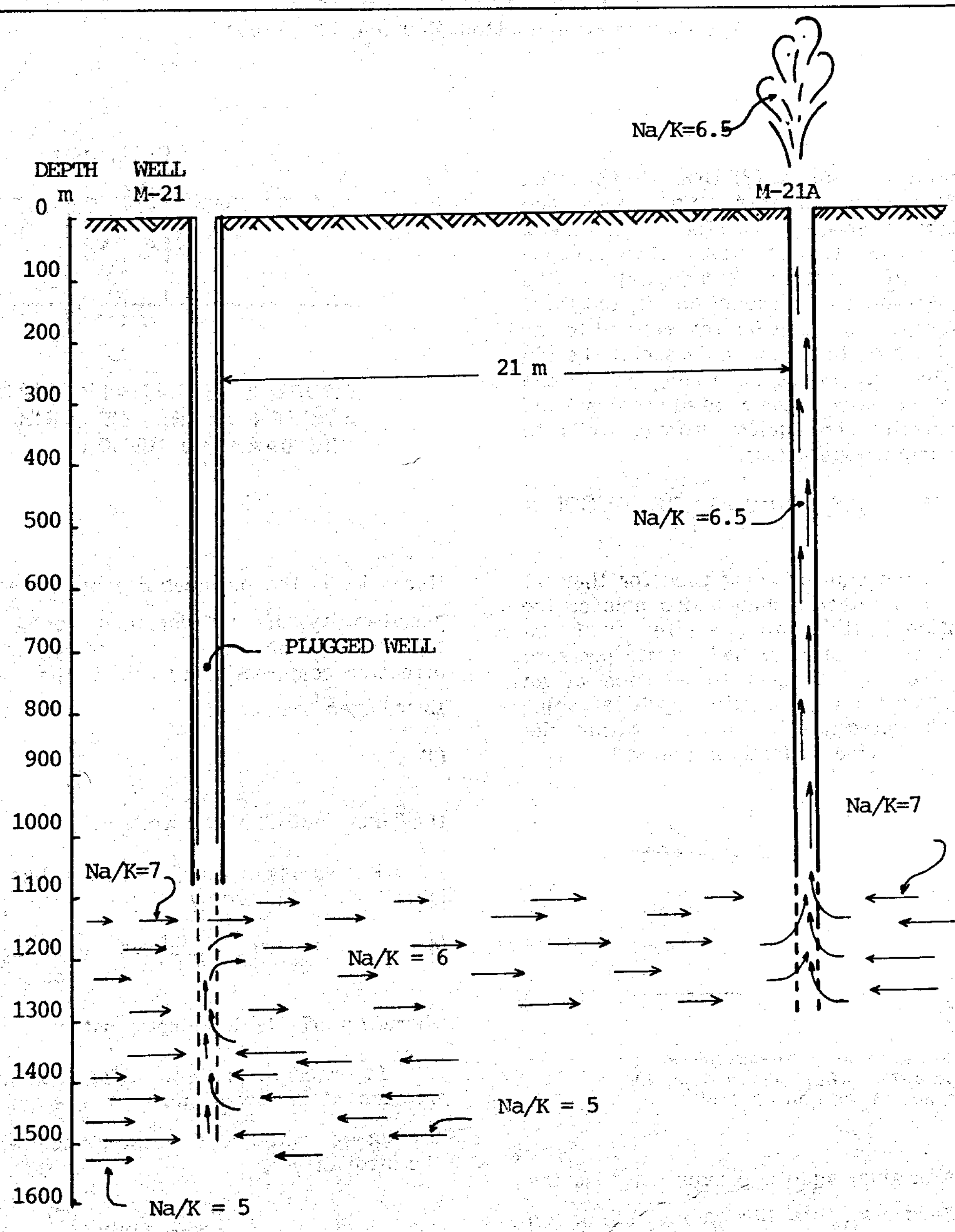

FIGURE 8. VISUALIZATION OF THE PRODUCTION MECHANISM OF THE WELL M-21A

DEPTH CONSTRAINTS ON THERMAL STORAGE WELLS

G. O. Morrell and R. E. Collins
The University of Houston, Houston, TX 77004

INTRODUCTION

At the recent (10-12 May 1978) DOE Workshop on Thermal Energy Storage in Aquifers, held at Lawrence Berkeley Laboratory, Berkeley, California, downhole pumps were suggested as providing satisfactory production capacity for aquifer thermal storage wells. This problem of assuring adequate production capacity for aquifer thermal storage wells is intimately related to the problem of water flashing to steam and associated scale formation within the well production tubing and in the aquifer. This note addresses these related problems and defines depth constraints on aquifer storage wells to assure successful pumping operations.

WELL BORE PRESSURES DURING PRODUCTION CYCLE

Assuming that the aquifer being used for thermal storage functions as a laterally unbounded aquifer the pressure distribution within the aquifer will be essentially uniform at the original hydrostatic pressure after a brief shut-in period upon termination of an injection cycle. During the production cycle at volumetric rate, q, the pressure distribution within the aquifer will be as shown schematically in Figure 1.

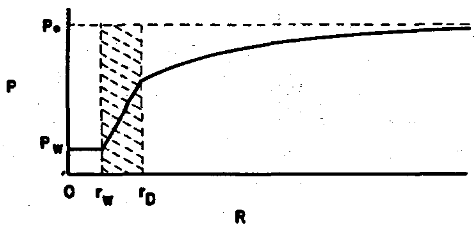

FIGURE I. PRESSURE AS A FUNCTION OF DISTANCE FROM THE WELL AFTER CONSTANT PRODUCTION FOR A PERIOD OF TIME.

Here P_0 is original aquifer pressure, r_w is the well bore radius and r_D is the radius defining a "damaged" zone of lower permeability about the well. The temporal history of this pressure distribution will be determined as the solution of the differential equation[1]

(1) $$\frac{k}{\mu}\frac{1}{r}\frac{\partial}{\partial r}\left(r\frac{\partial P}{\partial r}\right) = c\,\frac{\partial P}{\partial t}$$

provided that the water remains liquid.

The solution of Eq. (1) can be approximated[2], for the permeability distribution of Figure 2, to yield the temporal evolution of the pressure at the well bore as

(2) $$P_w(t) = P_0 - \frac{q\mu}{2\pi kh}\left(\frac{k}{\mu}\ln\frac{r_D}{r_w}\right) + \frac{q\mu}{4\pi kh}\,Ei\left(-\frac{\phi\mu c r_D^2}{4kt}\right)$$

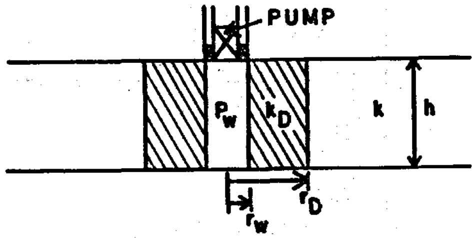

FIGURE 2. SCHEMATIC DIAGRAM OF AQUIFER NEAR THE WELL SHOWING THE DAMAGED REGION.

Here k is the permeability of the aquifer, k_D the permeability of the damaged zone, h is aquifer thickness, μ the water viscosity, ϕ the porosity, c the effective compressibility and t the elapsed time. Van Everdingen[2] calls

(3) $$S = \frac{k}{k_D}\ln\frac{r_D}{r_w}$$

the "Skin Factor" of the well.

For values of $\phi\mu c r_D^2/4kt$ less than 0.5, Equation (2) is well approximated by

(4) $$P_w = P_0 - \frac{q\mu}{4\pi kh}\left(2S + \ln\frac{4kt}{\phi\mu c r_D^2} - \gamma\right)$$

where $\gamma = .577216$ is Eulers constant.

In order to prevent water flashing to steam, the pressure at the well must be greater than the vapor pressure of water at the storage temperature[3], T, hence the inequality

(5) $$P_w \geq P_{boiling}(T)$$

must be satisfied.

In normally pressured aquifers the original ambient pressure, P_0 is the sum of the atmospheric pressure and the weight of a vertical column of water of length equal to the depth of the formation, d; thus the original pressure is

(6) $$P_0 = \rho_0 g d + P_{atm}$$

where ρ_0 is the original density of water in the formation, g is the acceleration of gravity, and P_{atm} is atmospheric pressure.

From Equations 4, 5, and 6 it is found that in order to maintain the liquid phase within the well bore at the aquifer the depth of the formation must satisfy

$$(7) \quad d \geq \frac{P_{boiling}(T) - P_{atm}}{\rho_0 g} + \frac{q\mu}{4\pi k h \rho_0 g}\left(2S + \ln \frac{4kt}{\phi \mu c r_D^2} - \gamma\right)$$

Hence the minimum depth depends upon two main factors: The storage temperature fixes the first term in Eq. 7, while formation properties, water properties and production variables enter into the second term.

Using the density of pure water for ρ_0 and converting to field units (pressure in psi, flow rate in gal/min, viscosity in centipoise, permeability in millidarcies, lengths in feet, compressibility in psi^{-1} and time in hours) Eq. 7 becomes

$$(8) \quad d \geq \frac{P_{boiling}(T) - 14.7}{.4335} + 5584.1 \frac{q\mu}{kh}\left(2S + \ln(.0010547 \frac{kt}{\phi \mu c r_D^2}) - \gamma\right)$$

The viscosity is temperature dependent according to[4]

$$(9) \quad \mu = 10^{-4}\, 241.4 \times 10^{[247.8/(T + 133.15)]}$$

which is valid for liquid water along the steam-water boundary of the phase diagram from 0°C to 300°C. Using this in Eq. (8) the curves of Figures 3, 4 and 5 were computed. These curves show the minimum depths required at different storage temperatures to prevent steam formation within the well bore, at the aquifer face, for flow rates of 500, 1000, and 2000 gal/min. with values of other parameters as given in Table I.

TABLE I.

k	=	permeability = 100 to 600 md
h	=	aquifer thickness = 230 feet
S	=	Skin factor = 2.5 to 25
t	=	time of production = 16 hours
ϕ	=	porosity = .2
c	=	compressibility of water = $5.00 \times 10^{-6} psi^{-1}$
r_D	=	radius of damage = 1 foot

The time of production used was 16 hours in order to simulate an 8 hour storage/16 hour retrieval operation, as contemplated by us for diurnal storage of solar energy[5]. The curve for zero flow rate (the uppermost solid line) reflects the increase in the vapor pressure of water with increasing temperature. Also shown in these figures are power requirements for pumping water to the surface.

A first order estimate of the power required for the downhole pump at a given depth and storage temperature was made by requiring that the pressure at the wellhead be greater than the vapor pressure of water,

$$(10) \quad P_{TOP} > P_{boiling}(T)$$

Since the pressure at the top is given by

$$(11) \quad P_{TOP} = P_W + \Delta P_{pump} - \rho g d - \Delta P_{fric} > P_{boiling}(T)$$

where ΔP_{pump} is the pressure increase across the pump, $\rho g d$ is the static head of the liquid column and ΔP_{fric}, is the pressure drop due to flow in the production tubing, and we require

$$(12) \quad P_W > P_{boiling}(T)$$

then we have the requirement for the pump

$$(13) \quad \Delta P_{pump} > \rho g d + \Delta P_{fric} .$$

The power is given by

$$(14) \quad \text{Power} = \Delta P_{pump} \cdot q > \rho g d q + q \cdot \Delta P_{fric} .$$

The dotted lines of Figures 3, 4, and 5 show the depth above which a pump of the designated power could be used at the given flow rate if ΔP_{fric} is negligible compared to the static head $\rho g d$. The increase in depth with temperature exhibited by these curves is due to the decrease in the density of water with increasing temperature.

The dotted lines of Figures 3, 4, and 5 show the depth above which a pump of the designated power could be used at the given flow rate if ΔP_{fric} is negligible compared to the static heat $\rho g d$. The power needed to lift against the static head is given by the power requirements of Curve 1 (q=0) for each figure. The increase in depth with temperature exhibited by these curves is due to the decrease in the density of water with increasing temperature.

The power requirements for injection into the aquifer can be found by the same methods as used above. However, to a good approximation, the injection pumping power for an eight hour storage period and an injection flow rate of twice the withdrawal rate is given by the difference in power requirements of Curve 1 and the curve with the desired values of the skin factor and permeability. The correct figure to use in this procedure is the one with the flow rate equal to the injection rate.

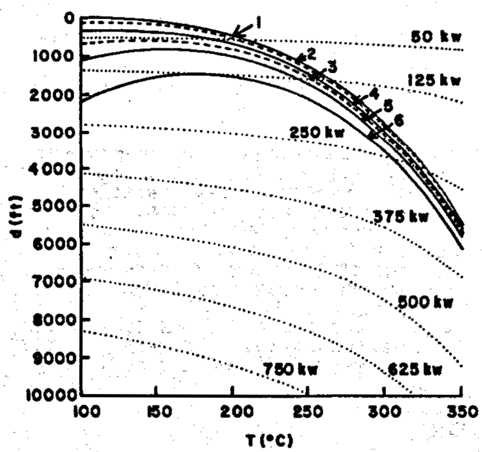

FIGURE 3. MINIMUM DEPTH REQUIRED TO PREVENT STEAM FORMATION IN A PUMPED AQUIFER HOT WATER STORAGE WELL AT VARIOUS STORAGE TEMPERATURES AND A FLOW RATE OF 500 GAL/MIN. ALSO SHOWN (DOTTED CURVES) IS MAXIMUM DEPTH, AS A FUNCTION OF TEMPERATURE, FROM WHICH A PUMP, OF THE INDICATED POWER, CAN LIFT THE WATER.

CURVE 1. q=0 GAL/MIN
2. S=2.5, k=600 md
3. S=2.5, k=100 md
4. S=25, k=600 md
5. S=25, k=200 md
6. S=25, k=100 md

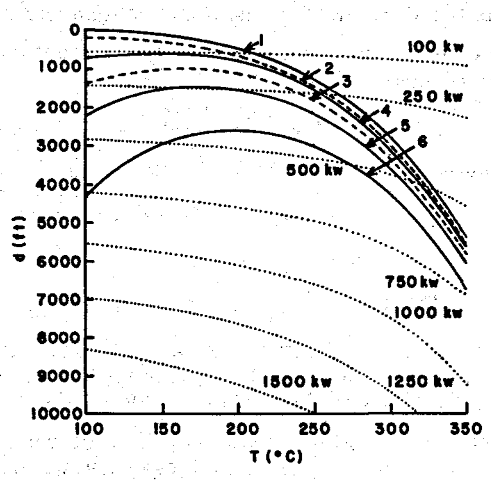

FIGURE 4. MINIMUM DEPTH REQUIRED TO PREVENT STEAM FORMATION IN A PUMPED AQUIFER HOT WATER STORAGE WELL AT VARIOUS STORAGE TEMPERATURES AND A FLOW RATE OF 1000 GAL/MIN. ALSO SHOWN (DOTTED CURVES) IS MAXIMUM DEPTH, AS A FUNCTION OF TEMPERATURE, FROM WHICH A PUMP, OF THE INDICATED POWER, CAN LIFT THE WATER.

CURVE 1. q = 0 GAL/MIN 4. S = 25, k = 600md
2. S = 2.5, k = 600md 5. S = 25, k = 200md
3. S = 2.5, k = 100md 6. S = 25, k = 100md

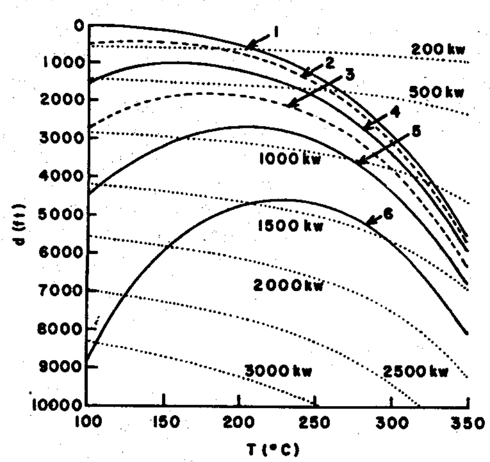

FIGURE 5. MINIMUM DEPTH REQUIRED TO PREVENT STEAM FORMATION IN A PUMPED AQUIFER HOT WATER STORAGE WELL AT VARIOUS STORAGE TEMPERATURES AND A FLOW RATE OF 2000 GAL/MIN. ALSO SHOWN (DOTTED CURVES) IS MAXIMUM DEPTH, AS A FUNCTION OF TEMPERATURE, FROM WHICH A PUMP, OF THE INDICATED POWER, CAN LIFT THE WATER.

CURVE 1. q = 0 GAL/MIN 4. S = 25, k = 600md
2. S = 2.5, k = 600md 5. S = 25, k = 200md
3. S = 2.5, k = 100md 6. S = 25, k = 100md

DISCUSSION

The most striking feature of these three figures is that for equal changes in k, S, and q, the additional depth required at low temperatures is greater than at high temperatures. Hence for some conditions a high temperature storage system could be operated at less total depth than could a low temperature system. This can be understood from the forms of Equations (8) and (9).

According to Equation (9) the viscosity decreases by a factor of about 3.5 as the temperature increases from 100° C to 350° C. Thus increased storage temperature reduces the viscosity and therefore reduces the pressure drop required for pumping. This viscosity effect on the pressure drop in the aquifer tends to counteract the effect of the increase in vapor pressure with temperature thus enhancing the viability of high temperature storage as compared to low temperature storage.

The exact constraint on depth for an aquifer storage system depends upon the specific parameters of the well-aquifer system. Once a storage temperature and maximum flow rate have been selected the most important variables are the permeability and thickness of the formation and the value of the skin factor, S. The value of S will in general depend upon drilling and completion techniques used to install the well.

It is important to note that the permeability was not varied with depth in these calculations but was varied over a range of 100 to 600 md. Higher permeabilities generally exist at shallow depths. However the trends exhibited in these figures still hold true. It should also be noted that these curves were computed for a fixed aquifer thickness of 230 ft. Aquifers used for hot water storage should have as large a permeability-thickness product as possible in order to minimize the depth required.

The skin factor S is of course dependent upon a particular well and aquifer. From Eq. (3) it is seen that the value of S is determined primarily by the reduced value of the permeability near the wellbore. Water flashing to steam in the damaged region will result in the deposition of dissolved materials which are soluble in the hot water but relatively insoluble in steam. This can result in a further reduction in permeability, and increased skin factor, and hence an increased occurrence of flashing.

For example at 300° C and 1246 psi, silica, the principal constituent of sandstone, has a solubility of 0.068 weight per cent. If the flow rate is 1000 gal/min. and all the water flashes to steam then silica is being deposited at a rate of 2.6×10^2 ft^3/min. For continuous flashing and deposition at this rate, the total pore space would be filled up in a few days of production. Of course effects of mineral deposition would become noticeable much earlier as the permeability in the damaged region would decrease, hence the Skin Factor would increase and the flow rate would drop.

Power requirements of the downhole pump depend upon the depth, flow rate and storage temperature. For example at 300° C and a flow rate of 2000 gpm using typical aquifer properties the minimum depth required is 5000 ft. and the pumping power is more than 25% of the net electric power which can be generated from the retrieved hot water. An aquifer with zero skin factor and very large permeability would still have to be at least 2800 ft. deep and the pump would need about 9% of the available power.

At lower temperatures the minimum depth and power required are reduced but the dependence upon the variables is much stronger. At 150° C and a flow rate of 500 gpm the minimum depth ranges from a few hundred feet to a few thousand feet depending upon the aquifer properties. Power requirements could be very small or as much as 15% or more.

In summary then, aquifer storage at high temperatures requires the use of downhole pumps with large power requirements. Therefore it appears that aquifer storage will not be competitive for heat storage for subsequent electric power generation.

REFERENCES

1. R. E. Collins; Flow of Fluids Through Porous Media, The Petroleum Publishing Co., Tulsa, Oklahoma, (1977).

2. A. F. Van Everdingen; "The Skin Effect and Its Influence on the Productive Capacity of a Well," Trans. AIME 198, 171 (1953).

3. R. C. Weast, Ed.; "Vapor Pressure of Water Above 100° C," Handbook of Chemistry and Physics, 54th Edition, p. D-160, (1974).

4. C. R. Faust and J. W. Mercer; "Finite-Difference Model of Two-Dimensional, Single-, and Two-Phase Heat Transport in a Porous Medium - Version I," U.S. Geological Survey Report 77 - 234 (1977).

5. R. E. Collins and K. E. Davis; "Geothermal Storage of Solar Energy for Electric Power Generation," Proc. Int. Conf. on Solar Heating and Cooling, Negat Veziroglu, Ed., Univ. of Miami (Dec. 1976).

RESPONSE OF PRESSURE CHANGES IN A FLUID FILLED CAPILLARY TUBE

C.W. Miller and J. Haney

Lawrence Berkeley Laboratory
Earth Sciences Division
Berkeley, California 94720

Abstract

An analysis was done on the transmission of a pressure change through a fluid filled capillary tube. The effects of viscosity (μ), compressibility (c_t), and temperature changes with time ($\partial T/\partial t$) on the signal propagation were investigated. For small disturbances (less than 1% of the bulk modulus), the propagation of the pressure signal, P, was characterized by a diffusion like equation,

$$\frac{\partial P}{\partial t} = \frac{R^2}{8\mu c_t} \frac{\partial^2 P}{X^2} - \frac{\beta}{c_t} \frac{\partial T}{\partial t}$$

where R is the tubing radius and β is the volumetric expansitivity. For large disturbances, compressibility effects are more important and a wavelike equation with damping results. An experiment was run to test the numerical model and excellent agreement was found. Recommendations were made as to the best operation of the tool.

Introduction

Well testing is an established method of assessing reservoir properties. However, accurate pressure measurements are essential. Due to the harsh environment of a geothermal well (high temperature and high content of dissolved solids and gases), most existing downhole pressure measurement devices cannot be used. For single phase flow in the wellbore, down-hole pressure changes can be obtained from wellhead measurements by taking into account gravity effects and frictional losses. For two-phase flow in the wellbore, the modeling of the flow is not yet sufficiently accurate to obtain downhole pressures from wellhead data. One device that can measure and record pressure at high temperatures (700°F) is the Kuster pressure tool.[1] However, the tool has several limitations: the accuracy and resolution is less than desired; downhole pressure cannot be monitored at the surface; and it does not have the capability to record pressure for longer than 12 hours. The tool is also subject to mechanical problems.

A method of continuously monitoring downhole pressures in geothermal wells was proposed by Fournier[2]. This method utilizes a fluid filled capillary tube downhole with a pressure gage at the surface. The fluid used can be either a gas or a liquid which does not undergo a phase change at the temperatures and pressures of the system and is usually less dense than water. The stainless steel tubing presently used by LBL in geothermal well tests is approximately 8,000 ft. in length with an O.D. of 0.094 in. and an I.D. of 0.054 in. Tubing with an I.D. of 0.026 in. has also been used. The tubing is attached to a larger chamber downhole. The large chamber minimizes changes in the brine/fluid interface level, provided this interface remains in the chamber. The chamber, used at LBL, is 10 ft. long. Changes in downhole pressure are transmitted through the fluid to the pressure transducer located at the surface and are recorded with the Sperry Sun or Hewlett Packard System. It is important to specify, however, that care be taken in using the data obtained. Changes in downhole pressure are not sensed simultaneously at wellhead because of the compressibility and/or viscosity of the fluid. High frequency signals are attenuated more and have a greater phase lag than lower frequencies. Because transient pressure signals are just a sum of different frequencies, a signal waveform generated at one end of a capillary tube will arrive as a different waveform at the other end. The amount of distortion depends on the signal shape itself. Any temperature changes in time along the tube create additional pressure signals which further distort the downhole signal. These effects must be corrected to obtain the desired, accurate pressure measurements.

This problem has been considered previously because there are many applications in which a fluid is used to transmit pressure signals, e.g., fluidic amplifiers. One of the first delineating papers on the subject was given by A.S. Iberall[3], who considered the attenuation of oscillating pressures in instrument lines. A number of other researchers (Brown[4], Kantola[5], Karem[6], and Schuder[7]) have considered this problem of the response of a general pressure transient signal. Unfortunately, they have dealt with small disturbances, and they have not included outside temperature effects. (A small disturbance has been defined as a pressure step change of less than 1% of the bulk modulus.) When oil is the fluid, pressure changes as large as 2,000 psi still qualify as a small disturbance. On the other hand, when gas is used, the pressure change must be less than (.01)P when P is the pressure in the tube. For a pressure level of 2,000 psi, a pressure change of only 20 psi would qualify as a small disturbance.

This paper gives the equations and solution procedures for both small and large disturbances. The problem is solved numerically, although an analytic solution can be obtained in some cases.

These will be presented in a future report. For the small disturbance case, a diffusion-like equation results. For the large disturbance, the equation is similar to a wave equation with damping. In both of these cases, the environmental temperature changes, which occur in the geothermal well, have been included in the solution.

Using the solution procedure developed at LBL, this paper will look at the effect of the capillary tubing on the downhole pressure signals. It will consider the effects of tubing size, type of fluid (nitrogen versus silicone oil), and temperature effects.

Defining Equations

In general, to determine the fluid response in the tube, the Navier-Stokes equations of momentum, mass, and energy must be solved. Because the capillary tubing is so small, the fluid at any point inside the tube will be assumed to be at the same temperature as the water or water/steam mixture surrounding the tube in the well. Temperature changes are controlled then by the geothermal fluid. Given the changes in time of the temperature profile along the well, only the equations of mass and momentum need be solved.

One-dimensional, transient flow along the x-axis is assumed. The continuity equation is

$$\frac{\partial \rho}{\partial t} + \frac{\partial}{\partial x}(\rho u) = 0. \qquad (1)$$

The momentum equation is

$$\frac{\partial(\rho u)}{\partial t} + \frac{\partial(\rho u^2)}{\partial x} = -\frac{\partial p}{\partial x} - \rho g - \mu\left[\frac{1}{r}\frac{\partial}{\partial r}\left(r\frac{\partial u}{\partial r}\right) + \frac{\partial^2 u}{\partial_x^2}\right]. \qquad (2)$$

Because the tube diameter is so small, the radial gradient term will be larger than the axial term in most cases. Then the viscous term can be approximated as a friction factor times an average velocity squared:

$$\mu\left[\frac{1}{r}\frac{\partial}{\partial r} r \frac{\partial u}{\partial r}\right] = \frac{1}{2}\frac{f\rho u^2}{D}$$

This form is a good approximation for a fully developed profile. For the laminar case, a fully developed profile results for a given pressure gradient if $\nu t/R^2 > 0.5$.[6] For $R = 7 \times 10^{-4}$m, $\nu = 5 \times 10^{-5}$ m^2/sec (gas); this condition is true when $t > 10^{-2}$ sec. Because time changes of interest are greater than 10^{-2} sec, a fully developed profile is assumed at all times for both the laminar and turbulent cases. The momentum equation now is

$$\frac{\partial}{\partial t}\left(\rho u\right) + \frac{\partial}{\partial x}\left(\rho u^2\right) = -\frac{\partial p}{\partial x} - \rho g - \frac{1}{2}\frac{f\rho u^2}{D}. \qquad (3)$$

For the laminar case, the friction factor, f, is 64/Re, where Re is the Reynolds number. ($Re = uD/\nu$). For the turbulent case ($Re > 1,760$), an equation for f as a function of Re for a smooth tube was determined to be

$$f = 0.18\, Re^{-0.2} \quad (1,760 < Re < 10^7).$$

Also, since it is only changes in pressure that are of interest, the static gravity balance is subtracted out. The pressure is written as $p_o + P'$ and the density as $\rho_o + \rho'$ where $dp_o/dx = -\rho_o g$.

The tubing length is L. The downhole chamber is at x = 0, and the pressure gage is at x = L. The initial condition is that the fluid is quiescent, $u(x, t{=}0){=}0$, and only a static gravity profile exits in the tube, $p_o(x) = -\int_0^x \rho_o g dx + P_r$. The boundary conditions are

$$u\,(L,\, t > 0) = 0$$

$$\left.\begin{array}{c} P\,(0,\, t > 0) \\ \text{or} \\ P\,(L,\, t > 0) \end{array}\right\} \text{ is specified,}$$

$$T\,(x,\, t \geq 0) \quad \text{is known from the fluid in the well.}$$

Small Disturbance

A small disturbance will mean that the flow is laminar and that convection effects in the momentum equation can be neglected. This is true, as stated, for a disturbance that is less than 1% of the bulk modulus. For a gas to satisfy these conditions, $\Delta P < .01P$. However, for a liquid, a ΔP of the order of 1,000 psi can usually be described as a small disturbance because the changes in density are so small. The momentum and continuity equations can be simplified further so a diffusion-like equation results.

For a small disturbance, u will be small as well as $\Delta\rho$. The continuity equation reduces to

$$-\frac{1}{\rho}\frac{\partial \rho}{\partial t} = \frac{\partial u}{\partial x} \qquad (4)$$

if second order terms ($u\partial\rho/\partial x$ in this equation) are neglected.

The derivative of the momentum equation is taken with respect to x and $\partial u/\partial x$ is replaced by Eq. 4.

$$\frac{\partial}{\partial x}\left[\rho\frac{\partial u}{\partial t}\right] = -\frac{\partial^2 P'}{\partial x^2} - g\frac{\partial \rho'}{\partial x} - \frac{8\mu}{R^2}\frac{\partial u}{\partial x}. \qquad (5)$$

The left hand side is 2nd order and is neglected. Then

$$\frac{\partial^2 P'}{\partial x^2} = -g\frac{\partial \rho'}{\partial x} + \frac{8\mu}{R^2}\frac{1}{\rho}\frac{\partial \rho}{\partial t}.$$

An equation of state is used to relate density to pressure and temperature:

$$\frac{1}{\rho}\, d\rho = \beta dT + c_t dP \qquad (6)$$

where β is -volumetric expanstivity and c_t is the isothermal compressibility. (The temperature changes must be known.)

$$\frac{\partial^2 P'}{\partial x^2} = -g \frac{2\rho'}{\partial x} + \frac{8\mu}{R^2} [\beta \frac{\partial T}{\partial t} + c_t \frac{\partial P'}{\partial t}]$$

or

$$\frac{\partial P'}{\partial t} = \frac{R^2}{8\mu c_t} \frac{\partial^2 P'}{\partial x^2} - \frac{\beta}{c_t} \frac{\partial T}{\partial t} + \frac{R^2 g}{8\mu c_t} \frac{\partial \rho'}{\partial x} \qquad (7)$$

The first term is the diffusion of a pressure pulse down a tube with a diffusion coefficient of $R^2/8\mu c_t$. The second term gives the pressure pulse generated by any temperature changes in time. The last term is due to changes in the balance of gravity effects in the tube and for oil in the tube, it is quite small. The solution to the equation subject to the stated boundary conditions is straight forward when the pressure is given downhole. The solution is not so simple if the pressure at wellhead is given and one must determine the downhole signal. Nevertheless, to make a comparison of the effects of different fluids, tubing sizes, and temperature changes, the downhole pressure was assumed and the resulting pressure signal arriving at the second end was calculated. Equation 7 was used to simulate the oil in the tubing.

Large Disturbance

For a gas filled line, most transient responses will be larger than 1% of the bulk modulus. (For an ideal gas, the bulk modulus is equal to the pressure.) Compressibility effects need to be included as well as damping effects. Simplifications used above for small disturbances cannot be made. The equations to be solved are the continuity, momentum and equation of state (Eqs. 1, 2, 6). A numerical solution was used throughout.

To solve the three equations numerically, the equations were combined to provide a solution for the new pressure. From this pressure, the new density was determined, and then the fluid velocity. The equations were combined by taking the $\partial/\partial x$ of the momentum equation (Eq. 2) and by subsituting $-\partial\rho/\partial t$ for $\partial(\rho u)/\partial x$ from the continuity equation:

$$\frac{\partial^2 \rho}{\partial t^2} = \frac{\partial^2}{\partial x^2} (\rho u^2) + \frac{\partial^2 P}{\partial x^2} + g \frac{\partial \rho}{\partial x} + \frac{\partial}{\partial x} [f \frac{1}{2} \frac{\partial u^2}{D}] \,. \qquad (8)$$

For laminar flow, the last term is rewritten as

$$\frac{1}{2D} \frac{\partial}{\partial x} (f\rho u^2) = \frac{8\mu}{R^2} \frac{\partial}{\partial x} (\frac{\rho u}{\rho}) = \frac{8\mu}{R^2} [- \frac{1}{\rho} \frac{\partial \rho}{\partial t} - \frac{\rho u}{\rho^2} \frac{\partial \rho}{\partial x}]$$

using $f = 64/Re$. Similarly, for turbulent flow, the last term reduces to

$$[\frac{0.09\mu^{-.2}}{D^{1.2}}] [\frac{-1.8(\rho u)^{0.8}}{\rho} \frac{\partial \rho}{\partial t} - \frac{(\rho u)^{1.8}}{\rho^2} \frac{\partial \rho}{\partial x}]$$

when f is approximated by $0.18\ Re^{-0.2}$. To relate changes in density to pressure changes, the equation of state is used.

This set of equations (1, 6, 8) was solved using a finite difference approximation. The pressure terms were evaluated in a implicit manner to avoid time step limitations. To eliminate stability problems, the friction effect was also evaluated implicity. Because of the large dissipating effect of the tube walls, shock waves (discontinuities) will not form. However, since increases in pressure are directly related to increases in dissipation, these two effects must be considered in a similar manner. To facilitate the programming, convection terms in the momentum equation were evaluated at old time steps, so a time limitation was imposed here. The pressure is determined by Eq. 8. Then the density is determined from the known imposed temperature and the new pressure. The new velocity is determined by Eq. 1 where $\partial(\rho u)/\partial x$ is evaluated implicitly.

The finite differenced equation for the pressure for a buildup is given below. The continuity equation is similarly differenced. The pressure, temperature and density are evaluated at node points while the velocity is determined at half node points. The resulting equation for the pressure is

$$[1+2r+s]P_i^{\ell+1} - r[P_{i+1}^{\ell+1} + P_{i+1}^{\ell+1}] =$$

$$(1+s)P_i^{\ell} - r \frac{\Delta x}{\Delta t} [\rho u_{i+\frac{1}{2}} - \rho u_{i-\frac{1}{2}}]^{\ell} +$$

$$r[\rho u_{i+\frac{1}{2}}^2 - 2\rho u_{i-\frac{1}{2}}^2 + \rho u_{i-3/2}^2]^{\ell} +$$

$$r \frac{g\Delta x}{2} [\rho_{i+1} - \rho_{i-1}]^{\ell} - s\frac{\Delta t}{\Delta x}(\frac{u}{\rho}) \left[\frac{P_{i+1} - P_{i-1}}{2}\right]^{\ell} -$$

$$[1+s] [T_i^{\ell+1} - T_i^{\ell}] \frac{\beta}{c_t}$$

where $r = (\Delta t/\Delta x)^2 (1/\rho c_t)$, and $s = (8\mu/R^2) (\Delta t/\rho)$, and where i denotes the spatial position and ℓ denotes the time step. An upwind difference scheme has been used for the convection terms.

Both the small and the large pressure disturbances can be handled. First, the solutions will be compared to experiments, and then a consideration of the effect of different tubing and different fluids will be considered.

Experiment

To determine if the equations developed do describe the fluid transmission line, an experiment was run. The experiment was done for the isothermal case. The capillary tubing used in the field was filled with nitrogen for one test, and with 10 centistoke silicone oil for the second test. The tubing was 8,000 ft. in length with an inner diameter of 0.054 in. The pressure was recorded at both ends, one with a Hewlett Packard gage, and the second with a Sperry Sun gage.

The tubing was filled with either nitrogen or oil and allowed to equilibrate at some initial pressure. The pressure at one end was then increased by Δp and held constant. The pressure was recorded at the second end. A nitrogen filled bottle at high pressure was used to provide the step change in pressure. Figure 1 is a sketch of the actual pressure measuring system. For the experiment, the downhole chamber was replaced with the nitrogen tank and a valve. The comparison between the experiment and the calculated response is shown in Figures 2, 3 and 4.

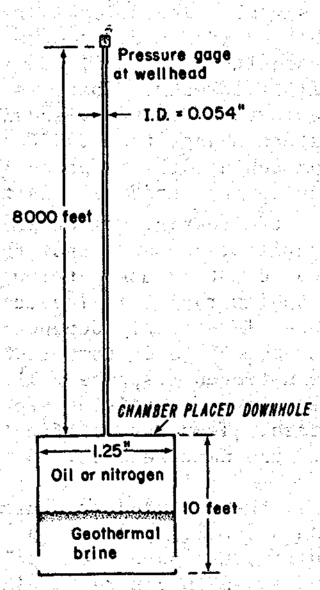

XBL 7810-2118

Figure 1. Schematic of downhole pressure measuring system.

Figure 2 shows the isothermal response of the tubing system to a step change in pressure for the oil filled tubing. The three cases shown are (1) p_i = 1109 psia with Δp = 490 psi; (2) p_i = 1598 psia with Δp = 478 psi; and (3) p_i = 2075 psia with Δp = 12 psi. On the graph, the step function is plotted along with the pressure measured at the second end. The tubing clearly distorts the signal. The response of the tubing is about 20 minues. The small disturbance equation matches the data quite well in all three cases. Figure 3 shows the response of the oil filled tubing at very low pressures, p_i = 14.7 psia with Δp = 1000 psi. This match is not good at the low pressures. It is likely that a gas bubble was trapped in the tube at the beginning of the experiment, and this bubble was the cause of the slow pressure response. On the whole, the small disturbance equation gave an excellent match with the experiment, and this equation will be used to model the oil filled tubing.

Figure 4 shows the experiment and the calculations for the nitrogen filled tube. Again, the experiment was run for constant temperature. The cases considered were (1) p_i = 587 psia with Δp = 454 psi; (2) p_i = 1520 psia with Δp = 820 psi; and (3) p_i = 1520 psia with Δp = 103 psi. The large disturbance equation was used to match the data. Again, the agreement is excellent. To illustrate that the small disturbance cannot be used, the calculation was done for case (1) using Eq. 7. Curve (c) in this figure is this calculation. It does not match the experiment at all. The calculated response is too fast. In deriving Eq. 7, some compressibility effects were neglected. These effects are important with the gas filled tubing and so the full set of equations (1, 2, 6) must be used.

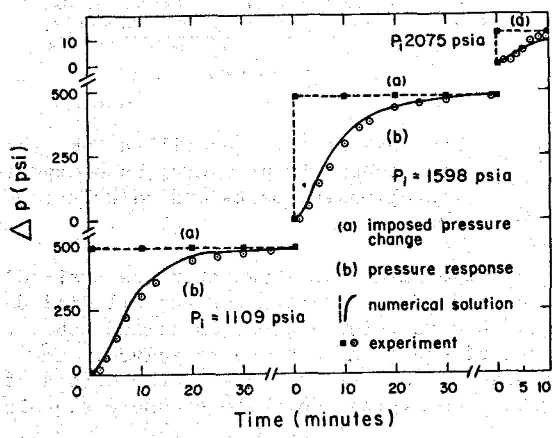

XBL 7810-2099

Figure 2. Response of oil filled tube to step change in pressure; both experimental measurements and calculations are shown.

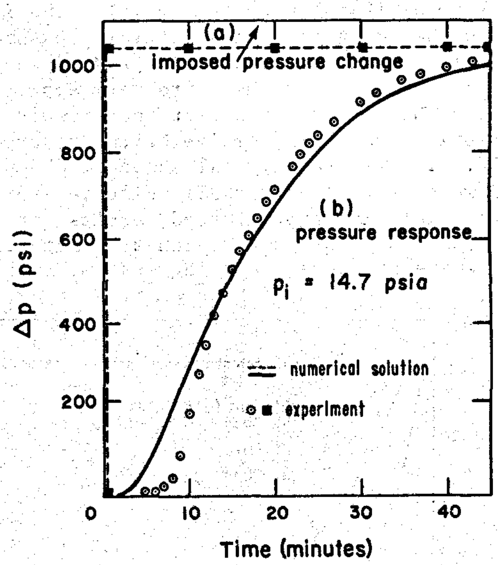

XBL 7810-2097

Figure 3. Response of oil filled tube to step change in pressure at low pressures; both experimental measurements and calculations are shown.

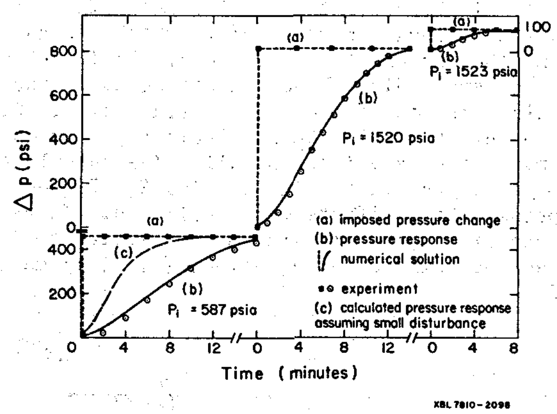

Figure 4. Response of nitrogen filled tube to step change in pressure; both experimental measurements and calculations are shown.

The experiment has shown that the small disturbance method is accurate for the oil filled tubing. However, for a nitrogen filled tube, the full set of equations need to be solved. The equations will be used to look at the effect of the tubing on typical downhole pressure signals.

Isothermal Pressure Signal Response

For the isothermal case, the effect of the tubing with the different fluids on a typical drawdown curve will be considered. Figure 5 gives a simulated downhole pressure change generated by the equation $p_{downhole} = 1980-180(1-e^{-t/5}) + 15 \ln[(t+10)/10]$ shown by curve (a). The first term in the equation is the initial pressure, the second term simulates a drop in pressure due to wellbore storage, and the third term approximates the straight line semilog plot that results at later times and is indicative of the reservoir itself. This is the typical shape of the pressure drawdown curve. A very small wellbore storage constant is being approximated, because it is the sharp changes in pressure which are distorted the most by the pressure measuring system.

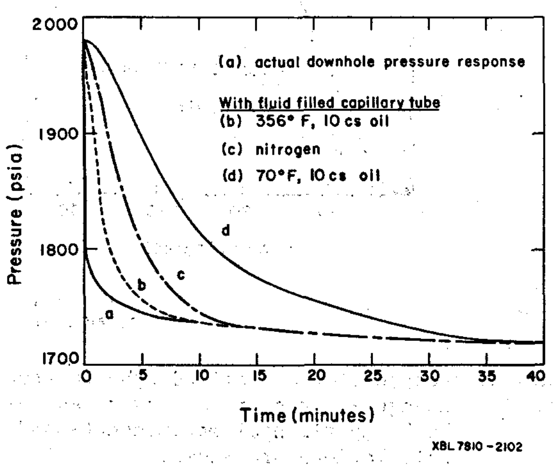

Figure 5. Comparison of the effect of different fluids in the downhole pressure measuring instrument on the measured pressure signal.

The other three curves shown in the figure are what would be measured at wellhead with the capillary tubing (0.054 in. tubing was used for this simulation). Curve (b) gives the response for 10 cs silicone oil at 356°F. The measured curve matches the actual downhole signal after approximately 5 minutes. Curve (c) shows the response for the nitrogen. This matches after about 10 minutes. Curve (d) shows the response at low temperatures with 10 cs silicone oil. The response is quite slow, taking at least 30 minutes for the measured signal to approach the actual downhole signal. The delay in response between curves (b) and (d) is due to the large increase in the viscosity of the oil when the temperature of the oil is lowered. There is an order of magnitude increase in the viscosity of the oil for a temperature change from 350°F to 70°F. For the oil filled tubing, the response is controlled by the diffusibility, $R^2/8\mu c_t$. As the viscosity increases, the damping effect is increased. From this comparison, one sees that the oil filled tubing should not be used at low temperatures unless the tubing radius is increased substantially. The nitrogen is strongly dependent on pressure. If pressures much lower than 1,000 psia are measured, the nitrogen response will be much slower. Of course, these comparisons are made for the isothermal case. Temperature effects will be considered in the next section.

Since the measured pressure signal is usually plotted on a semilog plot of p vs log time, the graphs in Figure 5 have been replotted in this manner and shown in Figure 6. The slow response of the tubing is quite evident here. All three signals eventually approach the semilog straight line. However, some configurations do faster than others. Because of this one might pick an incorrect straight line. This problem is especially evident from the low temperature oil filled tubing curve. As the measured response approaches the correct semilog straight line, the measured distorted signal is almost straight itself. If the test is stopped at this point, a slope too steep would be chosen. This same problem of two regions where the measured signal appears to be a straight line on the semilog plot is seen also with the high temperature oil curve. After 7 minutes, the measured curve approaches the actual downhole pressure. If the test was stopped at this point, an incorrect straight line might be chosen. For the isothermal case, an estimate of when the measured signal will have responded to a given pressure change is when $t > 10L^2/4k$, where $k = R^2/8\mu c_t$. For the low temperature oil, the signal takes at least 40 min. until the downhole and measured signal match. No additional responses can be tolerated during this time.

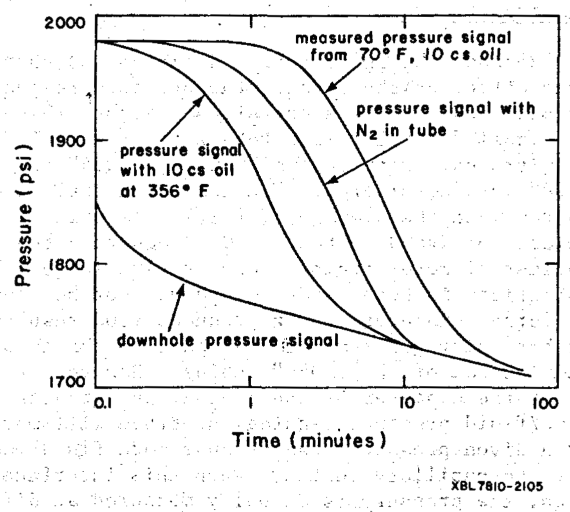

Figure 6. Comparison of the effects of the different measuring systems on the measured signal graphed on semi log plot.

With this measuring system, the very early time data of either pressure drawdown or buildup curves, is due to the measuring instrumentation and not due to the well itself. Figure 7 shows the signals obtained in the isothermal case with the oil filled tubing using two different early time drawdown curves. Curves 1 and 2 show the simulated drawdown curves, one with an early time drop of -180 $(1-e^{-t/5})$ and the second with a change of -180 $(1-e^{-t/50})$. The pressure signals calculated are given by 1' and 2' respectively. One might take the response curve 1' and try to analyze it like a wellbore storage effect. Actually, the slope of the curve is greater than 1 which should alert one to this error. What is being seen is the storage effect of the measuring tube. The flow rate out of the bottom of the tubing is not constant, so the slope of this measuring instrument storage will not be on a 1 to 1 plot. The actual data is not as smooth as that plotted, and this problem might not be evident immediately. Also, the large difference between curves 1 and 2 becomes much smaller with 1' and 2'. This means that if one is trying to obtain the actual downhole pressure from the measurements, any slight error in the data is magnified. For example, one might try to use curve 2' as the boundary condition at the top of the tube, and then try to obtain the downhole signal from it. Actual measured data will be scattered around curve 2'. If an experimental point were chosen closer to curve 1' than 2' because of the scatter in the data, the downhole signal obtained would be curve 1 instead of 2. There is an order of magnitude difference in the assumed storage constants between the two curves. This would be a significant error, when the error in the measurement was small.

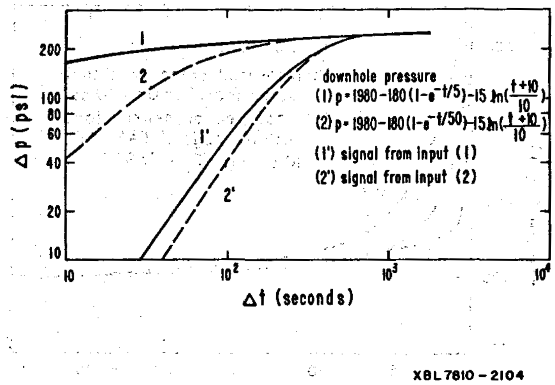

Figure 7. Comparison of the measured signal of different downhole pressures on a log-log plot.

From the isothermal comparisons, one sees that the high temperature oil gave the best response. However at these pressures, the nitrogen is not too bad. In either of these cases, the tubing response must not be interpreted as the response of the well itself.

Non-Isothermal Response

At high temperatures, the oil looked like it would respond faster than the nitrogen. This is altered when temperature effects are considered. Because the oil is almost incompressible, any increases in temperature are seen as large increases in pressure at that point. The pressure signal generated is $(\beta/c_t)\partial T/\partial t$. This means that, even though the pressure is dropping at one end, the measured signal may actually increase for awhile. This has been seen in field data (see Ref. 9). To alleviate this problem, the well is flowed until the change in temperature with time is less than say 1 C over 1 hour. Then, the flow rate is changed. Even in these circumstances, small temperature changes still take place in the geothermal well because of changes in heat loss out of the well and because of changes in the flash level. This will alter the measured pressure signal. Figure 8 shows this effect for the oil filled tube. In this graph, curve (a) is the desired signal and curve (b) is the signal measured for the isothermal case. Curve (c) is now the measured signal when the temperature at a point changes an average of 2.7°F over 10 minutes, i.e., in 10 minutes the temperature at the top of the well changes 5.4°F and at the bottom, the temperature is constant in time. The ΔT at other points in the well is just proportioned over the length of the well. This is a typical temperature change for a flow rate change of 100 gal/min to 200 gal/min. The actual temperature used was

$$T(x,t) = \frac{-3°C}{2400m}(x)e^{-t/(150\ \text{sec})} - \frac{13°C}{2400m}x + 181°C$$

The pressure response increases and then slowly decreases. Still, for this relatively small ΔT, the measured signal takes 10-20 minutes instead of 5 minutes to approach the desired signal.

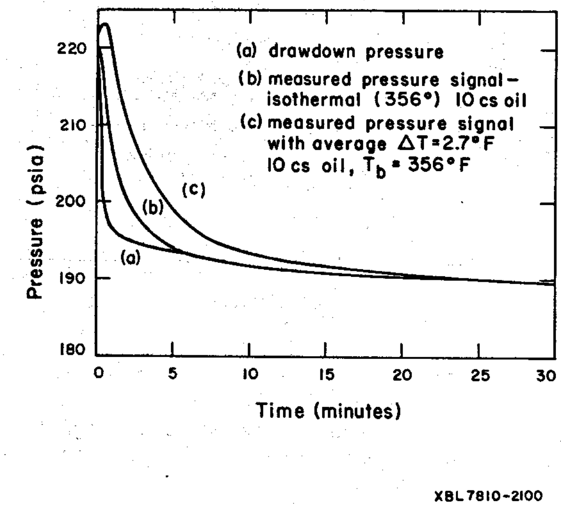

Figure 8. Temperature effects on the measured signal for an oil filled tube.

Figure 9 shows the same plot for the nitrogen filled tubing. The pressure increases very slightly at early time and then approaches the downhole signal in about 15 minutes. For the very small ΔT chosen, the oil filled tubing responds much slower. This is because of the term β/c_t. Although the oil filled tubing can respond faster for a given pressure change, the pressure at a point is increased about 25 times more with the oil for a given ΔT. The oil filled tubing at these pressures then looks much worse for small ΔT's. Of course these calculations are done assuming that the fluid heats up at the same rate. In the well itself, where the total heat capacity of the fluid is small compared with that of the fluid in the well, this assumption is valid. Above ground temperature changes in the fluid may not be at the same rate for both the oil and nitrogen. Still, this temperature effect can be controlled while that in the well cannot.

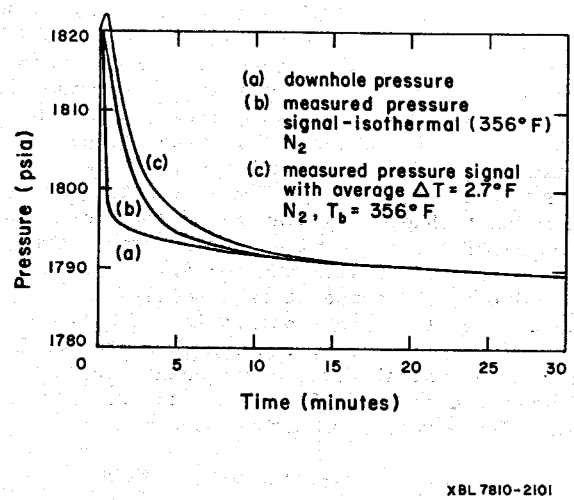

Figure 9. Temperature effects on the measured signal for a nitrogen filled tube.

Geometry Effects

Because the small tubing diameter has such a large effect on the signal, the pressure response was analyzed for different sizes. Figure 10 shows the signal for oil filled tubing and Figure 11 for the nitrogen. Diameters of 0.026", 0.054" and 0.108" were considered. The non-isothermal case was run with the average ΔT = 2.7°F as this is typical for drawdown tests. One sees that the smallest diameter tubing produces very large distortions in both cases and should not be used. The larger diameter tubing produces good results for both nitrogen and oil and should probably be used instead of the 0.054" tubing. However, the larger the diameter of the tubing, the greater the brine/fluid pressure sensing interface will move for a given pressure drop because more fluid must exit the capillary tubing. When this interface moves, the pressure is actually measured at different points. This is a greater problem with nitrogen than oil because of the larger density difference. The chamber diameter cannot really be increased because of the difficulty in getting it downhole.

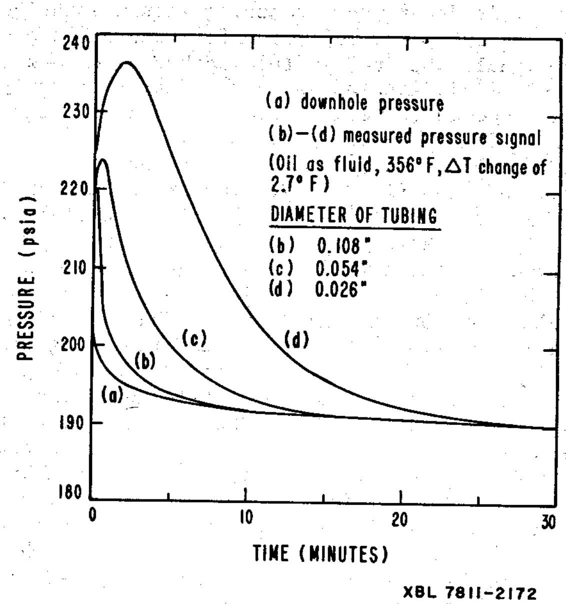

Figure 10. Effects of diameter on the measured signal for an oil filled tube.

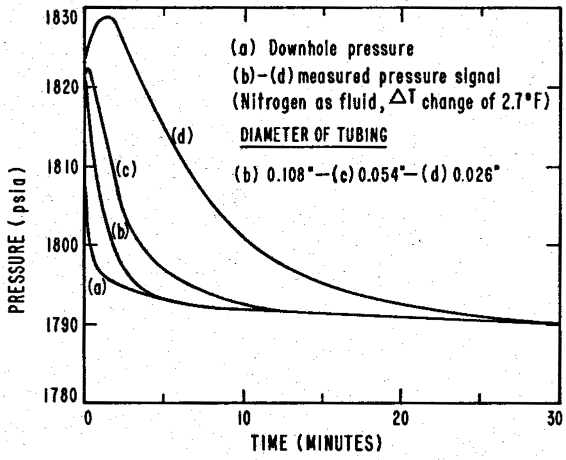

Figure 11. Effects of diameter on the measured signal for an nitrogen filled tube.

Conclusions

A method of calculating the pressure response of a fluid filled capillary tube has been determined for both large and small pressure disturbances. For a small disturbance and for constant temperature, the data will be the actual downhole signal when $t > 10L^2/4k$ for a given pressure change. If there is a temperature change or if the disturbance is large, another time estimate must be made. This has not been done yet.

(1) When the fluid filled capillary is used to measure downhole pressures, the signal is distorted. High frequencies are damped more than low frequencies.

(2) Any temperature changes, even slight, say 1/2°C, increase this distortion.

(3) One must be careful that the instrument response not be interpreted as the response of the well itself.

(4) The capillary tubing of 0.026" I.D. distorts the downhole signal significantly and should not be used. The tubing of 0.1" has a shorter response time and is still flexible. This size tubing would probably be the best for this type of instrumentation.

(5) If the temperature at the surface is controlled then a recommendation of the best fluid is oil when the temperature is high but not varying in time, and nitrogen when the temperature is low or for high temperatures when the temperature varies significantly with time. At low pressures and low temperatures, the tool should not be used.

As the response of the tubing has been determined, the actual downhole signal can be obtained. However, the exact time of the flow rate change must be known; and for the non-isothermal case, some idea of the temperature change with time is necessary. Given this information, one could guess the downhole pressure in a systematic way until the calculated pressure matches the measured signal. An analytic method for the small disturbance equation is being developed which would make the inversion simpler. No method, though can correct the signal without the necessary information on the temperature changes; and for that case, early time data cannot be used

Nomenclature

D	=	capillary tubing diameter
c_t	=	isothermal compressibility of fluid
f	=	friction factor
g	=	gravity
P_i	=	initial pressure
Δp	=	pressure change
p	=	pressure
p_o	=	static pressure
p'	=	$p-p_o$
P_r	=	reservoir pressure
r	=	radial direction
R	=	radius of capillary tubing
Re	=	Reynolds number, $\rho uD/\mu$
t	=	time
T	=	temperature
x	=	axial direction
u	=	velocity in axial direction
β	=	volumetric expansivity
ρ	=	density
ρ_o	=	static density
ρ'	=	$\rho-\rho_o$
ν	=	kinematic viscosity
μ	=	absolute viscosity

References

1. Matthews, C.S. and Russell, D.G., Pressure Buildup and Flow Tests in Wells, Monograph Series, Society of Petroleum Engineers of AIME, Dallas, Texas, (1967).

2. Fournier, R.O. and Truesdell, A.M., A Device for measuring downhole pressures and sampling fluids from geothermal wells, Geological Survey Research, U.S. Geol. Survey Prof. Paper 750-C, pp. C146-C150, (1971).

3. Iberall, A.S., "Attenuation of oscillatory pressures in instrument lines," Journal of Research, National Bureau of Standards, v. 45, (1950), R.P. 2115.

4. Brown, F.T., "The transient response of fluid lines," J. of Basic Engineering, Trans. ASME, Series D, v. 84, (Dec., 1962), p. 547.

5. Kantola, R., "Transient response of fluid lines including frequency modulated inputs," J. of Basic Engineering, Trans. ASME, Series D, v. 93, (June, 1971), p. 274.

6. Karem, J.I., Jr. and Leonard, R.G., "A simple yet theoretically based time domain model for fluid transmission line systems," J. of Basic Engineering, Trans. ASME, v. 95, (Dec., 1973), p. 498.

7. Schuder, C.B. and Binder, R.C., "The response of pneumatic transmission lines to step inputs," J. Basic Engineering, Trans. ASME, Series D, v. 81, (Dec., 1959), p. 578.

8. Schlicting, H., BOUNDARY LAYER FLOW, McGraw Hill, (1968).

9. Narasimhan, T.N., "Applications of well testing to liquid dominated geothermal systems," 1st Invitational Well Testing Symposium, LBL Report 7027, (Oct., 1977), p. 63.

TWO AND THREE DIMENSIONAL FINITE-ELEMENT SIMULATION
OF GEOTHERMAL EXPLORATION WITH REINJECTION

G. F. Pinder,* C. I. Voss*
Princeton University

The impact of cool water reinjection wells on the energy output of a producing geothermal well can be effectively simulated using an iterative finite-element reservoir model. While a correct system representation requires a three dimensional formulation, the system can also be described approximately using an areal two-dimensional model. Comparison of the two resulting solutions provide insight into the limitations of the vertically integrated model.

The geothermal reservoir simulator employs several unique features in its formulation. An asymmetric weighting function is used in conjunction with the energy convection term to provide an upstream-weighted effect. A block iterative finite-element scheme, similar to LSOR, is used along with the total increment method to solve the resulting set of non-linear algebraic equations.

*Present address: Stanford University

THE EFFECT OF THERMAL DISPERSION ON INJECTION OF HOT WATER IN AQUIFERS

*J.P. Sauty**, *A.C. Gringarten***, *P.A. Landel**

ABSTRACT

Two series of experiments on hot water injection, storage and recovery have been performed in France in 1976 and 1977. Analysis of temperature profiles in the aquifer and temperature spot measurement in the caprock provided detailed knowledge of the thermal behavior of the reservoir. The 1976 data were used to calibrate a numerical model that was then able to accurately predict the results of the second series of experiments performed in 1977.

The results give strong evidence of the existence of heat dispersion during injection and recovery operations with a resulting apparent thermal conductivity in the aquifer much higher than the one measured usually by conventionnal methods.

This phenomena is important for predicting the efficiency of heat storage or low temperature geothermal projects and cannot be neglected.

I - INTRODUCTION

The use of the classical heat conduction theory for analyzing heat transfer experiments in aquifers yields abnormally high thermal conductivity coefficients when calories are transported by a fluid with a high enough velocity.

In two experiments conducted in different locations hot water was injected at constant rate into a well, then produced immediatly from the same well at a higher flow rate. Average conductivities equal to 4.5 and 2.4 cal/m/s/d° were obtained (CLOUET, LEDOUX, 1975) : respectively 7.5 and 4 times the usual value (λ = 0.6 cal/m/s/d°) for a saturated sand and gravel formation.

Similar analysis of a serie of 4 successive hot water storage experiments performed by B.R.G.M. in the year 1977 lead to a still higher *apparent conductivity* λ of 12 cal/m/s/d° (20 times the expected value).

Characteristics of these various experiments are summarized in table I.

Such anomalies are explained in this paper by taking into account a kinematic dispersion effect in addition to thermal conductivity.

The numerous data accumulated during our experiments on the Bonnaud site allowed us to determine with precision a value of dispersivity from the calibrated apparent conductivity. It was found that this parameter was of the same order of magnitude as the dispersivities measured in the same field by means of chemical tracers, thus strongly conforting this concept suggested for porous media by GREENS, 1963 and BEAR, 1972. The fact that BEAR concluded to the small importance of dispersion relatively to thermal conduction appears to be due to the small dispersivity value measured in laboratory experiments while we are considering aquifer in situ behaviour where dispersivities are much higher (macrodispersivities).

* Bureau de Recherches Géologiques et Minières, Orléans, France

** formerly B.R.G.M. ; presently FLOPETROL, Melun France

	Aquifer thickness (m)	Injection			Production		Thermal Storage Radius (m)	Apparent conductivity $\tilde{\lambda}$ (cal/m/s/d°)	$\tilde{\lambda}/\lambda$
		temperature °C	Q_i (m^3/h)	t_i duration (d)	Q_p (m^3/h)	t_p duration (d)			
ENSMP* BURGEAP** at Neuilly 1974	10	19°	15	3	30	3	8	4.5	7.5
ENSMP* BURGEAP** at Noisy 1974	30	20°	115	3	130	3.7	12	1.8	4
BRGM*** at Bonnaud 1977	2.5	34°	3.4	6 3 6 6	3.4	6 3 6 6	10 7 10 10	12	20

TABLE I - Characteristics of several experiments of hot water storage

II - PROPOSED THEORY

When water is injected into an aquifer at a different temperature, transfer of heat takes place in many different ways in the aquifer and in the confining layers :

(A) in the aquifer, the average bulk movement of the liquid causes *heat convection* (forced convection induced by wells and/or advection by a regional flow of groundwater)

(B) Differenciations in the movement of each water particle results in *kinematic dispersion* ; the differences in velocities are due either :

1. to *velocity distribution* inside each pore tube (at the scale of one single pore) ;

2. to the *tortuosity* of the stream paths around the solid matrix (at the scale of several pores), with diffusion (or thermal conduction) contributing to exchanges between adjacent pathlines ;

and 3. to differences in the mean velocities between zones of different permeabilities (scale superior to that of local aquifer permeability *heterogeneities*).

(C) Heat is exchanged inside the aquifer between the water and the porous matrix. In fact, it is admitted (HOUPEURT, 1965) that temperature equilibrium is reached almost instantaneously (in less than 1 sec. for a Ø 1mm grain, 1 min. for Ø 1cm and 2 hrs for Ø 1dm). Considering the linear laws for heat conduction, the effects of the various heat exchanges with the solid matrix are similar to those of a linear instantaneous and reversible adsorption - desorption reaction with mass transfer : the final result is a delayed transfer which increases the time scale in the ratio of heat capacities (fluid capacity versus aquifer capacity). However, the conductivity inside the grains introduces a difference with respect to chemical adsorption, but this effect can be included into the global conduction term inside the aquifer.

(D) Natural heat conduction can result from density differences between warm and cold water. We do not take this factor into account as we consider shallow and generally anisotropic aquifers and limited temperature constrats.

(E) Finally, heat is transferred by thermal conduction from the aquifer to the surrounding layers.

Global partial differential equations for describing heat transfer within the aquifer can then simply be obtained from the ones describing mass transport by replacing the concentration C (mass per unit of water volume) by $\rho_F C_F\ \theta$ (thermal energy per unit of water volume) in the convective and dispersive terms and the solute mass storage by the heat energy variation of the aquifer : $\rho_A C_A\ \partial\theta/\partial t$ (SAUTY, 1977).

* Ecole Nationale Supérieure des Mines de Paris Paris, France

** Bureau de Géologie Appliquée, Neuilly, France

*** Bureau de Recherches Géologiques et Minières, Orléans, France

The result is :

$$\frac{\partial\theta}{\partial t} = \frac{1}{\rho_A C_A} \nabla \left((\bar{\bar{\alpha}}\ |\vec{V}|\rho_F C_F + \lambda_A)\vec{\nabla}\theta \right) - \frac{\rho_F C_F}{\rho_A C_A} \nabla(\vec{V}\theta) \qquad (1)$$

with θ : temperature
t : time
$\rho_F C_F$: heat capacity of water
$\rho_A C_A$: heat capacity of aquifer (matrix+water)
λ_A : heat conductivity of aquifer
$\vec{V}$: DARCY's flow velocity
$\bar{\bar{\alpha}}$: dispersivity tensor

It is possible to define an apparent thermal conductivity tensor within the aquifer :

$$\bar{\bar{\tilde{\lambda}}} = \begin{vmatrix} \lambda & 0 & 0 \\ 0 & \lambda & 0 \\ 0 & 0 & \lambda \end{vmatrix} + \rho_F C_F \cdot R^T \begin{vmatrix} \alpha_L & 0 & 0 \\ 0 & \alpha_T & 0 \\ 0 & 0 & \alpha_T \end{vmatrix} . |\vec{V}| \cdot R \qquad (2)$$

R being the rotation matrix from velocity axes into reference axes ;

α_L and α_T being respectively the longitudinal and transversal dispersivities.

In the direction of flow, the apparent thermal conductivity tensor reduces to :

$$\tilde{\lambda} = \lambda + \alpha_L \cdot \rho_F C_F \cdot |\vec{V}| \qquad (3)$$

III - FIELD EXPERIMENTS

Several heat storage and heat transfer experiments were performed in the years 1976 and 1977 in an alluvial, sand and gravel aquifer located at Bonnaud, France (North of Lyons). The aquifer was confined and well defined between two layers of clay (fig. 1). It had been devised previously for extensive tracer tests experiments in the period 1973 to 1975 (GAILLARD et al., 1976).

The heat transfer experiments included constant rate injection of hot water in one well and production at the same rate from another well (doublet), and two series of heat storage experiments from a central well C.

The first series of storage experiments consist of three successive injection and production cycles performed in 1976 ; they were used (1) by Ecole des Mines de Paris for evaluating the aquifer thermal characteristics from information obtained only at central well C and a few temperature point measurements in the caprock (LEDOUX, CLOUET d'ORVAL, 1977) ; and (2) by B.R.G.M. for modeling the whole aquifer and confining layers, with the help of temperature logs collected in eleven wells within 13 m from the central well C.

After calibration, the model was used to predict the results of the second series of single well storage experiments, performed in 1977. These consisted in four successive hot water injection and production cycles.

The model used by B.R.G.M. was axisymetric with a limited number of different layers (fig. 2). Although the real system was slightly anisotropic, a reasonable average thermal behaviour was obtained as a function of the distance from the central well and it was possible to correctly reproduce the actual temperatures in the eleven observation wells and at the nine points of measurements in the caprock, with only nine model of parameters.

In addition, a three-dimensionnal model was built and calibrated against both the doublet and the single well storage experiments. The values of the physical parameters used in the calibration of that model agreed well with thosed used in the axisymetric model, and indicated that the non exactly axisymetric heat and temperature distributions in the actual single well storage experiments were due to transmissibility heterogeneities ; these might be a consequence of local increases of permeability in the vecinity of some wells, following clean-up by air-lift.

The numerical code (ESTHER) used in the axisymetric model was checked against analytical solutions derived by RUBINSTEIN, 1972 for the injection phase and was found to give excellent results (fig. 4). This indicates that integration of P.D.E. is accurate, free of numerical dispersion, and that the parameters obtained from the calibration correspond indeed to the correct physical parameters of heat capacity, heat conductivity and dispersivity.

IV - MATHEMATICAL MODELING

Comparison between observed temperature variations at the central well and the simulations obtained with two different physical hypotheses is shown by figure 5 for the storage experiment performed in 1977 :

- First hypothesis : In equation (3), the dispersivity α_L is constant and uniform. The best calibration was obtained for α_L = 1 m (interrupted line).
- Second hypothesis : Dispersivity α_L is still constant with respect to time, but varies spatially with the distance r to the central well, so that : α_L/r = constant. As a result, the product $\alpha_L|\vec{V}|$ and the apparent conductivity (equation (3)) are uniform for radial flow (because velocity distribution in radial flow is such that $|\vec{V}|$. r = constant). The best calibration was obtained for α = 0.18 R (reinforced interrupted line), which yields an apparent conductivity of 12 cal/m/s/d° (see table I).

The model gives an excellent match, except for some minor differences during injection ; these are due to the fact that in the model an average temperature is calculated in a cylindrical node with a 2.7 m radius, while in the actual experiment the temperature is measured inside the well.

The apparent conductivity coefficient is much higher than the physical one ; this is caused by local *heterogeneities* of *permeability* in the vertical planes (which are apparent on the temperature logs) as well as in the horizontal plane.

The second hypothesis (*dispersivity* as a *linear function of distance)* corresponds to the case of a multilayer aquifer, without exchanges between the layers (HALEVY and MERCADO, 196). As the distance from the injection well increases, however, vertical exchanges result in stabilization of the global dispersivity over the entire aquifer thickness (MARLE et al., 1967) (fig. 6).

In the particular case of the Bonnaud aquifer, this stabilization occurs at a distance of about 30 m. For distances less than 20 m, a linear variation of the average dispersivity over the whole thickness is a good approximation (PEAUDECERF and SAUTY, 1978).

The calculated dispersivity (1 m on average for a storage radius of the order of 10 m) in in *good agreement* with the values obtained in similar conditions on the same site with *chemical tracers* (1.6 m with an experimental distance of 13 m) ; although, it would seem logical that heat dispersivity due to permeability heterogeneities be somewhat smaller, as heat conduction has a stronger effect on transverse exchanges than does molecular diffusion and transverse dispersion on solutes.

Spatial variation of dispersivity with respect to the distance to injection well is an interesting feature to introduce in dispersion models based on FICK's law : the same model would then be applicable to various distances whereas the use of a uniform dispersivity would only be valid for the distance over which an averaging parameter has been determined, unless all distances investigated are greater than the local scale of heterogeneity. In the present case, we obtained an excellent match of the thermal behaviours at the central well, as well as at observed distances up to 13 m.

Introducing this spatial variation of dispersivity appears to be a good solution for using FICK's law when local heterogeneities are not directly measurable but induce dispersion effects that are not negligible. This is then equivalent to using a purely convective three-dimensionnal model (at this scale microscopic dispersion is negligible) with a statistical permeability distribution : FICK's law with a spatial distribution of dispersivity is actually a statistical consequence of local changes in velocity around the mean value which causes convection.

V - HOT WATER STORAGE BY A SINGLE WELL

A general study of the influence of various physical parameters on hot water storage has been performed by B.R.G.M. (FABRIS et al., 1977 ; SAUTY et al., 1979b).

It has been shown that the thermal behaviour of an aquifer with confining rocks of infinite vertical extent can be characterized by two dimensionless parameters :

$Pe = \rho_F C_F \cdot Q/(\lambda_A \cdot 2\pi \cdot h)$

$\Lambda = (\rho_A C_A)^2 \cdot h^2/(\lambda_E \cdot \rho_E C_E \cdot t_i)$

providing the following dimensionless independent variables are used :

$t_R = t/t_i$

$\theta_R = (\theta - \theta_o)/(\theta_i - \theta_o)$

with (fig. 7) :

$\rho_F C_F$: heat capacity of injected fluid
$\rho_A C_A$: heat capacity of aquifer
$\rho_E C_E$: heat capacity of confining layers
λ_A : heat conductivity of aquifer
λ_E : heat conductivity of confining layers
h : aquifer thickness
Q : injected flow rate through the total aquifer thickness
t_i : duration of injection ;
$t_i = \rho_A C_A \cdot \pi \cdot R^2 \cdot h/(\rho_F C_F \cdot Q)$
R : thermal storage radius
t : time
θ : temperature produced at well bore
θ_o : initial reservoir temperature
θ_i : injected temperature

As dispersion may increase the apparent conductivity value by an order of magnitude, the Peclet number may be divided by a factor of 10. After several successive cycles of hot water injections, the water temperature during the production half cycle can then be sensibly reduced. This is illustrated on figure 8 from FABRIS et al., 1977 for $\Lambda = 10$, and two values of Peclet number : $Pe = 10$, $Pe = 1$; figure 9, from SAUTY et al., 1979b, gives another illustration for $\Lambda = 100$ and Peclet numbers which are respectively 100 and 10.

It is clear that disregarding this factor may result in overly optimistic prevision of heat recovery.

VI - GEOTHERMAL ENERGY PRODUCTION

Geothermal energy production with a doublet has been studied by B.R.G.M. (LANDEL, SAUTY ; 1978 ; SAUTY et al., 1979c) for different possible values of reservoir and exploitation characteristics (fig 10).

Only two dimensionless parameters are required:

$Pe = \rho_F C_F \cdot Q/(\lambda_A \cdot \pi \cdot h)$

$\Lambda = \rho_F C_F \cdot \rho_A C_A \cdot Qh/(\lambda_E \cdot \rho_E C_E \cdot D^2)$

with the dimensionless variables :

$t_R = 3 \cdot \rho_F C_F \cdot Q \cdot t/(\pi \cdot \rho_A C_A \cdot D^2 \cdot h)$

$\theta_R = (\theta - \theta_o)/(\theta_i - \theta_o)$

where D is the distance between injection and production wells.

As in heat storage, dispersion may be an important factor. If, for instance, we consider a doublet of average characteristics drilled in the Dogger formation near Paris, taking into account the thermal conductivity alone yield a Peclet number of 440 ; if we now take a high macroscopic dispersivity of 100 m (possible value in a fissured aquifer with wells 1000 m apart), the Peclet number becomes 3.

The temperature behaviour at the production well will then be much different (fig. 11), but the additional diffusion is not necessarily a disadvantage, however : breakthrough occurs much earlier, but the variation in temperature is slower. If some *loss in energy level* is acceptable, the doublet can be used for a longer time. A 20% reduction, for instance, will increase the example Dogger doublet lifetime 2.7 times, compared to that for Pe ∞, $\Lambda\infty$.

ACKNOWLEDGEMENTS

This publication presents partial results from several studies sponsored by Délégation Générale à la Recherche Scientifique et Technique (D.G.R.S.T.), Comité thermique et thermodynamique : (i) field experiment of hot water storage and doublet exploitation ; (ii) modelization fo the resulting data ; (iii) theoretical study of hot water storage in a deep aquifer, and by the Commission of the European Communities (CCE), Programme de Recherche et de Développement dans le domaine de l'Energie géothermique : theoretical study of the influence of physical characteristics on heat production by a geothermal doublet. For each of these studies a report and a publication is being prepared.

BIBLIOGRAPHY

BEAR (J.) .- Dynamics of fluids in porous media .- *New York, American Elzevier, 1972.*

CLOUET D'ORVAL (M.), LEDOUX (E.) .- Détermination in situ des paramètres du transfert de chaleur dans les aquifères en écoulement monophasique . *- Bull. BRGM, 2ème série, sect. III, n° 1, 1975*

GAILLARD (B.), GUIZERIX (J.), MARGAT (J.), MOLINARI (J.), PEAUDECERF (P.) .- Etude méthodologique des caractéristiques de transfert des substances chimiques dans les nappes. 5ème rapport, Synthèse de la recherche .- *Paris, Centre National de la Recherche Scientifique, Action thématique programmée Hydrogéologie, 1976.*

GREEN (D.W.) .- Heat transfer with flowing fluid through porous media .- *Ph.D. thesis, University of Oklahoma, 1963.*

FABRIS (H.), GRINGARTEN (A.C.), LANDEL (P.A.), NOYER (M.L.), SAUTY (J.P.) .- Etude des possibilités du stockage d'eau chaude en aquifère profond. 1er rapport d'avancement .- *Rapport BRGM 77 SGN 658 HYD.*

GRINGARTEN (A.C.), SAUTY (J.P.) .- A theoretical study of heat extraction from aquifers with uniform regional flow .- *Journ. Geophys. Res., vol. 80, n° 35, 1975, p. 4956-4962.*

LEDOUX (E.), CLOUET D'ORVAL (M.) .- Etude expérimentale d'un doublet géothermique. Interprétation des expériences "puits unique". .- *Délégation Générale à la Recherche Scientifique et Technique. Comité géothermie. Rapport de fin d'étude.*

MARLE (C.), SIMANDOUX (P.), PACSIRSKY (J.), GAULIER (C.) .- Etude du déplacement de fluides miscibles en milieu poreux stratifié .- *Revue de l'Institut Français du Pétrole, vol. XXII, n° 2, Février 1967.*

PEAUDECERF (P.), SAUTY (J.P.) .- Application of a mathematical model to the characterization of dispersion effects on groundwater quality .- *Prog. Wat. Tech. 1978, vol. 10, Nos 5/6, p.443-454, Pergamon Press.*

SAUTY (J.P.) .- Contribution à l'identification des paramètres de dispersion dans les aquifères par interprétation des expériences de traçage. *- Thèse doct.-ing., Univers. Grenoble, 1977.*

LANDEL (P.A.), SAUTY (J.P.) .- Etude de l'influence des caractéristiques physiques de l'aquifère et des roches encaissantes sur la température de l'eau au puits de production d'un doublet hydrothermique .- *Commission des Communautés Européennes. Final report. BRGM report 78 SGN 405 GTH, Orléans, 1978.*

RUBINSTEIN (L.I.) .- Thermal effect in oil reservoirs .- *Moscou : Nedra, 1972, chap. V to VIII (inc.).*

SAUTY (J.P.), THIERY (D.T.), GRINGARTEN (A.C.) LANDEL (P.A.) .- Calibration of heat transfer mathematical models after experiments of hot water injection in a superficial aquifer .- *to be submitted for publication in Water Resources Research, 1979a.*

SAUTY (J.P.), MENJOZ (A.), GRINGARTEN (A.C.), LANDEL (P.A.) .- A theoretical study of energy storage by means of hot water injection in an aquifer .- *to be submitted for publication in Journal of Geophysical Research, 1979b.*

SAUTY (J.P.), LANDEL (P.A.), GRINGARTEN (A.C.) .- Influence of physical characteristics of aquifer reservoir and confining rocks on heat production by a geothermal doublet .- *to be submitted for publication in Journal of Geophysical Research, 1979c.*

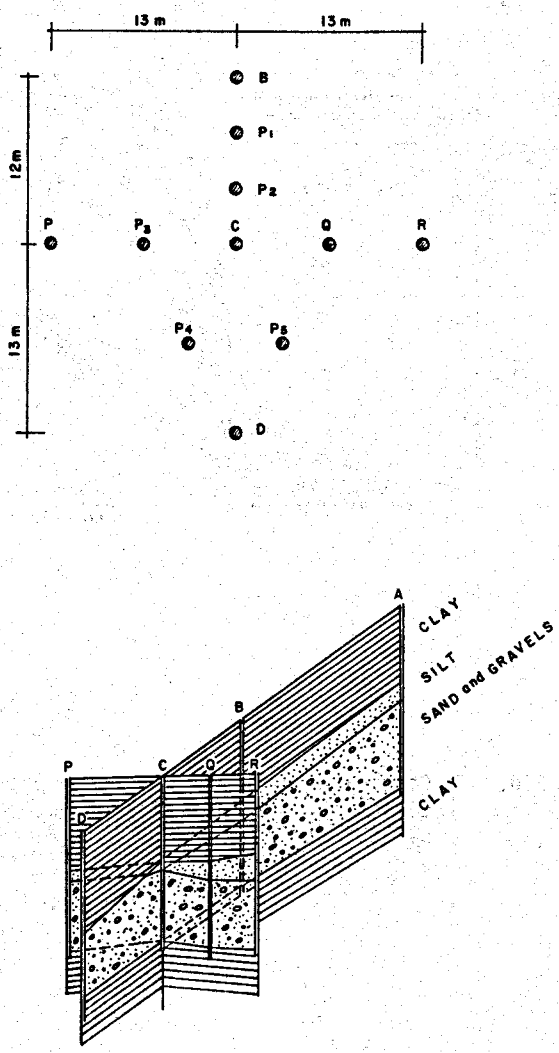

Fig. 1. Bonnaud (Jura)--Experimental site geological cross section and well positions.

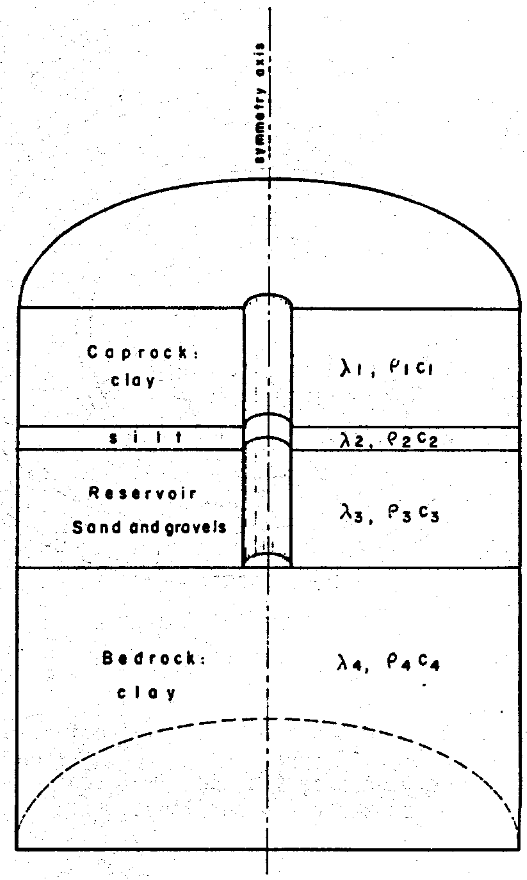

Fig. 2. Axisymmetric modelization of hot water injection at Bonnaud (Jura). List of adjusted parameters.

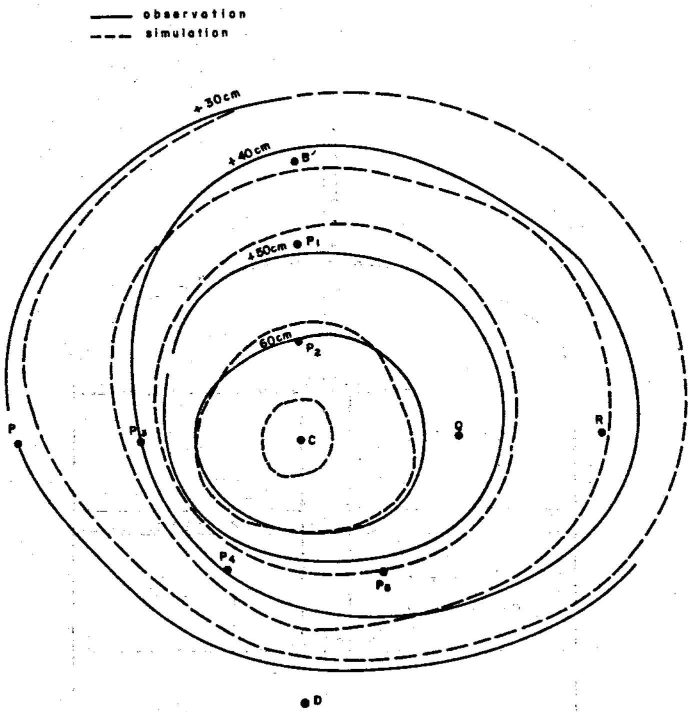

Fig. 3. Bonnaud (Jura)--Second injection in well C (October 1976). Comparison between observed and simulated piezometric contour lines.

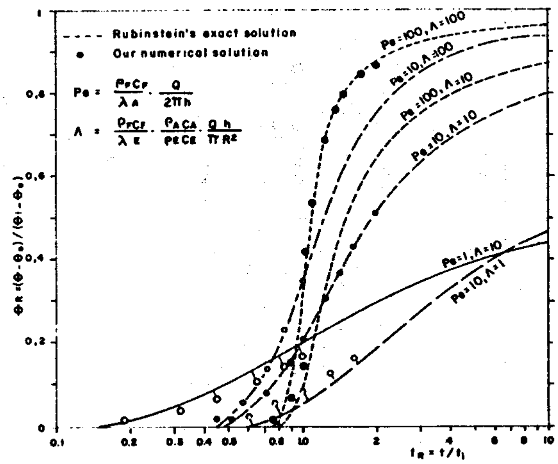

Fig. 4. Control of mathematical model precision against analytical solutions by Rubinstein, 1972.

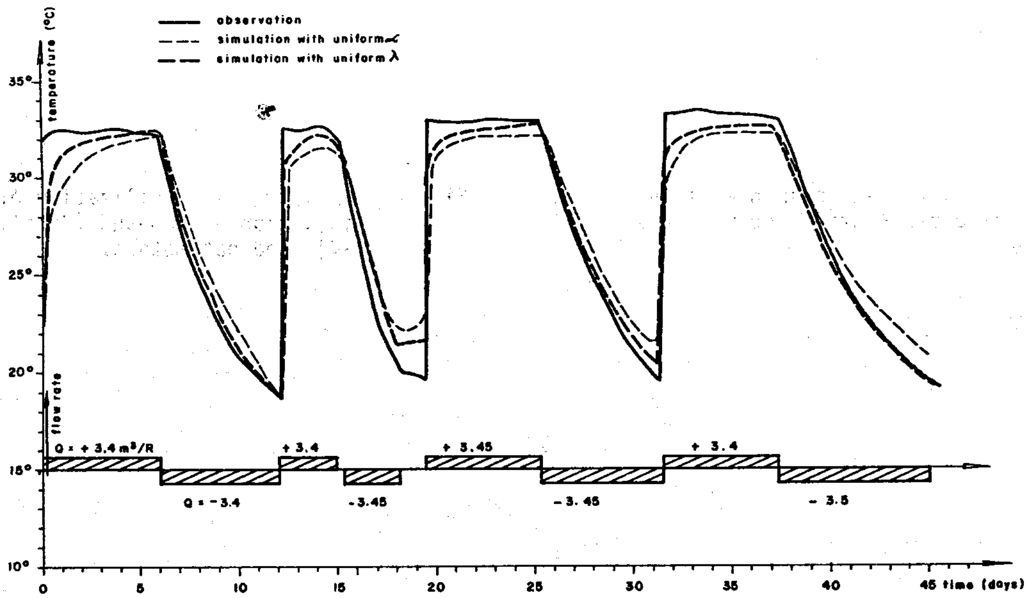

Fig. 5. 1977 hot water storage experiments at Bonnaud (Jura). Temperature evolution in central well.

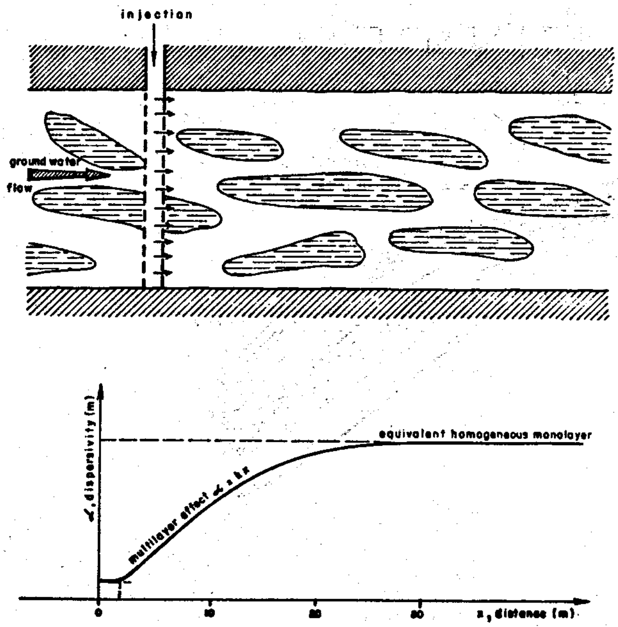

Fig. 6. Hot water storage experiments at Bonnaud (Jura). Effect of dispersivity variations with distance.

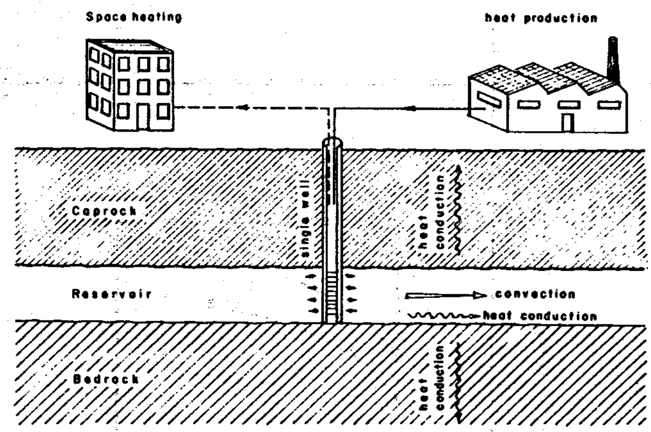

Fig. 7. Hot water storage with a single well.

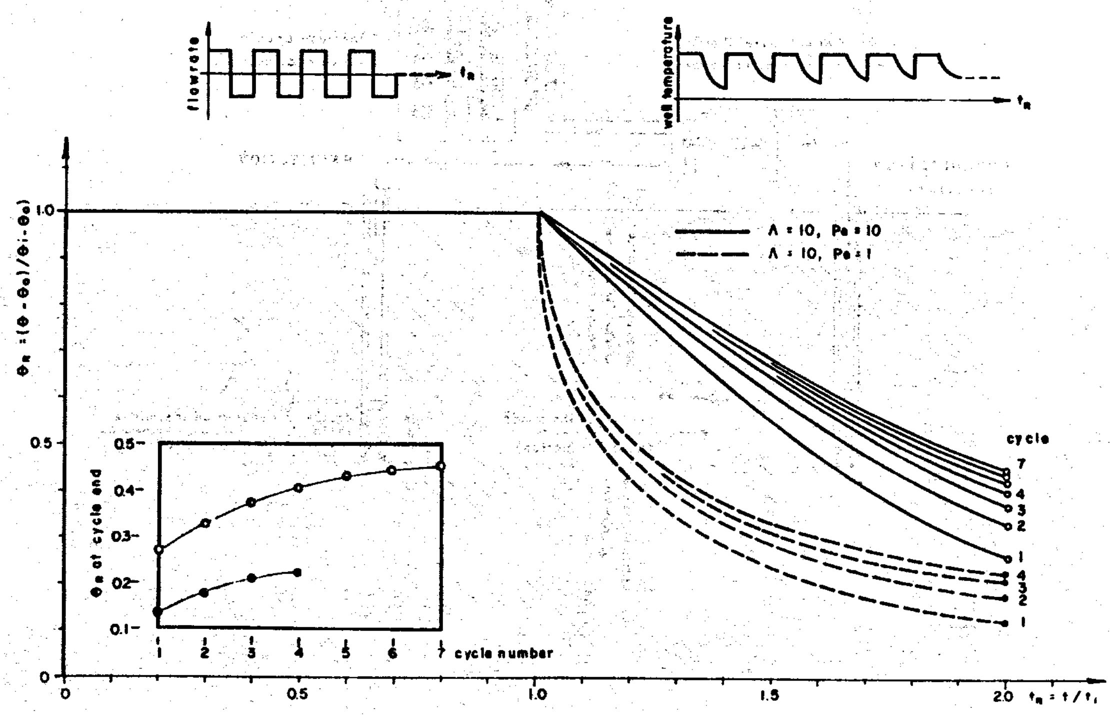

Fig. 8. Temperatures evolution at central well during successive cycles of hot water injection and production. Consequences of $\tilde{\lambda} = 10.\lambda$ (Pe = 1 instead of 10).

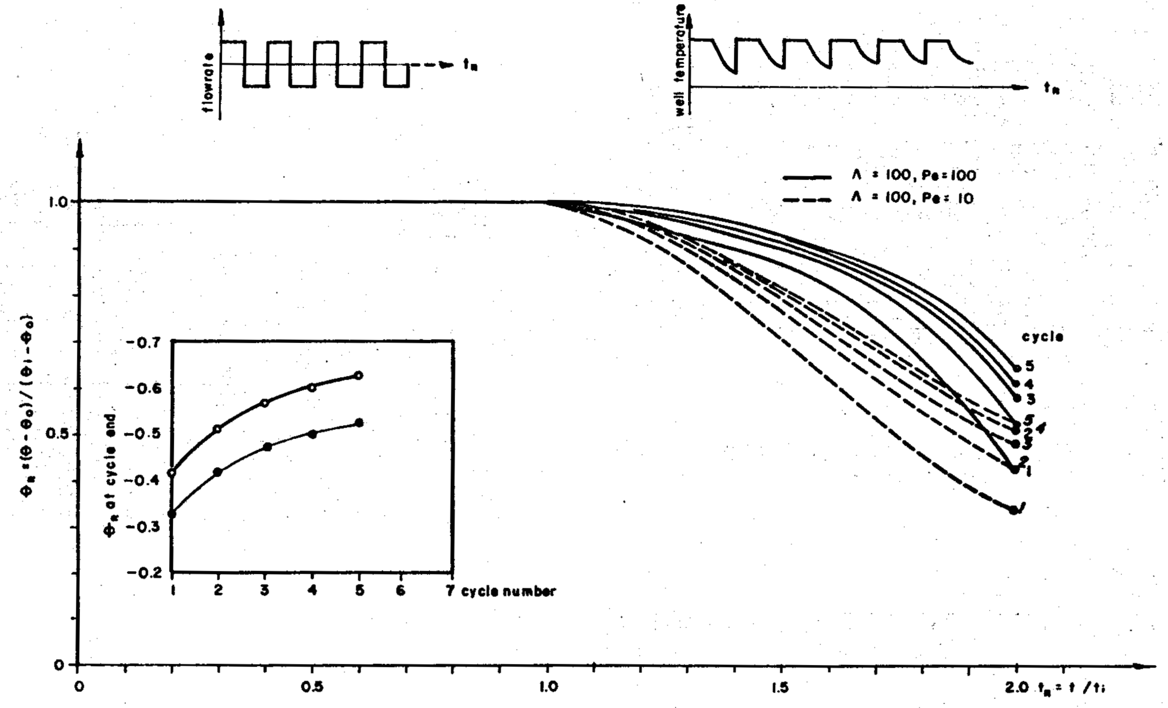

Fig. 9. Temperatures evolution at central well during successive cycles of hot water injection and production. Consequences of $\tilde{\lambda} = 10.\lambda$ (Pe = 10 instead of 100).

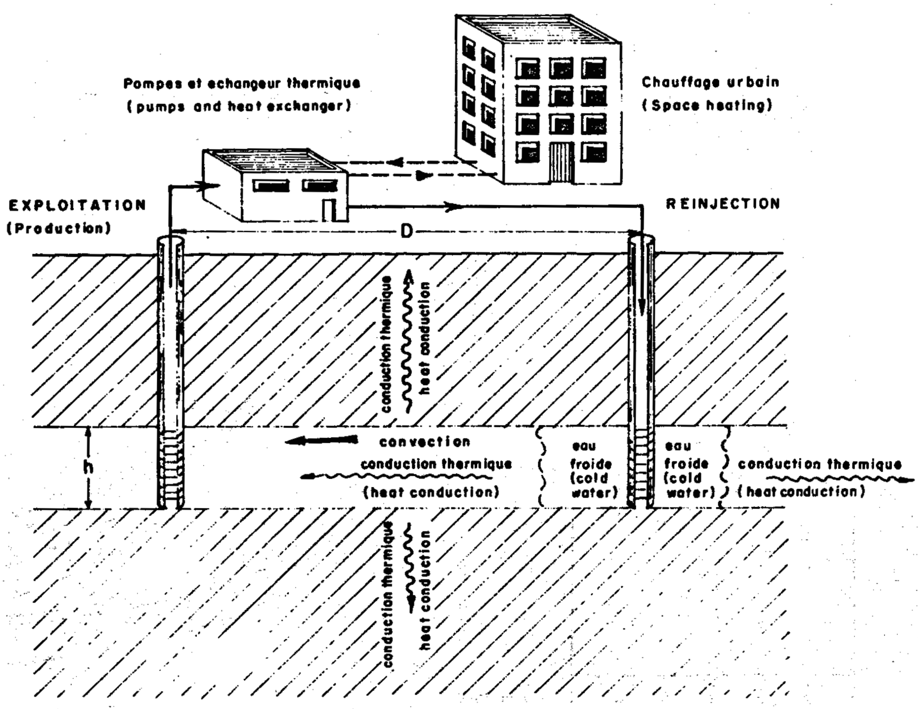

Fig. 10. Geothermal energy exploitation with a doublet.

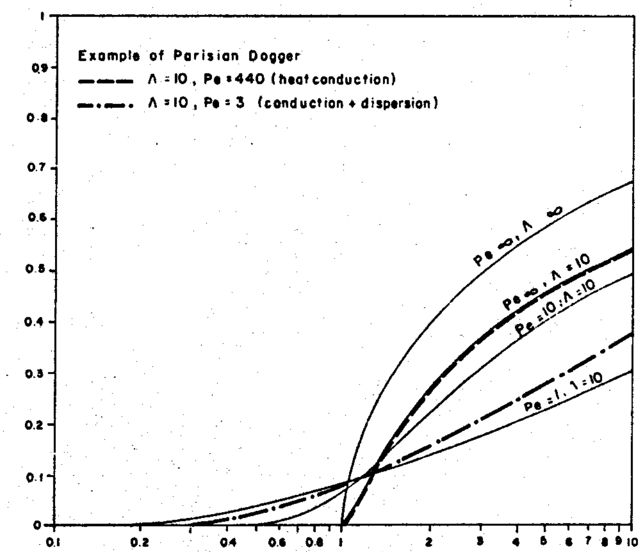

Fig. 11. Effect of Peclet number with apparent conductivity on geothermal doublet breakthrough curves. Theoretical type curves and example of exploitation in Parisian Dogger formation.

ATTENDEES

AAMODT, Lee
Los Alamos Scientific Laboratory
Route 5, Box 251
Santa Fe, New Mexico 87501
(505) 667-4318

ADAMS, John A.S.
Rice University
Department of Geology
P.O. Box 1892
Houston, Texas 77001
(713) 527-4891

ALLMAN, David W.
E G & G Idaho
685 Davidson Drive
Idaho Falls, Idaho 83401
(208) 522-5771

ANDERSON, Merlin
Halliburton Services
P.O. Box 1431
Duncan, Oklahoma 73533
(405) 251-3137

ANDERSON, Terry O.
Section Supervisor
Electrical Research & Development
Halliburton Services
P.O. Box 1431
Duncan, Oklahoma 73533
(405) 251-3081

BARKMANN, Peter
Geologic Applications G-9
Los Alamos Scientific Laboratory
P.O. 1603
Los Alamos, New Mexico 87545
(505) 667-6711

BENSON, Sally
Lawrence Berkeley Laboratory
1 Cyclotron Road
Berkeley, California 94720
(415) 843-2740

BLAIR, Allen
Los Alamos Scientific Laboratory
Mail Station 570
Los Alamos, New Mexico 87545
(505) 667-6722

BODVARSSON, Gunnar
Oregon State University
1377 N.W. Alta Vista Drive
Corvallis, Oregon 97330
(503) 752-4587 / (503) 754-2912

BRIGHAM, William E.
Stanford University
Stanford, California 94305
(415) 497-0611

CAMPBELL, Don A.
Manager - Reservoir & Planning
Republic Geothermal, Inc.
11823 E. Slauson Ave., Suite 1
Santa Fe Springs, California 90670
(213) 945-3661

CASTANIER, Louis M.
Stanford University
Stanford, California 94305

CATALDI, Ing. Carlo
ENEL - DSR
Centro Ricerca Geotermica
Piazza B. da Sassoferrato, 14
56100 Pisa, Italy
Tel. 22387 - 28092 - 573179

CINCO-LEY, Heber
Petroleum Engineering Department
Stanford University
Stanford, California 94305
(415) 497-4744 / (415) 497-1218

CLARK, George B.
Colorado School of Mines
Golden, Colorado 80401
(303) 279-0300 / 2409

COHEN, Lewis
Lawrence Berkeley Laboratory
1 Cyclotron Road
Berkeley, California 94720
(415) 843-2740

DOE, Thomas
Lawrence Berkeley Laboratory
Building 90, Trailer B
1 Cyclotron Road
Berkeley, California 94720
(415) 843-2740 / 6778

DOMINGUEZ, Ing. Bernardo
Superintendente General de Explotacion
Coordinadora Ejecutiva de Cerro Prieto
P.O. Box 248
Calexico, California 92231
Tels. 2-20-12, 2-20-13 y 2-23-40
ext. 131

DUNBAR, David
Woodward-Clyde Consultants
#3 Embarcadero Center
Suite 700
San Francisco, California 94111
(415) 956-7070 ext. 336

DYKSTRA, Herman
Petroleum Engineering Consultant
Suite I
4180 Treat Boulevard
Concord, California 94518
(415) 676-7464

EGGENSCHWILER, Mauricio
Department of Petroleum Engineering
Stanford University
Abrams G-F Escond Village
Stanford, California 94305
(415) 326-2985

ESCOBAR, David
C.E.L. (Comision Ejecutiva
Hidroelectrica del Rio Lempa)
San Salvador
El Salvador

FASSBENDER, Linda L.
Research Engineer
Economic Analysis Section
BATTELLE Pacific Northwest Laboratoies
Battelle Boulevard
Richland, Washington 99352
(509) 946-2247

FEATHERSTONE, John L.
Magma Power Company
2120 South 9th Street
El Centro, California 92243
(714) 353-1810

GALBRAITH, Robert M.
Lawrence Berkeley Laboratory
1 Cyclotron Road
Berkeley, California 94720
(415) 843-2740, ext. 6750

GARDNER, Murray C.
Geothermal Exploration Services
1340 Ponderosa Drive
Ashland, Oregon 97520
(503) 482-2605

GARG, Sabodh K.
Systems, Science and Software
P.O. Box 1620
La Jolla, California 92038
(714) 453-0060

GILMAN, Jeffrey A.
Woodward-Clyde Consultants
#3 Embarcadero Center
San Francisco, California 94111
(415) 956-7070

GORANSON, Colin
Lawrence Berkeley Laboratory
1 Cyclotron Road
Berkeley, California 94720
(415) 843-2740

GOYAL, Keshav
Lawrence Berkeley Laboratory
1 Cyclotron Road
Berkeley, California 94720
(415) 843-2740

GRAF, Alexander N.
Lawrence Berkeley California
1 Cyclotron Road
Berkeley, California 94720
(415) 843-2740 ext. 6756

GULATI, Mohinder S.
Union Geothermal Division
Union Oil Company of California
2099 Range Avenue
Santa Rosa, California 95406
(707) 542-9543

HANEY, Joe
Lawrence Berkeley Laboratory
1 Cyclotron Road
Berkeley, California 94720
(415) 843-2740, ext. 6452

HAWS, Gerald W.
Advanced Engineer
Oil Recovery Department
Research Division
Marathon Oil Company
7400 South Broadway
P.O. Box 269
Littleton, Colorado 80160
(303) 794-2601

HELM, Donald C.
Lawrence Livermore Laboratory
P.O. Box 808, L-398
Livermore, California 94550
(415) 422-9980

HILL, John H.
Lawrence Livermore Laboratory
P.O. Box 5507, L-453
Livermore, California 94550
(415) 522-3880

HOLMAN, Bill
San Francisco Operations Office
Department of Energy
1333 Broadway
Oakland, California 94612
(415) 273-7151

HOPKINS, Deborah
Lawrence Berkeley Laboratory
1 Cyclotron Road
Berkeley, California 94720
(415) 843-2740, ext. 6777

HOWARD, John H.
Lawrence Berkeley Laboratory
1 Cyclotron Road
Berkeley, California 94720
(415) 843-2740 ext. 5961

HOYER, Dan P.
Civil Engineer
Siting Department
Pacific Gas and Electric Company
77 Beale Street
San Francisco, California 94106
(415) 781-4211

HSU, Sungnan
Mechanical Research Department
Halliburton Services
P.O. Box 1431
Duncan, Oklahoma 73533
(405) 251-3350

IRVINE, Jeff
Lawrence Berkeley Laboratory
1 Cyclotron Road
Berkeley, California 94720
(415) 843-2740 ext. 5522

JACOBSON, Jimmy J., DSc
Sr. Research Scientist
Geophysicist
Applied Engineering and Development Section
BATTELLE Pacific Northwest Laboratories
Battelle Boulevard
Richland, Washington 99352
(509) 946-3653

JAVANDEL, Iraj
Pahlavi University
c/o University of California
Hearst Mining Building
Berkeley, California 94720

JUPRASERT, Serisak (Max)
Lawrence Berkeley Laboratory
1 Cyclotron Road
Berkeley, California 94720
(415) 843-2740

KASAMEYER, Paul W.
Geophysicist
Lawrence Livermore Laboratory
P.O. Box 808
Livermore, California 94550
(415) 447-1100

KOENIG, James B.
Geothermal Exploration Services
901 Mendocino Avenue
Berkeley, California 94707
(415) 524-9242

KRUGER, Paul
Civil Engineering Department
Stanford University
Stanford, California 94305
(415) 497-4123

KUMATAKA, Mark K.
Reservoir Engineer
Geothermal Resources Division
AMINOIL USA
1250 Coddington Center
Santa Rosa, California 95401
(707) 527-5332

KUNZMAN, William J.
Marathon Oil Company
P.O. Box 269
Littleton, Colorado 80120
(303) 794-2601

KUO, M.C. Tom
Research Engineer
Occidental Research Corporation
2100 S.E. Main
Irvine, California 92714
(714) 957-7332

LaMORI, Phillip N.
Manager of Geothermal Research
Occidental Research Corporation
2100 S.E. Main Street
P.O. Box 19601
Irvine, California 92713
(714) 957-7302

LEE, Naii
Department of Nuclear Engineering
University of California
Berkeley, California 94720
(415) 642-1480

LIGUORI, Paolo Emilio, dr. ing.
ELC - Electroconsult
8, Chiabrera
Milan, Italy 20151
Tele. 306502

LIPPMANN, Marcelo
Lawrence Berkeley Laboratory
1 Cyclotron Road
Berkeley, California 94720
(415) 843-2740, ext. 5035

LONG, Jane
Lawrence Berkeley Laboratory
1 Cyclotron Road
Berkeley, California 94720
(415) 843-2740, ext. 6657

LUND, John W.
Professor
Civil Engineering Technology Department
Oregon Institute of Technology
Klamath Falls, Oregon 97601
(503) 882-6321

MAASSEN, Brian W.
Engineer
Union Geothermal Division
Union Oil Company of California
2099 Range Avenue
Santa Rosa, California 95406
(707) 542-9543

MACIAS, Luis
Civil Engineering Department
Stanford University
Stanford, California 94305
(415) 497-4123

MAEDER, Paul F.
Brown University
Providence, Rhode Island 02912
(401) 863-2655
(415) 321-4069 (Palo Alto)

MANGOLD, Donald C.
Lawrence Berkeley Laboratory
1 Cyclotron Road, Bldg. 90/1024F
Berkeley, California 94720
(415) 843-2740, ext. 6459

MAVOR, Matt
Chevron Oil Field Research Company
P. O. Box 446
La Habra, California 92631
(213) 691-2241

McCUNE, Conwell C.
Chevron Oil Field Research Company
P. O. Box 446
La Habra, California 92631
(213) 691-2241

McEDWARDS, Donald G.
Lawrence Berkeley Laboratory
1 Cyclotron Road, Bldg. 90/1024E
Berkeley, California 94720
(415) 843-2740, ext. 6456

McLEAN, John S.
U. S. Geological Survey
3017 Delano Place, N.E.
Albuquerque, New Mexico 87106
(505) 766-3357

MEIDAV, Tsvi
40 Brookside Avenue
Berkeley, California
(415) 658-5330

MERCADO, Ing. Sergio
Instituto de Investigaciones Electricas
Div. Fuentes de Energia
Apdo. 475
Cuernavaca, Morelos
Mexico
4-13-65
4-13-51

MERCER, Jerry W.
U. S. Geological Survey
P. O. Box 26659
Albuquerque, New Mexico 87125
(505) 766-2246

MEYER, Charles F.
General Electric Tempo
P. O. Drawer QQ
Santa Barbara, California 93102
(805) 965-0551

MILLER, Constance W.
Lawrence Berkeley Laboratory
1 Cyclotron Road, Bldg. 90/1024H
Berkeley, California 94720
(415) 843-2740, ext. 6454

MOLLOY, Martin W.
Senior Program Coordinator
Geothermal Energy Division
Department of Energy
San Francisco Operations Office
1333 Broadway
Oakland, California 94612
(415) 273-7943
FTS 536-7943

MOODY, Marla M.
Lawrence Livermore Laboratory
P. O. Box 808, L453
Livermore, California 94550
(415) 422-3840

MORRELL, Glenn
Physics Department
University of Houston
Houston, Texas 77036
(713) 749-1874

MORSE, John G.
Hydrologist/Reservoir Engineer
Lawrence Livermore Laboratory
P. O. Box 808, L-224
Livermore, California 94550

NARASIMHAN, T. N.
Lawrence Berkeley Laboratory
1 Cyclotron Road, Bldg. 90/1012D
Berkeley, California 94720
(415) 843-2740, ext. 5655

NIEMI, Warren Lee
E G & G Idaho, Inc.
1294 St. Clair
Idaho Falls, Idaho 83401
(208) 526-0282

NOBLE, John
Lawrence Berkeley Laboratory
1 Cyclotron Road, Bldg. 90/1024G
Berkeley, California 94720
(415) 843-2740, ext. 5943

OWEN, Larry
Lawrence Livermore Laboratory
P. O. Box 808, L-220
Livermore, California 94550
(415) 422-3967

PETERSEN, Carol
GeothermEx, Inc.
901 Mendocino Avenue
Berkeley, California 94707
(415) 525-7096

PHILLIPS, Lynette
University of Southern California
1400 W. Lambert, #189
La Habra, California 90631
(213) 697-1282

PRIDDY, Charles P.
Senior Mineral Resources Engineer
California State Lands Commission
100 Oceangate, Suite 300
Long Beach, California 90802
(213) 590-5211

PRUESS, Karsten
Lawrence Berkeley Laboratory
1 Cyclotron Road, Bldg. 90/1024
Berkeley, California 94720
(415) 843-2740, ext. 5142

QUONG, Roland
Lawrence Livermore Laboratory
P. O. Box 808
Livermore, California 94550
(415) 422-7093

RAGNARSDOTTIR, Kristen V.
University of Iceland
28, Keeppsvegur
105 Reykjavik, Iceland
35-102

RINEY, T. David
Systems, Science and Software
P. O. Box 1620
La Jolla, California 92038
(714) 453-0060

ROGERS, Phila J.
Lawrence Berkeley Laboratory
1 Cyclotron Road, Bldg. 931/429
Berkeley, California 94720
(415) 843-2740, ext. 5771

ROSS, Don V.
U. S. Geological Survey
2465 E. Bayshore Road, Suite 400, Rm. 401
Palo Alto, California 94303
(415) 323-8111, ext. 2851

RUDISILL, Jacob M.
Thermal Power Company
601 California Street
San Francisco, California 94108
(415) 981-5700, ext. 162

SALTUKLAROGLU, Mehmet
ELC-Electroconsult
Melchor Ocampo 463-3°
Mexico 5 D.F.
Mexico
560-03-67

SANYAL, Subir K.
3761 Barrington Drive
Concord, California 94518
(415) 497-0691

SAUTY, Jean-Pierre
B.R.G.M. BP 6009
45018 Orleans/Cedex
France

SCHATZ, John F.
Lawrence Livermore Laboratory
P. O. Box 808
Livermore, California 94550
(415) 422-3958

SCHROEDER, Ronald C.
Lawrence Berkeley Laboratory
1 Cyclotron Road, Bldg. 90/1012C
Berkeley, California 94720
(415) 843-2740, ext. 5560

SCHWARZ, Werner J.
Lawrence Berkeley Laboratory
1 Cyclotron Road
Berkeley, California 94720
(415) 843-2740 ext. 6468

SHARMA, P.N.
Central Ground Water Board, Ind.
Jamuegar House,
Mansiugh Road
Delhi 11001
New Delhi, India

SIDDIQUI, Khaleeq (Kelly) Uddin
U.S. Geological Survey
Conservation Division
Western Region
Suite 400 - Room 401
2465 East Bayshore Road
Palo Alto, California 94303
(415) 323-6111 ext. 2851

STORM, Donna
Woodward-Clyde Consultants
#3 Embarcadero Center
San Francisco, California 94111
(415) 956-7070, ext. 325

STRELTSOVA-ADAMS, Tanya
Rice University
2368 Dunstan
Houston, Texas 77005
(713) 524-5590 - home
(713) 965-4656 - office

TSANG, Chin-Fu
Lawrence Berkeley Laboratory
1 Cyclotron Road
Berkeley, California 94720
(415) 843-2740 ext. 5728

VECHIL, Jack
Go-Wireline Services
5024 Airport Drive
Bakersfield, California 93308
(805) 399-9541

VENERUSO, A.F.
Sandia Laboratories
P.O. Box 5800
Albuquerque, New Mexico 87185
(505) 264-9162

VETTER, Otto
Vetter Research
3189 C Airway Avenue
Costa Mesa, California 92626
(714) 751-2945 / (714) 494-9907

WANG, Joseph
Lawrence Berkeley Laboratory
1 Cyclotron Road
Berkeley, California 94720
(415) 843-2740 ext. 6753

WEEKS, Edwin P.
Hydrologist
Water Resources Division
U.S. Geological Survey
P.O. Box 3355
Lubbock, Texas 79452
(806) 762-7654

WEISS, Richard B.
Harding-Lawson Associates
55 Mitchell Boulevard
San Rafael, California 94902
(415) 472-1400

WHELAN, James A.
Naval Weapons Center
China Lake, California 93555
(714) 939-2700

WITHERSPOON, Paul A.
Lawrence Berkeley Laboratory
1 Cyclotron Road
Berkeley, California 94720
(415) 843-2740 ext. 5082

YOUMANS, A.H.
Vice President
Research & Engineering
Dresser Atlas Division
Dresser Industries, Inc.
P.O. Box 1407
Houston, Texas 77001
(713) 784-6501

ZAIS, Elliot
Elliot Zais & Associates
Engineering Consultants
7915 N.W. Siskin Drive
Corvallis, Oregon 97330
(503) 757-9795

ZOLOTUKHIN, Anatoly B.
Stanford University
Stanford, California 94303

LATE REGISTRANTS

AWN, Raji Camille
University of California
Berkeley, California 94720
(415) 527-5563

CHENY, Jim
University of California at Davis
Department of Civil Engineering
Davis, California 95616
(916) 752-1438

FRIES, Bernard A.
Chevron Research
576 Standard Avenue
Richmond, California 94802
(415) 237-4411

HANSON, Jonathan M.
Lawrence Livermore Laboratory
P. O. Box 808, L-224
Livermore, California 94550
(415) 422-6502

PRABHAKAR, Vinod
University of California
412 O'Brien Hall
Berkeley, California 94720

SHOWERS, Carolin
University of California
2225 Hearst Avenue, #5
Berkeley, California 94709
(415) 841-7627

VIANNAY, Caroline
University of California
1121 Spruce Street
Berkeley, California 94707
(415) 525-3091

WERES, Oleh
Lawrence Berkeley Laboratory
1 Cyclotron Road
Berkeley, California 94720
(415) 843-2740, ext. 5625

NAME INDEX